MODIFIED RESPONSE SPECTRUM ANALYSIS FOR COMPUTING SEISMIC DEMANDS OF
MULTI-TOWER BUILDING SHARING A COMMON PODIUM

Mr. Tarek Youssef

A Thesis Submitted in Partial Fulfillment of the Requirements

for the Degree of Master of Engineering in Civil Engineering

Department of Civil Engineering

FACULTY OF ENGINEERING

Chulalongkorn University

Academic Year 2019

การปรับปรุงวิธีวิเคราะห์สเปกตรัมผลตอบสนองสำหรับคำนวณแรงที่ต้องต้านทานในอาคารสองตึกที่
ใช้ฐานร่วมกัน

นายทาเรก ยูสเซฟ

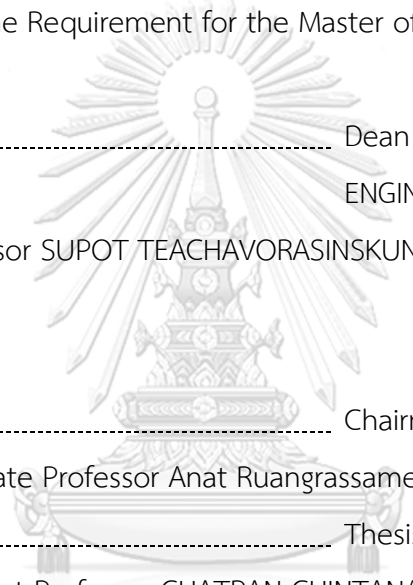|	
Thesis Title	MODIFIED RESPONSE SPECTRUM ANALYSIS FOR COMPUTING SEISMIC DEMANDS OF MULTI-TOWER BUILDING SHARING A COMMON PODIUM
By	Mr. Tarek Youssef
Field of Study	Civil Engineering
Thesis Advisor	Assistant Professor CHATPAN CHINTANAPAKDEE, Ph.D.

Accepted by the FACULTY OF ENGINEERING, Chulalongkorn University in Partial Fulfillment of the Requirement for the Master of Engineering

-- Dean of the FACULTY OF
ENGINEERING
(Professor SUPOT TEACHAVORASINSKUN, D.Eng.)

THESIS COMMITTEE

-- Chairman
(Associate Professor Anat Ruangrassamee, Ph.D.)

-- Thesis Advisor
(Assistant Professor CHATPAN CHINTANAPAKDEE, Ph.D.)

-- External Examiner
(Assistant Professor Nuttawut Thanasisathit, Ph.D.)

ทาเรก ยูสเซฟ : การปรับปรุงวิธีวิเคราะห์สเปกตรัมผลตอบสนองสำหรับคำนวณแรงที่ต้อง
ต้านทานในอาคารสองตึกที่ใช้ฐานร่วมกัน. (MODIFIED RESPONSE SPECTRUM ANALYSIS
FOR COMPUTING SEISMIC DEMANDS OF MULTI-TOWER BUILDING SHARING A
COMMON PODIUM) อ.ที่ปรึกษาหลัก : ผศ. ดร.ฉัตรพันธ์ จินตนาภักดี

การออกแบบอาคารที่มีรูปทรงไม่สม่ำเสมอควรทำการวิเคราะห์ด้วยวิธีแบบประวัติเวลาไม่เชิง
เส้น (Nonlinear Response History Analysis, NLRHA) ซึ่งถือว่าเป็นวิธีการวิเคราะห์ที่มีความถูกต้อง
ที่สุด ปัจจุบันวิธี NLRHA ไม่เป็นที่นิยมใช้ในการออกแบบในทางปฏิบัติเนื่องจากมีความซับซ้อน ดังนั้น
มาตรฐาน ASCE 7-16 จึงอนุญาตให้วิศวกรสามารถใช้วิธีสเปกตรัมผลตอบสนอง (Response Spectrum
Analysis, RSA) ในการออกแบบได้กับทุกอาคาร งานวิจัยนี้มีวัตถุประสงค์เพื่อตรวจสอบความถูกต้องของ
วิธี RSA ในการออกแบบอาคารที่มีรูปทรงไม่สม่ำเสมอโดยเฉพาะอาคารที่มีสองตึกใช้ฐานร่วมกัน และ
ทดลองใช้วิธี Modified Response Spectrum Analysis (MRSA) ซึ่งได้มีการเสนอไว้สำหรับคำนวณแรง
เฉือนสำหรับการออกแบบองค์อาคารแนวดิ่ง กับอาคารที่มีรูปทรงไม่สม่ำเสมอซึ่งเป็นอาคารตัวอย่างใน
การศึกษานี้ การศึกษานี้เริ่มด้วยการออกแบบอาคารตัวอย่างด้วยวิธี RSA ตามที่วิศวกรปฏิบัติโดยทั่วไป
จากนั้นทำการวิเคราะห์อาคารที่ออกแบบขึ้นด้วยวิธี NLRHA เพื่อหาค่าการตอบสนองที่คาดว่าจะเกิดขึ้น
จริงภายใต้แผ่นดินไหวที่กำหนดในมาตรฐานการออกแบบ และสมมุติว่าอาคารสองตึกใช้ฐานร่วมกันตั้งอยู่
ที่กรุงเทพมหานครและเชียงใหม่เพื่อให้ผลการวิเคราะห์ครอบคลุมทั้งสองกรณีหลักในประเทศไทย อาคาร
ตัวอย่างประกอบด้วย 2 กรณี คือ (1) กรณีตึกมีความสูงเท่ากัน (same tower height, SH) และ (2)
กรณีตึกมีความสูงไม่เท่ากัน (different tower height, DH) ผลการศึกษาอาคารที่สองตึกมีความสูงไม่
เท่ากัน (DH) พบว่าแรงตามแนวแกนในแผ่นพื้นบริเวณส่วนฐานที่เชื่อมระหว่างสองตึกมีค่าเพิ่มขึ้นมาก
อย่างมีนัยสำคัญเทียบกับกรณีที่ตึกมีความสูงเท่ากัน (SH) นอกจากนี้พบว่าวิธี RSA ให้ค่าประมาณของ
แรงที่ต้องต้านทานที่ต่ำเกินไปเมื่อเทียบกับผลการวิเคราะห์ด้วยวิธี NLRHA ในขณะที่วิธี MRSA สามารถ
ให้ค่าประมาณแรงเฉือนที่ถูกต้องดีทั้งในองค์อาคารแนวดิ่งและแผ่นพื้นแนวราบ ดังนั้นวิธี MRSA จึง
สามารถช่วยหลีกเลี่ยงการวิบัติแบบเปราะในองค์อาคารที่ไม่ยอมให้เกิดการครากหรือวิบัติ

สาขาวิชา	วิศวกรรมโยธา	ลายมือชื่อนิสิต ....
ปีการศึกษา	2562	ลายมือชื่อ อ.ที่ปรึกษาหลัก ....

6170452221 : MAJOR CIVIL ENGINEERING

Tarek Youssef : MODIFIED RESPONSE SPECTRUM ANALYSIS FOR COMPUTING SEISMIC DEMANDS OF MULTI-TOWER BUILDING SHARING A COMMON PODIUM. Advisor: Asst. Prof. CHATPAN CHINTANAPAKDEE, Ph.D.

To design irregular tall buildings, performance-based design (PBD) approach, which requires nonlinear response history analysis (NLRHA), is the most accurate method. However, PBD approach is not always used in the current design practice because of its complexity, and as allowed in ASCE 7-16, design engineer can use code-based approach such as response spectrum analysis (RSA) procedure. This paper aims to investigate the accuracy of RSA procedure when applied to irregular tall buildings, and in particular for multi-tower buildings sharing a common podium. Also, a modified response spectrum analysis (MRSA) procedure previously proposed for computing shear demand in regular tall buildings, was tried to apply to irregular tall buildings in this study, since elastic method is preferred in practice. Two hypothetical multi-tower buildings were designed for Bangkok and Chiang Mai sites of Thailand using the conventional RSA procedure, and then NLRHA is carried out. The effect of different tower heights is also investigated by analyzing two buildings. The first has two towers with the same heights (building SH), while the second has two towers with different heights (building DH). The out-of-synchronization behavior of the two towers in building DH leads to significant increase of axial forces in the podium floors. It was found that RSA underestimates force demands, while MRSA provides good estimates of shear force in vertical and horizontal elements. MRSA can significantly enhance the design of tall buildings by avoiding brittle failure.

Field of Study:	Civil Engineering	Student's Signature ....
Academic Year:	2019	Advisor's Signature ....

ACKNOWLEDGEMENTS

TABLE OF CONTENTS

LIST OF TABLES

LIST OF FIGURES

CHAPTER 1

INTRODUCTION

1.1 Background

Reinforced concrete (RC) shear walls are commonly used as lateral force resisting system in tall buildings. To design such structures to resist earthquake, design engineer has several choices either to follow prescriptive code-based approach, i.e., equivalent lateral force (ELF) and response spectrum analysis (RSA) procedure, or performance-based design (PBD) approach, which requires nonlinear response history analysis (NLRHA). PBD is an alternative approach for design of code-exceeding tall buildings; however, it is not always used in current design practice because of its complexity, such as nonlinear dynamic structural response and analysis, nonlinear structural model, selection and scaling of appropriate ground motions, and significant computational efforts.

As allowed in ASCE 7-16, the RSA procedure is widely used in current practice to compute design demands of structures. However, there are limitations on height, type and irregularity of structural system that can be used in ASCE 7-16. For example, in building frame system, the special RC shear wall is limited to 48.8 m for seismic design category D to F; and the ordinary RC shear wall is not permitted for seismic design category D and E; and structural system with vertical irregularity of type 5b (extreme week story irregularity) assigned to seismic design category D is not permitted according to ASCE 7-16. Structural irregularities are one of the major causes of damage amplification under seismic action as it can increase in seismic demands of a structural system. The dynamic response of irregular structures is an issue that is explicitly warned against in design guidelines. However, design engineers do not pay much attention on those limitations, and they use RSA procedure in the code to compute the design demands of tall building with RC shear walls with height taller than 48.8m, which is not compliant to the scope of the prescriptive code. This can lead to unsafe design of tall building because RSA procedure has been found to underestimate the actual demands computed from NLRHA procedure. For example, RSA method have been found to underestimates design shear force of tall RC wall

buildings, which can lead to brittle failure mode (Khy & Chintanapakdee, 2017; Khy et al., 2019; Najam & Warnitchai, 2018) and it cannot predict inelastic deformation locations where ductile detailing should be implemented to avoid brittle failure mode. The concept of RSA procedure is to reduce the elastic demand by response modification factor R, and to amplify the displacements by deflection amplification factor C_d in order to predict the real inelastic displacement that may results from a strong earthquake. Also, building codes assumes that shear forces are limited by flexural yielding, and they would be reduced in the same manner as bending moment. However, it was proved by many researchers that shear forces can still increase after flexural yielding occurs.

In European Committee for Standardization (2004) and New Zealand Standard (2006), there is no structural height limit as in ASCE 7-16, and there is no requirement to use PBD approach to design of tall buildings. RSA procedure can be used for all types of buildings; however, there are provisions about design shear force and bending moment for RC wall in these two codes. The main idea is to avoid brittle shear failure and unintended yielding location along the height of the wall. Shear force and bending moment in RC wall are computed by a design envelop using amplification factor method to scale up the force demands computed by ELF or RSA procedure before being used as design demands (EC8-1, 2004; NZS 3101, 2006). However, there is no such amplification method yet in ASCE 7-16 because maybe PBD approach is used for design of code-exceeding tall buildings in US (SEAONC 2007; LATBSDC 2017). It should be noted that such amplification factor method used in EC8-1 (2004); NZS 3101 (2006) cannot be applied for the case-study buildings in Bangkok because of its special tectonic and geological setting which leads to significantly different spectral shape comparing to the general code spectrum.

Modern tall buildings are often having irregular shapes, and multiple tower buildings are often a typical building that used in many countries around the world. The vertical lateral force resisting system that could be used for such kind of structure is RC shear walls. The seismic force resisting system is composed of vertical and horizontal elements. Diaphragms are horizontal planar elements that serve to

transfer lateral forces to vertical elements of the lateral force resisting system. Diaphragms are designed to resist in-plane and out-of-plane forces, where the source of out-of-plane forces induced in slabs are due to gravity loads, while the in-plane forces can develop due to lateral loads.

In multiple tower buildings, large diaphragm transfer forces should be anticipated at podium level, or where plane of resistance change. Therefore, diaphragms are an essential part of the seismic force resisting system and require design attention by the structural engineer to ensure that the structural system performs adequately during earthquake shaking. Multiple tower buildings sharing a common podium were not prevalent up to recent years since such structures were designed using seismic joints, forcing the response of the towers to be independent of each other. Therefore, although there is a scarce amount of relevant research in the literature, analysis of multiple towers sharing a common podium is a subject that is not yet adequately investigated. As well, considering code requirements, there is also a need for development of more practical approaches to be used for analysis and design of such structures.

A modified response spectrum analysis (MRSA) has been proposed by Khy et al. (2019), and it was found that MRSA method can significantly improve the underestimation of RSA in computing shear demand forces. However, MRSA method was adopted for regular building, and diaphragm forces are not yet studied. Irregular tall buildings should also be investigated to ensure safe design of these structures. Weakness or critical failure modes in irregular tall buildings such as force transfer mechanism in diaphragm at podium-tower intersection or at setback level, floor acceleration, and other inelastic deformations and internal forces should be investigated. Therefore, improved seismic analysis procedure for design of floor diaphragms in irregular RC shear wall tall buildings is proposed. The selected buildings are shown in the Figure 1.1, where the first has two towers with the same height (building SH), while the second has two towers with different heights (building DH).

      (a) SH   (b) DH
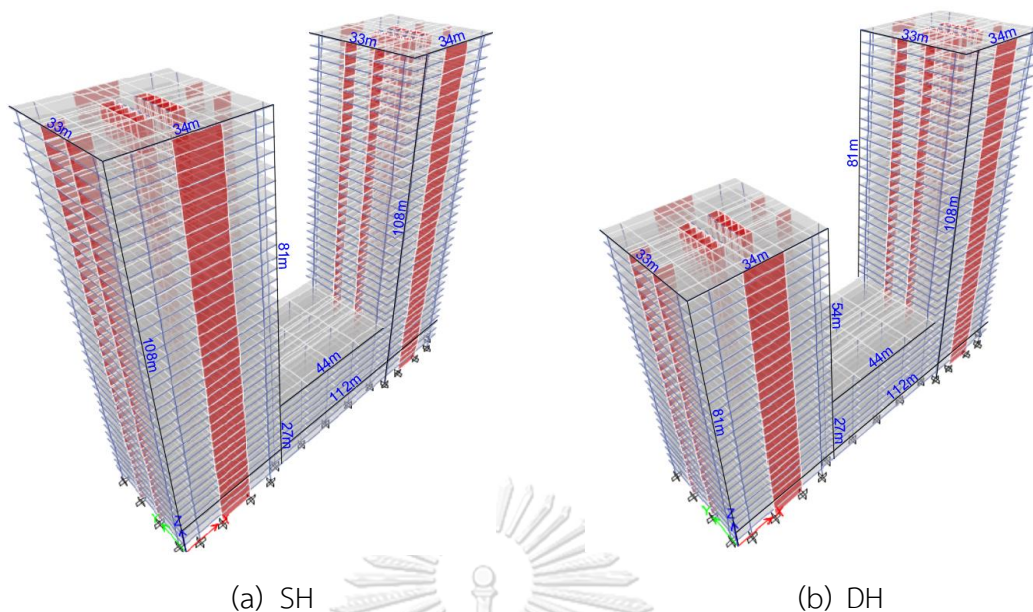
Figure 1.1 Multiple towers with, (a) same height, (b) different height.

1.2 Objectives

The main objectives of this study are the followings:

1) To check the accuracy of conventional RSA and previously proposed MRSA method when applied to irregular tall buildings.

2) To improve the design of diaphragms, by predicting the actual in plane forces that may results from an earthquake event.

3) To investigate the critical failure modes, and identify the locations that needs design attention.

1.3 Scope of research

The scope of this study are the followings:

1) Two irregular tall buildings are used to be designed in Bangkok (soft soil, site class F) and Chiang Mai (stiff soil, site class D) sites of Thailand.

2) Both buildings composed of multiple towers with a common podium, where one of the buildings consists of two towers with same height, while the other consist of two towers with different height.

3) Six and ten matched spectral acceleration ground motion are employed for Bangkok and Chiang Mai, respectively.

4) Soil structure interaction is not considered, and support were assumed to fixed at the base.

5) The buildings are designed according to ACI 318M-14 (American Concrete Institute, 2014) with earthquake load by mean of RSA procedure in ASCE 7-16 (American society of Civil Engineers, 2016) and wind load according to Thai code.

1.4 Research methodology

The procedure to conduct this study is outlined as follows:

1) Create the linear mathematical model using ETABS software (Computers and Structures, 2018).

2) Compute the design demands that results from all factored load combinations including gravity load, wind load according to Thai code, and seismic forces from RSA procedure in ASCE 7-16.

3) Design the structural system according to ACI 318M-14, such that the design strength of structural components is slightly larger than the design demands obtained from the factored load combination.

4) Analyze the structures by NLRHA procedure using PERFORM-3D (Computers and Structures, 2018) to evaluate the accuracy of RSA and MRSA methods.

5) Investigate the critical failure mode of the structure by using NLRHA results.

6) Compute the force response reduction factor of each mode by using modal pushover analysis.

7) Check the applicability of MRSA method if to be used for diaphragm design, and propose a new method to improve the design of diaphragms if needed.

8) Identify the critical location that needs a special detailing and design attention.

1.5 Research significance

1) The findings of this study emphasize that MRSA provides reasonably accurate design demands for irregular tall buildings with multiple towers sharing a common podium.

2) The findings of this study can contribute to the future revision of seismic design standard in Thailand.

3) This study contributes to better understanding of seismic behavior of irregular tall buildings, in which conventional RSA procedure cannot capture.

CHAPTER 2

LITERATURE REVIEW

2.1 Analysis methods

2.1.1 Response history analysis (RHA)

The governing equation for a multi-degree of freedom system subjected to earthquake ground motion $\ddot{u}_g(t)$ is defined as:

$$\mathbf{m}\ddot{\mathbf{u}}(t) + \mathbf{c}\dot{\mathbf{u}}(t) + \mathbf{k}\mathbf{u}(t) = -\mathbf{m}\iota\ddot{u}_g(t) \tag{2.1}$$

$$\mathbf{P}_{eff}(t) = -\mathbf{m}\iota\ddot{u}_g(t) \tag{2.2}$$

where $\mathbf{m}$, $\mathbf{c}$, and $\mathbf{k}$ are mass, damping and stiffness matrix, respectively; $\ddot{\mathbf{u}}(t)$, $\dot{\mathbf{u}}(t)$, and $\mathbf{u}(t)$ are acceleration, velocity, and displacement vector time history, respectively. The right hand side of Eq. (2.1) can be expressed as $\mathbf{P}_{eff}(t)$, as shown in Eq. (2.2), where ι is the influence vector. The spatial distribution of effective earthquake forces over the height of the building is defined by the vector $\mathbf{s} = \mathbf{m}\iota$. This force distribution can be expanded as a summation of modal inertia force distribution.

$$\mathbf{s} = \mathbf{m}\iota = \sum_{n=1}^{N} \Gamma_n \mathbf{m}\phi_n \tag{2.3}$$

where ϕ_n is the nth mode shape of the structure, and Γ_n is the modal participation factor, which is a measure of the degree in which the nth mode participates in the response. The contribution of the nth mode to excitation vector $\mathbf{m}\iota$ is:

$$\mathbf{s}_n = \Gamma_n \mathbf{m}\phi_n \tag{2.4}$$

$$\Gamma_n = \frac{\phi_n^T \mathbf{s}}{\phi_n^T \mathbf{m}\phi_n} \tag{2.5}$$

The differential equations of Eq. (2.1) are coupled when at least one of the matrices is not diagonal; then all equations must be solved simultaneously, which is difficult to carry out. The problem can be solved easier if we convert the equations in term of displacement $\mathbf{u}(t)$ into equations in terms of modal coordinate vector $\mathbf{q}$. The

displacement vector $\mathbf{u}(t)$ can be written as a product of mode shape vector ϕ_n and modal coordinate $q_n(t)$:

$$\mathbf{u}(t) = \sum_{n=1}^{N} \phi_n q_n(t) \tag{2.6}$$

Substitute Eq. (2.6) in the equation of motion and pre-multiplying by ϕ_n^{T} leads to the modal equation shown below.

$$\ddot{q}_n + 2\xi_n \omega_n \dot{q} + \omega_n^2 q_n = -\Gamma_n \ddot{u}_g(t) \tag{2.7}$$

where ξ_n is the modal damping ratio, and ω_n is the natural frequency mode n. Rewrite $q_n(t)$ as

$$q_n(t) = \Gamma_n D_n(t) \tag{2.8}$$

Substituting Eq. (2.8) in Eq. (2.7) leads to:

$$\ddot{D}_n + 2\xi_n \omega_n \dot{D}_n + \omega_n^2 D_n = -\ddot{u}_g(t) \tag{2.9}$$

Therefore, the modal response history analysis (RHA) is obtained using direct summation in time history of response from all modes as shown in Eq. (2.10) and Eq. (2.11), where the total displacement is:

$$\mathbf{u}(t) = \sum_{n=1}^{N} u_n(t) = \sum_{n=1}^{N} \Gamma_n \phi_n D_n(t) \tag{2.10}$$

And the total response is:

$$r(t) = \sum_{n=1}^{N} r_n(t) = \sum_{n=1}^{N} r_n^{st} A_n(t) \tag{2.11}$$

where r_n^{st} is the modal static response determined by static analysis due to external force $\mathbf{s}_n$; $A_n(t)$ is the pseudo-acceleration of nth mode SDF system obtained from $A_n(t) = \omega_n^2 D_n(t)$; and $D_n(t)$ is deformation of nth mode and it is obtained from dynamic analysis of SDOF system. If the modal peak responses are combined using SRSS or CQC combination rule the method is called modal response spectrum analysis (RSA).

2.1.2　Nonlinear response history analysis (NLRHA)

The governing equation for an inelastic multi-degree of freedom system subjected to earthquake ground motion $\ddot{u}_g(t)$ is defined as:

$$\mathbf{m}\ddot{u}(t) + \mathbf{c}\dot{u}(t) + \mathbf{f}_s(\mathbf{u},\dot{\mathbf{u}}) = -\mathbf{m}\iota\ddot{u}_g(t) \tag{2.12}$$

where $\mathbf{f}_s(\mathbf{u},\dot{\mathbf{u}})$ is the relation between structural resisting force and displacement that defines yielding and degradation of the structure.

2.1.3　Modal pushover analysis (MPA)

Nonlinear static analysis is used to investigate the force–deformation behavior of a structure for a spatial distribution of forces, typically lateral forces. Dropping the inertia and damping terms in Eq. (2.12) gives the nonlinear equation to be solved in a static problem:

$$\mathbf{f}_s(\mathbf{u}) = \mathbf{P} \tag{2.13}$$

The task is to determine the displacements $\mathbf{u}$ due to a set of given external forces $\mathbf{P}$, where the nonlinear force–deformation relation $\mathbf{f}_s(\mathbf{u})$ is known for the system to be analyzed. Chopra and Goel (2002) developed the modal pushover analysis that it is equivalent to the well-known response spectrum analysis (RSA) procedure. To develop a pushover analysis procedure consistent with RSA, they developed the following formulas:

$$\mathbf{f}_{no} = \Gamma_n \mathbf{m}\phi_n A_n \tag{2.14}$$

$$\mathbf{s}_n^* = \mathbf{m}\phi_n \tag{2.15}$$

where $\mathbf{f}_{no}$ is lateral force distributed over the height; $\mathbf{s}_n^*$ is the shape of the distributed lateral load over the height of the building. Nonlinear static analysis is conducted by pushing the building to reach the peak roof displacement (u_{rno}) of the nth mode estimated by:

$$u_{rno} = \Gamma_n \phi_{rn} D_n \tag{2.16}$$

where $D_n = A_n / \omega_n^2$. For elastic system; A_n is obtained from response spectra in the same way as in RSA procedure. The peak modal responses (r_{no}), each determined by one pushover analysis, can be combined by SRSS or CQC method to obtain an estimate of the peak value (r_o) of the total response.

2.2 Performance based-design (PBD)

The design of special and irregular tall buildings in seismically active regions varies dramatically from region to region. The performance-based design (PBD) approach is required in some countries, including Japan, China, and US, whereas many other countries do not require anything beyond traditional design practice that is based on equivalent lateral force and response spectrum analysis procedure (CTBUH 2008). In USA (SEAONC 2007; LATBSDC 2017), PBD is used for design of tall buildings exceeding 48.8 m (160 feet). In Japan, PBD is used for buildings taller than 60 m (Nakai et al., 2012), while in China, height limit on tall buildings is specified in Chinese code (GB 50011-2001) depending on seismic zone and structural system; for instant, the maximum height of code-design reinforced concrete structures is 80 m for highest seismic hazard. For taller buildings, PBD approach must be adopted.

Seismic design of a tall building following PBD principles requires explicitly consideration of two or more different-level earthquakes. In USA, two levels of ground shaking are considered, the Service-Level Earthquake (SLE) and the Maximum Considered Earthquake (MCE) (PEER TBI 2017; LATBSDC 2017). The SLE is defined as an earthquake with a 43-year return period (50% in 30 years) and the MCE is defined as an earthquake with 2475-year return period (2% in 50 years). Performance objectives are typically measured at the SLE and MCE design levels. For SLE, the building shall have capability to withstand moderate intensity earthquake with limited damages, and for MCE, the building shall be able to withstand strong earthquake with low probability of partial collapse. The performance is checked under individual level of earthquake. Linear response spectrum analysis (RSA) using elastic design spectrum is commonly used at SLE level, while nonlinear response history analysis (NLRHA) is generally used at MCE level to demonstrate adequate performance of high-rise buildings in regions of moderate-to-high seismic hazard. However, in regions of low seismic hazard, multi-mode response-spectrum analysis may be adequate according to Appendix B of CTBUH (2008).

2.3 Nonlinear static procedure (NSP) on irregular buildings

Nonlinear static procedure (NSP) by mean of pushover analysis is widely used because of its efficiency and capability to estimate seismic demands directly from site-specific hazard spectrum without the effort of selecting and scaling of ground motions as required by NLRHA. NSP is also recommended by rehabilitation code (ASCE 41-13, 2013; EC8-3, 2005). However, code-based NSP is limited to regular and first-translational mode dominant structure. In addition to higher-mode effect, in the case of asymmetric buildings, there is an additional source of errors in code-based NSP due to the coupled torsional-lateral displacement of the building. To consider this torsional effect, many pushover analysis methods have been proposed in the research field. Among many proposed methods for irregular buildings, two main approaches can be well recognized. The first approach is a combination of a nonlinear pushover analysis and linear elastic RSA (Cimellaro et al., 2014; Fajfar et al., 2005; Kreslin & Fajfar, 2012). The second approach is a combination of many independent nonlinear pushover analysis representing several mode responses with the application of a modal combination rule: square-root-of-sum-of-square (SRSS) or complete quadratic combination (CQC) (Chopra & Goel, 2004; Reyes & Chopra, 2011; Soleimani et al., 2017).

The first approach, named the Extended N2 method proposed by Fajfar et al. (2005) for application to plan irregular building, is the extended version of the N2 method proposed by Fajfar (2000). This extended N2 method was latter improved by Kreslin and Fajfar (2012) by considering higher-mode effects in both plan and elevation. In Extended N2 method, the peak response is estimated using the pushover analysis results multiplied by a "correction factor" to take into account for torsional and higher-mode effects. The correction factor is computed using linear elastic RSA on the assumption that the elastic envelop of lateral displacements is conservative with respect to the inelastic one. Cimellaro et al. (2014) proposed bidirectional pushover analysis (BPA) to improve the accuracy of the extended N2 method when applied to irregular building subjected to bidirectional ground motions. The main different with respect to the extended N2 method is that the BPA applies

lateral load patterns corresponding to the first mode in the two principal orthogonal directions simultaneously.

The second approach, called modal pushover analysis (MPA), was proposed by Chopra and Goel (2002) for regular buildings considering the higher-mode effect, and was extended by Chopra and Goel (2004) and Reyes and Chopra (2011) for asymmetric buildings subjected to unidirectional and bidirectional ground motions, respectively. This approach involves multiple pushover analysis of multi-degree of freedom (MDOF) systems, and multiple NLRHA of single-degree of freedom (SDOF) systems to get the target roof displacement for each mode. For irregular structure, the load pattern used in pushover analysis consists both lateral forces and a torque based on the elastic mode shape for each mode. The total peak responses are obtained by using SRSS or CQC modal combination rule. It was observed that there is abnormality of reversal in higher-mode pushover curve in MPA procedure; therefore, Soleimani et al. (2017) proposed energy-based modal pushover analysis (EMPA) to circumvent this issue. The overall procedure of EMPA is well comparable to MPA, but the capacity curve is established by energy-based approach. In this approach, the work done by lateral loads and a torque through pushover analysis is used to compute the displacement of a corresponding equivalent SDOF system.

2.4 Code guidelines on irregular buildings

Structural irregularities are one of the major causes of damage amplification under seismic action as it can increase in seismic demands of a structural system. Irregularities are generally classified into two major categories: horizontal and vertical irregularities. The first type is related to in-plan asymmetric building causing a substantial increase of torsional effects, and the second type involves variation of geometrical or structural properties along the height of the building leading to increase of the seismic demand in specific story. For design of an irregular structure in ASCE 7-16, there are several special considerations depending on seismic design category. For example, (1) structural system with extreme torsional irregularity, weak story or extreme soft story irregularity are not permitted for seismic design category E; (2) ELF procedure is not allowed for certain irregularities; (3) orthogonal load effect

is required for structure with nonparallel system irregularity assigned to seismic design category C through F; and (4) seismic demands of certain irregular structures are increased; for instance, load combination with over-strength factor is used for structural elements supporting discontinuous wall or frame; design force of diaphragm, collector, chord is increased by 25% for certain irregular types; redundancy factor (ρ) of 1.3 used to amplify horizontal earthquake load is required for extreme torsional irregularity and amplification of accidental torsional moment is required. EC8-1 (2004) does not have restriction on structural height or irregularities as considered in ASCE 7-16, and RSA procedure is applicable to all types of buildings. However, EC8-1 (2004) states more explicitly for non-regular building in elevation (Vertical irregularity) that the behavior factor (force response reduction factor in ASCE 7-16) of a structural system shall be decreased by a factor of 0.8, and ELF procedure is not permitted.

2.5 Special design considerations of diaphragms

One of diaphragm modeling concern is to determine whether the diaphragm can be modeled as a rigid or flexible element. This modeling assumption affects the distribution of lateral force in the structural system, due to a change in diaphragm relative stiffness. Rigid diaphragm assumptions mean that no in-plane deformation is taking place in slab elements, while the flexible or semi-rigid assumption allows for the in-plane deformation. American society of Civil Engineers (2016) suggest to idealize diaphragm as a rigid if span-to-depth ratio is 3 or less. Also, ASCE 7-16 provides analytical way to check diaphragm flexibility by checking the maximum in-plane deflection with average story drift under lateral loads obtained using equivalent lateral force (ELF) procedure, as shown in Figure 2.1.
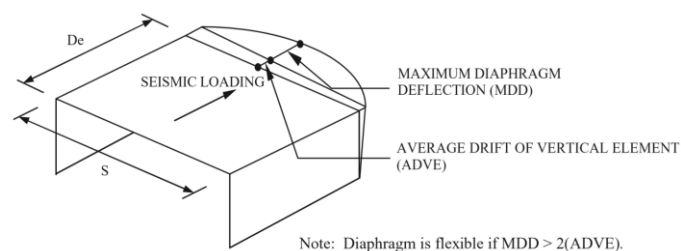
Figure 2.1 Flexible diaphragm condition according to ASCE 7-16.

American Concrete Institute (2019) (ACI 318-19) recommends design engineers to consider diaphragm flexibility in the cases where such effects will significantly affect the design actions. Also, a check of span-to-depth ratio could provide a guidance for engineers in some cases, as shown in Figure 2.2. Even though, such effect is considered for precast slabs, while it ignored in cast-in-place slabs, and this can show that even the construction process could affect the choice of these assumptions.
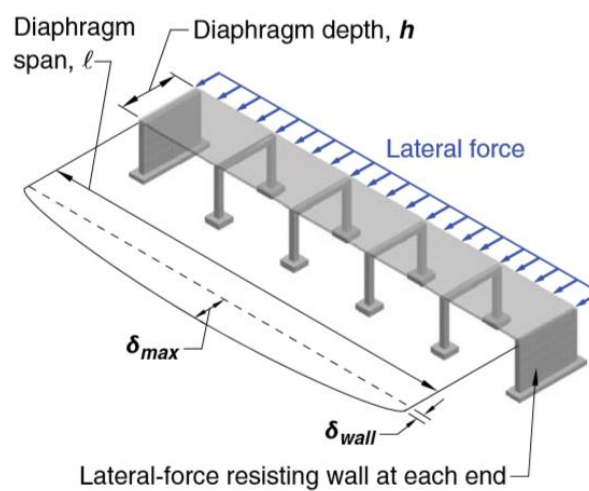
Figure 2.2 Diaphragm with long span-to-depth ratio (ACI 318-19).

ASCE 7-16 stated that the floor and diaphragms shall be designed to resist the seismic forces obtained from the analysis, but shall not be less than that determined in accordance with Eq. (2.17). Also, F_{px} in Eq. (2.17) shall not be less than $F_{px,min}$, and not exceed $F_{px,max}$.

$$F_{px} = \frac{\sum_i^n F_i}{\sum_i^n w_i} w_{px} \tag{2.17}$$

$$F_{px,min} = 0.2 S_{DS} I_e w_{px} \tag{2.18}$$

$$F_{px,max} = 0.4 S_{DS} I_e w_{px} \tag{2.19}$$

where F_{px} is the diaphragm design force, F_i is the design force applied at level i, w_i is the weight tributary to level i, w_{px} is the weight tributary to the diaphragm at level x, S_{DS} is design spectral response acceleration parameter at the short period range, I_e is the importance factor.

In addition, for structure assigned to seismic design category (SDC) C, D, E and F, ASCE 7-16 recommends to amplify the seismic forces by an overstrength factor for the purpose of designing the collector elements (same approach is followed in ACI code). The overstrength factor Ω_0 shall be multiplied by the horizontal earthquake load (Q_E) as shown in Eq. (2.20).

$$E_{mh} = \Omega_0 Q_E \qquad (2.20)$$

where E_{mh} is the horizontal seismic load effect used for the purpose of designing collectors. The horizontal earthquake load Q_E, shall be taken as the maximum value obtained from one of the following analysis methods, which are: ELF, RSA or forces obtained from Eq. (2.17). Also, the value of E_{mh} need not exceed the maximum force that can develop in the element as determined by a rational plastic mechanism analysis or nonlinear response analysis utilizing realistic expected values of material strengths. Finally, the maximum effect obtained from Eq. (2.20) shall be used in appropriate load combinations described in the code.

Fleischman et al. (2005) proposed a methodology for design of precast concrete diaphragms under seismic demands. They mentioned that the seismic demands obtained from equivalent force procedure (ELF) may significantly underestimate diaphragm inertial forces for wall and frame structures. They aim to satisfy the design requirements at diaphragm level, joints and connections, and to provide adequate detailing at critical location. In addition, they recommend to amplify the design forces results from DBE event by an amplification factor Ω.

2.6 Causes of inaccuracy of the code-based approach

Various research studies have shown that the base shear computed from static and dynamic code procedure is significantly smaller than those that may result from a real earthquake event. For example, the distribution of static forces obtained from equivalent lateral force (ELF) method described in ASCE 7-16 is based on the first-mode of vibration. However, the contribution of higher modes to the elastic response produces base shear significantly larger than those resulting from the static

code procedure. The contribution of higher modes in the structural response of an RC wall becomes more critical when the RC wall starts to respond inelastically.

For RSA procedure, higher-mode effects are taken into account, but the building code assumes that all modes of response are equally affected by inelastic action by using a single force response reduction factor (R). However, previous researchers have found that inelastic behaviors of each mode were not identical, and higher modes were not significantly affected by inelasticity as the first mode (Khy et al., 2019; Rejec et al., 2012). Building codes assumes that shear forces are limited by flexural yielding, and they would be reduced in the same manner as bending moment. However, it was proved that shear forces can still increase after flexural yielding occurs (Blakeley et al., 1975). The excessive force demand needed to cause flexural yielding is due to flexural overstrength inherent in design. There are many sources of flexural overstrength such as expected material strength which is greater than the material strength used in the design, reduction factor used in the design, and minimum reinforcement requirement. Also, it was proved that increasing flexural overstrength by providing additional vertical steel reinforcement at the base of core walls, will leads to an amplification of shear forces at the base (Khy & Chintanapakdee, 2017). In other words, when flexural capacity at the base of the wall is reached, the flexural over-strength inherent in the design could increase shear force of the wall. As stated by Priestley et al. (2008) that the problem in conventional force-based seismic design is that the initial stiffness is not known at the start of the design process, because stiffness is dependent on the strength, and increasing or decreasing reinforcement to satisfy code requirements will change the member stiffness. In addition, the lateral force distribution based on elastic stiffness is illogical (Blakeley et al., 1975; Priestley et al., 2008).

2.7 Improved estimations of seismic force demand

Many subsequent studies have suggested different methods to account for higher-mode contribution of inelastic RC shear walls. Here, the proposed methods were classified into two approaches: amplification factor method, higher-mode-elastic method. These proposed methods were developed based on different

parametric studies such as structural configurations and ground motions; obviously, the results depend on these choices.

2.7.1 Amplification factor approach

The first early work of checking the accuracy of RSA procedure was performed by Blakeley et al. (1975), who shown that RSA underestimate shear forces, due to excessive force needed to reach flexural capacity at the base of RC shear wall. Blakeley et al. (1975) conduct a study on a 5 to 20 story building consisting of RC cantilever walls. They conclude that the base shear from nonlinear dynamic analysis can be much higher than would be derived by assuming a normal code lateral load distribution. They proposed a simple formula to amplify the demand shear forces.

$$V_o = \omega_v V_E \tag{2.21}$$

$$\omega_v = \begin{cases} 0.9 + \dfrac{n}{10} & \text{for } n \le 6 \\[2mm] 1.3 + \dfrac{n}{30} & \text{for } n \ge 6 \end{cases} \tag{2.22}$$

where V_o is the design base shear, V_E is the demand base shear, n is the number of stories, and ω_v is the base shear amplification factor.

The amplification factor formula proposed by Blakeley was used by Paulay and Priestley (1992), however they modify Eq. (2.21) by including flexural over-strength factor ϕ_o. Additionally, New Zealand Standard (2006) (NZS 3101) use the same formula proposed by Paulay and Priestly as shown in Eq. (2.23) to amplify the design shear force envelope of walls obtained from equivalent static analysis.

$$V_o^* = \omega_v \phi_o V_E \tag{2.23}$$

NZS 3101 recommends to modify the shear and moment envelope of structural walls obtained from equivalent static and modal analysis to allow for higher-mode effects. The bending moment envelope is based on the nominal flexural strength of the wall at the critical section of the primary plastic hinge, which is identified as point B in Figure 2.3. The reason for formation of plastic hinge at point B is due to the moment drop below this level, and the drop of moment phenomena

take place in many podium structures, were the walls are supported at an intermediate height, by lower walls or frames. For most non-podium type walls, points A and B will be co-incident. The identified points below are defined as: for point B the bending moment corresponds to the nominal flexural strength $(M_{n,B})$, while the mid-height moment (M_C) is calculated from:

$$\frac{M_{n,B}}{2} \leq \frac{M_{E,C}}{0.85}\left[1+\frac{n_t-1}{4}\right] \leq 2M_{E,C} \tag{2.24}$$

where n_t is the total number of stories and $M_{E,C}$ is the bending moment at point C found in an equivalent static or modal response spectrum analysis for design actions at point C.
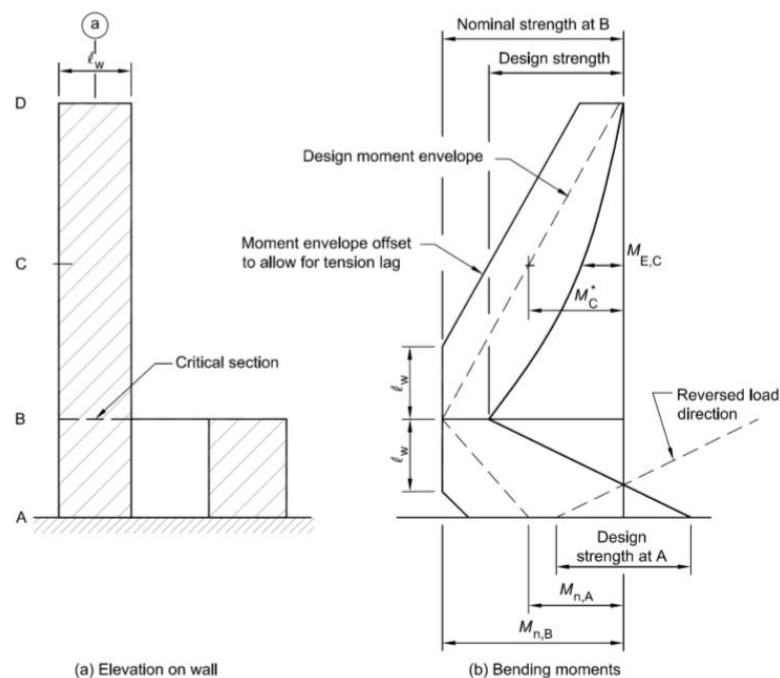
Figure 2.3 Capacity design bending moment envelope (NZS 3101).

Priestley et al. (2008) proposed a simplified capacity design approach for RC cantilever wall, similar to the one recommended by NZS 3101. This method amplifies shear force from direct displacement-based design (DDBD), where the shear capacity design envelope is defined by a straight line between the base and top of the wall as shown in Figure 2.4 (b). The design base shear is defined as:

$$V_b^o = \phi^o \omega_v V_{Base} \tag{2.25}$$

$$\omega_v = 1 + \frac{\mu}{\phi^o} C_{2,T} \tag{2.26}$$

$$C_{2,T} = 0.067 + 0.4(T_i - 0.5) \le 1.15 \tag{2.27}$$

and the design shear force at the top of the wall is defined as:

$$V_n^o = C_3 V_{Base}^o \tag{2.28}$$

$$C_3 = 0.9 - 0.3T_i \ge 0.3 \tag{2.29}$$

where V_b^o is the design base shear, ϕ^o is the flexural over-strength factor, ω_v is the dynamic amplification factor, V_{Base} is the base shear computed from DDBD, μ is the displacement ductility demand, T_i is the initial period.

The moment capacity envelope shown in Figure 2.4 (a), proposed by Priestley et al. (2008), is defined by the overstrength base moment capacity $\phi^o M_{Base}$ obtained from DDBD analysis method, and a mid-height overstrength moment demand $M_{0.5H}^o$ computed from Eq. (2.30).

$$M_{0.5H}^o = C_{1,T}\phi^o M_{Base} \tag{2.30}$$

$$C_{1,T} = 0.4 + 0.075T_i\left(\frac{\mu}{\phi^o} - 1\right) \tag{2.31}$$
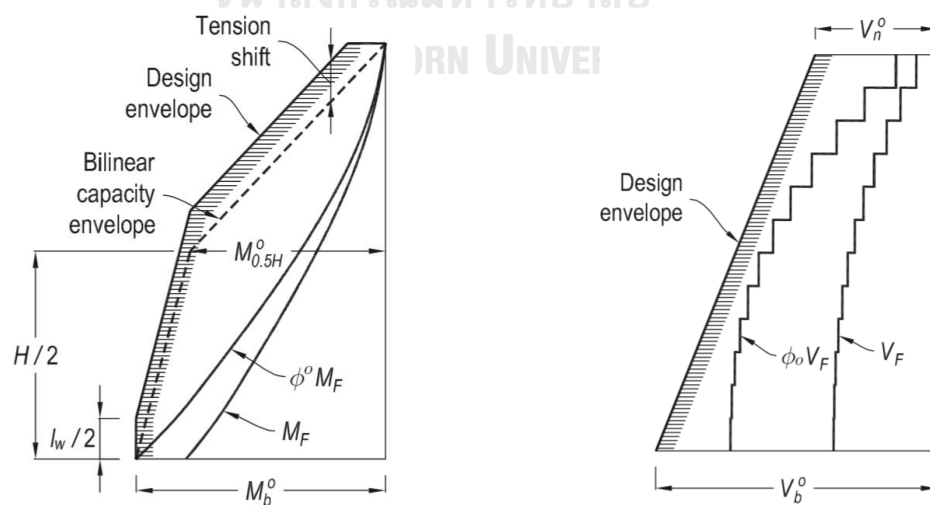
(a) Capacity design moment envelope   (b) Capacity design shear envelope

Figure 2.4 Capacity design envelopes for cantilever walls (Priestly et al., 2008).

The Canadian Standard Association (2004) (CSA) accounts for shear amplification in RC walls using capacity design shear envelope approach. The shear demand at the base is required to be amplified by overstrength factor which is taken as the ratio of probable moment capacity "M_p" over the design bending moment "M_f" as shown in the equation (2.32). For location above the hinge zone, the shear force is amplified by the ratio of the factored moment resistance "M_r" over the design bending moment "M_f". The shear force envelope computed from both equations should be used, and the probable moment capacity is computed using expected material strength. Both equations shall not exceed shear limit "$V_{\text{limit}_{base}}$" determined from the elastic shear forces reduced with $R_dR_o = 1.3$, where R_d and R_o are the ductility-related and overstrength-related force reduction factors, respectively.

$$V_p = V_f \left(\frac{M_p}{M_f} \right)_{base} \tag{2.32}$$

$$V_{ah} = V_f \left(\frac{M_r}{M_f} \right)_{top} \tag{2.33}$$
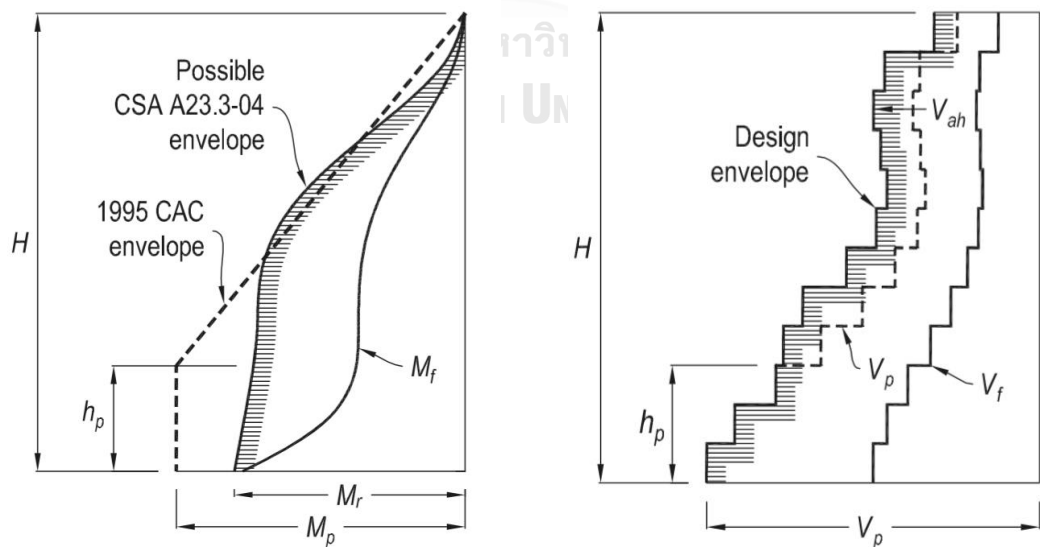
(a) Capacity design moment envelope   (b) Capacity design shear envelope

Figure 2.5 Capacity design envelopes for cantilever walls (CSA, 2004).

Boivin and Paultre (2012) proposed a new capacity design method for the Canadian Standard Association (2004), accounting for higher mode amplification effects in regular ductile RC cantilever walls. The proposed method was based on a parametric study of a ductile RC cantilever wall, designed according to National Building Code of Canada (2010) (NBCC) and CSA standards, and subjected to the ground motion excitation of Vancouver, which has the highest urban seismic risk in Canada. The concept of capacity design moment envelope proposed by Priestley et al. (2008) was adopted for the new proposed method and was modified in what follows based on the CSA standard.

$$M_r = \gamma_b M_f \tag{2.34}$$

$$M_{0.5H} = \alpha_M M_{nb} \tag{2.35}$$

where M_r is the required moment resistance at the base, M_f is the design demand of bending moment obtained from a linear elastic analysis, γ_b is the minimum factored base overstrength which is equal to 1.7, M_{nb} is the nominal base moment capacity, $M_{0.5H}$ is the mid-height moment, α_M is the ratio of mid-height to base moment determined from Table 2.1.

Table 2.1 Proposed α_M values for determining the mid-height moment $M_{0.5H}$.

$R_d R_o / \gamma_\omega$	$T_1 \le 0.5$	$T_1 \ge 1.0$
2.80	0.50	0.62
1.87	0.50	0.55
≤1.40	0.50	0.50

The proposed capacity design shear envelope is based on that of Rutenberg and Nsieri (2006), which is illustrated in Figure 2.6. The design base shear V_{pb} is calculated as follow:

$$V_{pb} = \bar{\omega}_v V_{phase} \le V_{\text{limit}_{\text{base}}} \tag{2.36}$$

$$V_{phase} = V_f \left(\frac{M_p}{M_f} \right)_{base} \tag{2.37}$$

$$\bar{\bar{\xi}} = 1.5 - T_1 \quad \text{for } 0.5 \le \bar{\bar{\xi}} \le 1 \tag{2.38}$$

where $\bar{\omega}_v$ is the dynamic shear amplification factor obtained from Table 2.2, $V_{\text{limit}_{\text{base}}}$ is the elastic base shear force limit reduced by 1.3, V_f and M_f are the demand shear and moment, M_p is the base probable moment capacity of the wall, $\bar{\xi}$ is height ratio.

Table 2.2 Proposed $\bar{\omega}_v$ values.

$R_d R_o / \gamma_\omega$	$T_1 \leq 0.5$	$T_1 \geq 1.0$
2.80	1.0	2.0
1.87	1.0	1.5
≤ 1.40	1.0	1.0
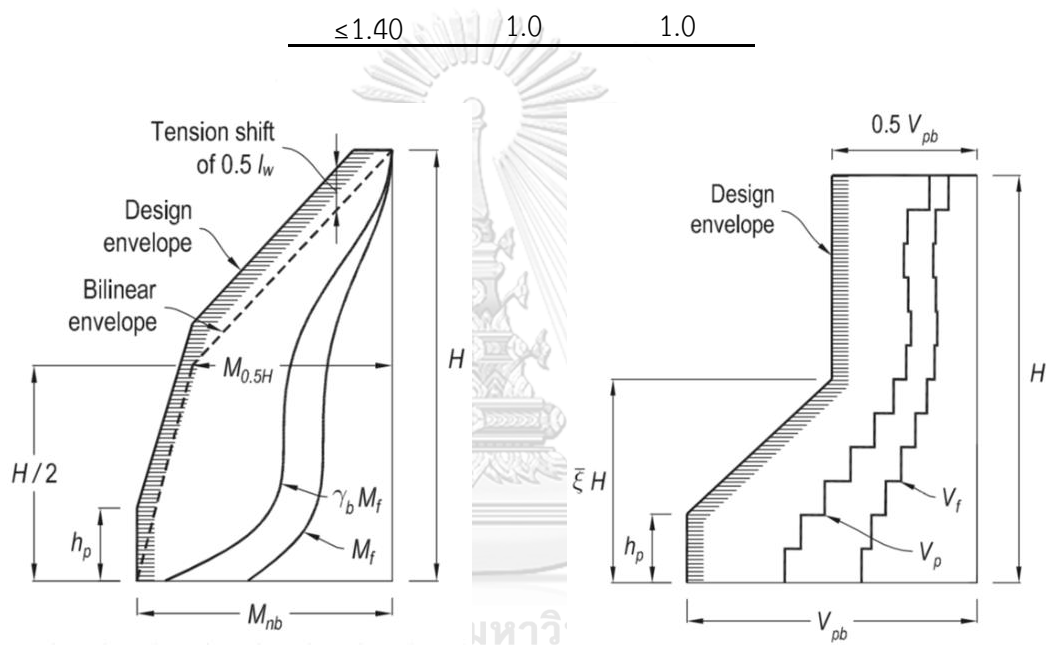
(a) Moment Capacity Envelope (b) Shear Force Capacity Envelope

Figure 2.6 Capacity design envelopes for cantilever walls (Boivin and Paultre, 2012).

Luu et al. (2013) conduct a study for examining the seismic behavior of a moderately ductile (MD) RC shear walls designed according to National Building Code of Canada (2010) and Canadian Standard Association (2004). The walls were subjected to high frequency eastern north America earthquake. The results obtained from response spectrum analysis (RSA) procedure were compared to nonlinear response history analysis (NLRHA) results. The results indicate that current code provisions for MD shear walls need to be modified. They propose a new base shear

amplification factor ω_v, applied to the base shear V_d, obtained from RSA as shown in equations below.

$$V_b = \omega_v V_d \tag{2.39}$$

$$\omega_v = \begin{cases} 1.6 + 0.7(\gamma_w - 1) + 0.2(T - 0.5) & \text{if } 0.5 \le T \le 1.5 \text{ sec} \\ 1.8 + 0.7(\gamma_w - 1) - 0.1(T - 1.5) & \text{if } 1.5 \le T \le 3.5 \text{ sec} \end{cases} \tag{2.40}$$

where γ_w is the base flexural over-strength.

Chao et al. (2007) conducted a study on 4 type of steel moment frames from 3 to 10 stories tall. They concluded that code lateral force distributions do not represent the maximum force distributions that may be induced during nonlinear response, which may lead to inaccurate predictions of deformation and force demands. They proposed new lateral force distribution based on inelastic behavior of the studied buildings.

$$F_i = C'_{vi} V \tag{2.41}$$

$$C'_{vi} = (\beta_i - \beta_{i+1}) \left(\frac{w_n h_n}{\sum_{j=1}^n w_j h_j} \right)^{\alpha T^{-0.2}} \tag{2.42}$$

$$\beta_i = \frac{V_i}{V_n} = \left(\frac{\sum_{j=1}^n w_j h_j}{w_n h_n} \right)^{\alpha T^{-0.2}} \tag{2.43}$$

where β_i is the shear distribution factor at level i; V_i and V_n, are the story shear forces at level i and at the top (nth) level; w_j is the seismic weight at level j; h_j is the height of level j from the base; w_n is the weight at the top level; h_n is the height of roof level from the base; T is the fundamental period; F_i is the lateral force at level i; and V is the total design base shear.

Filiatrault et al. (1994) conduct an analytical investigation on the shear demand obtained from nonlinear time-history analysis of ductile flexural walls designed for three different seismic zones in Canada. They conclude that the walls can experience a brittle shear failure even if the shear strengths are established by the Canadian standards. They observe that 77% of the cases, the computed dynamic

shear demand is higher than the current code shear strength. Finally, they propose for the Canadian code a force modification factor for shear, and one for modifying flexural forces.

2.7.2 Higher-mode-elastic approach

Eibl and Keintzel (1988) perform a parametric study on 2 to 5 story RC cantilever walls, that aims to check the accuracy of response spectrum analysis (RSA) method when compared to inelastic response history analysis. A base shear magnification factor was proposed to amplify the shear force demand obtained from RSA. They assumed that the contribution of the first two modes is important, were the first mode should be reduced by q, while the second mode remain elastic.

$$V_{Ed} = \sqrt{(V_{Ed,1}^{'})^2 + (q.V_{Ed,2}^{'})^2} \tag{2.44}$$

where V_{Ed} is the design seismic shear at the base of the wall, $V_{Ed,1}^{'}$ and $V_{Ed,2}^{'}$ is the reduced shear force at the base of wall due to the 1st and 2nd mode respectively, q is the behavior factor used in the design. A further simplification of Eq. (2.44) is developed such that the ratio of the base shear from second mode to first mode is equal to $\sqrt{0.1} S_e(T_c)/S_e(T_1)$ and the flexural over-strength factor $\gamma_{Rd} M_{Rd} / M_{Ed}$, was added to the first mode shear, hence the following expression is derived:

$$V_{Ed} = \varepsilon.V_{Ed,1}^{'} \tag{2.45}$$

$$\varepsilon = q\sqrt{\left(\frac{\gamma_{Rd} M_{Rd}}{q M_{Ed}}\right)^2 + 0.1\left(\frac{S_e(T_c)}{S_e(T_1)}\right)^2} \leq q \tag{2.46}$$

where ε is the magnification factor, M_{Ed} is the design bending moment at the base of the wall, M_{Rd} is the design flexural resistance at the base of the wall, γ_{Rd} is the factor to account for over-strength due to steel strain-hardening, T_1 is the fundamental period in the direction considered, T_c is the upper limit period, $S_e(T)$ is the ordinate of the elastic response spectrum.

Eibl and Keintzel (1988) formula described above was adopted by European Committee for Standardization (2004) (Eurocode 8, EC8), however they recommend to amplify the total demand shear force $(V_{Ed}^{'})$ obtained from the analysis (RSA or

ELF) as shown in Eq. (2.47). Also, the magnification factor ε is taken as 1.5 for walls with ductility class medium (DCM), while for walls classified as ductility class high (DCH), ε is computed using Eq. (2.46). The design shear force V_{Ed} is computed from the following equation:

$$V_{Ed} = \varepsilon . V_{Ed}^{'} \tag{2.47}$$

Priestley et al. (2008) stated that modal superposition approach can be non-conservative, particularly for structures braced with walls, since all modes are reduced by a single force-reduction factor (R). Nonlinear time history analysis (NLRHA) was conducted for multi-story RC wall buildings, and the results obtained were compared to the formula of capacity design envelope developed by NZS 3101, and to modal superposition approach. They conclude that the current capacity design envelops are generally non-conservative, and this inaccuracy is related to the displacement ductility demand. Priestley, et al. (2008) proposed a modified modal superposition (MMS), assuming that higher modes will behave elastically, and the inelastic action takes place in the first mode only. The design shear and bending moment profile is computed using the following formula:

$$V_{MMS,i} = \sqrt{V_{1D,i}^2 + V_{2E,i}^2 + V_{3E,i}^2 + ...} \tag{2.48}$$

$$M_i = 1.1\sqrt{M_{1,i}^2 + M_{2E,i}^2 + M_{3E,i}^2 + ...} \tag{2.49}$$

where $V_{MMS,i}$ and M_i are the design shear and moment at level i respectively, $V_{1D,i}$ and $M_{1,i}$ are the lesser of elastic first mode or inelastic (DDBD value) first-mode response at level i, $V_{2E,i}$ and $M_{2E,i}$ are the elastic modal shears and bending moment at level i for modes 2.

Rejec et al. (2012) conduct a study on a large number of single RC cantilever walls ranges from 4 to 20 stories, which designed to satisfy the requirements of Eurocode 8 (EC8) (CEN 2004). The aim of this study is to determine the reliability of the procedure in Eurocode 8 (EC8), and the formulation propsed by Eibl and Keintzel (1988), when compared to results obtained from nonlinear time history analysis (NLRHA). It was found that EC8 procedure estimate accuralty the base shear for some

of the studied cases, while it overestimate (up to 40%) the base shear for other cases. Also, they found that the constant maginfaction factor of 1.5 used for walls calssifed as DCM is non-conservative, and they recommends to apply the same procedure used for DCH walls to DCM walls. Eibl and Keintzel (1988) fourmla was found to be adequate in many cases, but it undersetiamte shear amplification for walls with fundemntal period larger than 2 sec. The author stated that the reason for these discrepancies lies in the inappropriate formulation of the upper bound for the shear magnification factor in the Eibl and Keintzel (1988) expression. Finally, they propose a to apply the magnifaction factor for shear forces obtained from first mode only as shown in Eq. (2.50), and the upper limit of the ε factor should be related to the total shear force, and should not be limited to q factor.

$$V_{Ed} = \varepsilon . V_{Ed,1}^{'} \tag{2.50}$$

$$\varepsilon = q \sqrt{\left(\min \left[\frac{\gamma_{Rd} M_{Rd}}{q M_{Ed}} ; 1 \right] \right)^2 + 0.1 \left(\frac{S_e(T_c)}{S_e(T_1)} \right)^2} \geq 1.5 \tag{2.51}$$

Şahin et al. (2013) conduct a study on a 4, 8 and 16 story RC wall buildings, designed to satisfy the requirements of Turkish Seismic Code (TSC 2007). A nonlinear response history analysis (NLRHA) was conducted, and compared to the demand results obtained from RSA. They conclude that, the results obtained from NLRHA were much larger than the results obtained from RSA. In addition, the dynamic shear amplification factor computed in the study was larger for buildings with long fundamental period (tall building). The Turkish Seismic Code recommends to amplify the design shear forces by a constant factor equal to 1.5. however, it was shown that the Turkish Seismic Design Code procedure needs some modification in order to provide an improved estimate of shear magnification factor.

Khy and Chintanapakdee (2017) conduct a study on RC split core walls in five buildings varying from 5 to 25 stories, located in Bangkok and Chiang Mai of Thailand were first designed by response spectrum analysis (RSA) procedure in ASCE 7-10. A nonlinear response history analysis (NLRHA) was conducted, and compared to the demand results obtained from RSA. They conclude that the results obtained from

NLRHA were significantly larger than those from RSA procedure. In addition, modal contribution of each mode to the base shear and base moment were studied, and they found that higher modes are primary contributors to base shear for tall building with long period, while base moment responses were always dominated by the first mode for all periods considered. Also, the accuracy of previously proposed formulas for estimating shear forces of RC walls, developed by Rejec et al. (2012), European Committee for Standardization (2004) (EC8), Priestley et al. (2008), and Luu et al. (2013) were studied and compared to NLRHA results. They conclude that Rejec, et al. (2012) formula provide good results for Bangkok in Y direction, while it overestimates shear demand in X direction, and Luu, et al. (2013) formula provide good results in Chang Mai for both directions.

Khy et al. (2019) conduct a study on six RC shear wall tall buildings ranging from 15 to 39 story. The buildings were assumed to be in Bangkok (soft soil, site class F) site of Thailand. The structural members were designed according to ACI 318M-14 considering all factored load combinations, and earthquake load developed using the RSA procedure in ASCE 7-10. A nonlinear response history analysis (NLRHA) was conducted to obtain benchmark results which were used to evaluate the accuracy of the RSA. They found that shear and moment forces computed from NLRHA was significantly larger than the design demand forces computed from RSA procedure. They stated that, the main reason of underestimated results computed from RSA is due to the use of a single (R) factor to reduce the force response of all modes. Also, a modal pushover analysis was conducted to determine the elasticity of each mode, and it was found that inelasticity of response in different modes were not the same. Finally, they proposed a modified response spectrum analysis (MRSA) procedure to improve the accuracy of the conventional RSA procedure. Two versions of the MRSA method were proposed to compute shear force demands. The first method $\mathrm{MRSA_{HE}}$ was based on a higher-mode elastic (HE) approach, and the second method $\mathrm{MRSA_{HI}}$ considered the inelasticity of higher modes which requires nonlinear static analysis. The methods are presented in heading (1) for $\mathrm{MRSA_{HE}}$, (2) for $\mathrm{MRSA_{HI}}$.

1) Modified RSA based on higher-mode elastic approach $(\mathbf{MRSA_{HE}})$

This approach is similar to what was proposed by Priestley et al. (2008), by assuming that the first mode is only affected by inealsticity. The shear forces in the structure using the $\mathbf{MRSA_{HE}}$ method are computed using Eq.(2.52). However, same approach can not be used for computing the bending moment in the structure, because it will increase shear force due to the increase of flexural strength and it will require a large vertical reinforcement due to a large bending.

$$V_{HE,i} = I \times \sqrt{\left(\frac{\text{SF} \times \Omega_0}{R} V_{1e,i}\right)^2 + V_{2e,i}^2 + V_{3e,i}^2 + ...} \qquad (2.52)$$

where $V_{HE,i}$ is the shear force at level i ; $V_{je,i}$ is the elastic modal shears of mode j at level i ; I is the importance factor; SF is the scale factor recommended by ASCE 7-16; Ω_0 is the overstrength factor.

2) Modified RSA based on higher-mode inelastic approach $(\mathbf{MRSA_{HI}})$

This approach requires a nonlinear structural model, and takes the inelasiticity of higher modes into account by using different force response reduction factor (R) for each mode. The $\mathbf{MRSA_{HI}}$ method is essentially equivalent to the modal pushover analysis (MPA) method proposed by Chopra and Goel (2002), but $\mathbf{MRSA_{HI}}$ does not include the task of extracting the desired response parameters at the target roof displacement from pushover databases as required by the MPA method. In the $\mathbf{MRSA_{HI}}$ method, the shear forces in the structure are computed from:

$$V_{HI,i} = I \times \sqrt{\left(\frac{V_{1e,i}}{R_1}\right)^2 + \left(\frac{V_{2e,i}}{R_2}\right)^2 + \left(\frac{V_{3e,i}}{R_3}\right)^2 + ...} \qquad (2.53)$$

where R_i is the force response reduction factor of mode i .

Najam and Warnitchai (2018) proposed a modified response spectrum analysis (RSA) procedure based on equivalent linearization concept, by examining three RC shear wall tall buildings. RSA procedure may lead to inaccurate estimation of demand forces that may results from nonlinear dynamic analysis. Reducing the elastic demand by a single factor (R) is inappropriate, because recent studies have

shown that it may not be appropriate to reduce the demand contributions of higher vibration modes by the same factor. This method is based on converting a nonlinear multi degree of freedom structure to an equivalent linear single degree of freedom system. Assumptions are that the nonlinear seismic demands can be approximately obtained by summing up the individual modal responses, and that the responses of each vibration mode can be approximately represented by those of an equivalent linear SDF system.

2.8 Summary

Many studies were conduct in order to enhance the performance of the available method such as equivalent lateral force (ELF) and response spectrum analysis (RSA), used in the seismic analysis. Nonlinear time history analysis (NLRHA) was set as the best accurate method in all of the previous studies. However, NLRHA is rarely used in practice due to the complexity of understanding the inelastic behavior of the structure, and due to the long time needed to conduct such analysis. Many research papers have confirmed that ELF and RSA methods underestimate the demand forces when compared to the results obtained from NLRHA. This issue was first recognized by Blakeley, et al. (1975), and due to his pioneer work, a lot of effort was consumed by researchers, to solve this issue. However it appears that a unique consensus is not avaliable yet.

Higher mode effects was mainly the reason of inaccuracy of the avaliable methods. Many of previous studies proposed an amplification factor to overcome this phenomena, while other proposed a higher mode elastic approach that assumes that inelasticity takes place in the first mode only. Most of the researchers focused on RC cantilever walls designed to have plastic hinge at the base. This may not be appropriate, since cracking and yielding may occure anywhere along the height of the building specially when dealing with irregullar building. New Zealand Standard (NZS 3101, 2006) provides a design moment envelope that's take into consideration the possibility of plastic hinge formation at the upper level, as shown in Figure 2.3. In addition, the amplification factor method was adopted by some of the international

standards such as NZS 3101 (2006), and EC8 (2004). However, the accuracy offered by this method is not warranted.

Higher mode elastic approach is more convenient to use in practical application. Almost all proposed method, assumes that higher modes will remain elastic, while the difference was in determining the first mode contribution to the total response. Eibl and Keintzel (1988) assumes that the first two modes are important, and then proposed a simplfied fourmla for comuting the design shear forces by multiplying the first mode shear by a magnification factor. Eurocode (EC8, 2004) adopted the same equation recommended by Eibl and Keintzel (1988), however they recommend to amplify the total demand shear force by the same magnification factor. Priestley (2008) proposed a modified modal superposition (MMS), assuming that higher modes will behave elastically, and the inelastic action is taken place in the first mode only. Khy and Chintanapakdee (2018), proposed two modified response spectrum analysis, to account for higher mode effect. The first method was based on assuming that higher modes remain elastic, and the first mode is multiplied by a coefficient. The second method is based on higher mode inelastic approach, which requires a nonlinear modal to perform a pushover analysis, and takes the inelasiticity of higher modes into account by using different force response reduction factor (R) for each mode.

The inaccuracy of RSA procedure is due to the use of one force reduction factor (R) for all modes, however recent studies have shown that it may not be appropriate to reduce the demand contributions of higher vibration modes by the same factor. Therefore, this study aims to evaluate the accuracy of RSA procedure when compared to NLRHA results. Also, this study will confirm the reliability of the modified response spectrum analysis proposed by Khy and Chintanapakdee (2018), when applied to irregular tall building.

CHAPTER 3

STRUCTURAL SYSTEMS AND EARTHQUAKE GROUND MOTIONS

3.1 Description of the studied buildings

Two hypothetical multi-tower buildings are used in this study and they were designed for two sites in Thailand; Bangkok (soft soil, site class F) and Chiang Mai (stiff soil, site class D). The first building consists of two towers with the same height (building SH), while the second has two towers with different heights (building DH), as shown in Figure 3.1. The structural system used to resist lateral forces is RC shear wall. The floor plans of every floor are identical with a uniform story height of 3m.

(a) SH   (b) DH
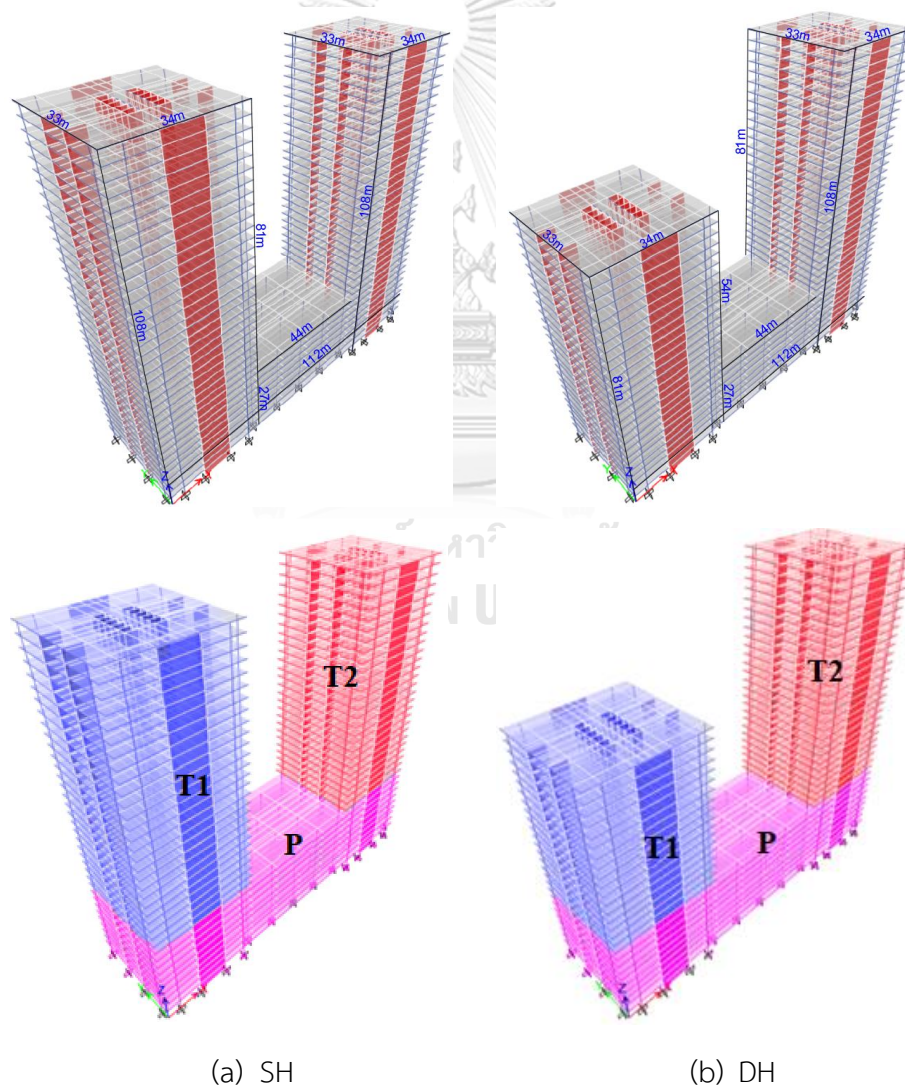
Figure 3.1 Towers denotation for building; (a) SH and (b) DH.
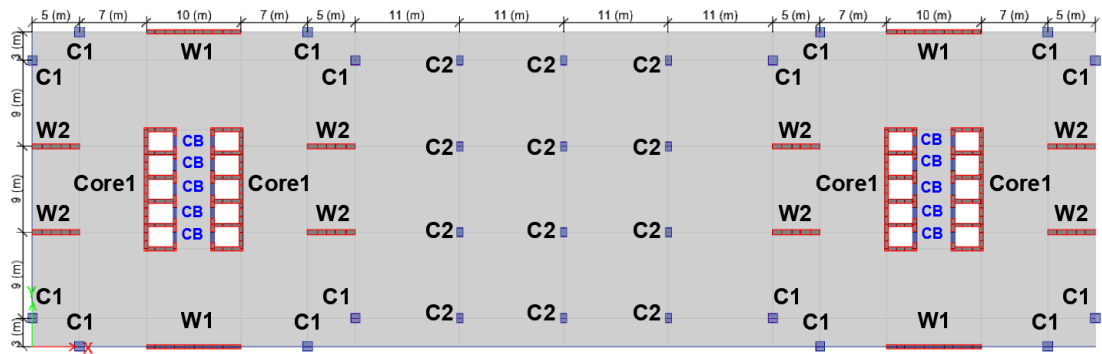
Figure 3.2 Podium floor plans (1st to 9th floor).

Figure 3.3 Tower floor plans (10th to top floor).

Multiple towers buildings are often a typical building that used in many countries around the world. The layout of the buildings was taken originally from an existing building in Bangkok, but the structural configuration was modified to the configuration shown in the figures above. Both buildings are 36-story RC shear wall tall buildings (including 9-story podium), with uniform story height of 3m. The Podium and towers are denoted by "P", "T1", and "T2" as shown in Figure 3.1 (more details are shown in Table 3.1). As shown in Figures 3.2 and 3.3, the structural element configurations are the same in both towers. Due to symmetry in structural element configurations and tower heights in building SH, both towers respond symmetrically. However, building DH have distinct torsional modes due to different heights of towers that lead to asymmetrical mode shapes. Structural elements with the same size are denoted by the same name, as shown in Figure 3.2 and 3.3. A constant thickness of 0.4m is provided for core walls along the height of the building, while planar shear wall thickness is varied from 0.5m at the base to 0.3m at the top floor.

Table 3.1 Structural characteristics and design details.

Building	SH			DH		
Tower	P	T1	T2	P	T1	T2
Number of stories	9	27	27	9	18	27
Total height (m)	27	81	81	27	54	81
Effective seismic weight (kN)	1,122,548			1,000,010		
Percentage of walls per floor area at the base	2.68%			2.68%		
Percentage of Columns per floor area at the base	0.63%			0.63%		
Maximum wall thickness (m)	0.5			0.5		
Maximum column cross section (m x m)	1 x 1			1 x 1		
$f_c^{'}$ for vertical element (MPa)	50			50		
$f_c^{'}$ for horizontal element (MPa)	35			35		
Vertical rebar yield strength f_y (MPa)	400			400		

The lateral force resisting system composed of RC walls, columns, and flat-slabs. The primary lateral force resisting system of the building consists of planar RC shear walls aligned only in X-direction, and core walls which are composed of coupled walls aligned in the X-direction, and cantilever walls aligned in the Y-direction. The lateral force resisting system was considered to be special RC shear wall whose design factors according to ASCE 7-16 are shown in Table 3.2, where R is the response modification factor, C_d is the deflection amplification factor, Ω_0 is the overstrength factor, and I is the importance factor. The structural members were designed according to factored load combinations presented in DPT (1301/1302-61, 2018). Gravity loads (live load and superimposed dead load) are assigned uniformly over the slabs with the values shown in Table 3.3, while wind loads were taken from Bangkok Building Control Act (Bangkok Metropolitan Administration, 2001) as shown in Table 3.4. P-delta effect is included before computing the modal properties of the buildings. The effective seismic weight was computed from all dead loads (DL+SDL) only.

Table 3.2 Design factors according to ASCE 7-16.

Factors	Values
R	6
C_d	5
Ω_0	2.5
I	1.25
Risk category	III
Site class	F
SDC	D

Design load combinations according to DPT (1301/1302-61, 2018) were used.

1) 1.4D + 1.7L

2) 0.75(1.4D + 1.7L) + 1.0E

3) 0.9D + 1.0E

4) 0.75(1.4D + 1.7L) + 1.6W

5) 0.9D + 1.6W

Table 3.3 Design gravity load

Load source	Value (kN/m^2)
LL	3.0
SDL	2.5

Table 3.4 Wind load pressure according to Bangkok Building Control Act (2001).

Building height (H)	Design Wind Pressure (kN/m^2)
$H \leq 10$ m	0.5
$10 < H \leq 20$ m	0.8
$20 < H \leq 40$ m	1.2
$40 < H \leq 80$ m	1.6
$H > 80$ m	2

Normally drift limit and other serviceability limit states control the design of tall buildings. Hence, to provide enough lateral capacity for the lateral force resisting system, design engineers increase the cross-sections of the structural elements. The modal properties of building are affected by changing element size due to a change in structure stiffness. Therefore, a statistical comparison of natural period and the percentage of structural element used at the base is done on several buildings (SW1 to SW6) taken from Khy and Chintanapakdee (2018), and compared to SH building (refer to Table 4.5 for natural periods of SH building).
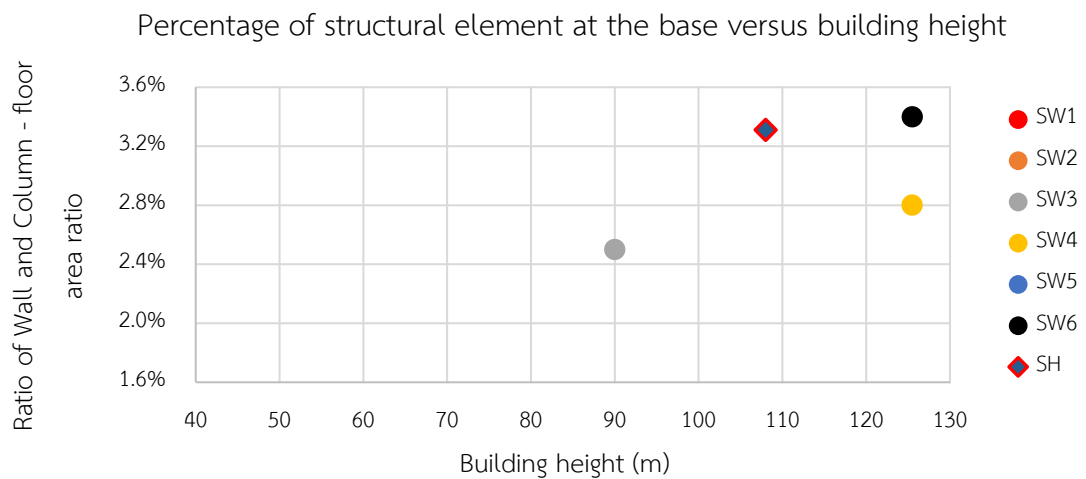
Figure 3.4 Percentage of structural element per floor area at base versus building height.
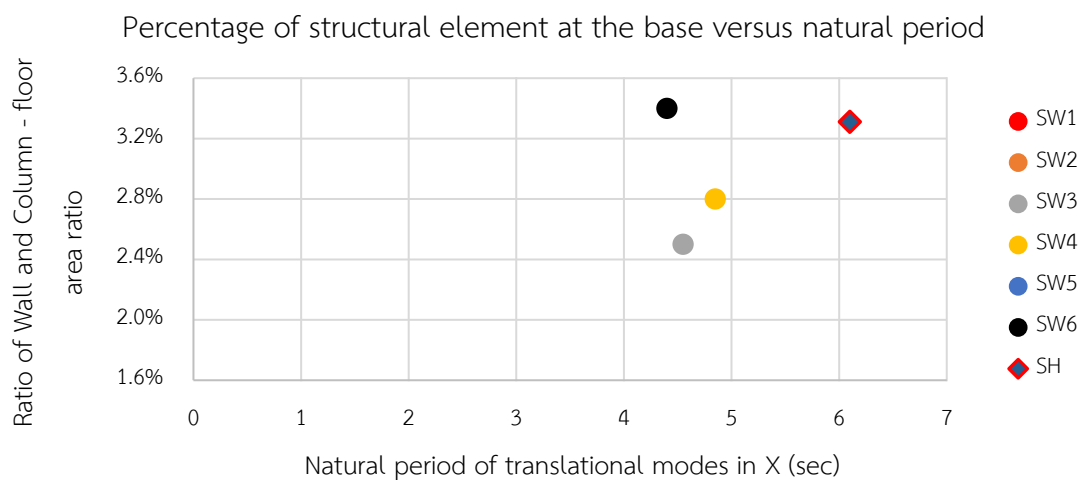
Figure 3.5 Percentage of structural element at base versus natural period in X direction.

Percentage of structural element at the base versus natural period
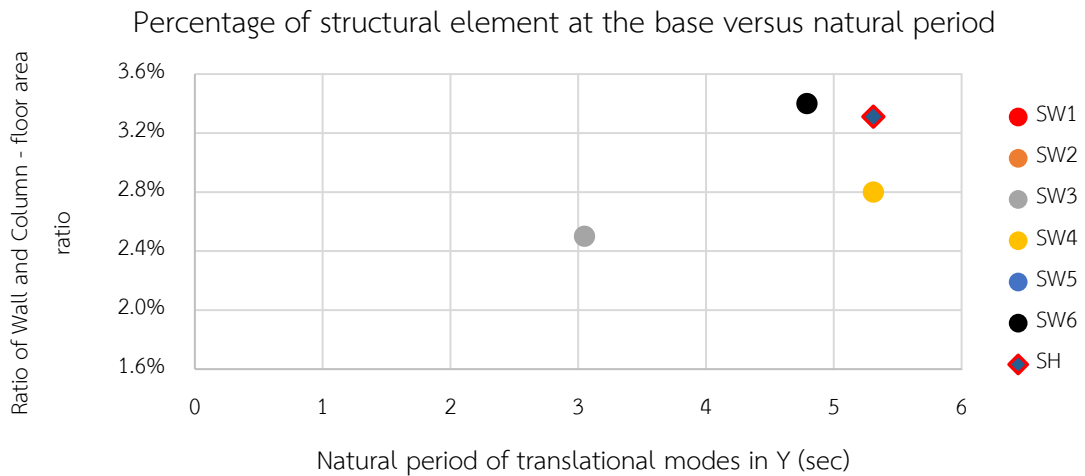
Figure 3.6 Percentage of structural element at base versus natural period in Y direction.

As shown in Figure 3.4, there is a trend between building height and percentage of structural elements used at the base of each building. The natural period of buildings depends on the configuration of structural elements which provides the lateral capacity of the building. Hence, any change in structural element configuration will leads to different lateral capacity and to a different modal property, even if the percentage of components is the same. The use of natural period of buildings rather than building height in comparison with the percentage of structural elements used at the base is more convenient because the effect of structural elements configuration on providing the lateral stiffness has been taken into consideration. The selected buildings in this study fit with the overall trend of other buildings.

3.2 Structural models

The analytical models were developed considering all serviceability limit state requirement of ASCE 7-16. ACI 318M-14 was used to compute member capacities, and to provide appropriate reinforcement detailing. The main assumptions done to construct the mathematical model are as follow:

1) Semi-rigid diaphragm was assigned to all podium floors, while a rigid diaphragm was assigned to each floor in towers T1 and T2.

2) Fixed supports were assigned at the base of all columns and structural walls.

3) Shear behavior of structural members was considered to be elastic and was modeled using uncracked gross shear stiffness.

4) The out-of-plane behavior of walls and slabs was assumed to be elastic with small effective stiffness of 0.25 $E_c I_g$.

The assumptions above were applied in both linear and nonlinear models.

3.2.1 Linear model

The linear structural model was developed using ETABS (CSI 2018) software (Computers and Structures, 2018). Cracked cross-section properties of structural members were used for analysis and design of the structural system. The criteria for selecting effective flexural stiffness of wall section was based on modulus of rupture (f_r) described in ACI 318M-14. If the tensile stress of a wall exceeds the modulus of rupture computed using Eq. (3.1), a cracked cross-section property of wall was used. It was found that cracked cross-section property should be used for all RC walls. The effective stiffness of structural members used in the linear analytical model is shown in Table 3.5.

$$f_r = 0.62\lambda\sqrt{f_c'}$$ (3.1)

where f_r is the modulus of rupture of concrete in MPa; f_c' is the compressive strength of concrete in MPa; and λ is a modification factor for concrete.

Table 3.5 Effective stiffness of structural members in linear model.

Elements	Flexural	Axial	Shear
Shear wall (In-plane)	0.35 $E_c I_g$	1.0 $E_c A_g$	1.0 GA_g
Shear wall (Out-of-plane)	0.25 $E_c I_g$	-	-
Slab (In-plane)	1.0 $E_c I_g$	1.0 $E_c A_g$	1.0 GA_g
Slab (Out-of-plane)	0.25 $E_c I_g$	-	-
Column	0.7 $E_c I_g$	1.0 $E_c A_g$	1.0 GA_g
Beam	0.35 $E_c I_g$	1.0 $E_c A_g$	1.0 GA_g

where E_c is the modulus of elasticity of concrete; I_g is the gross moment of inertia of cross section; A_g is the gross cross-sectional area; G is the shear modulus of concrete.

3.2.2 Nonlinear model

A nonlinear structural model was created in PERFORM-3D (Computers and Structures, 2018) software for pushover analysis and NLRHA. A nonlinear fiber element was used for walls and columns, while moment-rotation hinges were assigned for coupling beams. The nonlinear fiber behavior is controlled by the nonlinear stress-strain relation of concrete and steel material properties. The shear behavior is not considered in the fiber elements, assuming that the shear behavior of the structural elements will remain in the elastic range. The out-of-plane behavior of the wall and slabs was assumed to be elastic with small effective stiffness of 0.25 EI. The effective stiffness of structural members used in the nonlinear model is summarized in Table 3.6.

Table 3.6 Effective stiffness of structural members in the nonlinear model.

Elements	Flexural	Axial	Shear
Shear wall (In-plane)	Fiber	Fiber	1.0 GA_g
Shear wall (Out-of-plane)	0.25 E_cI_g	-	-
Slab (In-plane)	1.0 E_cI_g	1.0 E_cA_g	1.0 GA_g
Slab (Out-of-plane)	0.25 E_cI_g	-	-
Column	Fiber	Fiber	1.0 GA_g
Beam	0.35 E_cI_g	1.0 E_cA_g	1.0 GA_g

The nonlinear fiber behavior is determined by the nonlinear stress-strain relation of concrete and steel material properties. The stress-strain relation of concrete proposed by Mander et al. (1988) was adopted and represented by a tri-linear relationship as shown in Figure 3.7. Non-degrading concrete material was used, and the tensile strength of concrete was neglected. The steel material properties were taken from specifications of Thailand industrial standard (SD40 in TIS 24-2548). The expected strength was used in the model, as the actual strength is usually greater than the nominal strength specified by the designer. The expected material strength of concrete and steel were taken as 1.25 times the nominal strength. The cyclic degradation parameters for reinforcing steel proposed by Moehle et al. (2011) were used, as shown in Table 3.7.
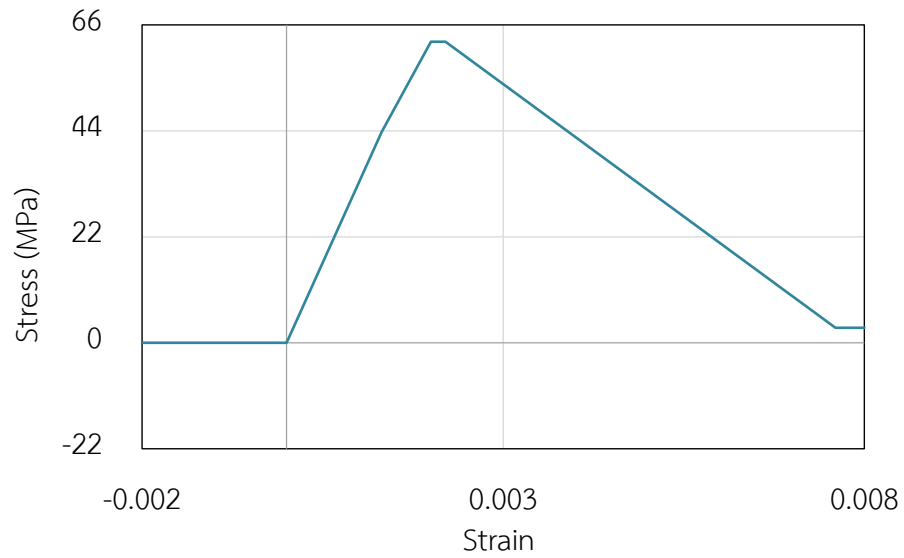
Figure 3.7 Stress-strain relationship of Unconfined concrete (f_c'=50MPa).
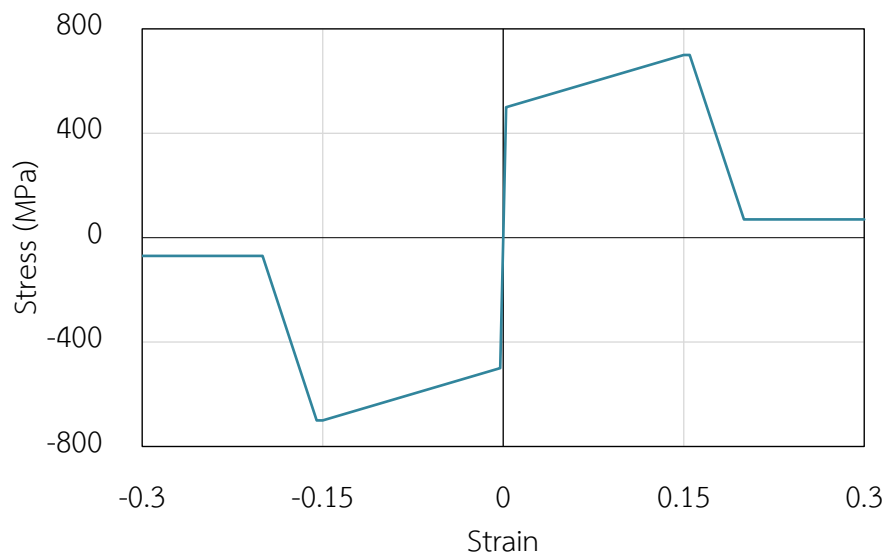
Figure 3.8 Stress-strain relationship of steel reinforcement.

Table 3.7 Cyclic degradation parameters for reinforcing steel (Moehle et al., 2011).

Points	Strain	Cyclic degradation factor
Y	0.00195	0.70
1	0.0025	0.68
2	0.004	0.64
3	0.006	0.62
X	0.09	0.6

Nonlinear fiber elements were used for RC walls to capture the in-plane axial-bending interaction (P-M) behavior along the height of the walls. The fiber-model cross-section consists of eight equally spaced concrete and steel fibers assigned to wall segments, as shown in Figure 3.9 (a).

For RC columns, the plastic hinge zones were modeled using nonlinear fiber element embedded at both ends. The remaining portion of column was assumed to remain elastic with an effective stiffness of 0.7 E_cI_g, as shown in Figure 3.9 (b). The length of the plastic zone was assumed to be equal to 0.5 of the least cross section dimension of the column section (Paulay & Priestley, 1992). The axial-bending interaction in both directions (P-M-M) was considered in the fiber elements assigned for RC columns.

RC coupling beams were modeled using moment-rotation hinge elements embedded at both ends. The modeling parameters are shown in Figure 3.9 (d) and the acceptance criteria were obtained from ASCE 41-13 (American Society of Civil Engineers, 2013). The yielding moment (M_y) of coupling beam was assumed to be equal the beam nominal capacity (M_n), while the ultimate bending moment (M_{ult}) is estimated by assuming M_{ult}/M_y=1.13 suggested by Haselton et al. (2008). The remaining portion of coupling beam was assumed to remain elastic with an effective stiffness of 0.35 E_cI_g, as shown in Figure 3.9 (c). The cyclic degradation parameters for coupling beams proposed by Naish et al. (2013) were used as shown in Table 3.8.

Table 3.8 Cyclic degradation parameters for coupling beams (Naish et al., 2013).

Model	Energy degradation factor					Unloading stiffness factor
	Y	U	L	R	X	
Moment-hinge	0.5	0.45	0.4	0.35	0.35	0.5

Most of the inelastic components in PERFORM-3D have the same form of force-deformation relationship with optional strength loss as shown in Figure 3.10. The degradation factors shown in Table 3.8 are related to points (Y, U, L, R, X) which are shown in Figure 3.10. These points define the F-D relationship.

(a) Wall fibers

(b) Column model

Concrete and
Steel Fibers

Elastic Element

(c) Beam model

Elastic element

Moment-hinge rotation

(d) M-θ backbone curve
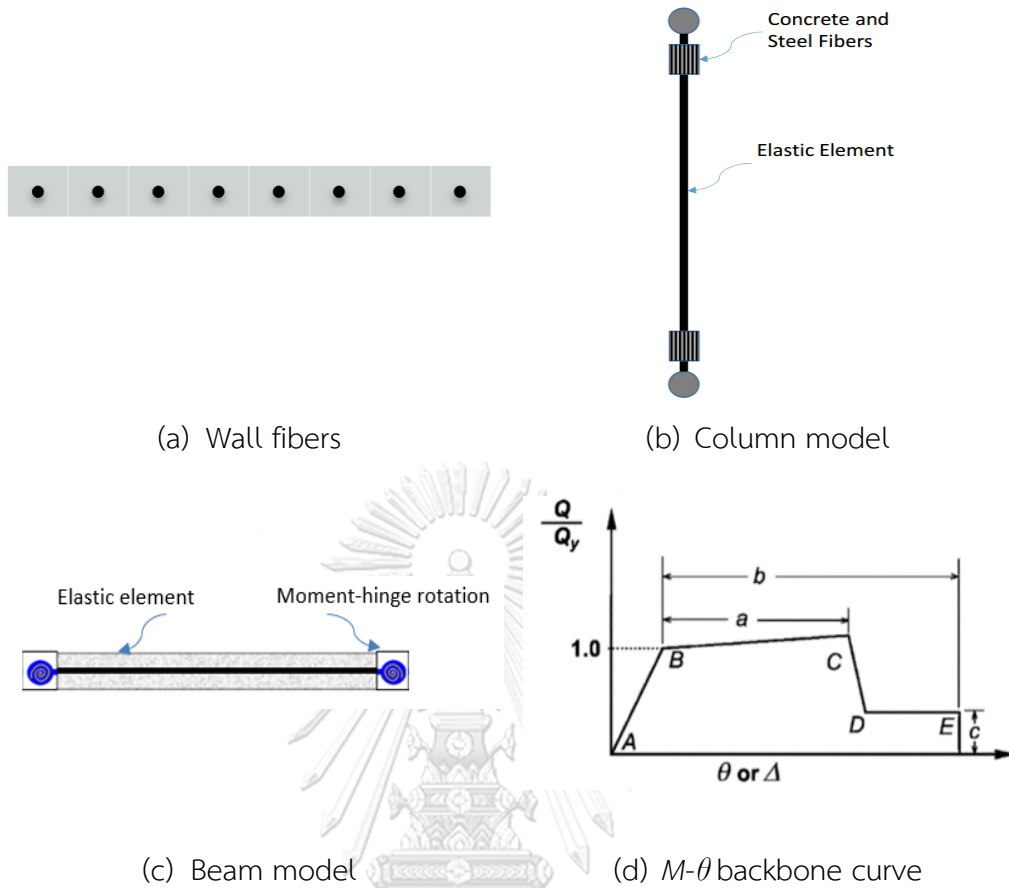
Figure 3.9 Nonlinear components.
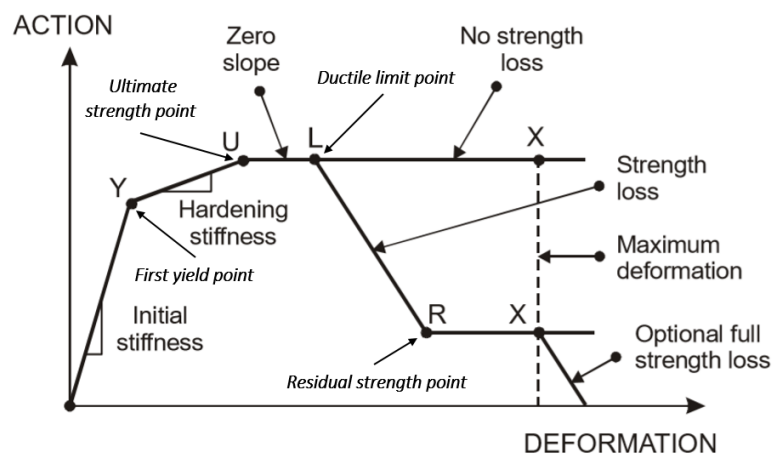
Figure 3.10 PERFORM force-deformation relationship (Computers and Structures, 2018).

3.3 Description of earthquake ground motions

The earthquake ground motion used in this study were obtained from a similar study conducted for RC tall buildings in Bangkok and Chiang Mai sites (Khy & Chintanapakdee, 2018). The uniform hazard spectrum (UHS) for both sites is obtained from Thai code (DPT 1301/1302-61). Khy and Chintanapakdee (2018) selects several ground motions records that have similar seismic mechanisms to Bangkok and Chiang Mai, and they will be used in this study for both LRHA and NLRHA.

3.3.1 Bangkok earthquake ground motions

Bangkok site located on soft soil (site class F), were a long period earthquake is expected to have most influence on that site. Also, tall buildings in Bangkok faces a risk from distant large earthquakes, due to resonance phenomena. The uniform hazard spectrum (UHS) for Bangkok is significantly different from the typical code spectrum, and it is obtained from Thai code (DPT 1301/1302-61) (Department of Public Work and Town & Country Planning, 2018) as shown in Figure 3.11. The design spectrum (UHS) obtained from Thai code belongs to design basic earthquake (DBE) having 10% probability of exceedance in 50 years. The UHS shown in Figure 3.11 is for 2.5% damping ratio.

For RSA and the proposed MRSA methods, uniform hazard spectrum (UHS) is used, while for NLRHA, consistent ground motions need to be used to ensure that the analysis results from different methods are compatible for comparison; hence, UHS spectral matching ground motions were used in NLRHA. The UHS spectral matching ground motions used in this study were taken from Khy and Chintanapakdee (2018) , who conduct a similar study for RC tall buildings in Bangkok. Six ground motions having similar seismic mechanisms as in Bangkok were used for NLRHA (Figure 3.13). The individual matching spectra, the mean value of matching spectra, and the target spectrum (UHS) for 2.5% damping ratio in Bangkok zone 5 are shown in Figure 3.12.
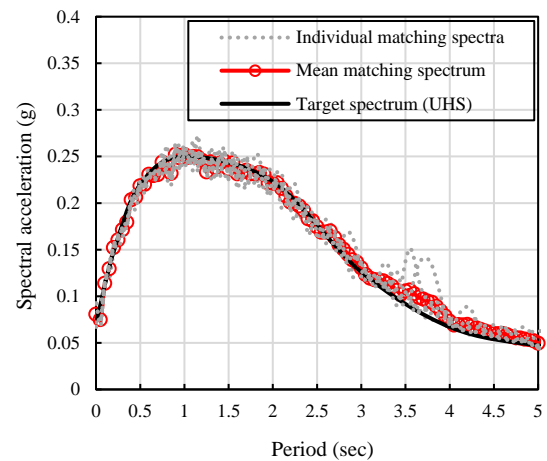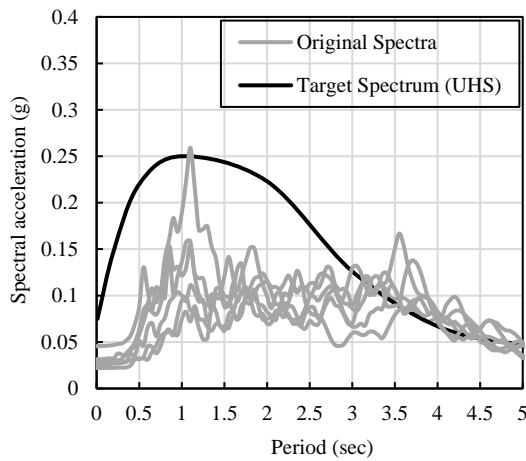
Figure 3.11 Original spectra of CMS ground motions conditioned at 3 sec and target spectrum for 2.5% damping ratio in Bangkok zone 5.

Figure 3.12 Individual matching spectra, mean matching spectrum, and target spectrum for 2.5% damping ratio in Bangkok zone 5.
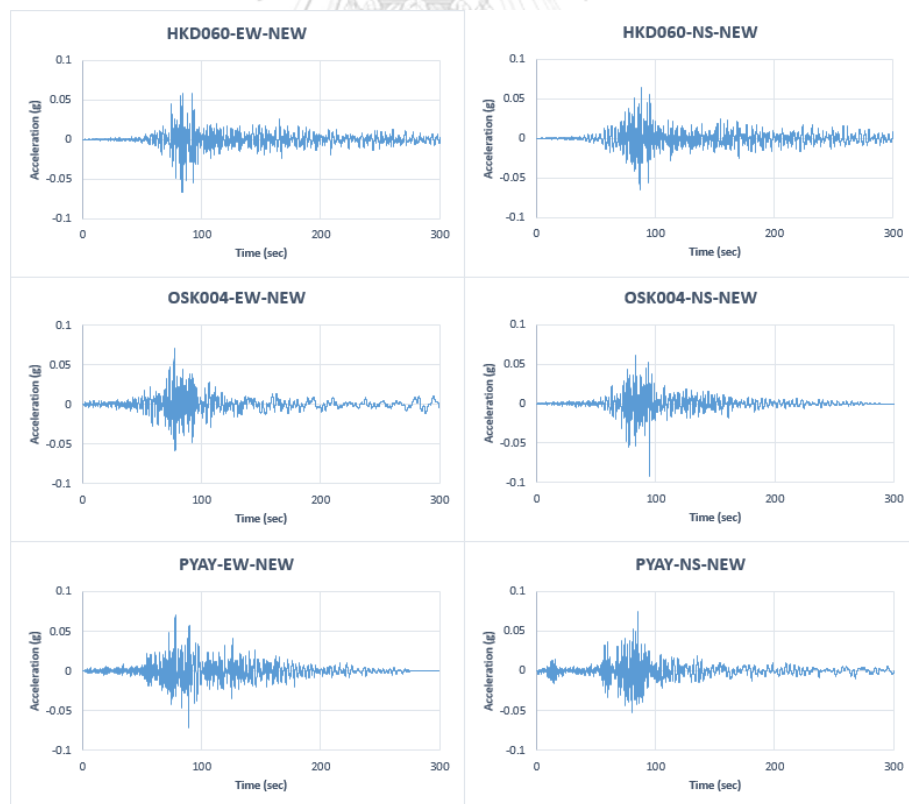
Figure 3.13 Six UHS spectral matching ground accelerations in Bangkok used for LRHA and NLRHA.

3.3.2 Chiang Mai earthquake ground motions

Chiang Mai site located on stiff soil (site class D), where the target spectrum (UHS) was developed using the procedure described in ASCE 7-16, for a response spectral parameter of S_s = 0.963g, and S_1 = 0.248g. The damping factor formula (Eq.(A.1)) in ASCE 41-13 was used to obtain the design spectrum curve that corresponds to 2.5% damping. The spectral matching ground accelerations were obtained using ten ground motions that have similar seismic mechanism of the studied site (Khy & Chintanapakdee, 2018). The original spectra of ground motions are shown in Figure 3.14, while the matching spectra is shown in Figure 3.15. The UHS spectral matching ground motions are shown in Figure 3.16.
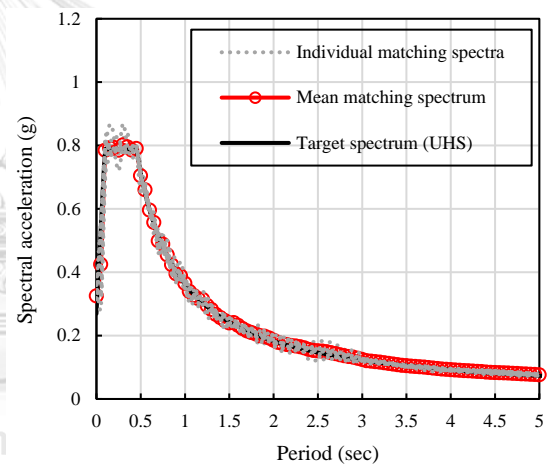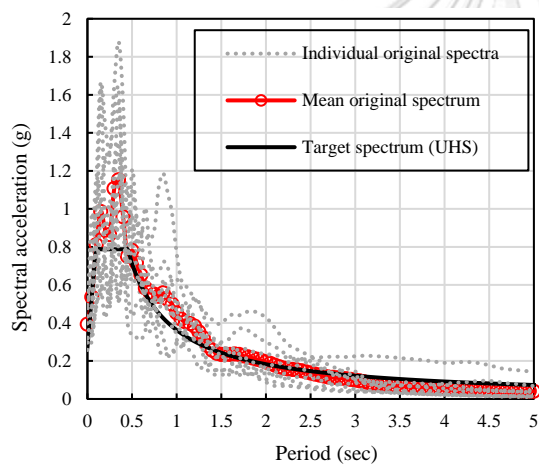
Figure 3.14 Individual original spectra, mean original spectrum, and target spectrum for 2.5% damping ratio in Chiang Mai.

Figure 3.15 Individual matching spectra, mean matching spectrum, and target spectrum for 2.5% damping ratio in Chiang Mai.
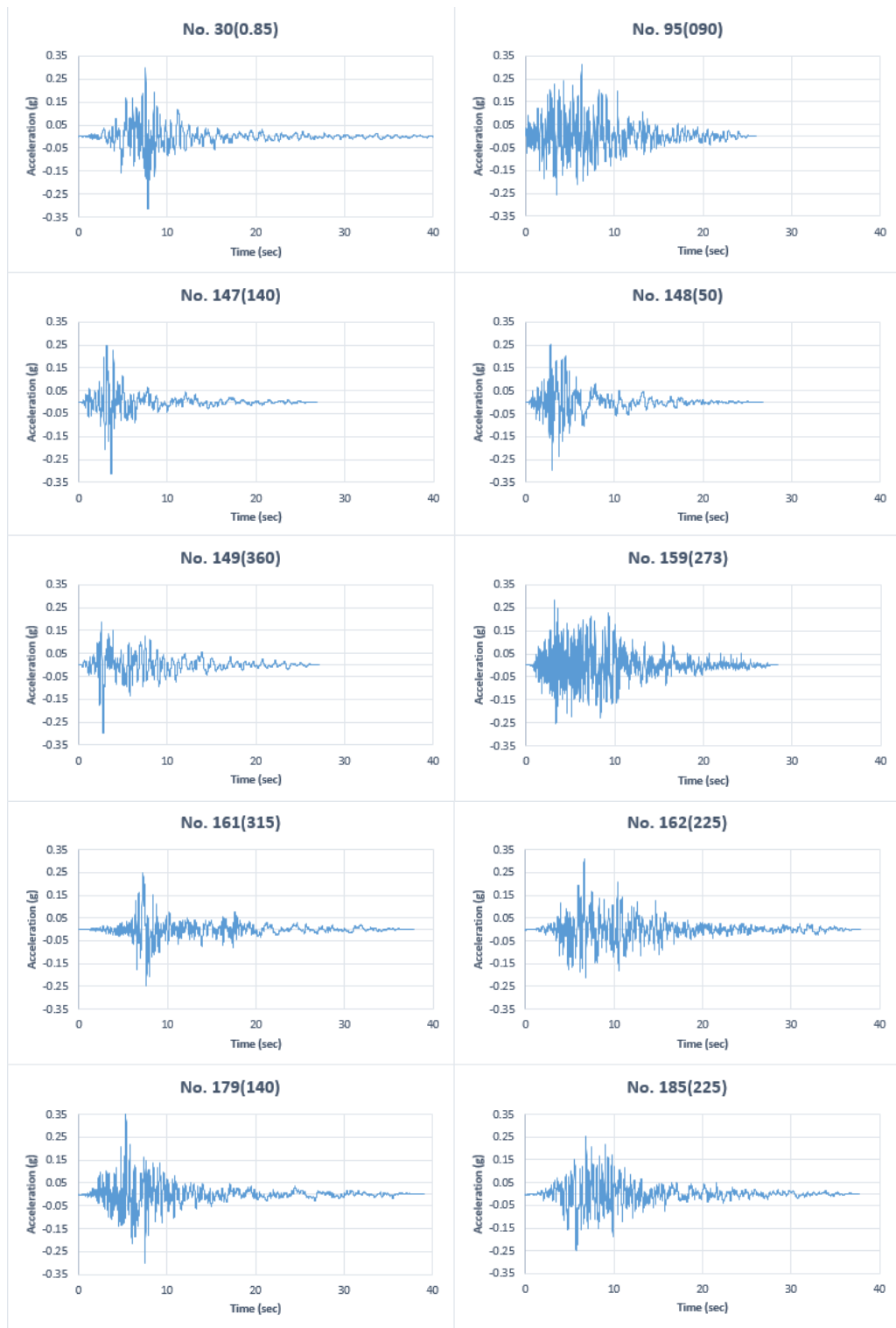
Figure 3.16 Ten UHS spectral matching ground accelerations in Chiang Mai used for LRHA and NLRHA.

CHAPTER 4

MODIFIED RESPONSE SPECTRUM ANALYSIS

4.1 Introduction

This chapter presents response behavior of the studied buildings using response spectrum analysis (RSA) procedure in ASCE 7-16, modal pushover analysis (MPA), linear response history analysis (LRHA) and nonlinear response history analysis (NLRHA). The NLRHA was conducted to evaluate the accuracy of other methods, as it considered to be the most accurate method. The accuracy of RSA procedure is firstly evaluated. The MPA procedure was used to estimate the inelasticity of modal responses. Finally, the accuracy of the previously proposed modified response spectrum analysis (MRSA) methods for computing shear demand is evaluated. Here, two irregular tall RC shear-wall buildings (Figure 3.1) and earthquake ground motions for Bangkok and Chiang Mai (section 3.3) were employed. The ground motions were applied separately in each principle direction of the building at a time for all analysis methods and vertical earthquake was not considered.

4.2 Response spectrum analysis procedure

The RSA procedure in ASCE 7-16 was adopted in this study. The demand forces computed from RSA procedure were obtained with the use of the linear model described in Section 3.2.1, and the design spectral acceleration curve (target spectrum) shown in Figure 3.11 and 3.14. P-delta effect was considered by including gravity loads of all dead load (DL & SIDL) plus 25% of live load. A constant viscous modal damping of 2.5% was provided. The design factors R, C_d, Ω_0, and I were taken from ASCE 7-16 with the values of 6, 5, 2.5, and 1.25 respectively, as shown in Table 3.2. The concept of RSA procedure described in building codes is to reduce the elastic demand by response modification factor (R), and to amplify the displacements by a factor (C_d), in order to predict the real inelastic displacement that may results from a strong earthquake. Complete Quadratic Combination (CQC) rule was used to combine all modal responses. For simplicity, the concept of RSA procedure is outlined below using square root of sum of squares (SRSS) method.

$$V_t = \frac{I}{R}\sqrt{V_1^2 + V_2^2 + V_3^2 + \ldots} \tag{4.1}$$

$$M_t = \frac{I}{R}\sqrt{M_1^2 + M_2^2 + M_3^2 + \ldots} \tag{4.2}$$

where V_t and M_t are the total reduced elastic shear force and bending moment demand, respectively; V_i and M_i are the elastic shear force and bending moment of the ith mode, respectively.

As recommended by ASCE 7-16, the design forces obtained from RSA should be scaled such that RSA base shear (V_t) is not less than 85% of equivalent lateral force base shear (V_{ELF}). Table 4.1 summarizes the values of the scaling factor (SF) for this purpose, where EQX and EQY represents earthquake directions in X and Y, respectively. It should be noted that ELF method was used in this study for computing the scale factor only, because it is not permitted by ASCE 7-16 to use ELF method for design of building exceeding 48m.

$$F_{RSA} = SF \times F_t \tag{4.3}$$

$$\delta_{RSA} = \frac{C_d}{R}\sqrt{\delta_1^2 + \delta_2^2 + \delta_3^2 + \ldots} \tag{4.4}$$

$$SF = 0.85 V_{ELF}/V_t \tag{4.5}$$

where F_{RSA} represents the design (scaled) elastic demand of shear and bending moment; F_t represents the reduced elastic demand of shear and moment (V_t and M_t); SF is the scaling factor computed according to ASCE 7-16; δ_{RSA} is the total amplified displacement or drift; and δ_i is floor displacements or drift of ith mode.

Table 4.1 Scaling factor for buildings in Bangkok.

Building	SH		DH	
Direction	EQX	EQY	EQX	EQY
$0.85V_{ELF}$	20,964	20,964	18,675	18,675
V_t	11,630	13,936	9,027	9,887
SF	1.80	1.50	2.10	1.89

Table 4.2 Scaling factor for buildings in Chiang Mai.

Building	SH		DH	
Direction	EQX	EQY	EQX	EQY
$0.85V_{ELF}$	37,559	37,559	33,459	33,459
V_t	19,532	28,466	17,070	20,986
SF	1.92	1.32	1.96	1.59

Due to scaling of reduced elastic demand of RSA procedure, it is more convenient to know the effective response modification factor R_{eff} used in the analysis, instead of knowing R factor. The factor R_{eff} is the ratio between the unreduced elastic base shear (without the use of R and I factor) and design base shear (V_{RSA}). Summarized results are shown in Table 4.3 and 4.4 for Bangkok and Chiang Mai buildings, respectively.

Table 4.3 Effective response modification factor (R_{eff}) used for Bangkok buildings.

Building	SH		DH	
Formula	$R_{eff,x}$	$R_{eff,y}$	$R_{eff,x}$	$R_{eff,y}$
$R_{eff} = \dfrac{R}{SF \times I}$	2.7	3.2	2.3	2.5

Table 4.4 Effective response modification factor (R_{eff}) used for Chiang Mai buildings.

Building	SH		DH	
Formula	$R_{eff,x}$	$R_{eff,y}$	$R_{eff,x}$	$R_{eff,y}$
$R_{eff} = \dfrac{R}{SF \times I}$	2.5	3.7	2.4	3.0

The elastic response of RSA procedure is obtained by combining 30 modes of vibration, to achieve a minimum of 90% of mass participation as recommended by ASCE 7-16. The modal mass participation ratio for the first 20 modes of building SH and DH is shown in Table 4.5 and 4.6, respectively.

Table 4.5 Mass participation ratios for translation in X and Y directions and rotation about Z-axis for building SH.

Mode number	Period (sec)	UX	UY	RZ
1	6.10	61%	0	0
2	5.31	0	58%	0
3	5.23	0	0%	60%
4	4.56	0%	0	0
5	2.88	0	0	0%
6	2.84	0	0	3%
7	1.50	16%	0	0
8	1.05	0%	0	0
9	1.01	0	20%	0
10	1.00	0	0%	18%
11	0.79	0	0	0%
12	0.76	0	0	0%
13	0.66	8%	0	0
14	0.43	0%	0	0
15	0.42	0	10%	0
16	0.41	0	0	6%
17	0.37	0	0%	0
18	0.36	4%	0	0
19	0.34	0	0	1%
20	0.25	0	4%	0
		89%	91%	89%

Table 4.6 Mass participation ratios for translation in X and Y directions and rotation about Z-axis for building DH.

Mode number	Period (sec)	UX	UY	RZ
1	5.55	49%	0%	0%
2	5.27	0%	33%	26%
3	3.21	0%	22%	36%
4	3.06	13%	0%	0%
5	2.81	0%	3%	1%
6	1.77	0%	0%	1%
7	1.29	11%	0%	0%
8	1.00	0%	11%	8%
9	0.78	0%	1%	1%
10	0.77	8%	0%	0%
11	0.61	0%	9%	10%
12	0.48	2%	0%	0%
13	0.46	0%	1%	0.3%
14	0.40	0%	4%	3%
15	0.38	5%	0%	0%
16	0.36	0%	0.3%	0.1%
17	0.27	0%	5%	2%
18	0.23	0%	1%	3%
19	0.23	1%	0%	0%
20	0.22	0%	1%	0%
		89%	91%	91%

SH building was used in this study as a reference building for comparison with DH building. As shown in Table 4.5 and 4.6, in order to obtain translational mode of Y direction for SH building, more number of modes were needed. This due to symmetry of towers' response, while is not the case for building DH. Due to different heights of towers in building DH, a coupled translational-torsional response in each mode is obtained. Another interesting behavior was realized in SH building where

some modes have zero mass participation ratios; e.g., modes 4, 8, 12, 14, 17, as shown in Table 4.5. This is due to symmetrical mode shape in both towers. This means that if one of the towers moves toward the positive X-direction, the second tower will move toward the negative X-direction, as shown in Figure 4.1. The first two translational modes (ignoring modes with zero mass participation) in each direction for SH and DH buildings are shown in Figure 4.2 and 4.3, respectively.

    (a) Mode 4 - X   (b) Mode 8 - X   (c) Mode 3 – Y   (d) Mode 10 - Y
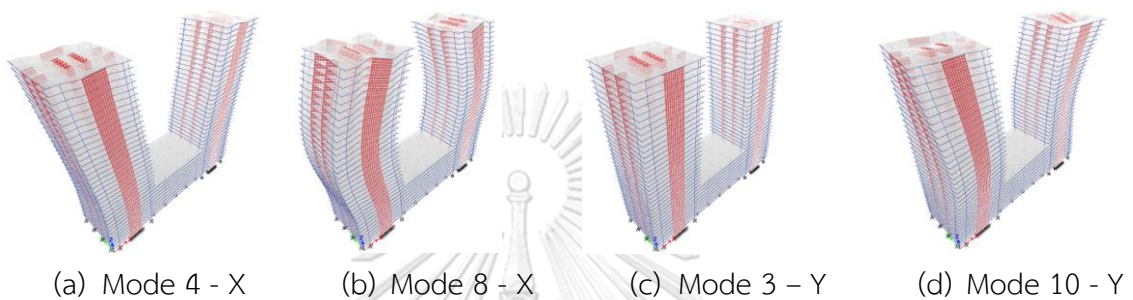
Figure 4.1 Three-dimensional mode shapes with zero mass participation ratios for SH building.

    (a) Mode 1 - X   (b) Mode 7 - X   (c) Mode 2 - Y   (d) Mode 9 - Y
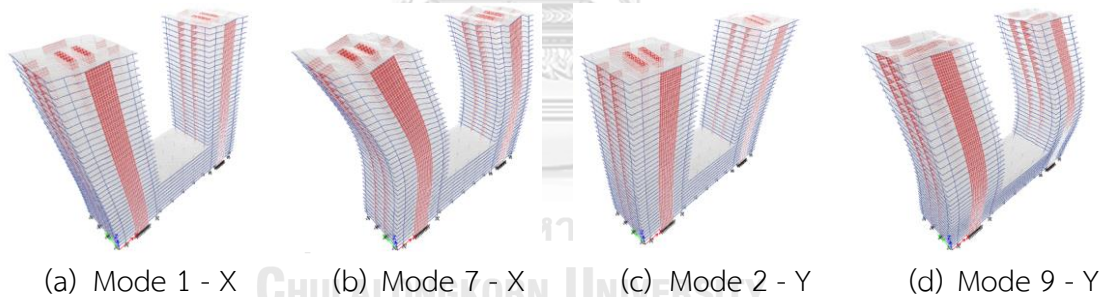
Figure 4.2 Three-dimensional mode shapes corresponding to translation in X- and Y-directions of SH building.

    (a) Mode 1 - X   (b) Mode 4 - X   (c) Mode 2 - Y   (d) Mode 3 - Y
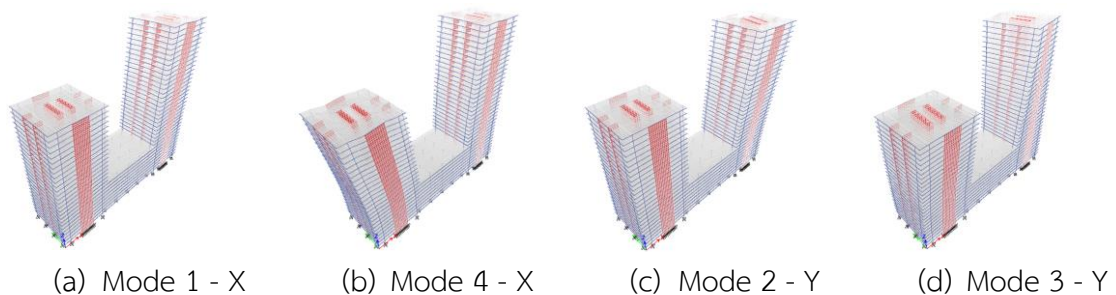
Figure 4.3 Three-dimensional mode shapes corresponding to translation in X- and Y-directions of DH building.

Theoretically, symmetrical mode shapes with opposite sign will lead to a zero modal participation factor Γ_n, and zero effective modal mass M_n^*, computed from the following equations (Chopra, 2012).

$$\Gamma_n = \frac{L_n}{M_n} = \frac{\phi_n^T \mathbf{m}\boldsymbol{\iota}}{\phi_n^T \mathbf{m}\phi_n} \tag{4.6}$$

$$M_n^* = \frac{(L_n)^2}{M_n} \tag{4.7}$$

$$\bar{M}_n^* = M_n^* / \sum \mathbf{m} \tag{4.8}$$

where M_n is the modal mass; ϕ_n is the nth mode shape of the structure; $\boldsymbol{\iota}$ is the influence vector; $\mathbf{m}$ is the mass matrix; $\bar{M}_n^*$ is the modal mass participation ratio; and $\sum \mathbf{m}$ denotes the total mass of structure (effective seicmic weight). In addition, zero modal participation factor will lead also to zero modal response, because the modal response quantities are computed with the use of the participation factor, as shown in equations below.

$$\mathbf{f}_n = \Gamma_n \mathbf{m}\phi_n A_n \tag{4.9}$$

$$\mathbf{u}_n = \Gamma_n \phi_n D_n \tag{4.10}$$

where $\mathbf{f}_n$ is peak value of equivalent static force in the nth mode; A_n is the nth mode pseudo-acceleration spectrum ordinate; $\mathbf{u}_n$ is the nth modal displacement; D_n is the deformation spectrum ordinate obtained from A_n / ω_n^2; and ω_n is the natural frequency of mode n.

4.3 Comparison of LRSA and LRHA results

In this section, comparison of results between linear response spectrum analysis (LRSA) and linear response history analysis (LRHA) is presented. linear RSA (without R and C_d) model was used, and it will be referred to as LRSA. Linear RSA (with R and C_d) procedure, which is the practical way that most of engineers follow is also presented, and it will be referred to as RSA (Eq.(4.3)). CQC modal combination rule was used for linear RSA to obtain total responses, while modal response histories were summed to obtain the total response of LRHA. The aim of this

comparison is to check the accuracy of combining peak response by modal combination rule (CQC) rather than time history, and to check the compatibility of UHS spectral matching ground motions selected in this study, before using them in NLRHA. However, it was found that LRSA provides similar results to LRHA with minor error, as shown in Figure 4.4 and 4.5. More details about structural element forces are presented in APPENDIX B.

A cracked cross-section property described in section 3.2.1 was used for all linear models described in this section. The results of LRHA are presented as the mean value of the peak results obtained from all the ground motion selected for each location. Normalized results are presented, where floor displacement is normalized by total building height H, story-drift is normalized by story height h, story shear is normalized by the effective seismic weight W, and overturning moment is normalized by WH. The results of story shear and overturning moment presented in Figure 4.4 and 4.5 are the sum of the forces in the two towers. For example, the story shear at level 35 is the sum of shear in towers T1 and T2 at level 35, and the overturning moment at the bottom of story 35 is equal to story force of level 36 (in T1 and T2) multiplied by the height of story 36 and 35, plus the force of story 35 multiplied by the height of story 35. Floor displacements and drifts are taken at center of mass of the taller tower, which is tower T2. Note that in SH building both towers respond symmetrically.

It was found that LRSA and LRHA provide similar results, with minor error in terms of all of the response quantities shown in Figure 4.4 and 4.5. RSA provides similar results of floor displacement and drift ratio as LRSA and LRHA, but with minor difference, while it underestimates force demand. The force demand obtained from RSA is the reduced elastic demand by the factor R, which is more convenient to compare RSA with NLRHA, to estimate the level of nonlinearity in structures, and to evaluate the accuracy of RSA method.
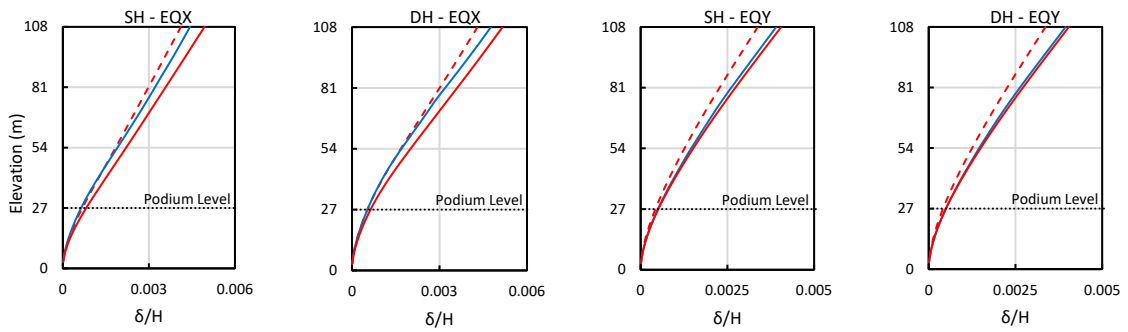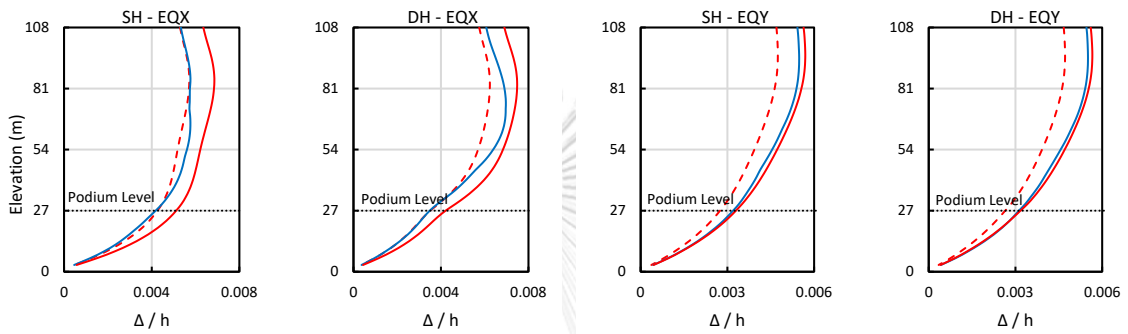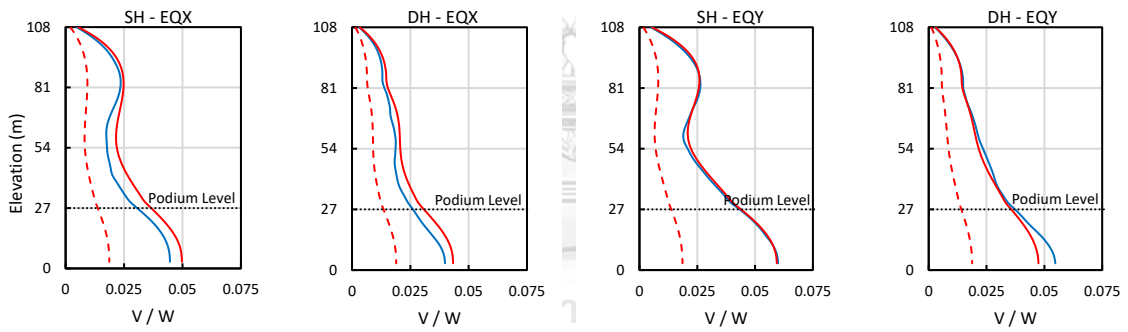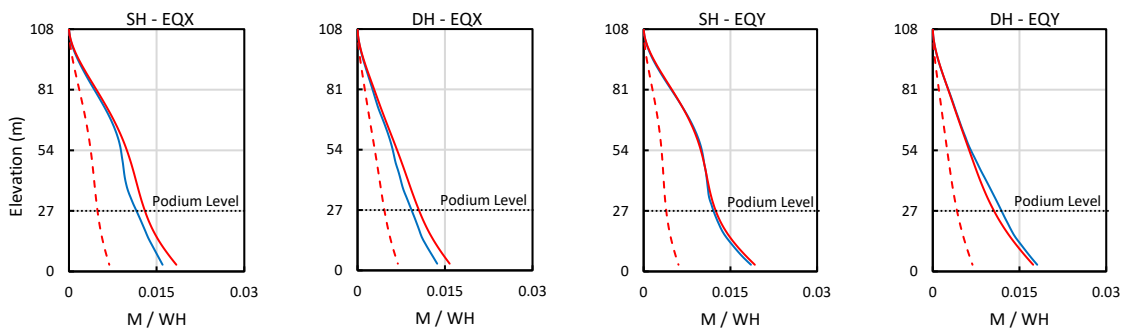
Figure 4.4 (a) Floor displacement (b) Inter-story drift ratio (c) Story shear (d) Story overturning moment, for Bangkok buildings, due to earthquake in both directions.
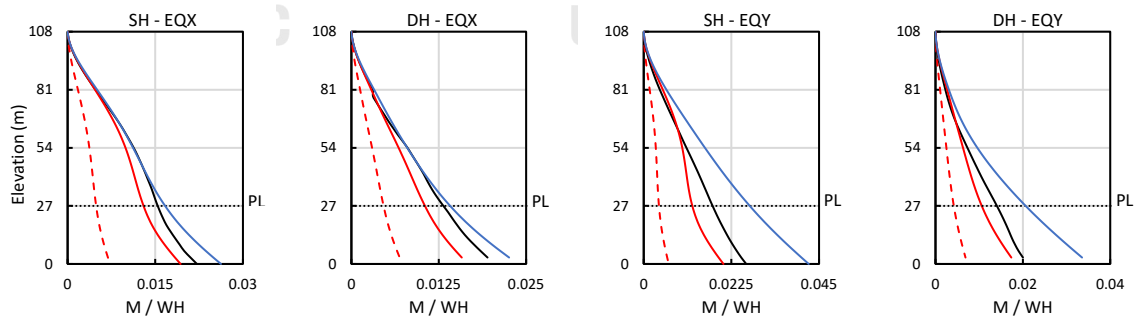
(a) Floor displacement

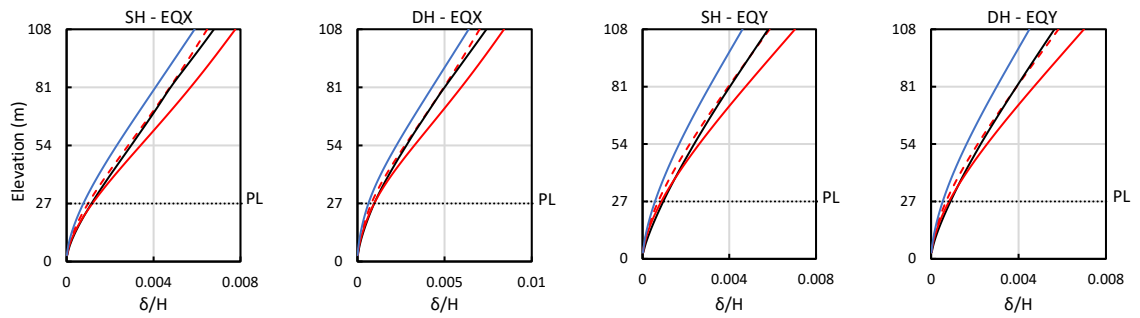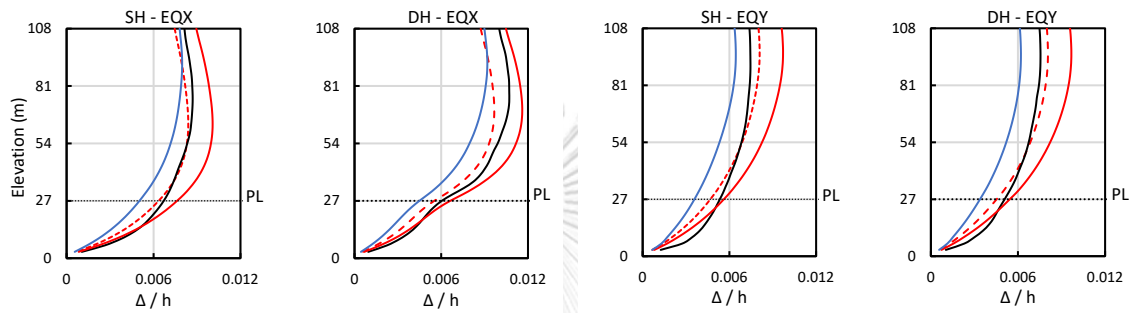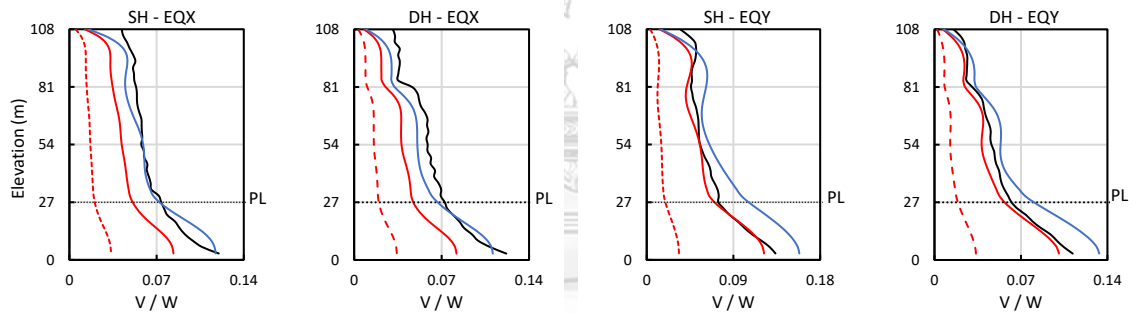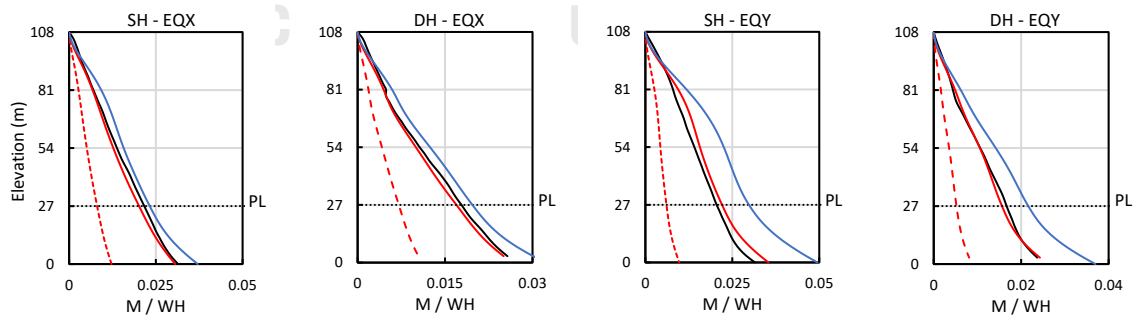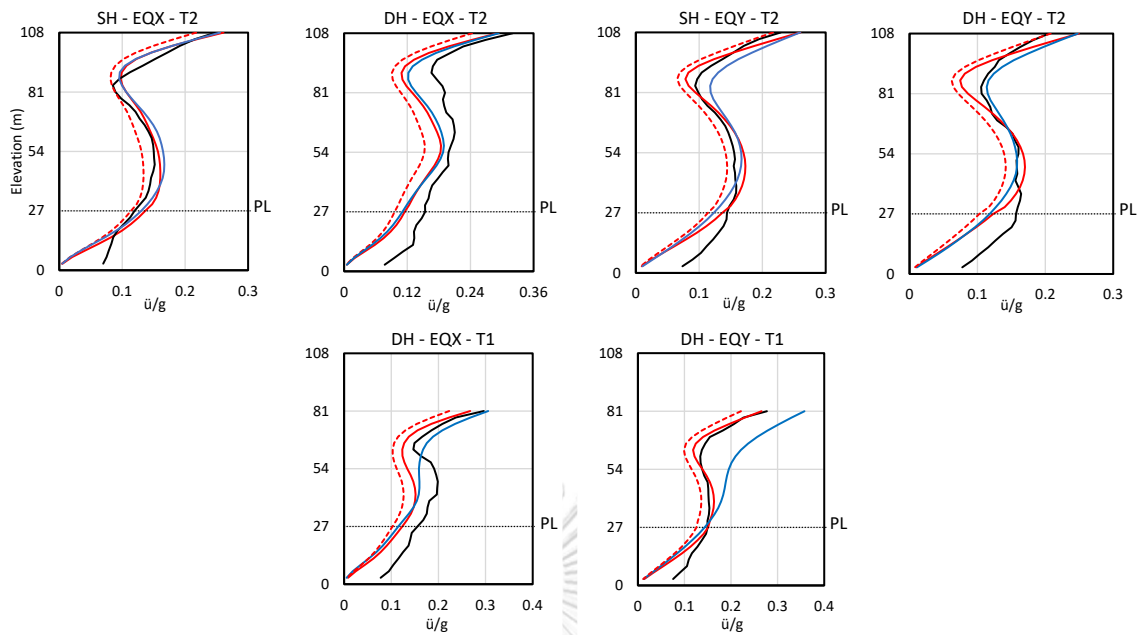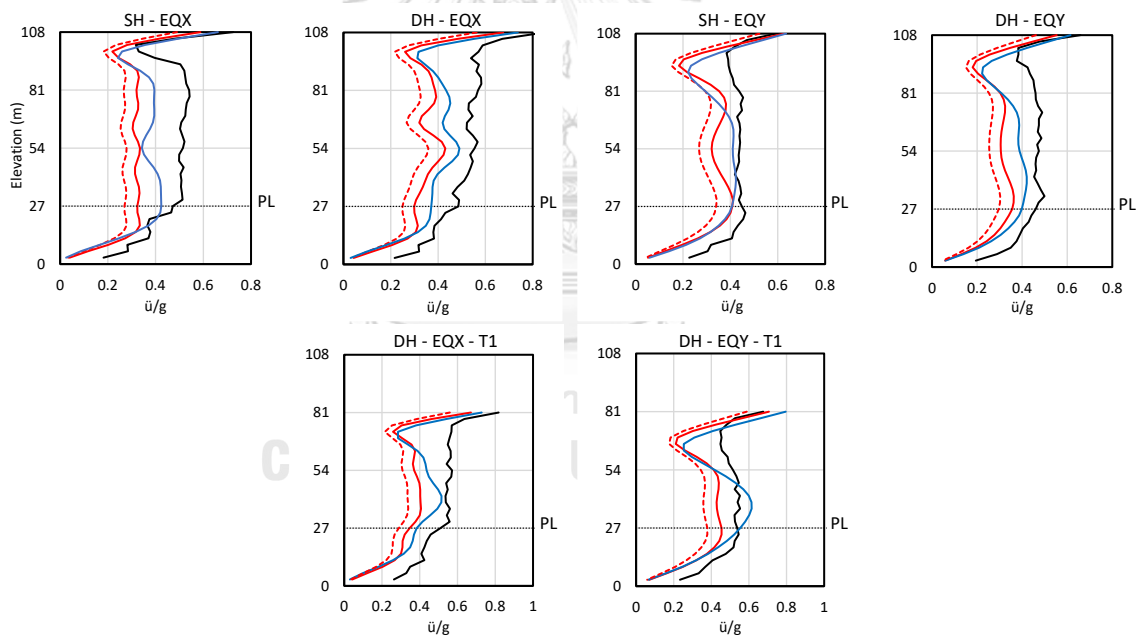(b) Inter-story drift ratio

(c) Story shear

(d) Story overturning moment

- - - RSA ——— LRSA ——— LRHA
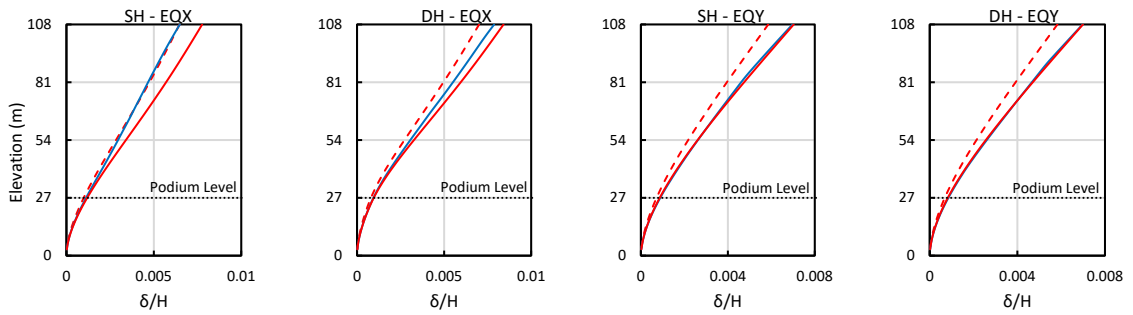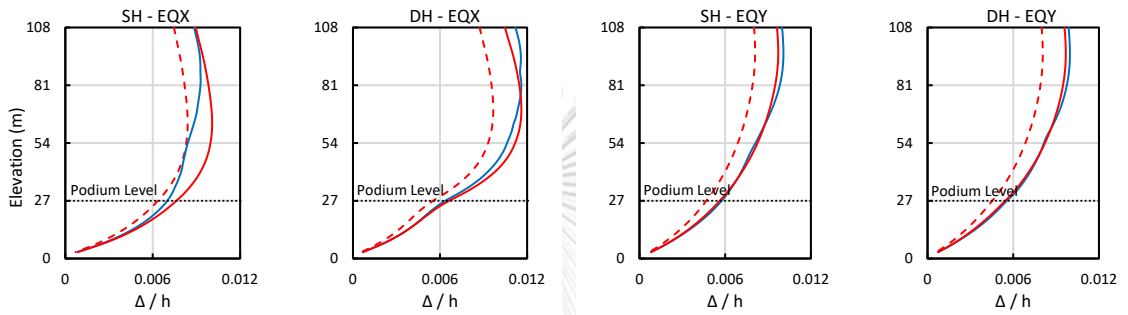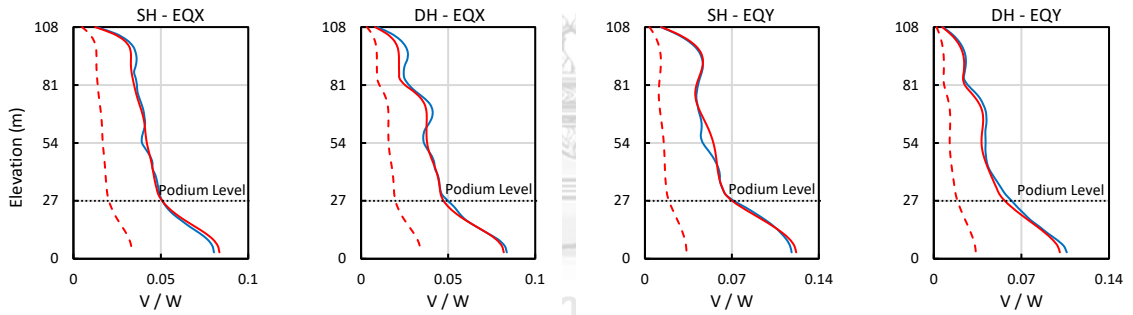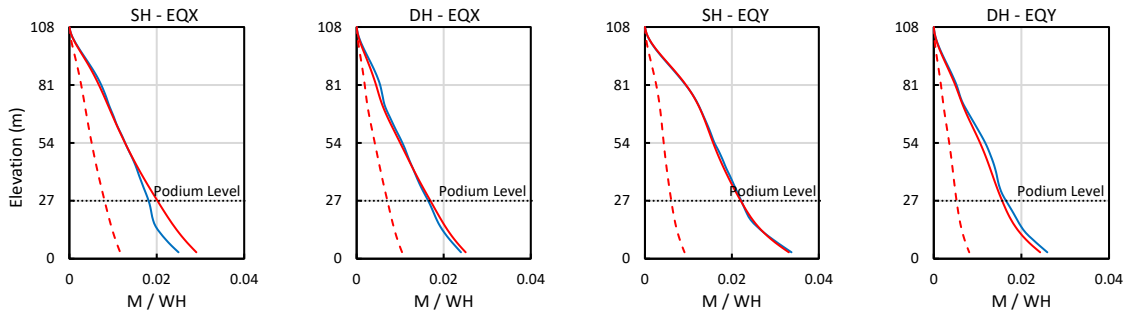
Figure 4.5 (a) Floor displacement (b) Inter-story drift ratio (c) Story shear (d) Story overturning moment, for Chiang Mai buildings, due to earthquake in both directions.

4.4 Nonlinear Response Time History Analysis (NLRHA) results

In this section, a comparison between linear RSA and NLRHA is presented. The nonlinear analytical model described in section 3.2.2 was used for conducting NLRHA using PERFORM-3D software (CSI 2018). The matched spectral ground motions shown in Figure 3.13 and 3.16 were used for NLRHA. A linear model computed using uncracked cross section properties of structural members (LRSA$_{uncracked}$), which have the same initial stiffness as the nonlinear model is presented in this section. The reason for using the LRSA$_{uncracked}$ model is to show the reduction of force in the nonlinear model due to the inelastic effect. In addition, RSA (Eq.(4.3)) and LRSA (without R and C_d) model shown previously in section 4.3 are also presented in this section. Note that RSA and LRSA model are computed using a cracked cross-section property of structural members as described in section 3.2.1. Results from, LRSA$_{uncracked}$, LRSA, and RSA are compared with NLRHA results as shown in Figure 4.6 and 4.7. More details about structural element forces are presented in APPENDIX C.

The analysis is performed using step-by-step integration through time, using the constant average acceleration method (also known as Newmark β =1/4 method). The numerical solution is obtained at every input time step of the ground motions, which varies between 0.005 to 0.01 sec. A constant damping ratio of 2.49% was assigned to all significant modes, while 0.1% damping ratio was assigned to Rayleigh damping model, which is based on the initial stiffness of the structure (Chopra & McKenna, 2016). The results of NLRHA are presented as the mean value of the peak results obtained from all the ground motions selected for each location. Normalized results are presented, where floor displacement is normalized by total building height H, story drift is normalized by story height h, story shear is normalized by the effective seismic weight W, and story overturning moment is normalized by WH, as shown in figures 4.6 and 4.7. Absolute floor accelerations are normalized by gravitational acceleration g, as shown in Figure 4.8, where the title of each figure shows the building name, earthquake direction, and tower name.
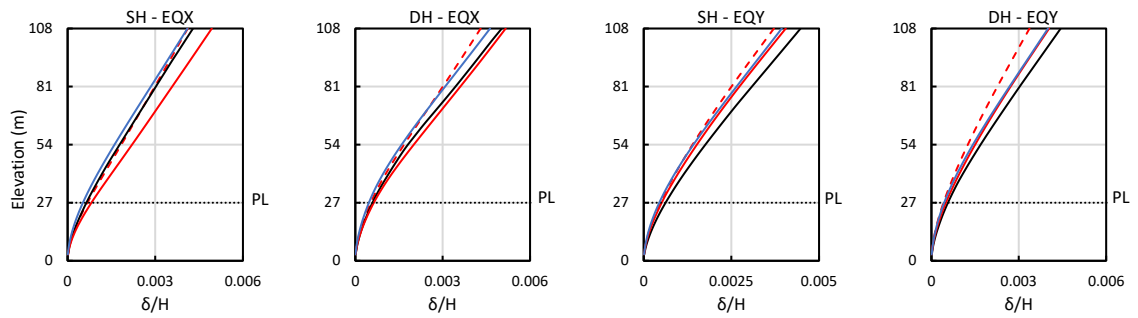
(a) Floor displacement
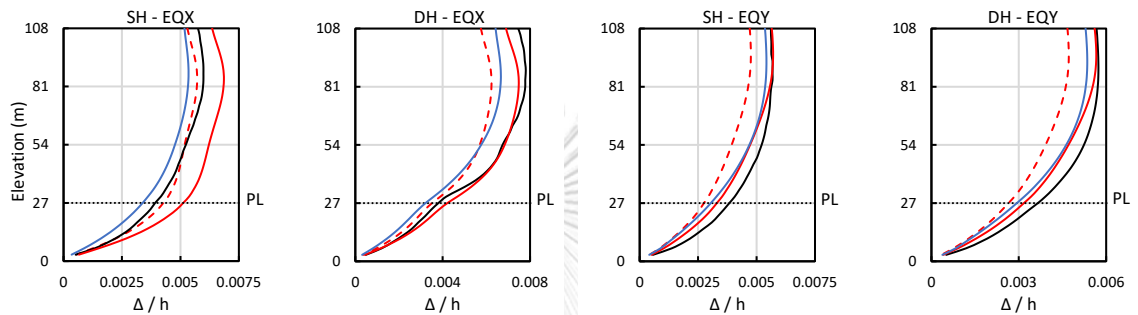
(b) Inter-story drift ratio
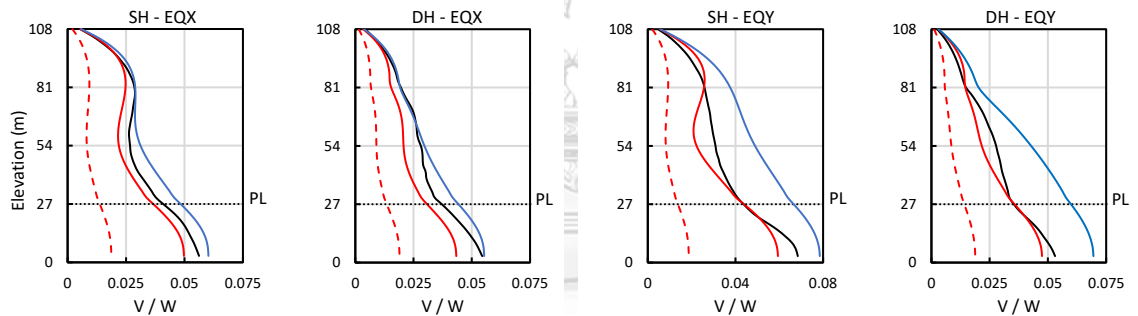
(c) Story shear

(d) Story overturning moment

Figure 4.6 RSA and NLRHA results of (a) Floor displacement (b) Inter-story drift ratio (c) Story shear (d) Story overturning moment, for Bangkok buildings, due to earthquake in both directions.

Figure 4.7 RSA and NLRHA results of (a) Floor displacement (b) Inter-story drift ratio (c) Story shear (d) Story overturning moment, for Chiang Mai buildings, due to earthquake in both directions.

Figure 4.8 Absolute floor accelerations for buildings in (a) Bangkok (b) Chiang Mai.

4.5 Inelasticity of modal responses

The inelasticity of response in each mode was investigated using modal pushover analysis (MPA). Linear and nonlinear structural model were used to conduct MPA. The linear model used has the same initial stiffness as the nonlinear model, which is different from the linear model described in 3.2.1, that was used for computing the demand forces of RSA. The lateral load distribution for conducting MPA was applied in proportion to the distribution of mass in the plane of each floor diaphragm, multiplied by mode shape in the direction under consideration ($\mathbf{m}\phi_n$). The first three translational modes in each direction were considered in this study (refer to Table 4.5 and 4.6). It should be noted that modes with zero mass participation ratio in SH building were ignored and mode number 8 in DH building was used instead of mode number 5 (mode number 8 contributes more to the total response). The modal contribution of the first three translational modes to story shear is shown in Figure 4.9 for both buildings in each direction. The modal contribution to story displacement shown in Figure 4.10 can clarify the location of the target roof displacement selected to construct the shear-roof displacement relation. For example, second mode in the Y-direction for DH building is contributing to story displacements of tower T1 only; hence, roof displacement of tower T1 was used for obtaining the pushover curve.

The base shear-roof displacement relation is shown in Figure 4.11 and 4.12 for all studied buildings, where base shear is normalized by building weight W, and roof displacement is normalized by building height H. The target roof displacement for the first translational mode in each direction was computed using displacement coefficient method in ASCE 41-13 (American Society of Civil Engineers, 2013). The target roof displacements for higher modes were assumed to be equal to the elastic response computed by modal analysis of the linear structural model considering cracked cross section of structural members. The force response reduction factor R_i is taken as the ratio of base shear of the linear to the nonlinear model at the target roof displacement. Summary of the force response reduction factors are shown in

Figure 4.13. The gravity loads of all dead loads plus 25% of live load were applied before pushover analysis.

(a) Bangkok buildings

(b) Chiang Mai buildings
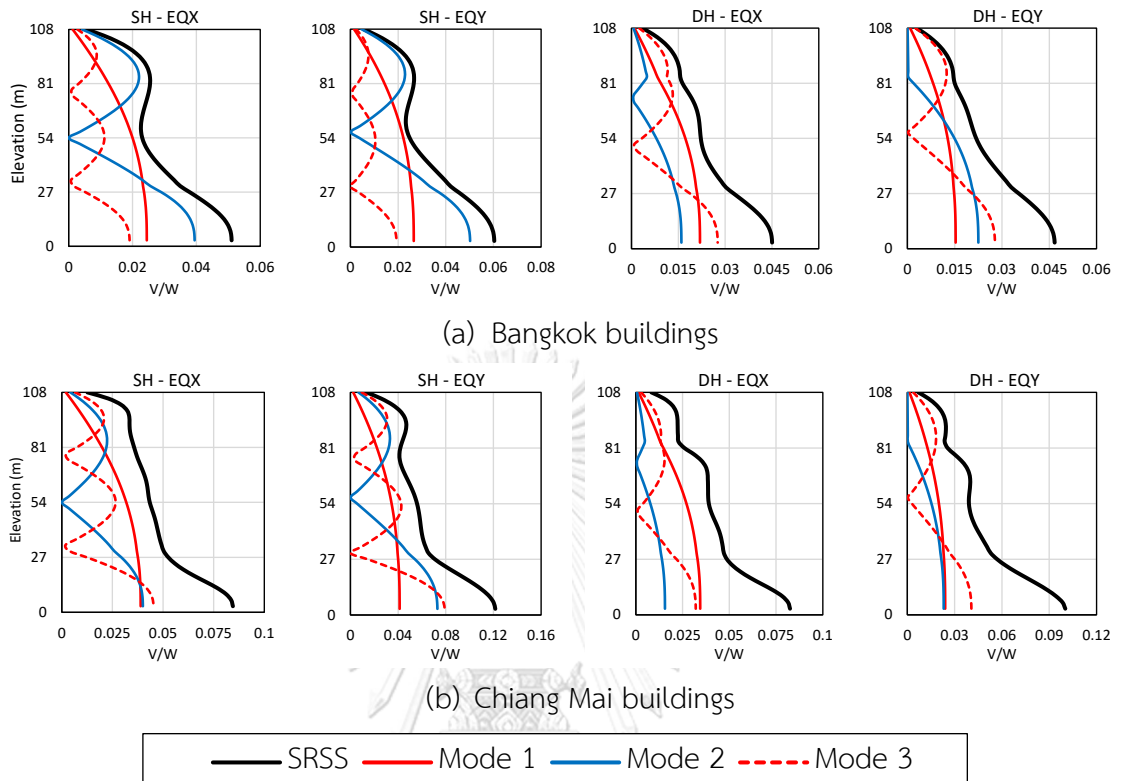
Figure 4.9 Modal contribution to story shear for both buildings in (a) Bangkok (b) Chiang Mai.
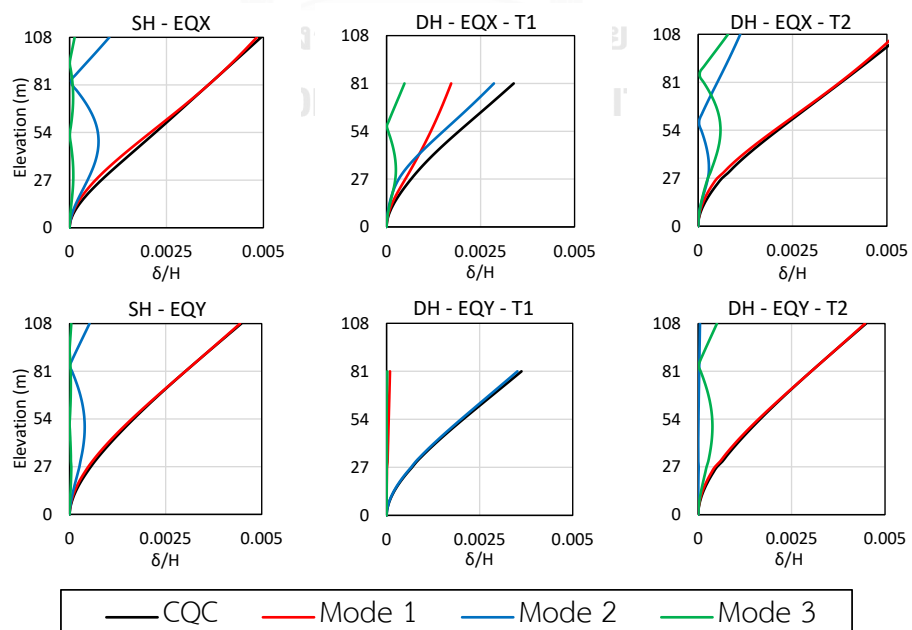
Figure 4.10 Modal contribution to story displacement.
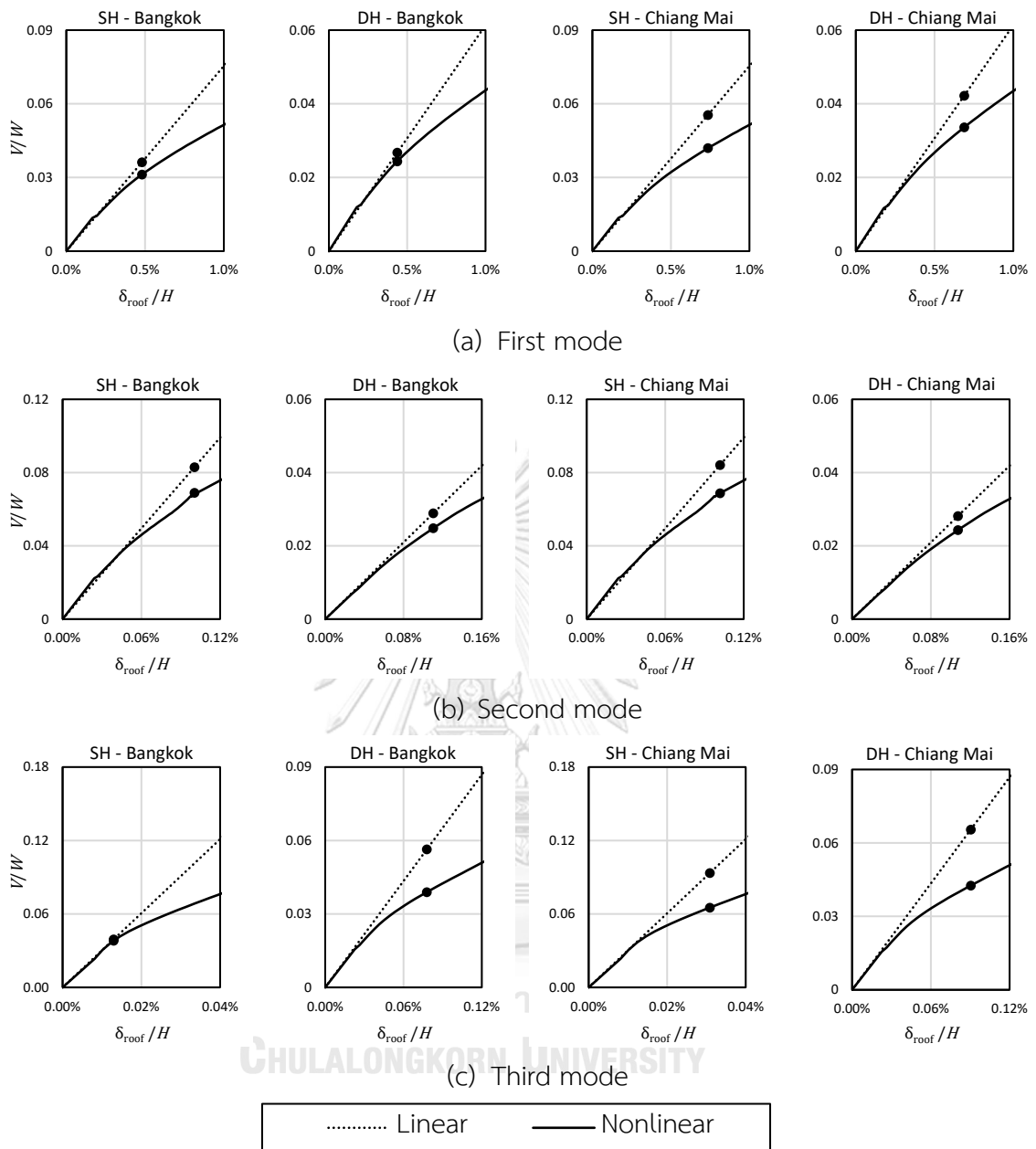
Figure 4.11 Linear and nonlinear pushover curves along with the target roof displacements of the first three translational modes in X-direction of buildings in Bangkok and Chiang Mai: (a) first mode; (b) second mode; and (c) third mode. The black dots in each figure indicate the target roof displacement.
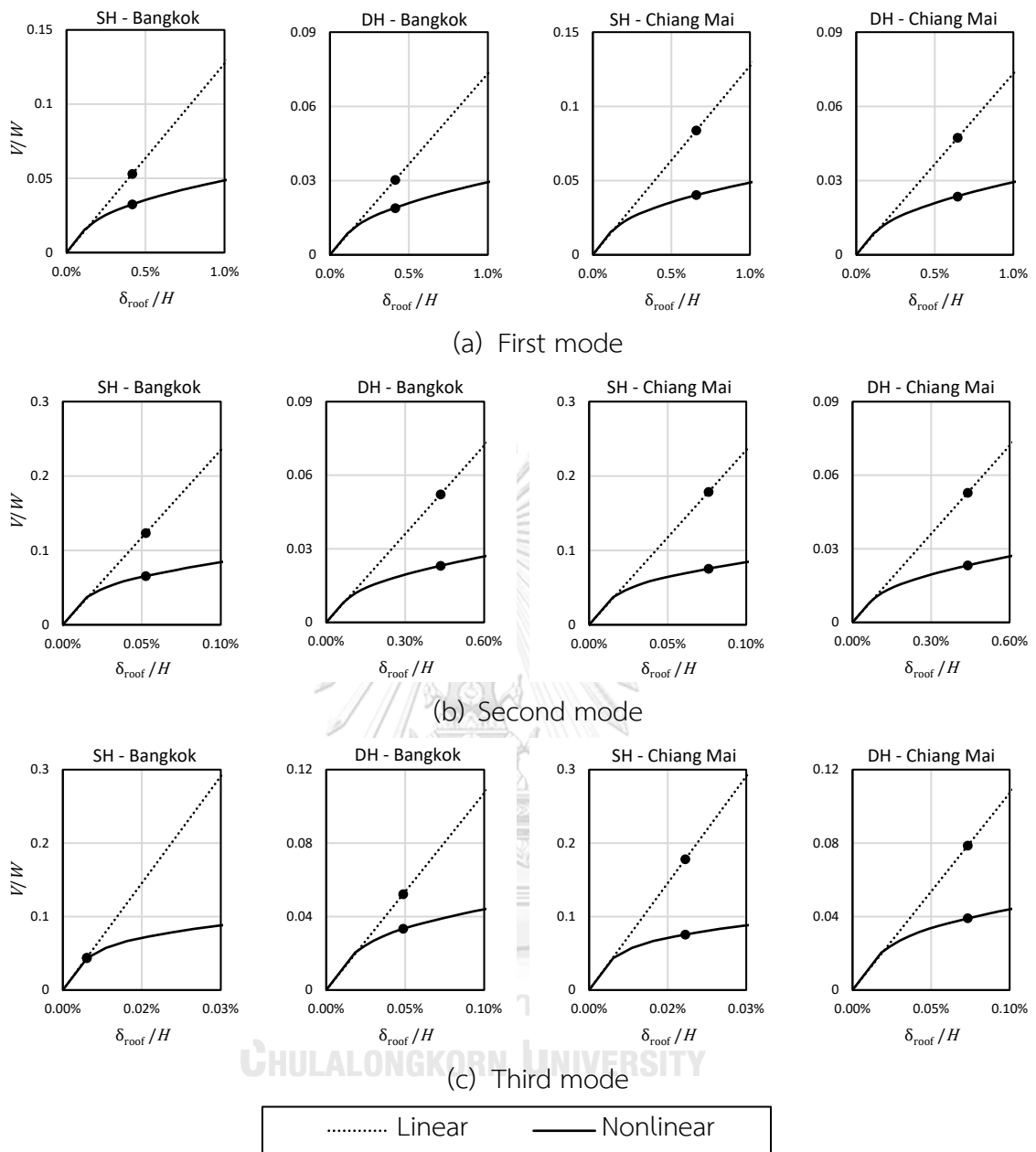
Figure 4.12 Linear and nonlinear pushover curves along with the target roof displacements of the first three translational modes in Y-direction of buildings in Bangkok and Chiang Mai: (a) first mode; (b) second mode; and (c) third mode. The black dots in each figure indicate the target roof displacement.

(a) X -direction   (b) Y -direction
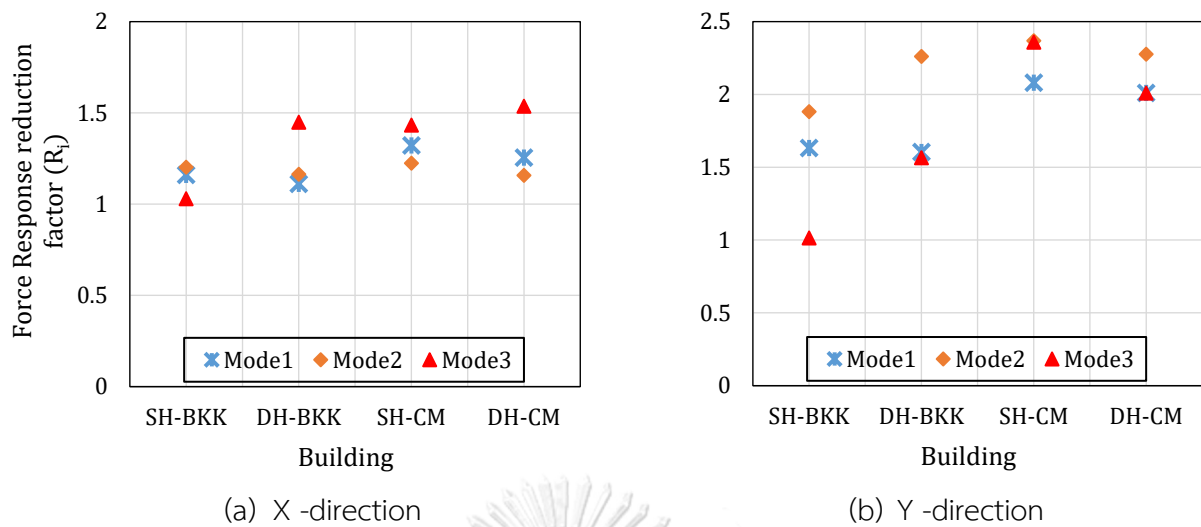
Figure 4.13 Force response reduction factor of the first-three translational modes for case studies in Bangkok and Chiang Mai: (a) X-direction; and (b) Y-direction.

It was found that the level of inelasticity of response in different modes were different, and the force response reduction factor R_i ranges between 1 to 2.3, which is about 2.5 to 6 times lowers than the response modification factor (R=6) used in the design of these buildings. The force response reduction factor increases with increasing mode order for most buildings. In general, the force response reduction factor ranges between 1 to 1.5 for all modes in the X-direction, while it ranges between 1 to 2.5 for all modes in the Y-direction. The R_i factor of the first translational mode in X-direction was generally close to 1 for all buildings, while it ranges between 1.5 to 2 for the first mode in Y-direction.

4.6 Accuracy of modified response spectrum analysis (MRSA)

In this section, the modified response spectrum analysis (MRSA) procedure proposed by Khy and Chintanapakdee (2018) is conducted. Two versions of MRSA were proposed to compute the shear forces in RC shear walls, where the first method assumes that higher modes will behave elasticly, and the inelastic action will takes place in the first mode only, and it refered to as MRSA$_{HE}$. The second method takes into account the inelasticity of higher modes by estimating the force response reduction factor of each mode (R_i) using pushover analysis, and it refered to as MRSA$_{HI}$. The methods were proposed to estimate shear forces in structural

element with a more accuracy, when compared to NLRHA results. Moreover, Khy and Chintanapakdee (2018) suggest to compute the bending moments using RSA procedure described in the interantional codes (Eq. (4.3)), because bending moments computed from MRSA will require a large vertical reinforcement, and this will increase shear forces due to increase of flexural strength. The pushover analysis conducted to compute the force response reduction factor (R_i) is presented in section 4.5. It should be noted that MRSA$_{HI}$ requires a nonlinear model to compute the force respones reduction factor (R_i), while MRSA$_{HE}$ can be applied directly in linear model. Both methods were applied using a linear model with effective stiffness corresponding to cracked cross-section properties of structural members, as presented in section 3.2.1. The shear forces in the structure using the MRSA$_{HE}$ and MRSA$_{HI}$ method are computed from Eq. (4.11) and (4.12) respectively.

$$V_{HE,i} = I \times \sqrt{\left(\frac{SF \times \Omega_0}{R} V_{1e,i}\right)^2 + V_{2e,i}^2 + V_{3e,i}^2 + ...} \tag{4.11}$$

$$V_{HI,i} = I \times \sqrt{\left(\frac{V_{1e,i}}{R_1}\right)^2 + \left(\frac{V_{2e,i}}{R_2}\right)^2 + \left(\frac{V_{3e,i}}{R_3}\right)^2 + ...} \tag{4.12}$$

where I is the importance factor, SF is the scaling factor computed using Eq. (4.4), Ω_0 is the overstrength factor, $V_{je,i}$ is the elastic modal shears of mode j at level i; R_i is the force response reduction factor of mode i.

The total combined elastic shear demand was obtained by considering 30 modes of vibration using ETABS software. For MRSA$_{HE}$, the elastic first-mode shear multiplier ($SF \times \Omega_0 / R$) is summarized in Table 4.7. Story shear and story overturning moment from RSA, MRSA, and NLRHA are shown in Figure 4.14. More details about structural element forces are presented in APPENDIX D.

Table 4.7 Elastic first-mode shear multiplier ($SF \times \Omega_0 / R$) for MRSA$_{HE}$.

Building	SH		DH	
Direction	X	Y	X	Y
Bangkok	0.75	0.63	0.88	0.79
Chiang Mai	0.80	0.55	0.82	0.66
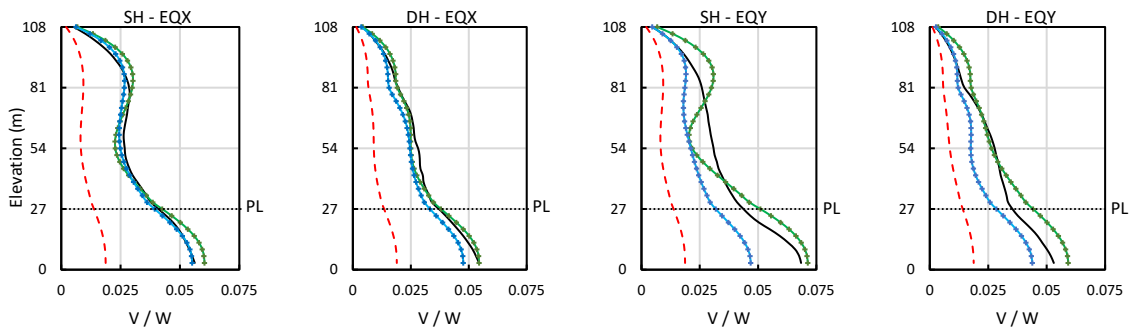
(a) Story shear for Bangkok buildings
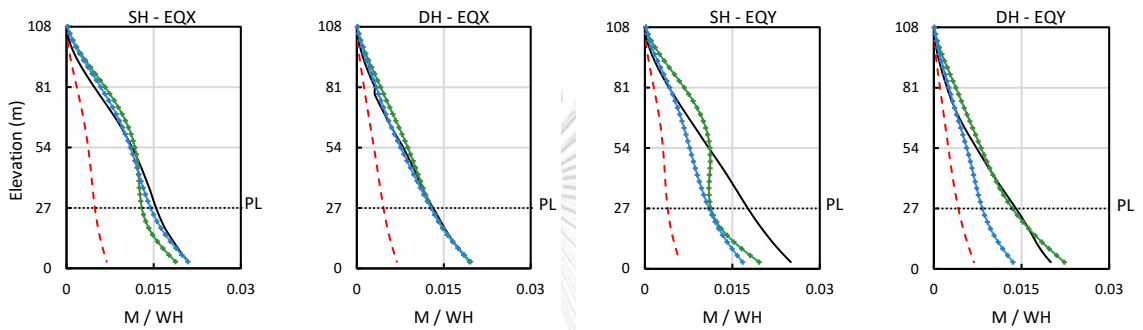
(b) Story overturning moment for Bangkok buildings
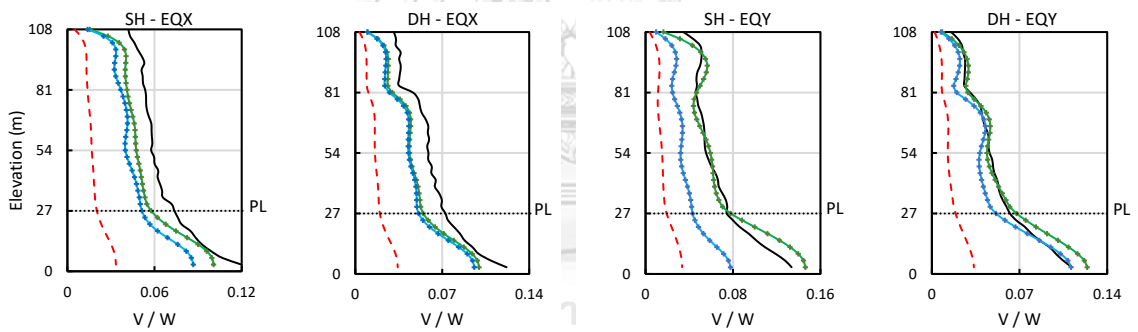
(c) Story shear for Chiang Mai buildings
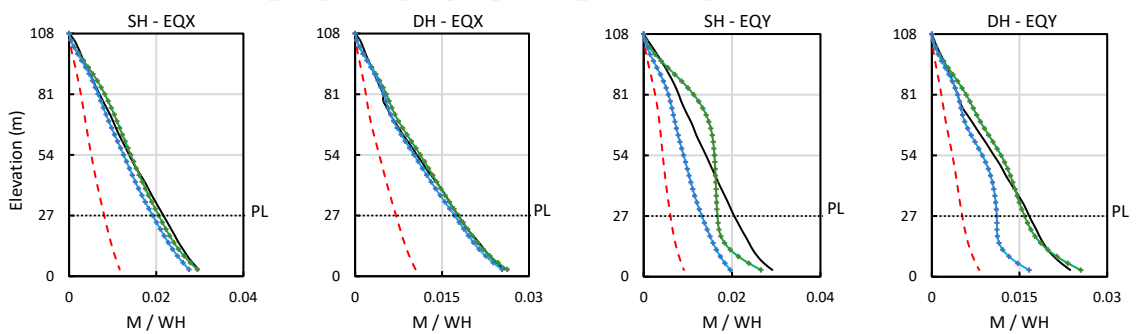
(d) Story overturning moment for Chiang Mai buildings

Figure 4.14 Story shear and story overturning moment for both buildings located in Bangkok and Chiang Mai.

The modified response spectrum analysis (MRSA) procedure is outlined as follow:

1) Compute demand forces using RSA procedure, as described in Eqs. (4.1) and (4.2).

2) Compute scaling factor (*SF)* which is the ratio of 85% of base shear from static analysis (ELF) and dynamic analysis (RSA).

3) Compute bending moment demand using Eq. (4.3), and provide the required flexural reinforcement corresponding to this demand.

4) Compute shear demand from MRSA procedure, using Eq. (4.11) or (4.12).

5) If Eq. (4.12) is to be used, a nonlinear model is needed in order to estimate the force response reduction factor of each mode (R_i)

4.7 Summary

The main findings of this Chapter are summarized as the followings:

1) RSA procedure underestimates force demands when compared to NLRHA results. The design (reduced) shear demand obtained from RSA procedure is not sufficient and it could lead to brittle shear failure in RC shear walls, if used in the design.

2) For buildings in Bangkok, RSA procedure provides fair results of floor displacements, inter-story drift ratios, and absolute floor accelerations, while estimating those response quantities by elastic value would be more accurate than those obtained by procedure in ASCE 7-16. For buildings in Chiang Mai, RSA procedure provides accurate estimates of inelastic floor displacements and story drift ratios computed from NLRHA, while RSA procedure and other elastic methods underestimates the absolute floor accelerations computed from NLRHA (Figure 4.8).

3) The inelastic behaviors of each mode were not identical, and higher modes were significantly affected by inelasticity as the first mode. The force response reduction factor (R_i) increases with increasing mode order for most buildings.

4) The $MRSA_{HE}$ method provides good estimates of shear forces for both studied RC shear wall tall buildings in Bangkok and Chiang Mai, except that it slightly underestimates the shear forces due to earthquake in the X-direction for both buildings in Chiang Mai (refer to Table 4.8). The $MRSA_{HE}$ is preferred to be used in the design practice as it can be applied directly using a linear structural model.

5) The $MRSA_{HI}$ method provides good estimates of shear forces due to earthquake in the X-direction for both studied buildings in Bangkok, while it slightly underestimates the shear forces due to earthquake in the X-direction for both buildings in Chiang Mai. For earthquake in the Y-direction, $MRSA_{HI}$ method underestimates the shear forces in building SH, while it provides fair results for building DH (refer to Table 4.9).

Table 4.8 Summary of accuracy of $MRSA_{HE}$ method.

Building	SH		DH	
Direction	X	Y	X	Y
Bangkok	Accurate	Accurate	Accurate	Accurate
Chiang Mai	Fair	Accurate	Fair	Accurate

Table 4.9 Summary of accuracy of $MRSA_{HI}$ method.

Building	SH		DH	
Direction	X	Y	X	Y
Bangkok	Accurate	Underestimates	Accurate	Fair
Chiang Mai	Fair	Underestimates	Fair	Accurate

CHAPTER 5

CONCLUSIONS AND RECOMMENDATIONS

5.1 Conclusions

In this study, two hypothetical multi-tower buildings subjected to earthquake ground motions expected in Bangkok and Chiang Mai were first designed using seismic demands determined by conventional RSA procedure in ASCE 7-16. Results from nonlinear response history analysis (NLRHA), which is the most accurate method, were used as benchmark values to evaluate the accuracy of the other methods. Since elastic methods are preferred in practice, a modified response spectrum analysis (MRSA) previously proposed to compute shear force in regular building was tried in this study to irregular tall buildings. Two version of MRSA were used, the first is based on higher-mode elastic approach denoted as $MRSA_{HE}$, and the second is based on a higher-mode inelastic approach denoted as $MRSA_{HI}$. The main findings of this study are summarized as follow:

1) RSA procedure underestimates design demand when compared to NLRHA. Due to overstrength inherent in the design, and by providing the required detailed reinforcement in locations where flexural yielding occurs, RSA procedure can be sufficient for computing bending moments of structural RC shear walls. However, the design (reduced) shear demand obtained from RSA procedure is not sufficient and it could lead to brittle shear failure in RC shear walls, if used in the design.

2) RSA procedure provides good estimate of floor displacements, inter-story drift ratios, while estimating those response quantities by elastic value would be more accurate than those obtained by procedure in ASCE 7-16.

3) $MRSA_{HE}$ provides good estimates of shear forces for both studied RC shear wall tall buildings, while $MRSA_{HI}$ provides accepted results for most buildings, but it underestimates shear forces due to earthquake in Y-direction for SH building. Therefore, $MRSA_{HE}$ is preferred to be used in the design practice as it

provides good estimate of shear forces in RC shear walls and in diaphragm slabs, and it can be applied directly in a linear structural model.

4) Diaphragms are usually designed to remain elastic or nearly elastic for forces acting within their plane under factored load combinations. Hence, designing diaphragm components (chords and collectors) using the unreduced elastic demand of RSA procedure is preferred. However, It was found that the two versions of MRSA provide good estimate of shear and bending moments in diaphragm slabs, much better than the use of the unreduced elastic demand of RSA procedure (Figures D.22 to D.25). In addition, it was found that the demand forces in diaphragms of the lower stories (story 1 to 4) obtained from NLRHA are always larger than the demand forces obtained from the elastic methods.

5) The effect of changing towers heights is also investigated by analyzing two buildings, the first building consists of two towers with the same heights (building SH), and the second building consist of two towers with different heights (building DH). It was found that, changing towers height leads to a significant change in building response with a dominant translational-torsional coupling phenomenon in most of modes. All RC walls of building DH aligned in the X-direction experienced severe discontinuity of demand forces at the podium level (e.g., Figures C.4 and C.5), while such phenomenon is not seen in members of SH building. The discontinuity of pier forces in DH building is due to a large contribution of axial forces developed in podium floors. Asymmetrical mode shapes in towers of DH building leads to a significant increase in axial forces in podium floors (Figures C.26 and C.27).

6) The two versions of MRSA provide good estimate of shear and bending moment forces in RC columns for Bangkok buildings (Figures D.9 to D.14), while for RC columns in Chiang Mai buildings, the MRSA methods and other elastic methods are incapable of estimating well the shear forces below the podium level (Figures D.15 to D.17).

5.2 Recommendations for future studies

The modified response spectrum analysis based on higher mode inelastic approach MRSA$_{HI}$ was recommended by Khy et al. (2019) as it can provide higher accuracy than the MRSA$_{HE}$ method, which is contradictory to the finding of this study. The main difference between both studies is that Khy et al. has studied regular buildings without significant coupling effect between translational and torsional modes such that each dominant translational mode in a building can be identified, and the inelasticity of each mode can be investigated through uncoupled-mode assumption, while buildings in this study have a significant coupling between translational and torsional modes. The reason for underestimation could be due to inaccuracy of estimating the force response reduction factor (R_i) in asymmetrical buildings, where coupling between translational and torsional responses in each mode is present. Therefore, a better estimation of the force response reduction factor (R_i) is needed by using another pushover analysis method that accounts for the torsional effect in asymmetrical buildings. Also, the present study considered unidirectional earthquake when applied to structures. Tall buildings subjected to bi-directional earthquake ground motions should also be studied.

APPENDIX A

DESIGN CONSIDERATIONS AND TECHNICAL GUIDANCE

A.1 Studied building

In this section, SH building (Figure 3.1) was used as an example to explain the design process followed in this study. The lateral force resisting system is considered to be a special RC shear wall whose design factors are: R =6, C_d =5, Ω_0 =2.5, I =1.25 (Table 3.2). The location of the building was considered to be in Chiang Mai. Gravity loads, wind loads, and load combinations are shown in section 3.1.

A.2 Design spectrum

The spectral acceleration parameters at short period (S_S) and at 1s (S_1) were taken from DPT 1301/1302-61 with the values of 0.963 and 0.248 respectively. The ASCE 7-16 procedure was used to obtain the design spectral acceleration curve. It should be noted that the design spectrum in ASCE 7-16 is for a 5% damping ratio. To obtain a spectrum with a 2.5% damping ratio as recommended by PEER (2017) for tall buildings, the damping factor formula in ASCE 41-13 was adopted (Eq. (A.1)).

$$B_1 = 4 / [5.6 - \ln(100\beta)] \tag{A.1}$$

where β is the effective viscous damping ratio.

Table A.1 Basic parameters (ASCE 7-16).

Site class	D
S_S	0.963
S_1	0.248
Short-period site coefficient "F_a"	1.115
Long-period site coefficient "F_v"	1.904
Spectral parameter adjusted for site class effect "$S_{MS} = F_a \times S_S$"	1.074
Spectral parameter adjusted for site class effect "$S_{M1} = F_v \times S_1$"	0.472
Design spectral parameters at short period "$S_{DS} = (2/3) \times S_{MS}$"	0.716
Design spectral parameters at long period "$S_{D1} = (2/3) \times S_{M1}$"	0.315
$T_0 = 0.2\, S_{D1}/S_{DS}$	0.088
$T_S = S_{D1}/S_{DS}$	0.440
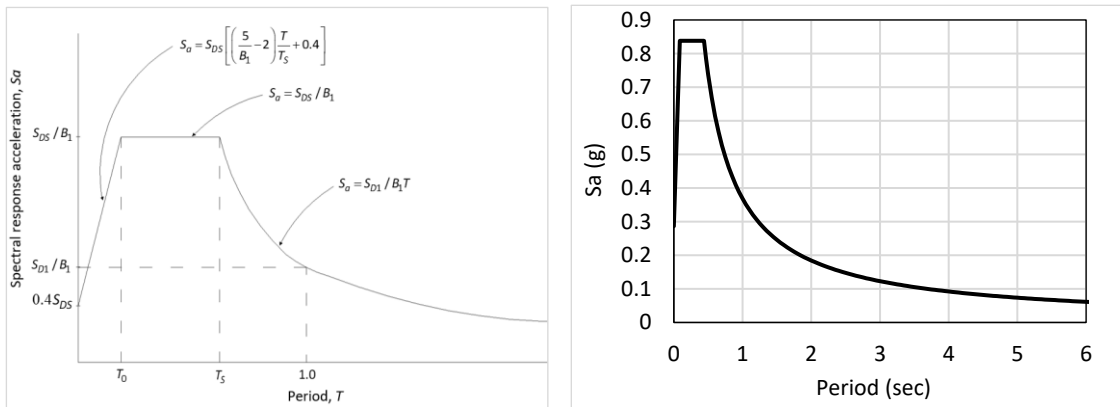
(a) Design response spectrum   (b) Chiang Mai design spectrum

Figure A.1 Design spectrum.

A.3 Effective seismic weight

The effective seismic weight "W" of a structure shall include the total dead load, and sometimes a portion of live load. Live load is included only when designing areas used for storage, ... etc. In this study, the effective seismic weight is computed from all dead loads (DL+SDL) only. The weight of the structural element is computed using the volume of the structural element multiplied by the unit weight of concrete (24 kN/m^3). Structural elements with the same size are denoted by the same name in Figure A.2. Elements dimensions, thickness, length, and number of structural elements are shown in Table A.2, Table A.3, Table A.4, and Table A.5.
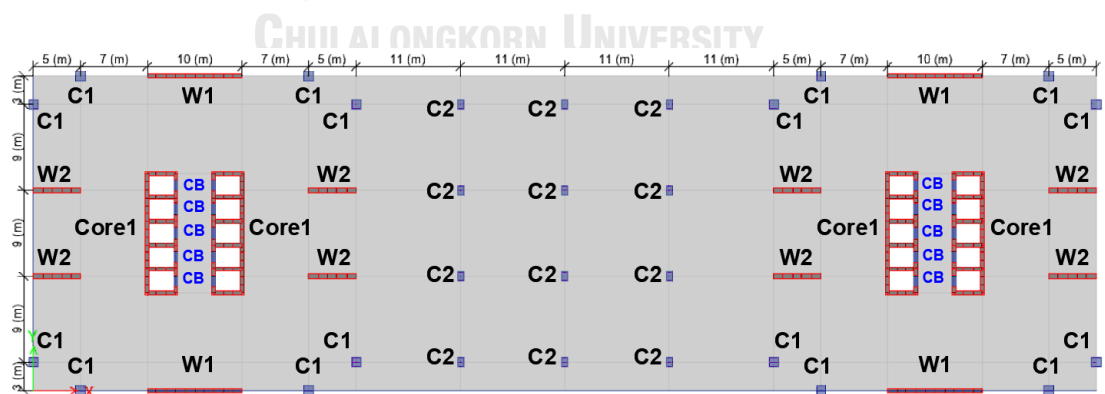
Figure A.2 Denotation of the structural elements in SH building.

Table A.2 Structural element dimension.

Symbol	Story Range	Cross section (mm x mm) / Thickness (mm)
C1	All Stories	1000 x 1000
C2	$1^{st} - 9^{th}$	600 x 1000
Core 1	All Stories	400
W1 & W2	$1^{st} - 6^{th}$	500
	$7^{th} - 9^{th}$	450
	$10^{th} - 18^{th}$	400
	$19^{th} - 27^{th}$	350
	$28^{th} - 36^{th}$	300
CB	All Stories	400 x 800

Table A.3 Walls thickness and length in stories of SH building.

Story	Wall thickness (m)	Wall length (m)
P (1st to 6th)	0.5	80
	0.4	148
P (7th to 9th)	0.45	80
	0.4	148
T1 or T2 (10th to 18th)	0.4	114
T1 or T2 (19th to 27th)	0.35	40
	0.4	74
T1 or T2 (28th to 36th)	0.3	40
	0.4	74

Table A.4 Number of columns and cross section dimensions in SH building.

Towers	Column cross section	Number of columns
P	1 x 1	16
	1 x 0.6	12
T1	1 x 1	8
T2	1 x 1	8

Table A.5 Dimensions of horizontal component.

Towers	Slab area (m²)	Slab thickness (m)	CB length (m)	CB dim. (m²)
P	3546	0.3	24	0.8 × 0.4
T1	1047	0.3	12	0.8 × 0.4
T2	1047	0.3	12	0.8 × 0.4

Table A.6 Summary of stories weight.

Weight of one story in range					
Story range	1st - 6th	7th – 9th	10th - 18th	19th - 27th	28th - 36th
Slab weight (kN)	25,066	25,066	7,401	7,401	7,401
Columns weight (kN)	1,640	1,640	565	565	565
Wall weight (kN)	7,012	6,730	3,223	3,082	2,941
Coupling beam weight (kN)	181	181	90	90	90
SDL (kN)	8,865	8,865	2,618	2,618	2,618
Total	42,765	42,482	13,898	13,757	13,615

Note that the weight of stories sharing different cross-section from two-level should be modified. For example, story 36 shares only half of the length of the vertical element (columns and walls), while story 9 does not share any weight in the middle region from the above stories. The effective seismic weight equals the summation of stories weight, and it is equal to W=1,112,548 kN. Stories weight is shown in more detail in Table A.7.

A.4 Equivalent lateral force procedure

The approximated fundamental period (T_a) and upper limit period (T_{max}) in ASCE 71-6 are computed as follow:

$T_a = C_t \times h_n^x = 0.0488 \times 108^{0.75} = 1.635$ sec

$T_{max} = C_u \times T_a = 1.4 \times 1.635 = 2.289$ sec

where C_t and x are coefficients determined from table 12.8-2 in ASCE 7-16, h_n is the structural height, C_u is the upper limit coefficient determined from table 12.8-1 in ASCE 7-16.

The fundamental period used in ELF procedure is computed by

$T = \min(T_{max}, T_{etabs}) = \min(2.289, 6.1) = 2.289$ sec

The Seismic response coefficient (C_s) is computed by

$$C_s = \frac{S_{DS}}{(R/I)} = \frac{0.716}{(6/1.25)} = 0.149$$

$$C_{s,max} = \frac{S_{D1}}{T(R/I)} = \frac{0.315}{2.289(6/1.25)} = 0.029$$

$C_{s,min} = 0.044 S_{Ds} I = 0.044 \times 0.716 \times 1.25 = 0.039$

Therefore, $C_{s,used} = 0.039$.

The ELF seismic base shear (V) is computed by

$V = C_s \times W = 0.039 \times 1,112,548 = 44,188$ kN

The vertical distribution of ELF seismic base shear (V) is computed by

$F_x = C_{vx} \times V$

$$C_{vx} = \frac{w_x h_x^k}{\sum w_i h_i^k}$$

where C_{vx} is vertical distribution factor, V is ELF base shear, w_i and w_x are the portion of the total effective seismic weight of the structure located or assigned to level i or x, h_i and h_x are the height from the base to level i or x, k is an exponent related to the structure period determined as follow:

- ✓ $k = 1$, if $T < 0.5$
- ✓ $k = 2$, if $T > 2.5$
- ✓ $k = 0.5T + 0.75$, if $0.5 < T < 2.5$

Table A.7 Vertical distribution of seismic load by ELF procedure in X-direction.

Tower	Level	w (kN)	h (m)	h^k	wh^k	C_{vx}	F_x (kN)
T1 or T2	36th	11,862	108	7,115	8E+07	0.033	1,477
	35th	13,615	105	6,745	9E+07	0.036	1,608
	34th	13,615	102	6,385	9E+07	0.034	1,522
	33th	13,615	99	6,034	8E+07	0.033	1,438
	32th	13,615	96	5,692	8E+07	0.031	1,357
	31th	13,615	93	5,360	7E+07	0.029	1,278
	30th	13,615	90	5,037	7E+07	0.027	1,201
	29th	13,615	87	4,724	6E+07	0.025	1,126
	28th	13,615	84	4,420	6E+07	0.024	1,053
	27th	13,686	81	4,125	6E+07	0.022	988
	26th	13,757	78	3,841	5E+07	0.021	925
	25th	13,757	75	3,566	5E+07	0.019	859
	24th	13,757	72	3,300	5E+07	0.018	795
	23th	13,757	69	3,045	4E+07	0.017	733
	22th	13,757	66	2,799	4E+07	0.015	674
	21th	13,757	63	2,563	4E+07	0.014	617
	20th	13,757	60	2,337	3E+07	0.013	563
	19th	13,757	57	2,120	3E+07	0.012	511
	18th	13,827	54	1,914	3E+07	0.010	463
	17th	13,898	51	1,717	2E+07	0.009	418
	16th	13,898	48	1,531	2E+07	0.008	373
	15th	13,898	45	1,355	2E+07	0.007	330
	14th	13,898	42	1,189	2E+07	0.007	289
	13th	13,898	39	1,033	1E+07	0.006	251
	12th	13,898	36	888	1E+07	0.005	216
	11th	13,898	33	753	1E+07	0.004	183
	10th	13,898	30	628	9E+06	0.003	153
P	9th	42,086	27	515	2E+07	0.009	379
	8th	42,482	24	412	2E+07	0.007	306
	7th	42,482	21	320	1E+07	0.005	238
	6th	42,623	18	239	1E+07	0.004	178
	5th	42,765	15	169	7E+06	0.003	127
	4th	42,765	12	111	5E+06	0.002	83
	3th	42,765	9	64	3E+06	0.001	48
	2th	42,765	6	30	1E+06	0.001	22
	1th	42,765	3	8	3E+05	0.000	6
	Total	1,122,548			2,524,067,007	1	44,188

The same ELF base shear is obtained in the Y-direction.

A.5 Design demands from modal response spectrum analysis

In this section, the procedure of calculating the scaling factor and design demand will be shown. The design factors R, C_d, Ω_0, and I were taken from ASCE 7-16 with the values of 6, 5, 2.5, and 1.25 respectively, as shown in Table 3.2. The concept of RSA procedure is discussed in section 4.2. The reduced dynamic demand from RSA (Eq. (4.1) and (4.2)) procedure is obtained as shown in Figure A.3. The design demand forces of RSA procedure are obtained by scaling the reduced demand by the scaling factor, as shown in Figure A.4. The calculation of the scaling factor is shown in Table A.8. Floor displacements and drift ratios are computed by multiplying the elastic spectrum by C_d/R, as shown in Figure A.5.
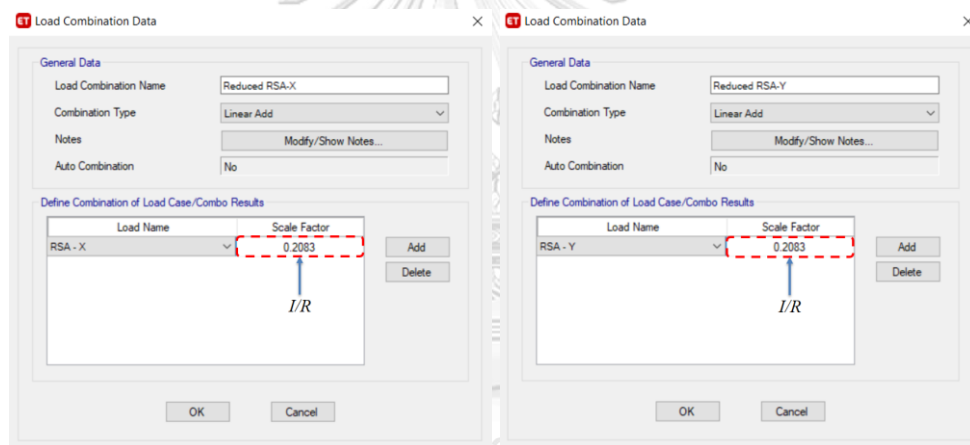
Figure A.3 Load combination in ETABS for obtaining the reduced dynamic seismic load of RSA procedure.

Table A.8 Calculation of scaling factor.

Direction	X-direction	Y-direction
V_{ELF}	44,188 kN	44,188 kN
$V_t = V_{dynamic} \times (I/R)$	19,532 kN	28,466 kN
$SF = 0.85\ V_{ELF} / V_t$	1.92	1.32
Design base shear of RSA	37,559 kN	37,559 kN

Note that V_t is obtained from the load combination shown in Figure A.3.
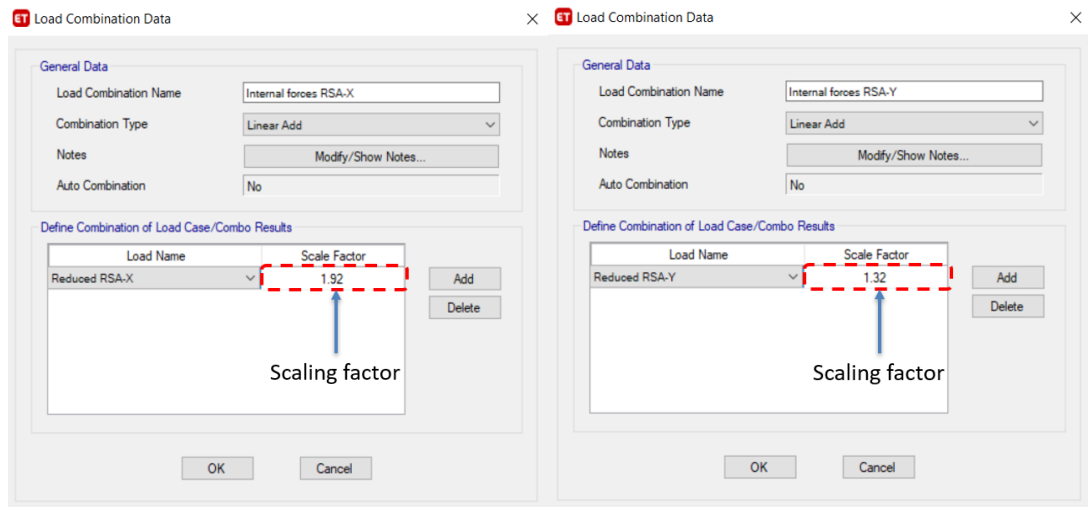
Figure A.4 load combination defined in ETABS for the scaled dynamic force.
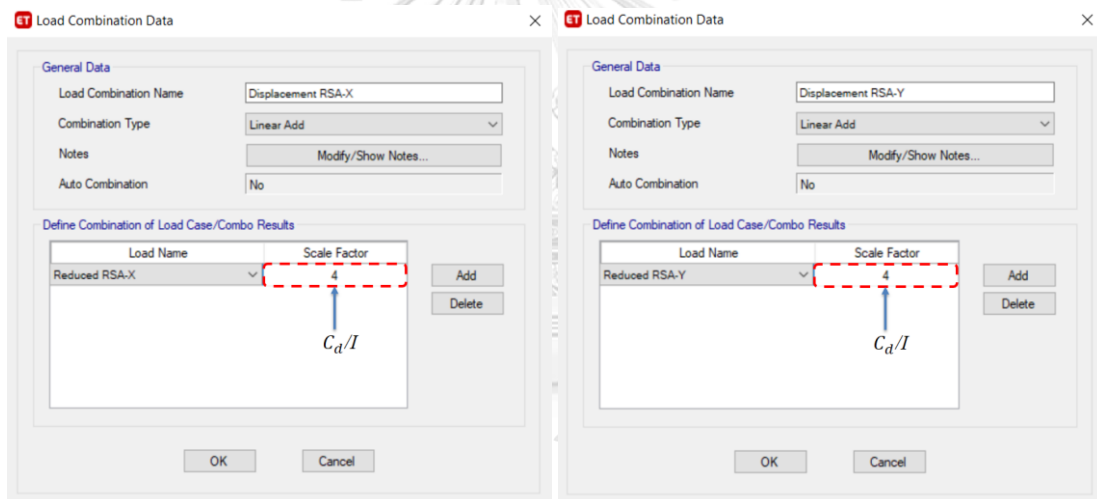
Figure A.5 load combination for predicting inelastic deformation.

A.6 Design story drift

The design story drift (Δ) is computed as the difference of the displacement (δ) at the centers of mass at the top and bottom of the story under consideration. The displacement at any level, used to compute the design story drift (Δ) shall be amplified by the factor C_d / I. In practice, it is more preferred to compute drift ratio using static lateral forces such as those from ELF procedure. If ELF seismic forces to be used for computing drift ratio, the lower bound of seismic response coefficient

($C_{s,min}$) need not be considered. In addition, seismic forces shall be computed using the fundamental period of structure without the upper limit (C_uT_a).

Table A.9 Inter-story drift ratio due to ELF seismic forces in the X-direction.

Story	Load Case/Combo	$U_x(\delta_i)$	$C_d\delta_i/I$	Story height	Story drift ratio (Δ)	Allowable story drift ratio (Δ_a)
		m	m	m		
Story36	ELF X - Drift	0.27	1.06	3	1.0%	1.5%
Story35	ELF X - Drift	0.26	1.04	3	1.0%	1.5%
Story34	ELF X - Drift	0.25	1.01	3	1.0%	1.5%
Story33	ELF X - Drift	0.24	0.97	3	1.0%	1.5%
Story32	ELF X - Drift	0.24	0.94	3	1.1%	1.5%
Story31	ELF X - Drift	0.23	0.91	3	1.1%	1.5%
Story30	ELF X - Drift	0.22	0.88	3	1.1%	1.5%
Story29	ELF X - Drift	0.21	0.85	3	1.1%	1.5%
Story28	ELF X - Drift	0.20	0.81	3	1.2%	1.5%
Story27	ELF X - Drift	0.19	0.78	3	1.2%	1.5%
Story26	ELF X - Drift	0.19	0.74	3	1.2%	1.5%
Story25	ELF X - Drift	0.18	0.71	3	1.2%	1.5%
Story24	ELF X - Drift	0.17	0.67	3	1.2%	1.5%
Story23	ELF X - Drift	0.16	0.63	3	1.2%	1.5%
Story22	ELF X - Drift	0.15	0.60	3	1.3%	1.5%
Story21	ELF X - Drift	0.14	0.56	3	1.3%	1.5%
Story20	ELF X - Drift	0.13	0.52	3	1.3%	1.5%
Story19	ELF X - Drift	0.12	0.48	3	1.3%	1.5%
Story18	ELF X - Drift	0.11	0.45	3	1.2%	1.5%
Story17	ELF X - Drift	0.10	0.41	3	1.2%	1.5%
Story16	ELF X - Drift	0.09	0.37	3	1.2%	1.5%
Story15	ELF X - Drift	0.08	0.34	3	1.2%	1.5%
Story14	ELF X - Drift	0.08	0.30	3	1.2%	1.5%
Story13	ELF X - Drift	0.07	0.27	3	1.1%	1.5%
Story12	ELF X - Drift	0.06	0.23	3	1.1%	1.5%
Story11	ELF X - Drift	0.05	0.20	3	1.0%	1.5%
Story10	ELF X - Drift	0.04	0.17	3	1.0%	1.5%
Story9	ELF X - Drift	0.04	0.14	3	0.9%	1.5%
Story8	ELF X - Drift	0.03	0.11	3	0.8%	1.5%
Story7	ELF X - Drift	0.02	0.09	3	0.7%	1.5%
Story6	ELF X - Drift	0.02	0.07	3	0.6%	1.5%
Story5	ELF X - Drift	0.01	0.05	3	0.6%	1.5%
Story4	ELF X - Drift	0.01	0.03	3	0.4%	1.5%
Story3	ELF X - Drift	0.00	0.02	3	0.3%	1.5%
Story2	ELF X - Drift	0.00	0.01	3	0.2%	1.5%
Story1	ELF X - Drift	0.00	0.00	3	0.1%	1.5%

Table A.10 Inter-story drift ratio due to ELF seismic forces in the Y-direction.

Story	Load Case/Combo	$U_y(\delta_i)$	$C_d\delta_i/I$	Story height	Story drift ratio (Δ)	Allowable story drift ratio (Δ_a)
		m	m	m		
Story36	ELF Y-Drift	0.25	0.99	3	1.2%	1.5%
Story35	ELF Y-Drift	0.24	0.96	3	1.2%	1.5%
Story34	ELF Y-Drift	0.23	0.92	3	1.2%	1.5%
Story33	ELF Y-Drift	0.22	0.89	3	1.2%	1.5%
Story32	ELF Y-Drift	0.21	0.85	3	1.2%	1.5%
Story31	ELF Y-Drift	0.20	0.82	3	1.2%	1.5%
Story30	ELF Y-Drift	0.19	0.78	3	1.2%	1.5%
Story29	ELF Y-Drift	0.19	0.74	3	1.2%	1.5%
Story28	ELF Y-Drift	0.18	0.71	3	1.2%	1.5%
Story27	ELF Y-Drift	0.17	0.67	3	1.2%	1.5%
Story26	ELF Y-Drift	0.16	0.64	3	1.2%	1.5%
Story25	ELF Y-Drift	0.15	0.60	3	1.2%	1.5%
Story24	ELF Y-Drift	0.14	0.56	3	1.2%	1.5%
Story23	ELF Y-Drift	0.13	0.53	3	1.2%	1.5%
Story22	ELF Y-Drift	0.12	0.49	3	1.2%	1.5%
Story21	ELF Y-Drift	0.11	0.46	3	1.1%	1.5%
Story20	ELF Y-Drift	0.11	0.42	3	1.1%	1.5%
Story19	ELF Y-Drift	0.10	0.39	3	1.1%	1.5%
Story18	ELF Y-Drift	0.09	0.36	3	1.1%	1.5%
Story17	ELF Y-Drift	0.08	0.33	3	1.0%	1.5%
Story16	ELF Y-Drift	0.07	0.29	3	1.0%	1.5%
Story15	ELF Y-Drift	0.07	0.26	3	1.0%	1.5%
Story14	ELF Y-Drift	0.06	0.23	3	0.9%	1.5%
Story13	ELF Y-Drift	0.05	0.21	3	0.9%	1.5%
Story12	ELF Y-Drift	0.04	0.18	3	0.9%	1.5%
Story11	ELF Y-Drift	0.04	0.15	3	0.8%	1.5%
Story10	ELF Y-Drift	0.03	0.13	3	0.8%	1.5%
Story9	ELF Y-Drift	0.03	0.11	3	0.7%	1.5%
Story8	ELF Y-Drift	0.02	0.09	3	0.6%	1.5%
Story7	ELF Y-Drift	0.02	0.07	3	0.6%	1.5%
Story6	ELF Y-Drift	0.01	0.05	3	0.5%	1.5%
Story5	ELF Y-Drift	0.01	0.04	3	0.4%	1.5%
Story4	ELF Y-Drift	0.01	0.02	3	0.3%	1.5%
Story3	ELF Y-Drift	0.00	0.01	3	0.3%	1.5%
Story2	ELF Y-Drift	0.00	0.01	3	0.2%	1.5%
Story1	ELF Y-Drift	0.00	0.00	3	0.1%	1.5%

A.7 Amplification of accidental torsion

Accidental torsion is caused by displacement of the center of mass each way from its actual location by a distance equal to 5 percent of the dimension of the structure perpendicular to the direction of the applied forces. Accidental torsion should be amplified if the value of A_x shown in figure below is greater than 1. The ELF seismic forces are used for checking accidental torsion effect.

$$\delta_{avg} = \frac{\delta_A + \delta_B}{2}; \qquad A_x = \left[\frac{\delta_{max}}{1.2\delta_{avg}}\right]^2$$
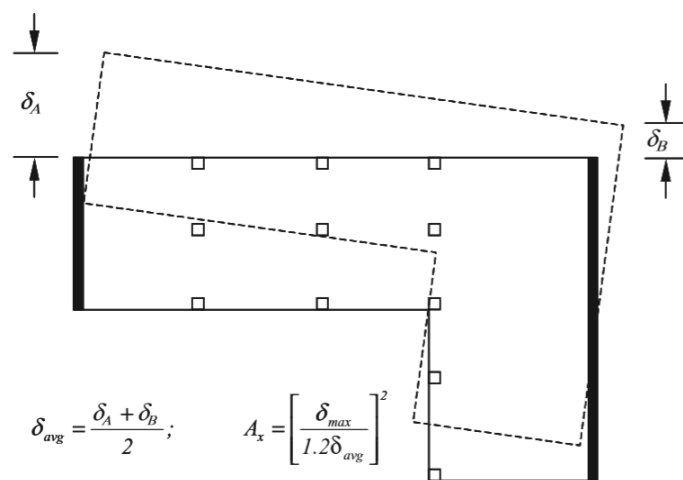
Figure A.6 Torsional amplification factor.
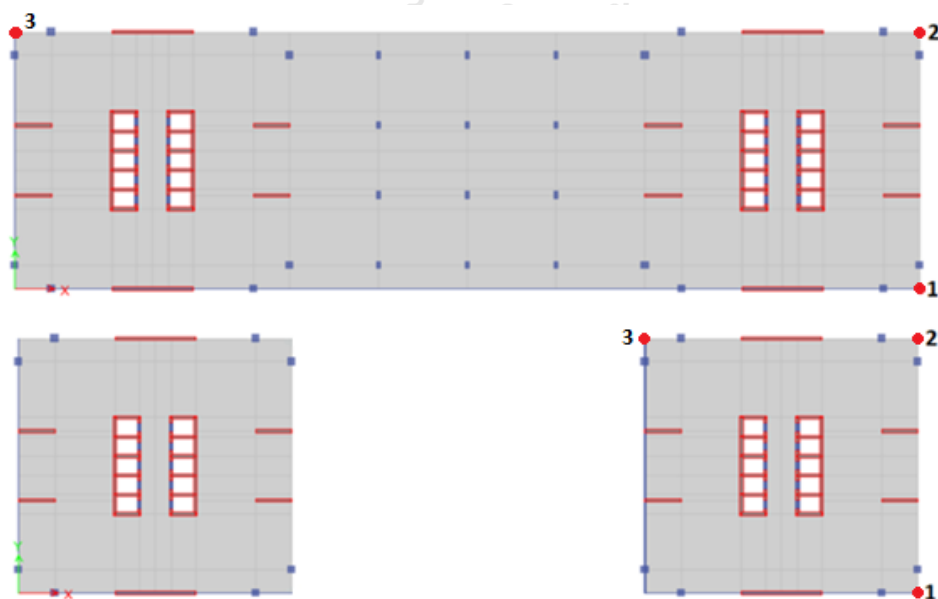
Figure A.7 Selected joints for checking accidental torsion.

Table A.11 Calculation of torsional amplification factor for earthquake along X-axis.

Story	Load Case/Combo	δ_1 m	δ_2 m	δ_{max} m	δ_{avg} m	Ax
36	ELF X+ecc	0.93	0.99	0.99	0.96	0.74
35	ELF X+ecc	0.91	0.97	0.97	0.94	0.74
34	ELF X+ecc	0.88	0.94	0.94	0.91	0.74
33	ELF X+ecc	0.85	0.91	0.91	0.88	0.74
32	ELF X+ecc	0.83	0.88	0.88	0.85	0.74
31	ELF X+ecc	0.80	0.85	0.85	0.83	0.74
30	ELF X+ecc	0.77	0.82	0.82	0.80	0.74
29	ELF X+ecc	0.74	0.79	0.79	0.77	0.74
28	ELF X+ecc	0.71	0.76	0.76	0.74	0.74
27	ELF X+ecc	0.68	0.73	0.73	0.71	0.74
26	ELF X+ecc	0.65	0.70	0.70	0.67	0.74
25	ELF X+ecc	0.62	0.66	0.66	0.64	0.74
24	ELF X+ecc	0.59	0.63	0.63	0.61	0.74
23	ELF X+ecc	0.56	0.59	0.59	0.58	0.74
22	ELF X+ecc	0.52	0.56	0.56	0.54	0.74
21	ELF X+ecc	0.49	0.52	0.52	0.51	0.74
20	ELF X+ecc	0.46	0.49	0.49	0.47	0.74
19	ELF X+ecc	0.43	0.45	0.45	0.44	0.74
18	ELF X+ecc	0.39	0.42	0.42	0.41	0.73
17	ELF X+ecc	0.36	0.38	0.38	0.37	0.73
16	ELF X+ecc	0.33	0.35	0.35	0.34	0.73
15	ELF X+ecc	0.30	0.31	0.31	0.31	0.73
14	ELF X+ecc	0.27	0.28	0.28	0.27	0.73
13	ELF X+ecc	0.24	0.25	0.25	0.24	0.72
12	ELF X+ecc	0.21	0.21	0.21	0.21	0.72
11	ELF X+ecc	0.18	0.18	0.18	0.18	0.72
10	ELF X+ecc	0.15	0.16	0.16	0.15	0.71
9	ELF X+ecc	0.13	0.13	0.13	0.13	0.71
8	ELF X+ecc	0.10	0.10	0.10	0.10	0.70
7	ELF X+ecc	0.08	0.08	0.08	0.08	0.70
6	ELF X+ecc	0.06	0.06	0.06	0.06	0.70
5	ELF X+ecc	0.04	0.04	0.04	0.04	0.70
4	ELF X+ecc	0.03	0.03	0.03	0.03	0.70
3	ELF X+ecc	0.02	0.02	0.02	0.02	0.70
2	ELF X+ecc	0.01	0.01	0.01	0.01	0.70
1	ELF X+ecc	0.00	0.00	0.00	0.00	0.70

Table A.12 Calculation of torsional amplification factor for earthquake along Y-axis.

Story	Load Case/Combo	δ_3 m	δ_2 m	δ_{max} m	δ_{avg} m	Ax
36	ELF Y+ecc	0.74	0.81	0.81	0.77	0.75
35	ELF Y+ecc	0.71	0.78	0.78	0.75	0.76
34	ELF Y+ecc	0.69	0.75	0.75	0.72	0.76
33	ELF Y+ecc	0.66	0.72	0.72	0.69	0.76
32	ELF Y+ecc	0.63	0.69	0.69	0.66	0.76
31	ELF Y+ecc	0.61	0.66	0.66	0.64	0.76
30	ELF Y+ecc	0.58	0.64	0.64	0.61	0.76
29	ELF Y+ecc	0.55	0.61	0.61	0.58	0.76
28	ELF Y+ecc	0.53	0.58	0.58	0.55	0.76
27	ELF Y+ecc	0.50	0.55	0.55	0.52	0.76
26	ELF Y+ecc	0.47	0.52	0.52	0.50	0.76
25	ELF Y+ecc	0.45	0.49	0.49	0.47	0.76
24	ELF Y+ecc	0.42	0.46	0.46	0.44	0.76
23	ELF Y+ecc	0.39	0.43	0.43	0.41	0.76
22	ELF Y+ecc	0.37	0.40	0.40	0.38	0.76
21	ELF Y+ecc	0.34	0.37	0.37	0.36	0.76
20	ELF Y+ecc	0.32	0.35	0.35	0.33	0.76
19	ELF Y+ecc	0.29	0.32	0.32	0.30	0.76
18	ELF Y+ecc	0.27	0.29	0.29	0.28	0.75
17	ELF Y+ecc	0.24	0.26	0.26	0.25	0.75
16	ELF Y+ecc	0.22	0.24	0.24	0.23	0.75
15	ELF Y+ecc	0.20	0.21	0.21	0.21	0.75
14	ELF Y+ecc	0.18	0.19	0.19	0.18	0.74
13	ELF Y+ecc	0.16	0.17	0.17	0.16	0.74
12	ELF Y+ecc	0.14	0.14	0.14	0.14	0.73
11	ELF Y+ecc	0.12	0.12	0.12	0.12	0.73
10	ELF Y+ecc	0.10	0.10	0.10	0.10	0.72
9	ELF Y+ecc	0.08	0.09	0.09	0.08	0.75
8	ELF Y+ecc	0.07	0.07	0.07	0.07	0.74
7	ELF Y+ecc	0.05	0.06	0.06	0.05	0.74
6	ELF Y+ecc	0.04	0.04	0.04	0.04	0.74
5	ELF Y+ecc	0.03	0.03	0.03	0.03	0.74
4	ELF Y+ecc	0.02	0.02	0.02	0.02	0.74
3	ELF Y+ecc	0.01	0.01	0.01	0.01	0.74
2	ELF Y+ecc	0.01	0.01	0.01	0.01	0.74
1	ELF Y+ecc	0.00	0.00	0.00	0.00	0.74

A.8 P-Delta effect

In P-Delta effect checking, the stability ratio (θ) is computed for each story by

$$\theta = \frac{P_x \Delta I_e}{V_x h_{sx} C_d}$$

where P_x is the total unfactored design gravity load at level x, Δ is the design story drift, I is the importance factor, V_x is the shear force at level x, h_{sx} is the story height, C_d is the deflection amplification factor.

There are three cases to check with stability ratio

1) if $\theta \leq 0.1$, P-Delta effect is not required

2) $\theta < 0.1 \leq \theta_{max}$, P-Delta should be considered by multiplying displacement and member forces by $1/1-\theta$

3) $\theta > \theta_{max}$, structure is unstable and shall be redesigned

$\theta_{max} = \frac{0.5}{\beta C_d} \leq 0.25$, where β is the ratio of shear demand to shear capacity. This ratio is conservatively taken as 1.0, but it was taken into account in this section. The ELF procedure described in section A.6 for computing design drift was also used for checking P-Delta effect. The P-Delta effect is taken into account in computing design story drift in section A.6, while the design story drift in this section is obtained without including the effect of P-Delta. Hence, there is a slight difference in design story drift and lateral forces in this section and in section A.6. As shown in Table A.13 and A.14, stability ratio exceeds 0.1 in mid-height regions. Therefore, P-Delta effect should be included in the structural model.

Table A.13 Checking of P-Delta effect in X-direction.

Level	Height (m)	V_x (kN)	P_x (kN)	Δ_i (m)	θ	θ_{max}	Check if $\theta < 0.1$
36th	3	448	10,804	0.028	0.06	0.25	ok
35th	3	935	25,205	0.028	0.06	0.25	ok
34th	3	1,394	39,605	0.029	0.07	0.25	ok
33th	3	1,827	54,006	0.029	0.07	0.25	ok
32th	3	2,234	68,406	0.030	0.08	0.25	ok
31th	3	2,616	82,807	0.030	0.08	0.25	ok
30th	3	2,973	97,208	0.031	0.08	0.25	ok
29th	3	3,307	111,608	0.032	0.09	0.25	ok
28th	3	3,619	126,009	0.032	0.09	0.25	ok
27th	3	3,910	140,409	0.033	0.10	0.25	ok
26th	3	4,182	154,951	0.034	0.10	0.25	Modify
25th	3	4,432	169,493	0.034	0.11	0.25	Modify
24th	3	4,664	184,035	0.034	0.11	0.25	Modify
23th	3	4,876	198,577	0.035	0.12	0.25	Modify
22th	3	5,070	213,119	0.035	0.12	0.25	Modify
21th	3	5,247	227,661	0.035	0.13	0.25	Modify
20th	3	5,408	242,203	0.035	0.13	0.25	Modify
19th	3	5,553	256,745	0.035	0.13	0.25	Modify
18th	3	5,684	271,287	0.035	0.14	0.25	Modify
17th	3	5,801	285,971	0.034	0.14	0.25	Modify
16th	3	5,905	300,654	0.034	0.14	0.25	Modify
15th	3	5,996	315,337	0.033	0.14	0.25	Modify
14th	3	6,075	330,021	0.032	0.14	0.25	Modify
13th	3	6,144	344,704	0.031	0.14	0.25	Modify
12th	3	6,202	359,387	0.030	0.14	0.25	Modify
11th	3	6,252	374,071	0.028	0.14	0.25	Modify
10th	3	6,292	388,754	0.027	0.14	0.25	Modify
9th	3	12,684	821,858	0.025	0.13	0.25	Modify
8th	3	12,763	866,999	0.023	0.13	0.25	Modify
7th	3	12,824	912,141	0.020	0.12	0.25	Modify
6th	3	12,868	957,282	0.018	0.11	0.25	Modify
5th	3	12,900	1,002,707	0.015	0.10	0.25	Modify
4th	3	12,920	1,048,131	0.013	0.09	0.25	ok
3th	3	12,931	1,093,555	0.010	0.07	0.25	ok
2th	3	12,936	1,138,980	0.006	0.04	0.25	ok
1th	3	12,937	1,184,404	0.002	0.02	0.25	ok

Table A.14 Checking of P-Delta effect in Y-direction.

Level	Height (m)	V_y (kN)	P_x (kN)	Δ_i (m)	θ	θ_{max}	Check if $\theta < 0.1$
36th	3	505	10,804	0.034	0.06	0.25	ok
35th	3	1,054	25,205	0.034	0.07	0.25	ok
34th	3	1,572	39,605	0.034	0.07	0.25	ok
33th	3	2,060	54,006	0.034	0.07	0.25	ok
32th	3	2,519	68,406	0.034	0.08	0.25	ok
31th	3	2,950	82,807	0.034	0.08	0.25	ok
30th	3	3,353	97,208	0.034	0.08	0.25	ok
29th	3	3,730	111,608	0.034	0.09	0.25	ok
28th	3	4,082	126,009	0.034	0.09	0.25	ok
27th	3	4,410	140,409	0.034	0.09	0.25	ok
26th	3	4,716	154,951	0.034	0.09	0.25	ok
25th	3	4,999	169,493	0.034	0.10	0.25	ok
24th	3	5,260	184,035	0.034	0.10	0.25	ok
23th	3	5,499	198,577	0.033	0.10	0.25	Modify
22th	3	5,718	213,119	0.033	0.10	0.25	Modify
21th	3	5,918	227,661	0.032	0.10	0.25	Modify
20th	3	6,099	242,203	0.032	0.11	0.24	Modify
19th	3	6,263	256,745	0.031	0.11	0.23	Modify
18th	3	6,410	271,287	0.031	0.11	0.23	Modify
17th	3	6,542	285,971	0.030	0.11	0.22	Modify
16th	3	6,659	300,654	0.029	0.11	0.22	Modify
15th	3	6,762	315,337	0.028	0.11	0.22	Modify
14th	3	6,852	330,021	0.027	0.11	0.21	Modify
13th	3	6,929	344,704	0.026	0.11	0.21	Modify
12th	3	6,995	359,387	0.024	0.10	0.21	Modify
11th	3	7,051	374,071	0.023	0.10	0.20	Modify
10th	3	7,096	388,754	0.021	0.10	0.19	ok
9th	3	14,305	821,858	0.020	0.06	0.18	ok
8th	3	14,394	866,999	0.018	0.07	0.16	ok
7th	3	14,463	912,141	0.016	0.07	0.14	ok
6th	3	14,513	957,282	0.014	0.07	0.13	ok
5th	3	14,548	1,002,707	0.012	0.08	0.12	ok
4th	3	14,571	1,048,131	0.010	0.08	0.11	ok
3th	3	14,584	1,093,555	0.007	0.08	0.11	ok
2th	3	14,589	1,138,980	0.005	0.09	0.10	ok
1th	3	14,591	1,184,404	0.002	0.09	0.10	ok

A.9 Designed section of SH building

The design of structural members was done using all factored load combinations including gravity loads, wind loads, and earthquake loads from RSA procedure. The accidental torsional effect was considered in the design process, by shifting the center of mass with a distance of 5 percent of structure dimension, perpendicular to the earthquake motion. The design process leads to minimum reinforcement requirements in most of structural members, while the design of the remaining members was governed by the gravity loads. The designed columns cross-sections are shown in Table A.15.
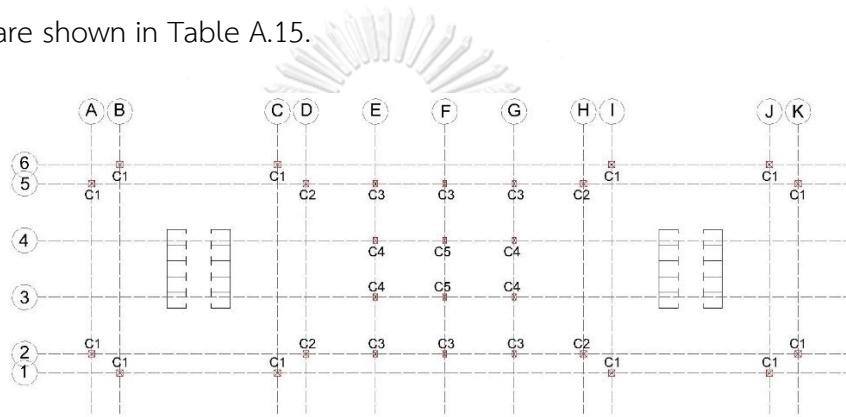
Figure A.8 Denotation of designed columns cross-sections.

Table A.15 Steel reinforcement of columns.

Story / Column	Story1	Story2	Story3	Story4-9	Story10-36
C1	28DB22	28DB22	28DB22	28DB22	28DB22
C2	28DB36	32DB28	28DB25		
C3	30DB16	30DB16			
C4	24DB36	28DB25	30DB16	30DB16	
C5	20DB36	28DB22			

The percentage of vertical steel reinforcement ($\rho = \dfrac{A_s}{A_c} \times 100$) used in walls is shown in Table A.16. The walls' names shown in Table A.16 are indicated in Figure A.9.
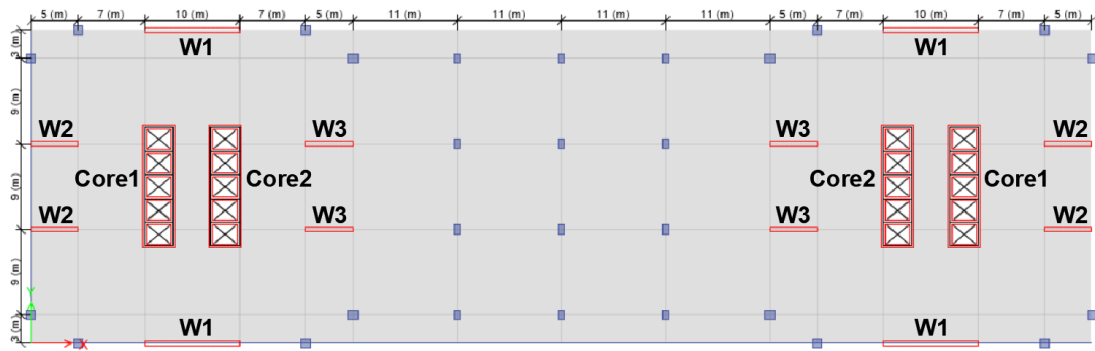
Figure A.9 Designed RC walls denotation.

Table A.16 Percentage of used vertical steel reinforcement in RC walls.

Floor	Walls thickness (cm)	Percentage of vertical reinforcement			
		Cores	W1	W2	W3
1				0.653	2.21
2					1.69
3	50		0.306	0.320	1.044
4					0.423
5-6					0.311
7-9	45	0.284	0.256	0.261	0.261
10-18	40		0.288	0.294	0.294
19-27	35		0.330	0.336	0.336
28-33			0.385		
34-35	30		0.510	0.392	0.392
36			1.292		

A.10 Structural irregularities

Irregularities are generally classified in two major categories: horizontal and vertical irregularities (ASCE 7-16). The first type is related to in-plan asymmetric building causing a substantial increase of torsional effects, and the second type involves variation of geometrical or structural properties along the height of the building leading to increase of the seismic demand in specific story.

A.10.1 Horizontal structural irregularities

1. Torsional irregularity (Type 1a)

Torsional irregularity shall be considered to exists when the maximum story drift, computed including accidental torsion, at one end of the structure transverse to an axis is more than 1.2 times the average of the story drifts of the two ends of the structure $(\delta_{\max} > 1.2\delta_{avg})$. Since, the torsional amplification factor (A_x) computed in section A.7 is smaller than 1, torsional irregularity does not exist.

2. Reentrant corner irregularity (Type 2)

Plan configurations of a structure and its lateral-force resisting system contain reentrant corners, where both projections of the structure beyond a re-entrant corner are greater than 15 percent of the plan dimension of the structure in the given direction. Since the plane layout is rectangular (no corners), re-entrant corner irregularity does not exist in the studied buildings.
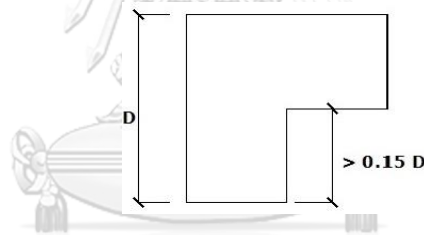
Figure A.10 Plan configuration of reentrant corner irregularity.

3. Diaphragm discontinuity irregularity (Type 3)

When a diaphragm has an opining greater than 50% of diaphragm area, or when there is a change in diaphragm stiffness of more than 50%, diaphragm discontinuity irregularity exits, as shown in Figure A.11. The diaphragm discontinuity irregularity does not exist in the studied buildings.
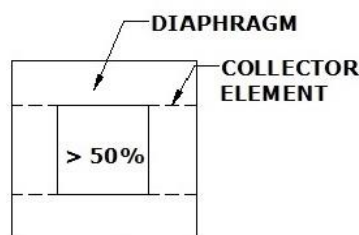
Figure A.11 Plan configuration of diaphragm discontinuity irregularity.

4. Out-of-plane offset irregularity (Type 4)

Defined to exist where there is a discontinuity in a lateral force-resistance path, such as an out-of-plane offset of at least one of the vertical elements, as shown in Figure A.12. The out-of-plane offset irregularity does not exist in the studied buildings.
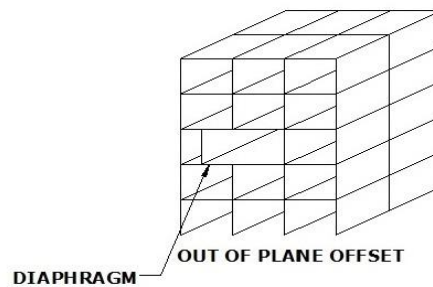
Figure A.12 Out-of-palne offset irregularity.

5. Nonparallel system irregularity (Type 5)

Defined to exist where vertical lateral force-resisting elements are not parallel to the major orthogonal axes of the seismic force-resisting system, as shown in Figure A.13. The nonparallel system irregularity does not exist in the studied buildings.

Figure A.13 Plan configuration of nonparallel system irregularity.

A.10.2 Vertical structural irregularities

1. Stiffness-soft story irregularity (Type 1a)

Defined to exist where there is a story in which the lateral stiffness is less than 70% of that in the story above or less than 80% of the average stiffness of the three stories above. The stiffness-soft story irregularity does not exist in the SH building, as shown in Table A.17.

Table A.17 Checking stiffness soft story irregularity along X-direction.

Floor	Load case	K_x (kN/m)	k_i/k_{i+1}	Check	$k_i/((k_{i+1...3})/3)$	Check
Story1	ELF X	22,159,251	205%	Regular	309%	Regular
Story2	ELF X	10,816,273	174%	Regular	227%	Regular
Story3	ELF X	6,222,206	139%	Regular	169%	Regular
Story4	ELF X	4,477,694	126%	Regular	146%	Regular
Story5	ELF X	3,566,350	119%	Regular	134%	Regular
Story6	ELF X	3,005,291	115%	Regular	128%	Regular
Story7	ELF X	2,620,008	112%	Regular	145%	Regular
Story8	ELF X	2,330,255	110%	Regular	175%	Regular
Story9	ELF X	2,118,325	218%	Regular	233%	Regular
Story10	ELF X	971,419	107%	Regular	114%	Regular
Story11	ELF X	906,148	107%	Regular	112%	Regular
Story12	ELF X	850,679	106%	Regular	111%	Regular
Story13	ELF X	805,736	105%	Regular	109%	Regular
Story14	ELF X	767,979	104%	Regular	108%	Regular
Story15	ELF X	735,573	104%	Regular	108%	Regular
Story16	ELF X	707,199	104%	Regular	107%	Regular
Story17	ELF X	681,845	104%	Regular	107%	Regular
Story18	ELF X	658,682	103%	Regular	107%	Regular
Story19	ELF X	636,982	103%	Regular	107%	Regular
Story20	ELF X	616,355	103%	Regular	107%	Regular
Story21	ELF X	596,328	103%	Regular	107%	Regular
Story22	ELF X	576,685	104%	Regular	108%	Regular
Story23	ELF X	556,813	104%	Regular	108%	Regular
Story24	ELF X	536,266	104%	Regular	109%	Regular
Story25	ELF X	514,588	105%	Regular	111%	Regular
Story26	ELF X	491,311	105%	Regular	112%	Regular
Story27	ELF X	465,947	106%	Regular	115%	Regular
Story28	ELF X	438,268	107%	Regular	118%	Regular
Story29	ELF X	408,123	109%	Regular	122%	Regular
Story30	ELF X	374,273	111%	Regular	129%	Regular
Story31	ELF X	336,105	115%	Regular	139%	Regular
Story32	ELF X	292,972	120%	Regular	156%	Regular
Story33	ELF X	244,334	129%	Regular	192%	Regular
Story34	ELF X	189,779	147%	Regular	-	-
Story35	ELF X	129,124	206%	Regular	-	-
Story36	ELF X	62,565	-	-	-	-

2. Weight (mass) irregularity (Type 2)

Defined to exist where the effective mass of any story is more than 150% of the effective mass of an adjacent story. The mass irregularity exists in SH building, as shown in Table A.18.

Table A.18 Checking weight (Mass) irregularity.

Floor	Weight (kN)	w_i/w_{i+1}	Status
Story1	42,765	100%	Regular
Story2	42,765	100%	Regular
Story3	42,765	100%	Regular
Story4	42,765	100%	Regular
Story5	42,765	100%	Regular
Story6	42,623	100%	Regular
Story7	42,482	100%	Regular
Story8	42,482	101%	Regular
Story9	42,086	303%	Irregular
Story10	13,898	100%	Regular
Story11	13,898	100%	Regular
Story12	13,898	100%	Regular
Story13	13,898	100%	Regular
Story14	13,898	100%	Regular
Story15	13,898	100%	Regular
Story16	13,898	100%	Regular
Story17	13,898	101%	Regular
Story18	13,827	101%	Regular
Story19	13,757	100%	Regular
Story20	13,757	100%	Regular
Story21	13,757	100%	Regular
Story22	13,757	100%	Regular
Story23	13,757	100%	Regular
Story24	13,757	100%	Regular
Story25	13,757	100%	Regular
Story26	13,757	101%	Regular
Story27	13,686	101%	Regular
Story28	13,615	100%	Regular
Story29	13,615	100%	Regular
Story30	13,615	100%	Regular
Story31	13,615	100%	Regular
Story32	13,615	100%	Regular
Story33	13,615	100%	Regular
Story34	13,615	100%	Regular
Story35	13,615	115%	Regular
Story36	11,862	-	-

3. Vertical geometric irregularity (Type 3)

Defined to exist where the horizontal dimension of the seismic force-resisting system in any story is more than 130% of that in an adjacent story, as shown in Figure A.14. This type of irregularity does not exist in the seismic force-resisting system. However, the studied buildings should be considered to have a vertical geometric irregularity, due to their 3D layout, which is two towers sharing a common podium.
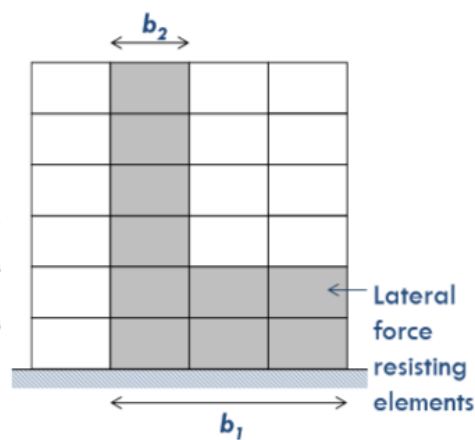
Figure A.14 Vertical geometric irregularity.

4. In-plane discontinuity irregularity (Type 4)

Define to exist where there is an in-plane offset of the vertical seismic force resisting system. The lateral force resisting system in the studied buildings are continuous over the height without in plane offset. Therefore, vertical structural irregularity type 4 does not exist.
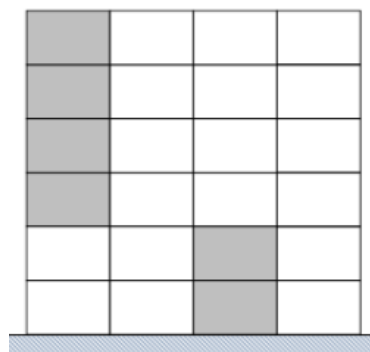
Figure A.15 In-plane discontinuity in vertical lateral force-resisting element.

The tables below show a summary of irregularities in building SH, where SH building is considered as vertically irregular (type 2 and 3) while horizontally regular. For DH building same irregularities are present, in addition to horizontal irregularity type 1a. Refer to ASCE 7-16 for other irregularities presented in the tables A.19 and A.20, and not discussed in this section.

Table A.19 Summary of horizontal structural irregularity in building SH.

Irregularity type	X-direction		Y-direction	
	Regular	Irregular	Regular	Irregular
Type 1a	✓	-	✓	-
Type 1b	✓	-	✓	-
Type 2	✓	-	✓	-
Type 3	✓	-	✓	-
Type 4	✓	-	✓	-
Type 5	✓	-	✓	-

Table A.20 Summary of vertical structural irregularity in building SH.

Irregularity type	X-direction		Y-direction	
	Regular	Irregular	Regular	Irregular
Type 1a	✓	-	✓	-
Type 1b	✓	-	✓	-
Type 2	-	✓	-	✓
Type 3	-	✓	-	✓
Type 4	✓	-	✓	-
Type 5a	✓	-	✓	-
Type 5b	✓	-	✓	-

A.11 Diaphragm demand forces

In this section, the procedure for obtaining the diaphragm demand forces from ETABS is discussed. In ETABS, the user can display the slab stress due to any kind of loads. However, it is more preferred to obtain the demand forces in terms of

a unit force, and not in terms of stress. The procedure for obtaining diaphragm internal forces is as follow:

1) Select slab elements and node at the cut line, then assign these objects into group as shown in Figure A.16 (do not assign any other elements such as walls and columns).

2) Define a section cut by selecting the previously defined group, as shown in Figure A.17.
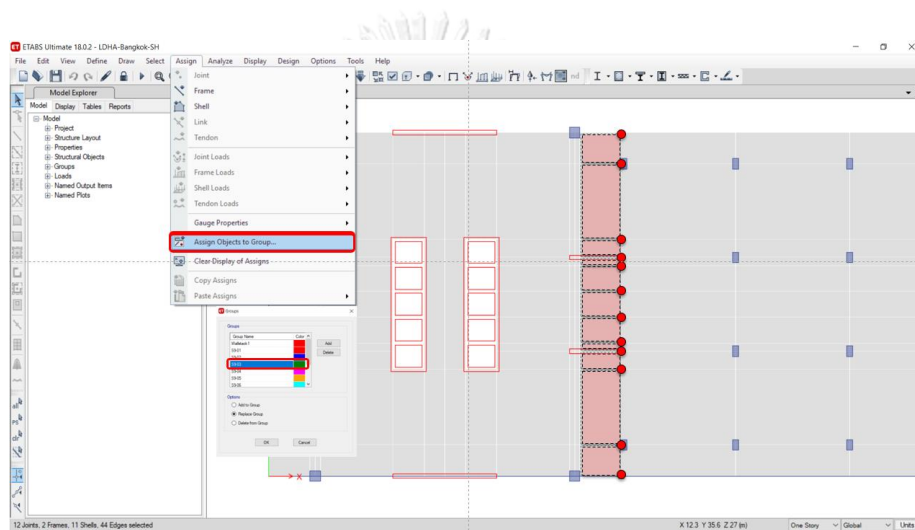
Figure A.16 Assigning slab elements and node into group.
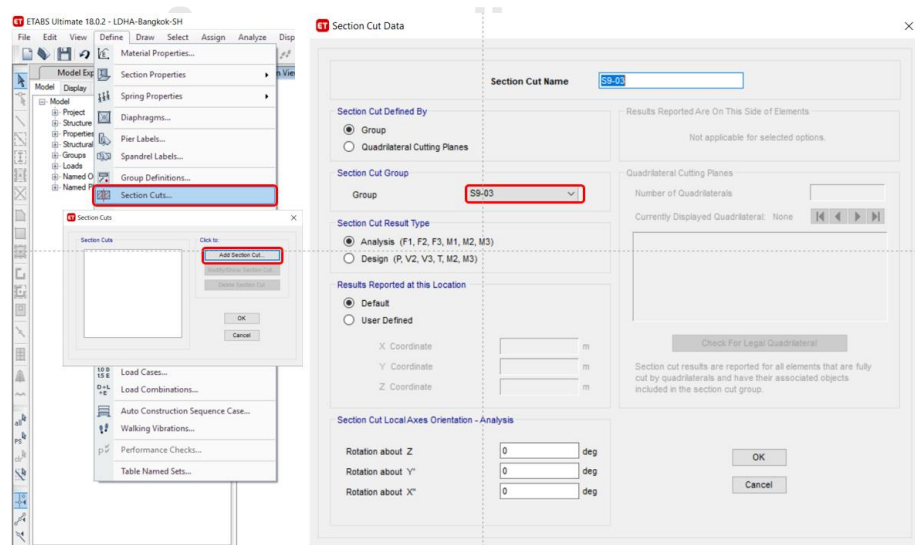
Figure A.17 Defining section cut for the previously defined section cut group.
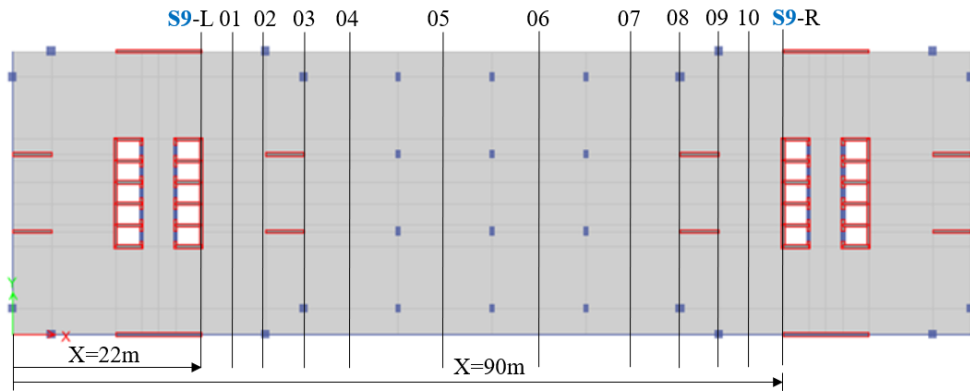
Figure A.18 Section-cut locations.
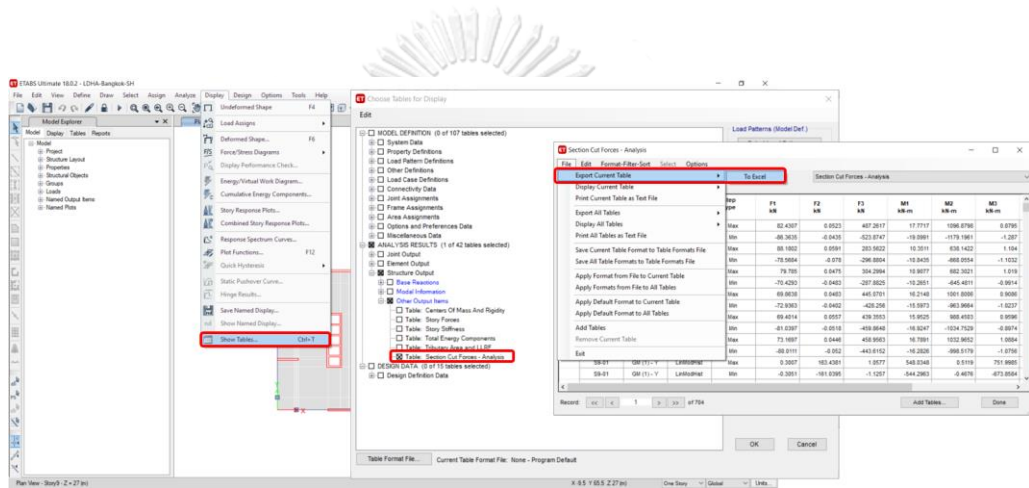
Figure A.19 Exporting results from ETABS.

Figure A.20 Rearranging results in excel (highlighted columns refer to in-plane shear and bending moment due to earthquake in the Y-direction).

APPENDIX B

LINEAR RESPONSE SPECTRUM ANALYSIS AND LINEAR RESPONSE HISTORY ANALYSIS

B.1 Vertical element forces

In this section, walls and columns forces obtained from LRSA and LRHA are presented for the two-buildings located in Bangkok and Chiang Mai. Due to symmetrical response in both towers in building SH, and symmetry of structural configuration in towers, some of the structural elements are sharing the same demand forces. For example, walls denoted in Figure B.1 as W1 are experiencing the same demand forces. Therefore, the results presented below may describes several structural elements at same time. In every building, structural elements that share the same demand force are denoted by the same name, as shown in Figures B.1 and B.2.
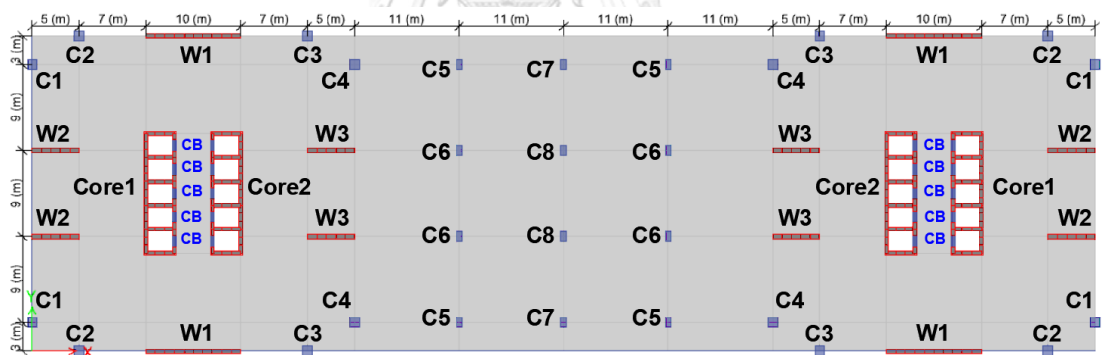
Figure B.1 Denotation of vertical members in building SH.
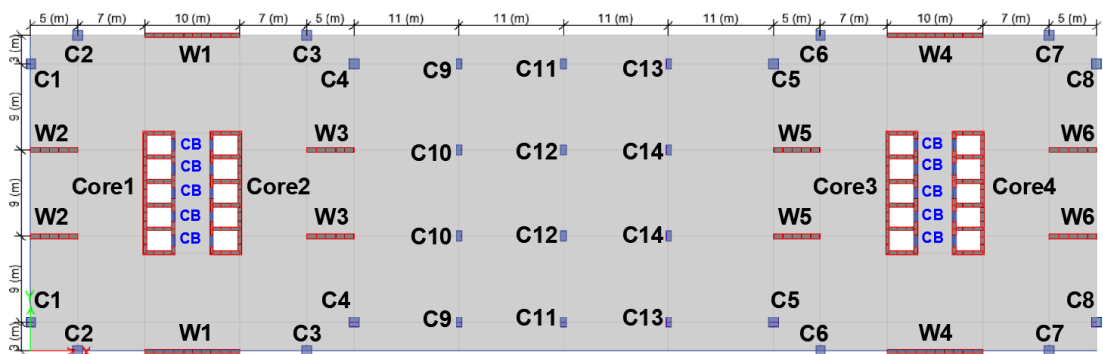
Figure B.2 Denotation of vertical members in building DH.

B.1.1 Wall forces
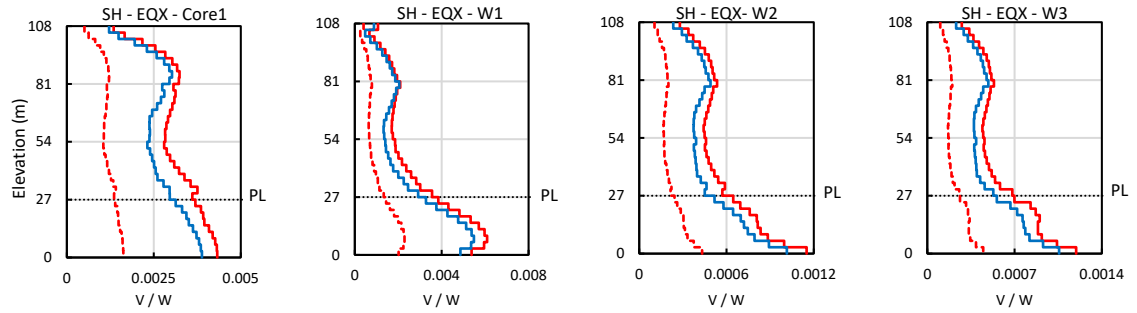
(a) Wall shear forces due to EQX
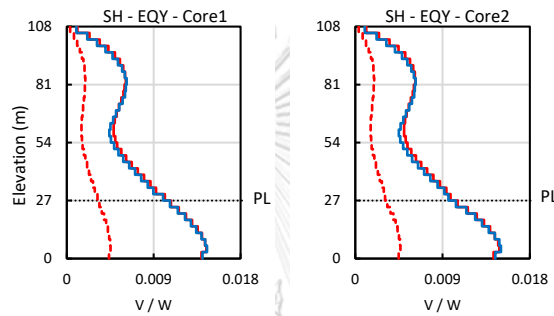
(b) Wall shear forces due to EQY

(c) Wall bending moment due to EQX

(d) Wall bending moment due to EQY

- - - - RSA ——— LRSA ——— LRHA
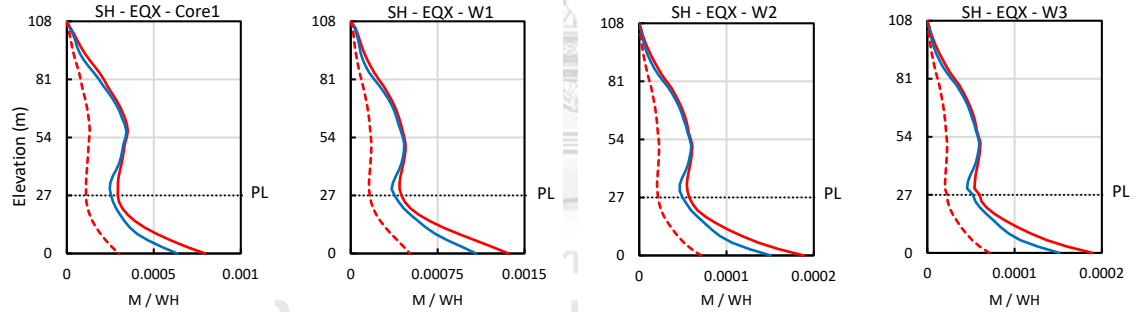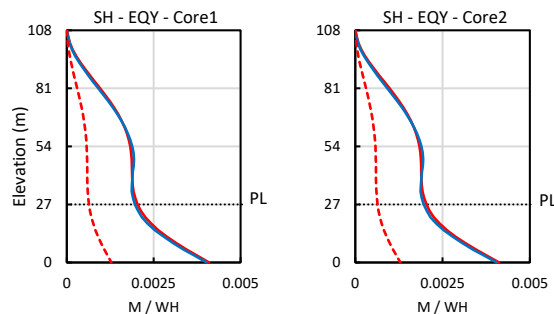
Figure B.3 Wall shear forces and bending moment of building SH located in Bangkok due to earthquake in X- and Y-direction.

(a) Wall shear forces due to EQX
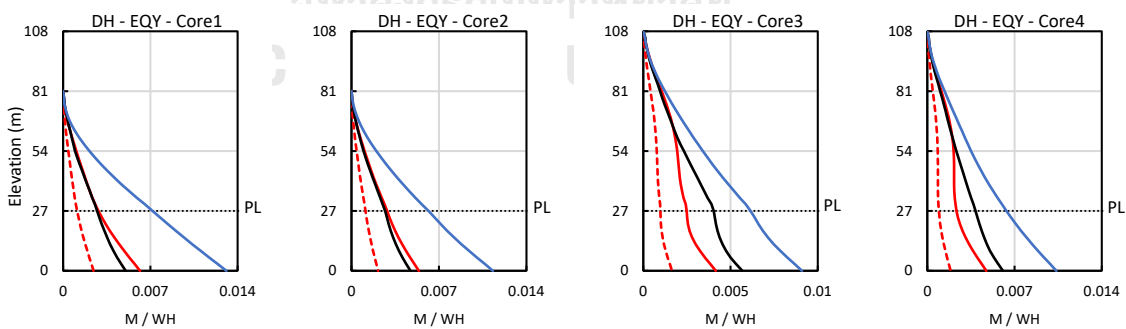
(b) Wall shear forces due to EQY

------- RSA ——— LRSA ——— LRHA
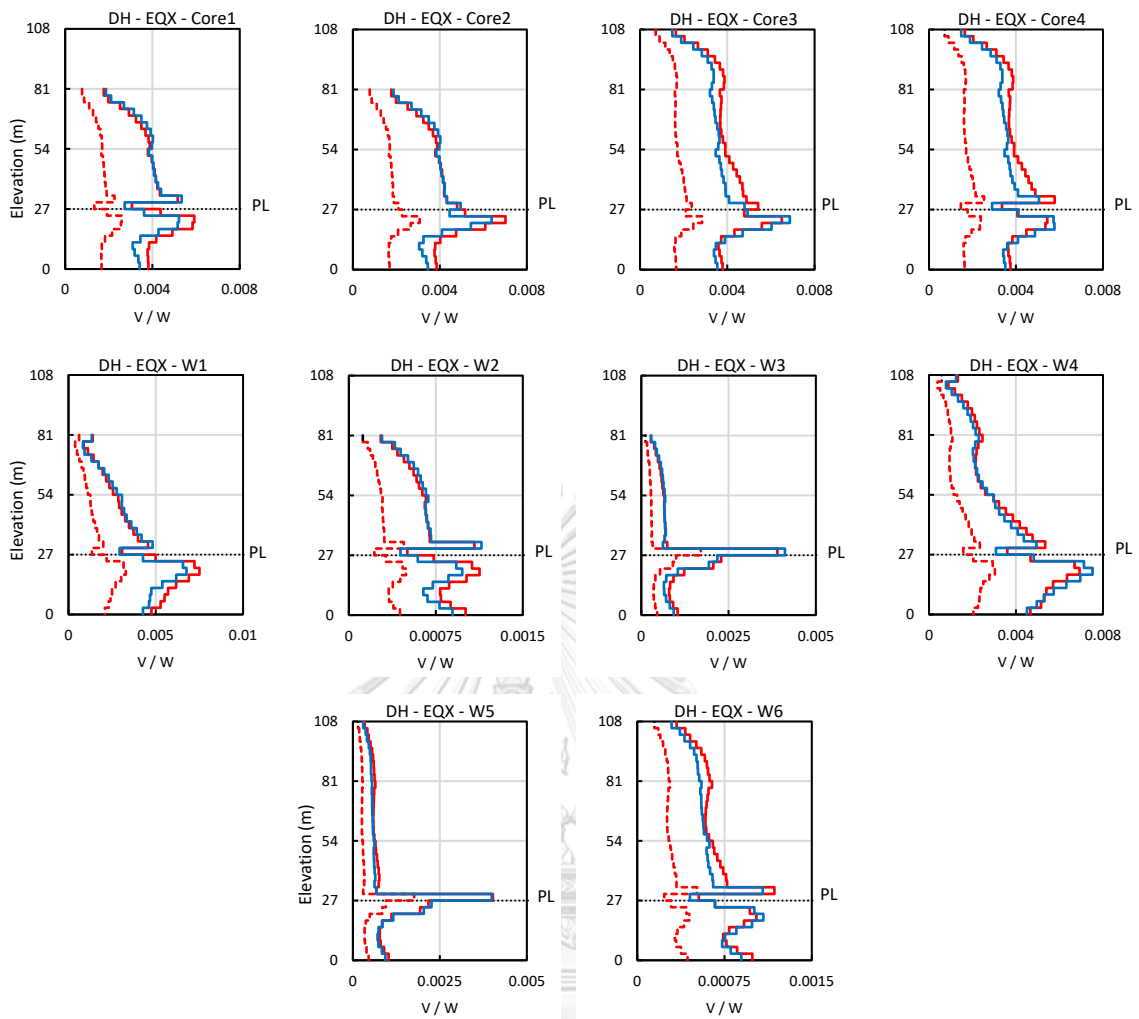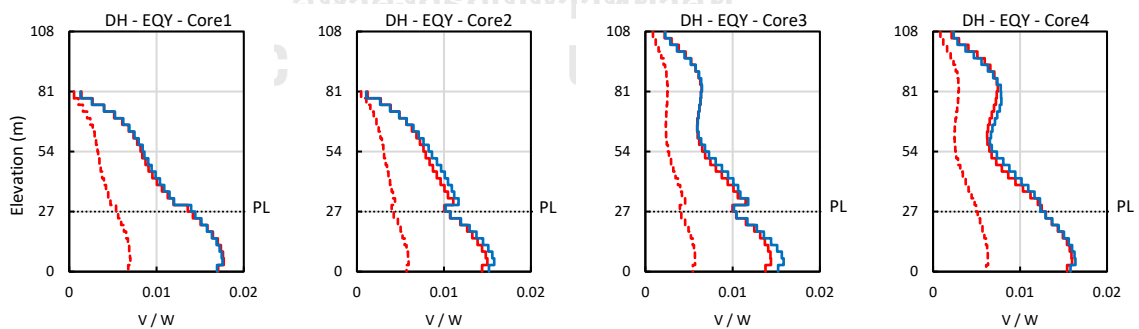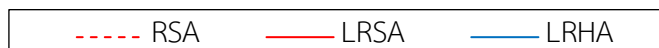
Figure B.4 Wall shear forces of building DH located in Bangkok due to earthquake in (a) X-direction (EQX); (b) Y-direction (EQY).
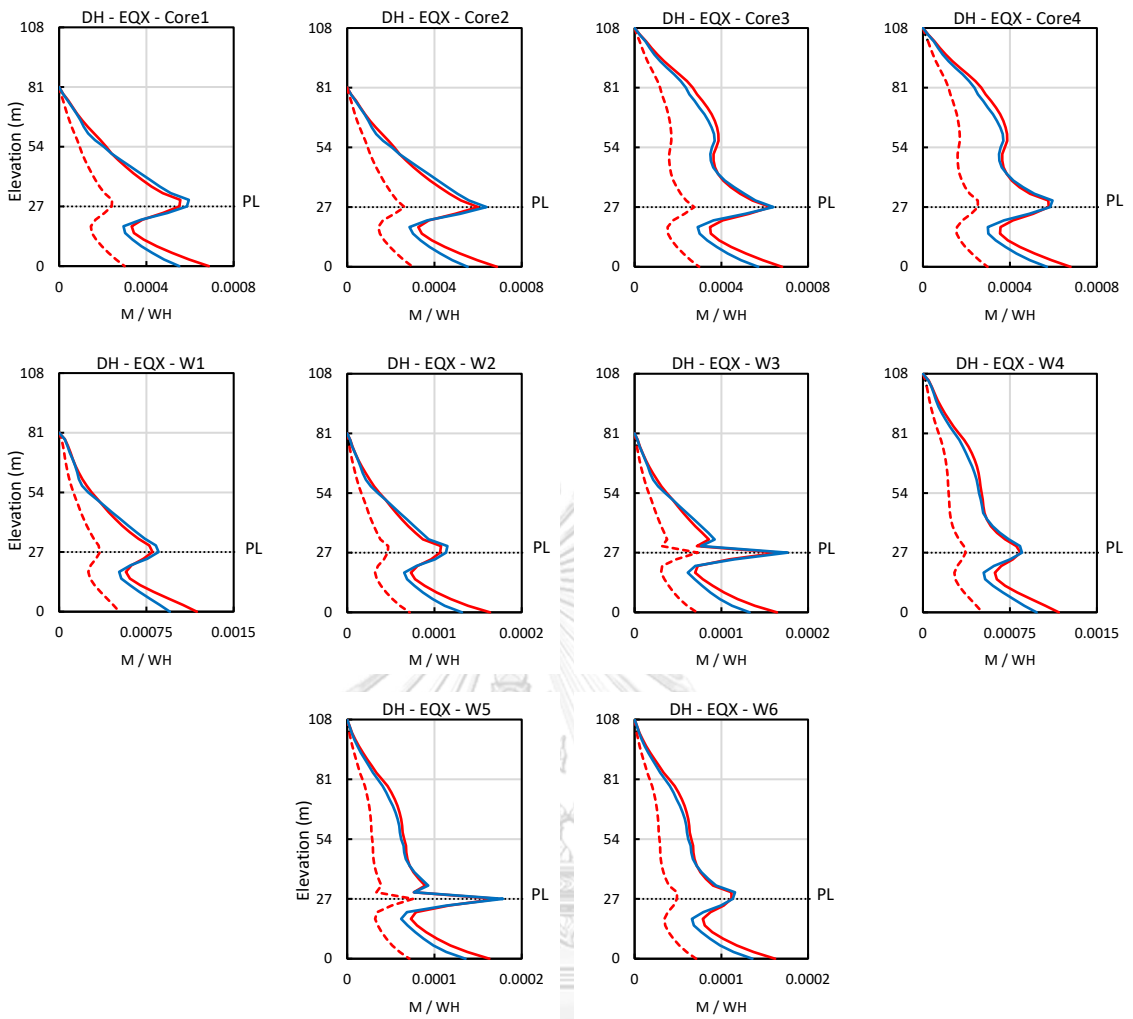
(a) Wall bending moment due to EQX
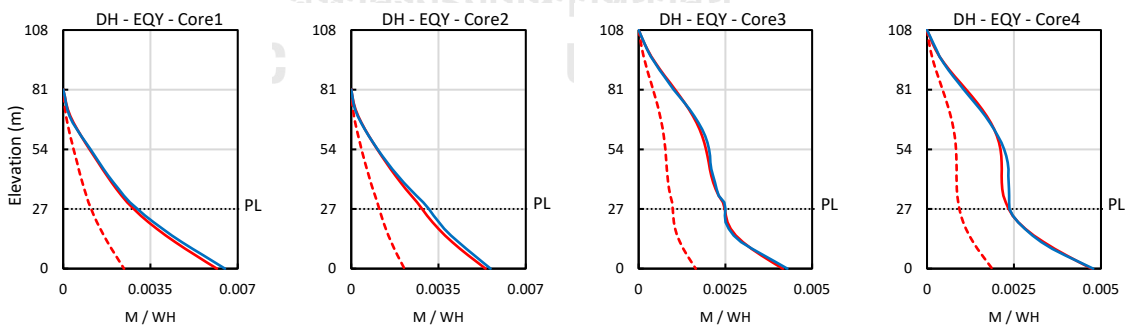
(b) Wall bending moment due to EQY

Figure B.5 Wall bending moment of building DH located in Bangkok due to earthquake in (a) X-direction (EQX); (b) Y-direction (EQY).
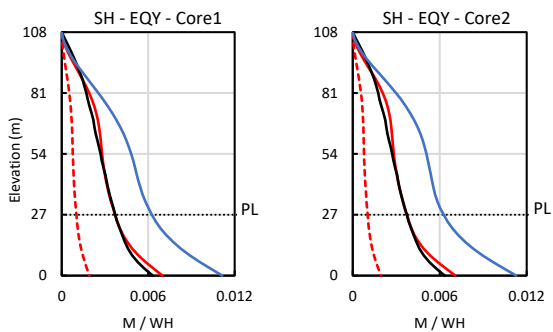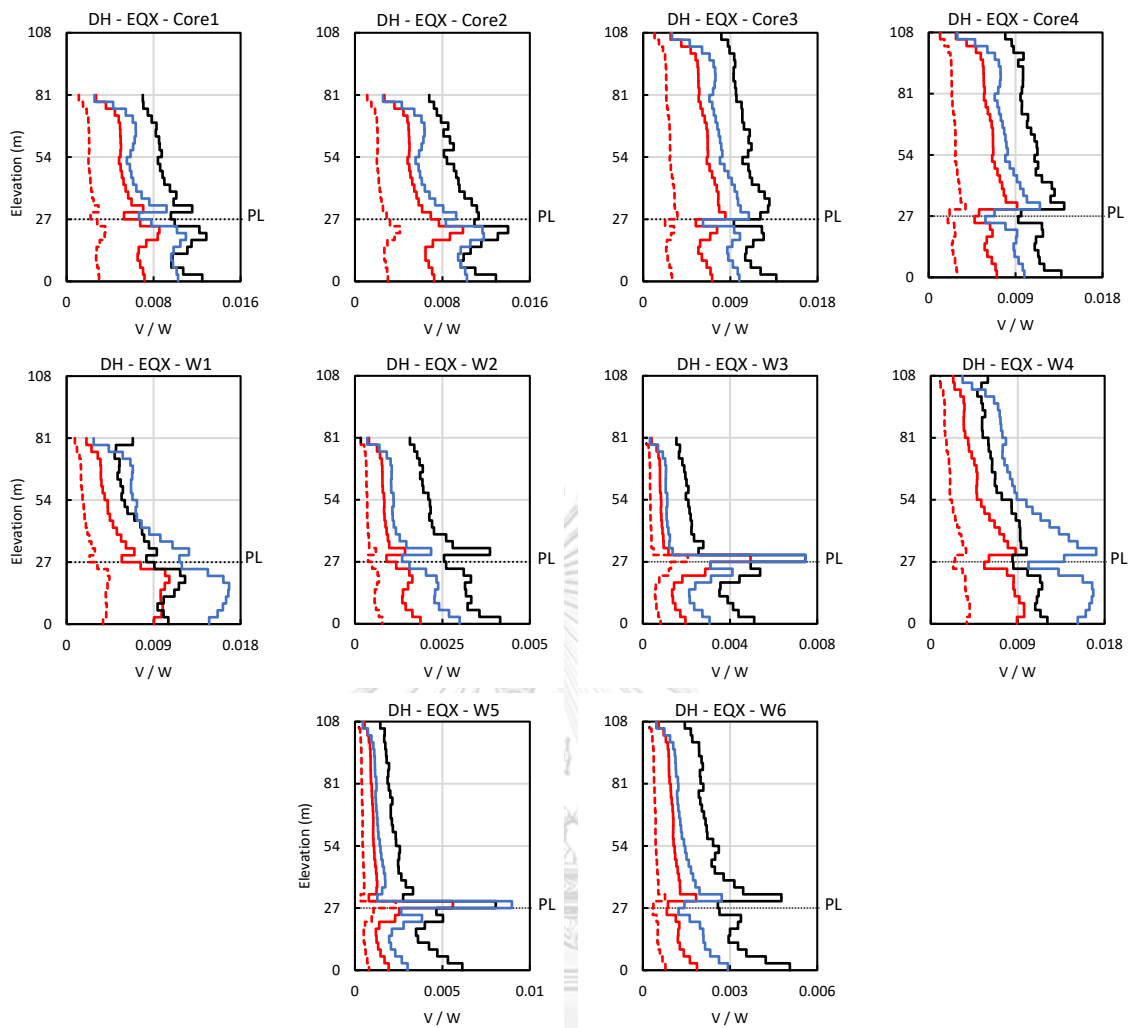
(a) Wall shear forces due to EQX

(b) Wall shear forces due to EQY
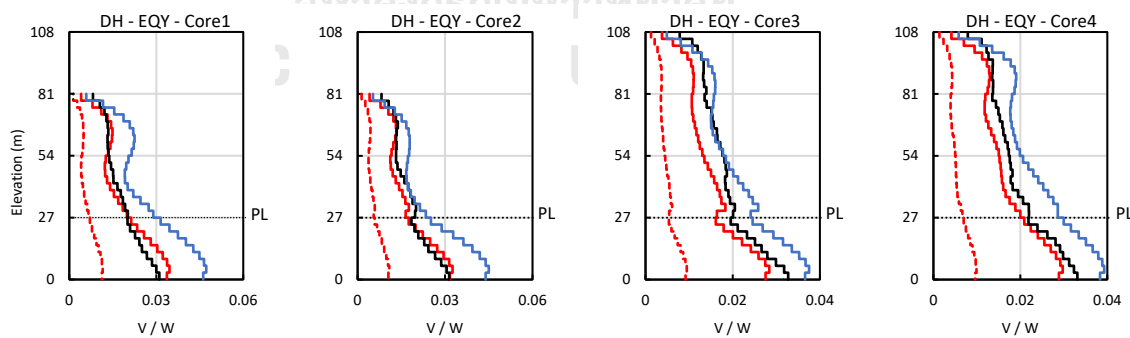
(c) Wall bending moment due to EQX

(d) Wall bending moment due to EQY

- - - - RSA ——— LRSA ——— LRHA
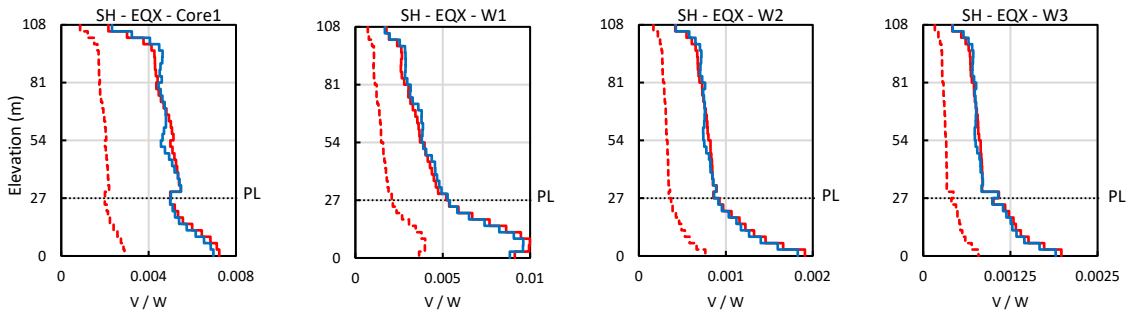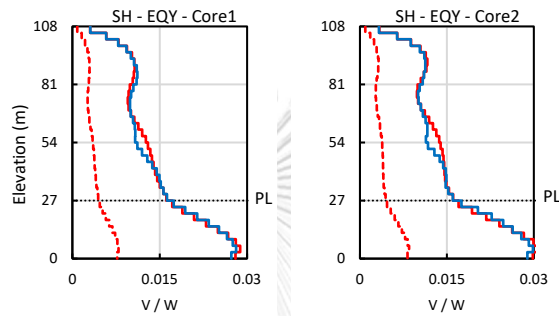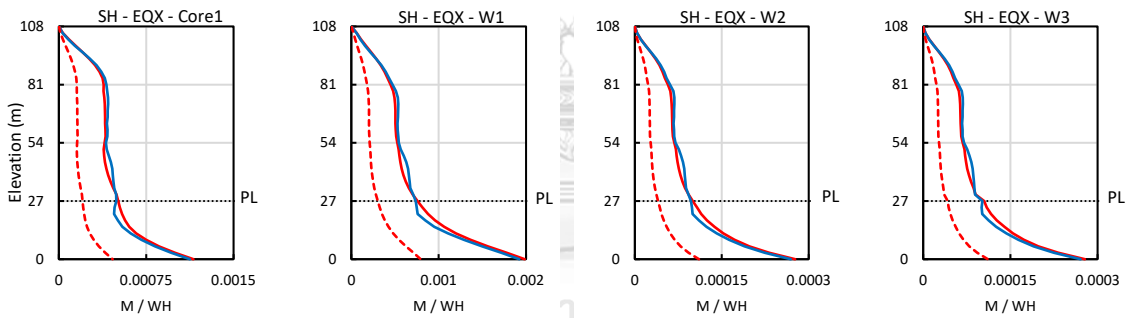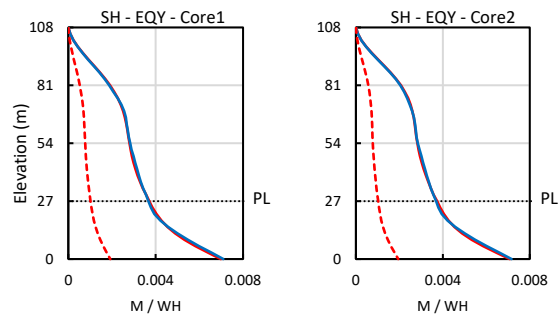
Figure B.6 Wall shear forces and bending moment of building SH located in Chiang Mai due to earthquake in X- and Y-direction.

(a) Wall shear forces due to EQX

(b) Wall shear forces due to EQY

RSA -----   LRSA ———   LRHA ———
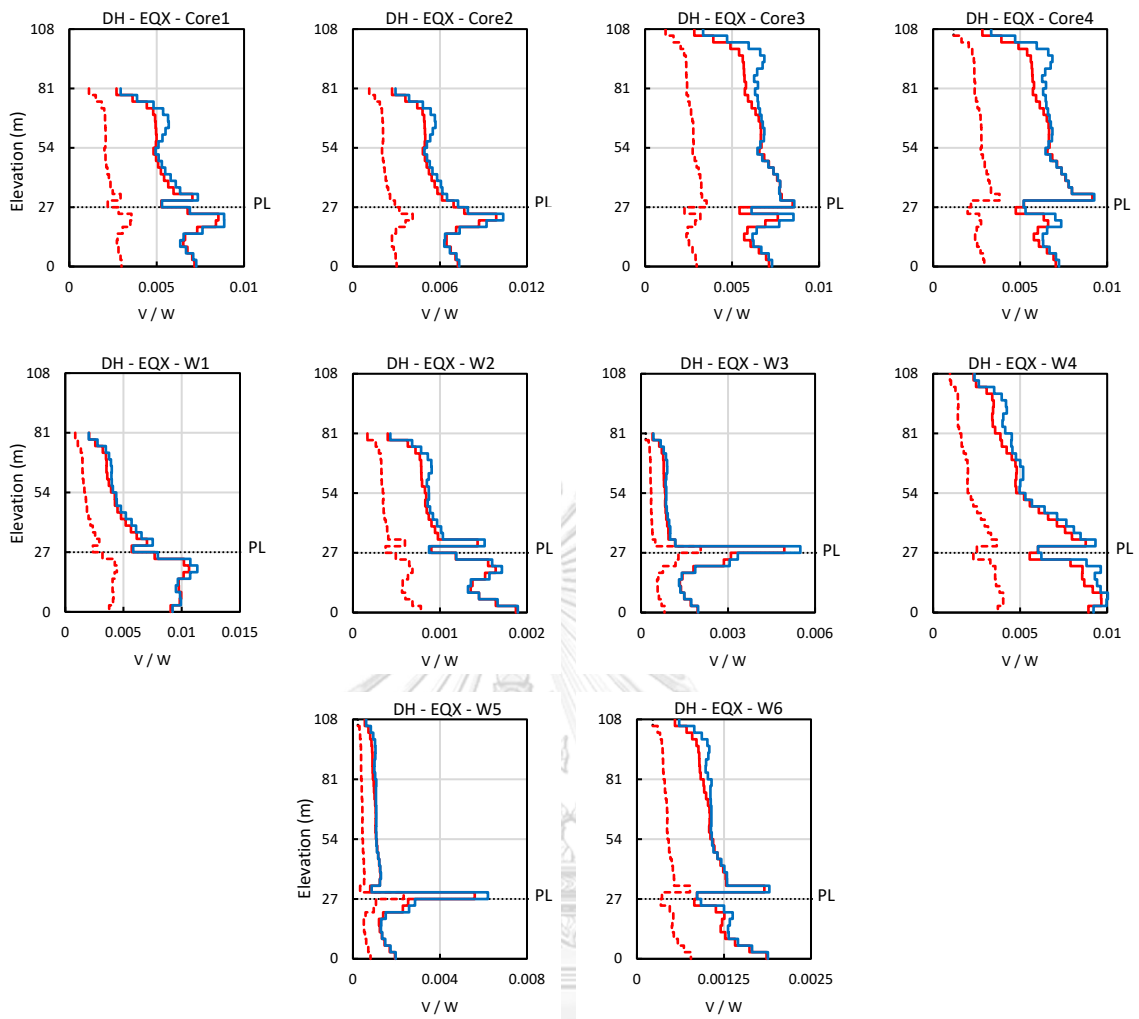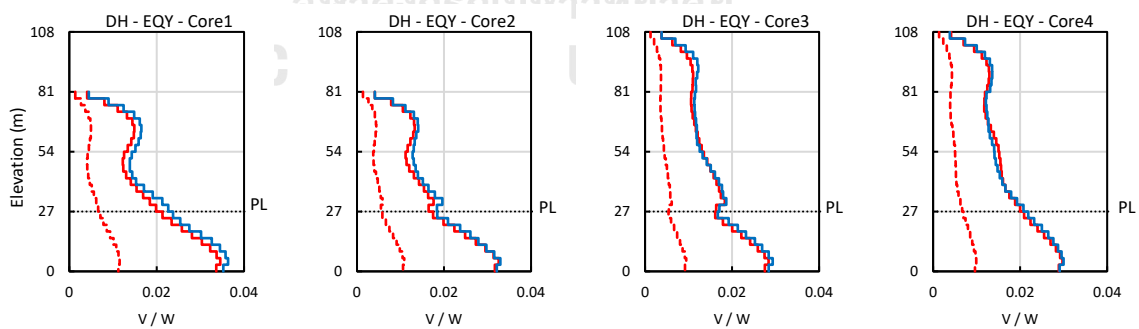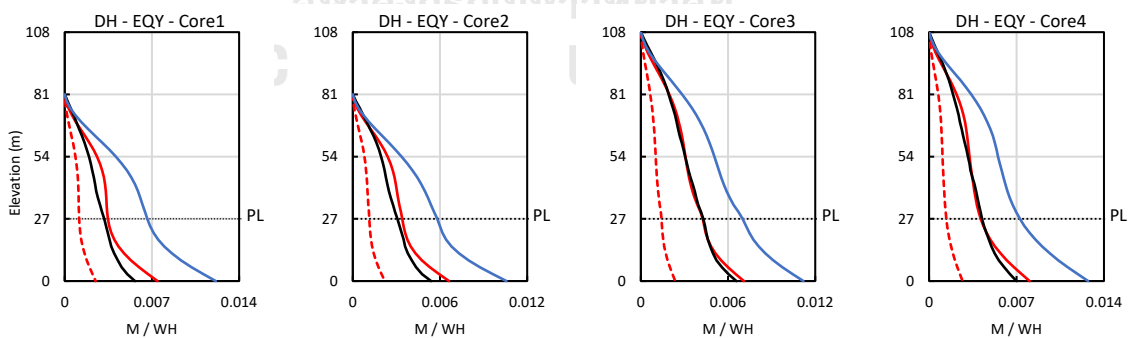
Figure B.7 Wall shear forces of building DH located in Chiang Mai due to earthquake in (a) X-direction (EQX); (b) Y-direction (EQY).

(a) Wall bending moment due to EQX
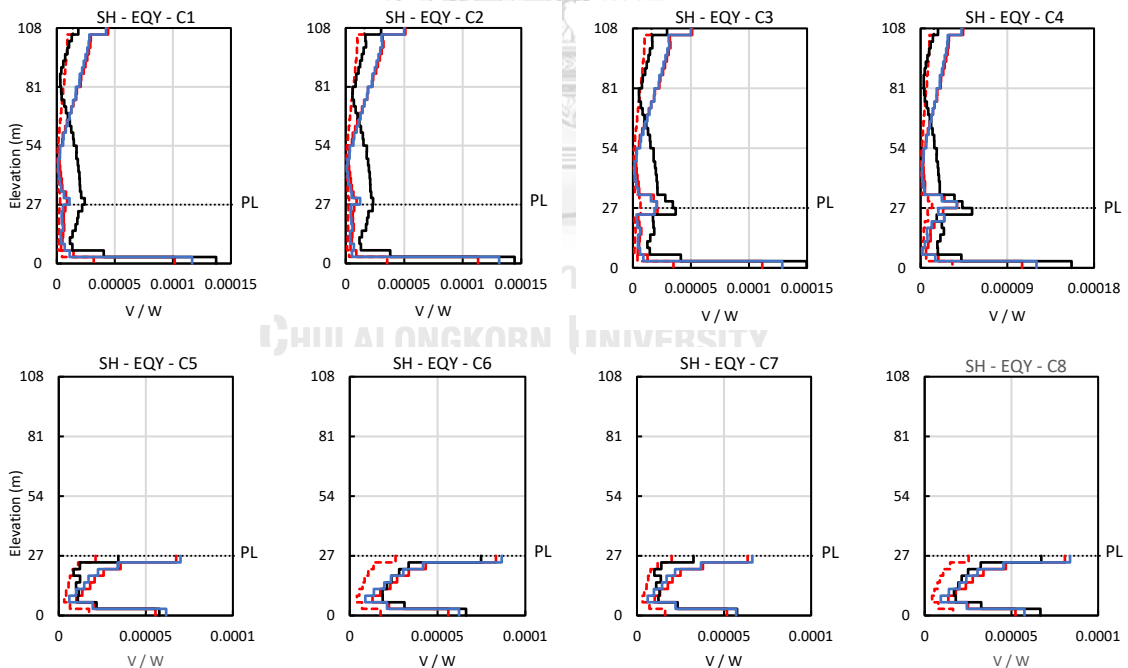
(b) Wall bending moment due to EQY

- - - - RSA ——— LRSA ——— LRHA
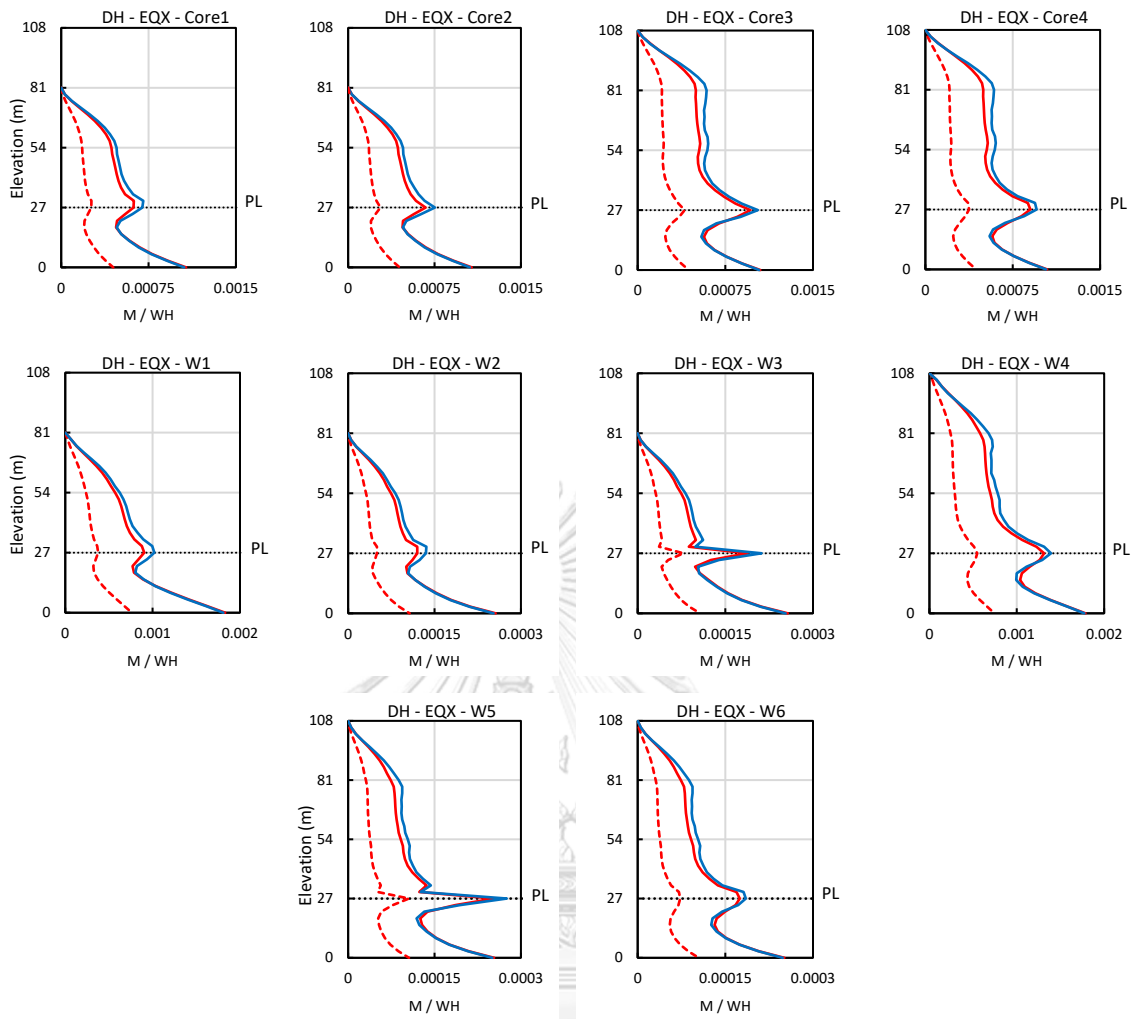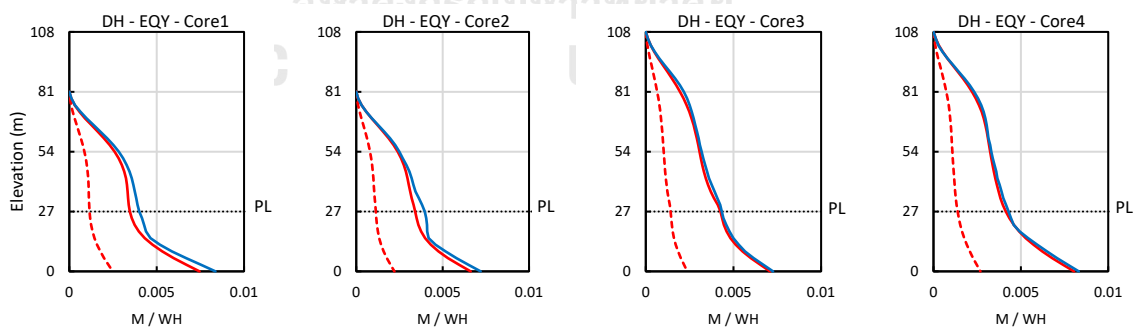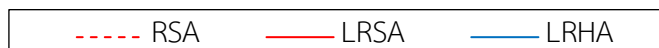
Figure B.8 Wall bending moment for building DH located in Chiang Mai due to earthquake in (a) X-direction (EQX); (b) Y-direction (EQY).

B.1.2 Column forces
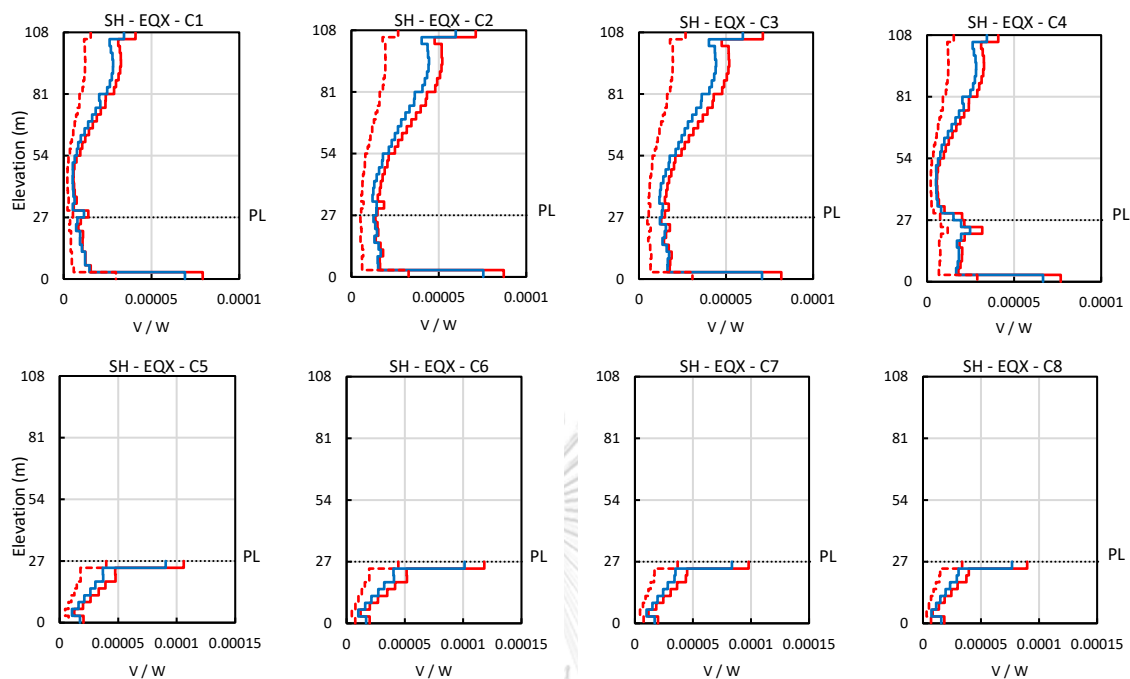
(a) Column shear forces due to EQX
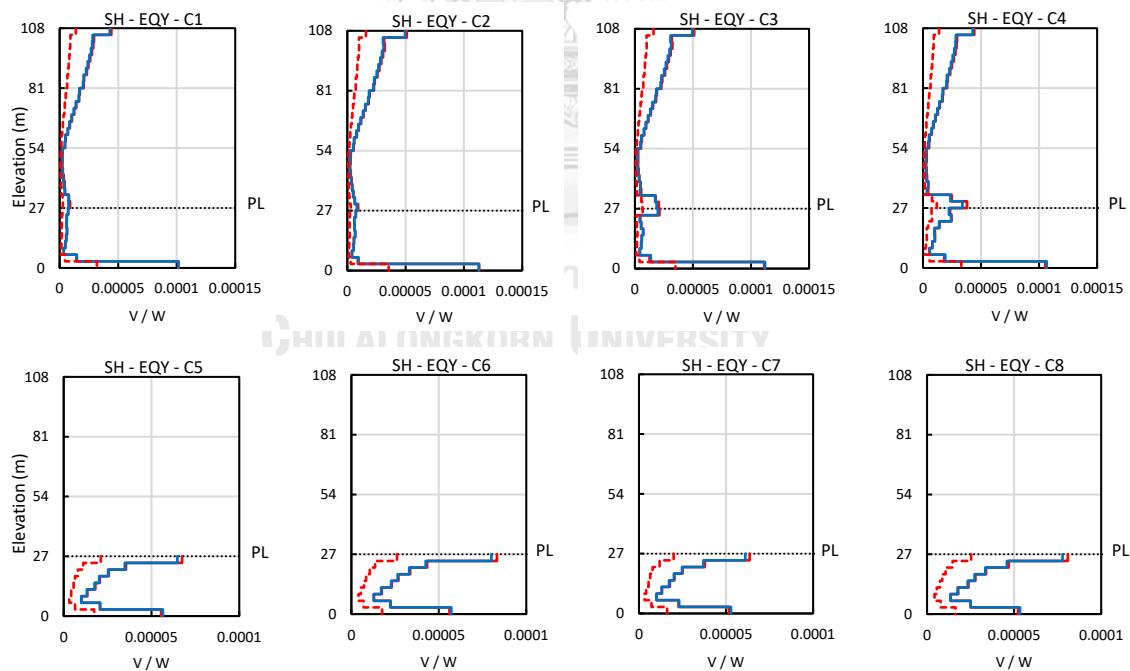
(b) Column shear forces due to EQY

Figure B.9 Column shear forces of building SH located in Bangkok due to earthquake in (a) X-direction (EQX); (b) Y-direction (EQY).
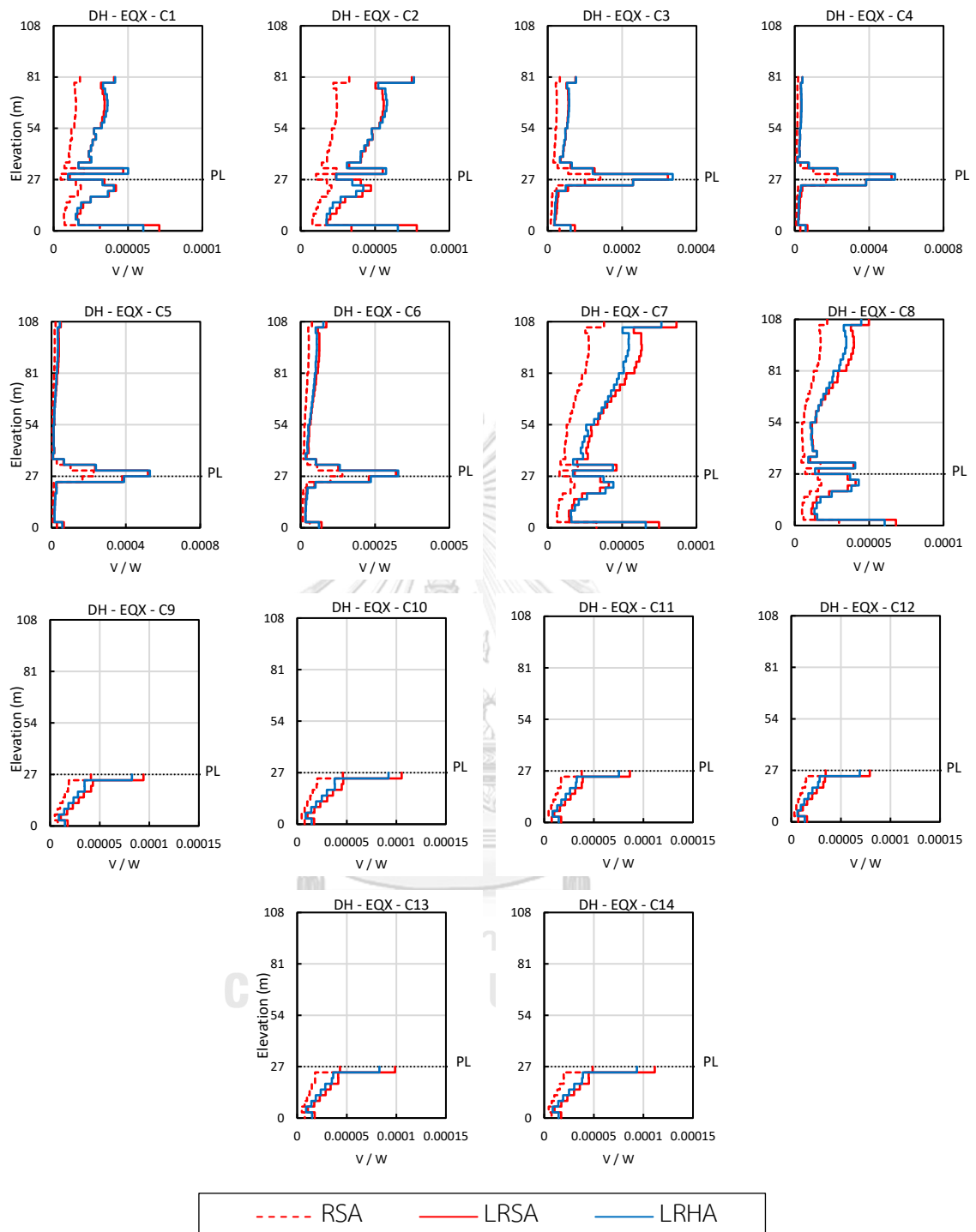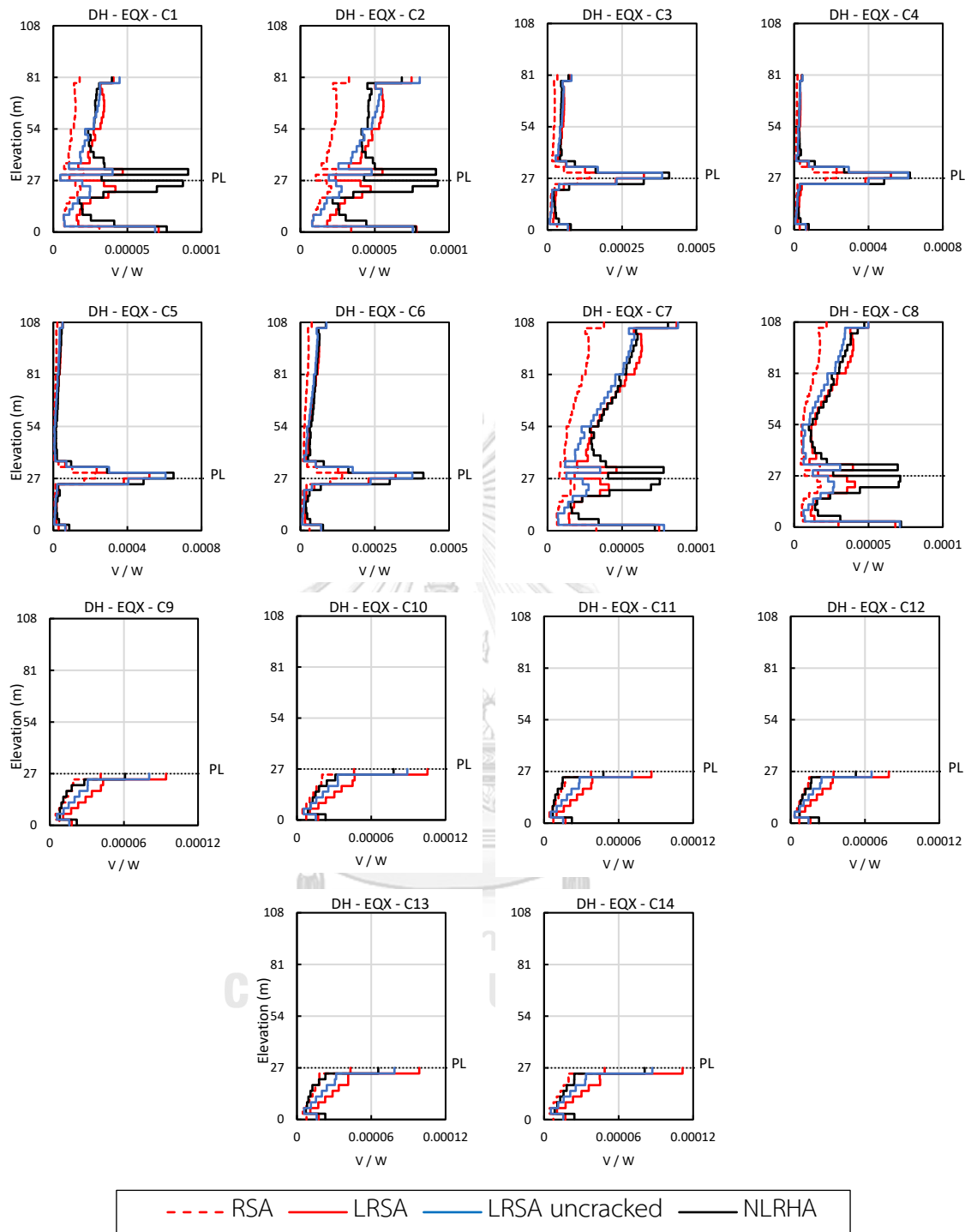
Figure B.10 Column shear forces of building DH located in Bangkok due to earthquake in X-direction (EQX).
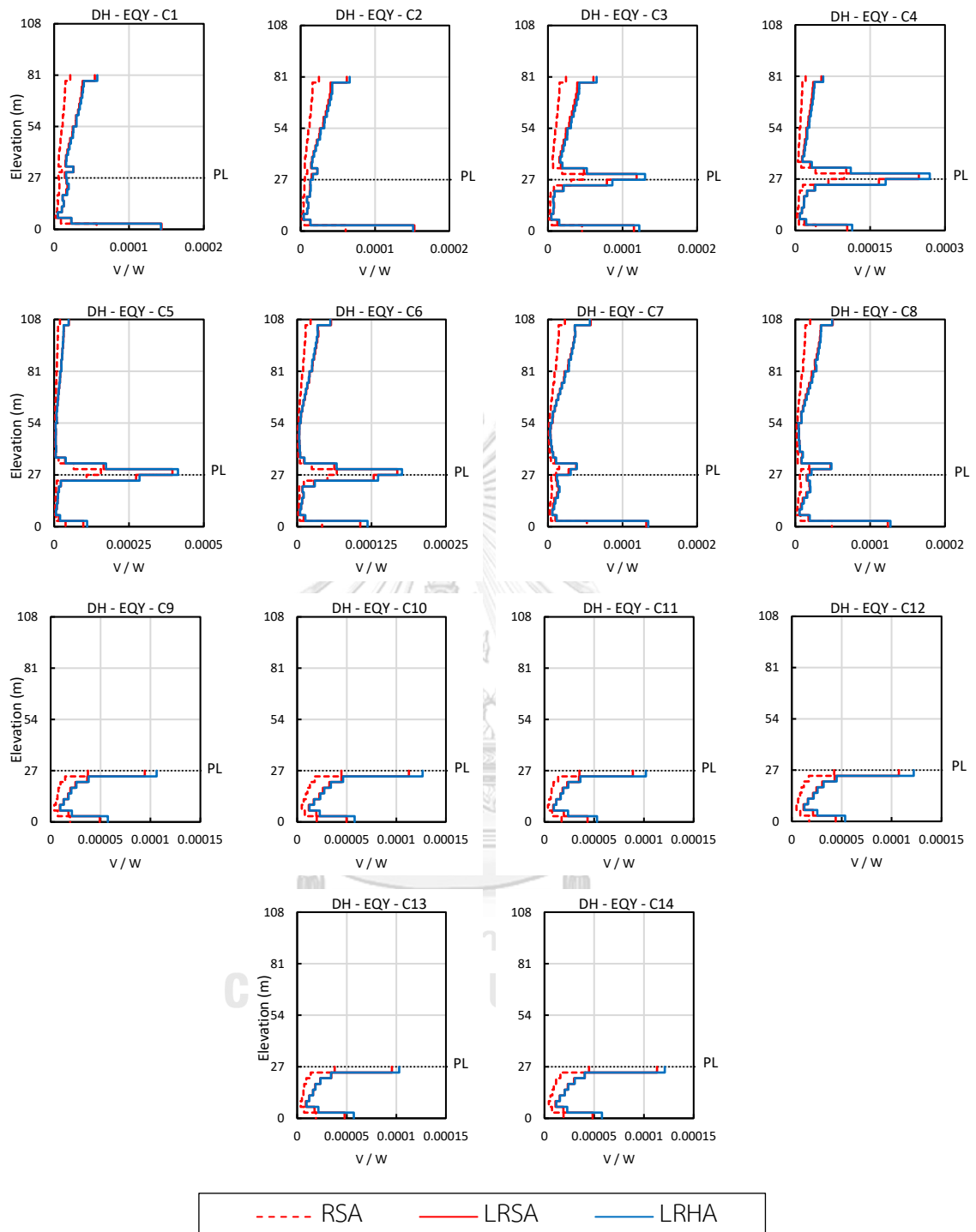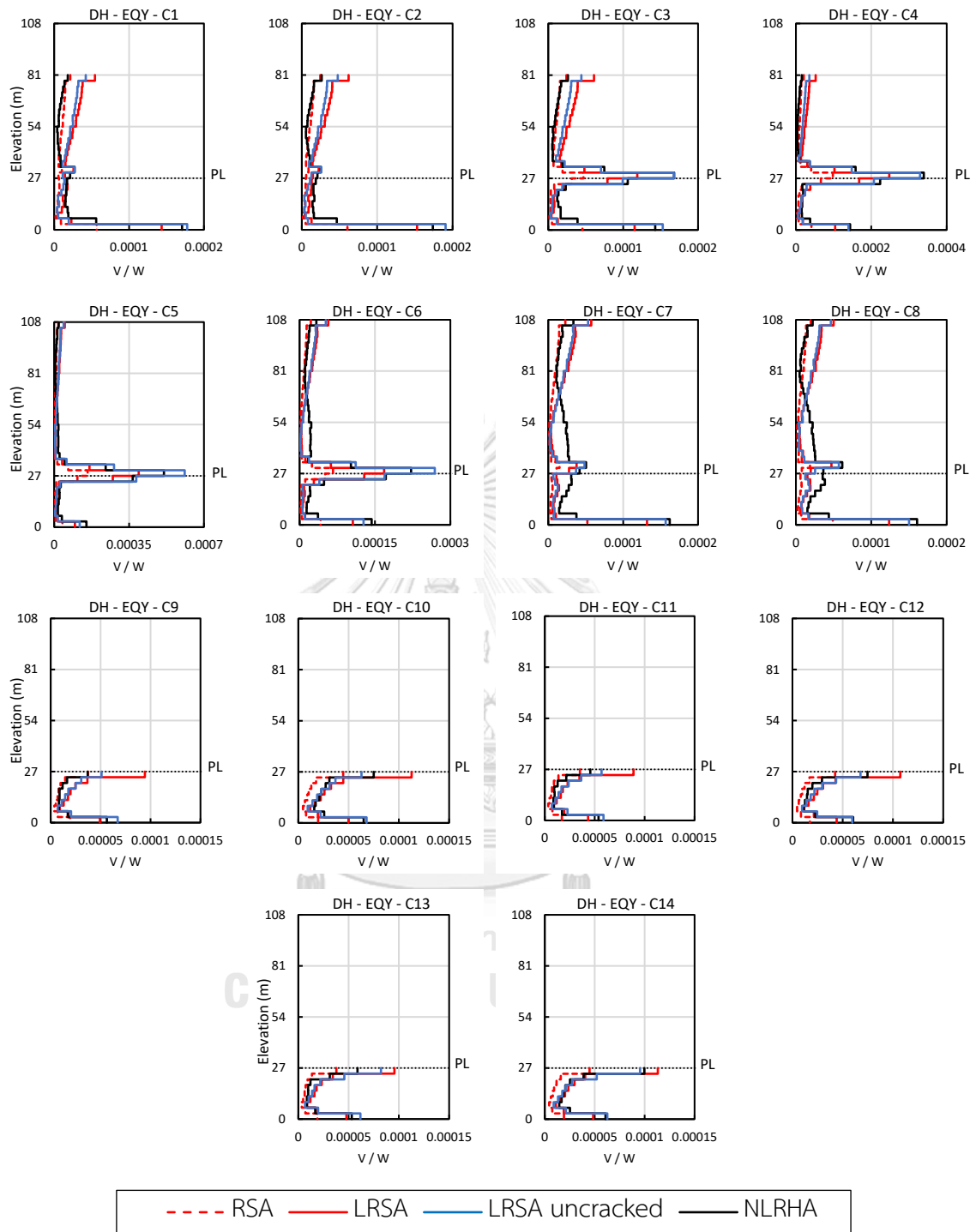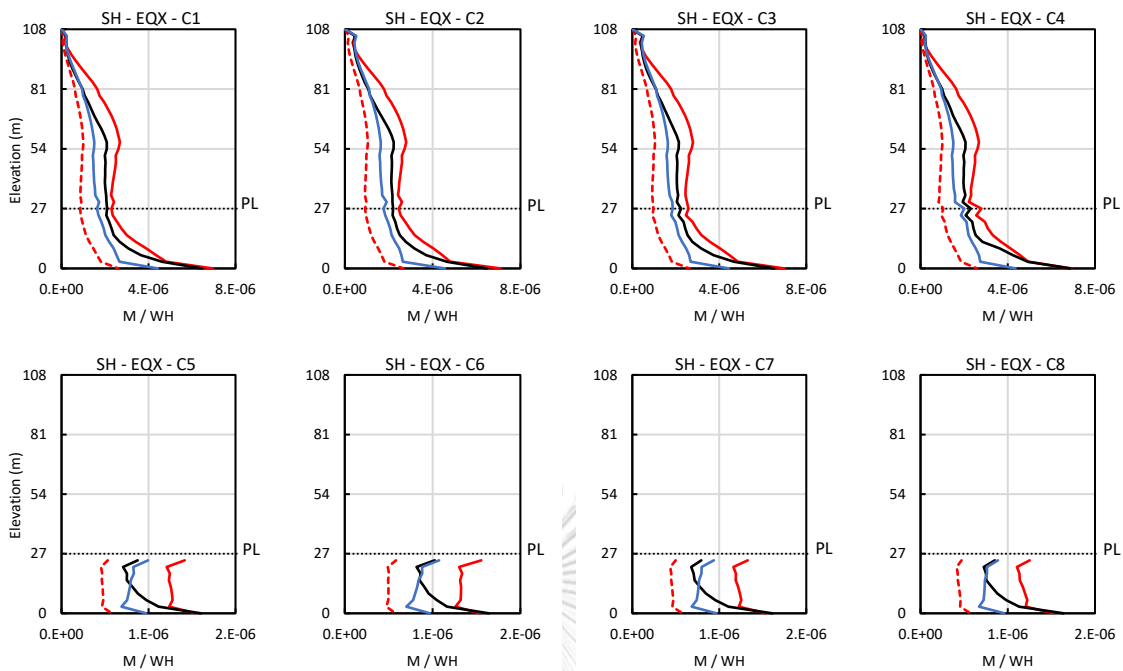
Figure B.11 Column shear forces for building DH located in Bangkok due to earthquake in Y-direction (EQY).

(a) Column bending moment due to EQX

(b) Column bending moment due to EQY

- - - - RSA ——— LRSA ——— LRHA
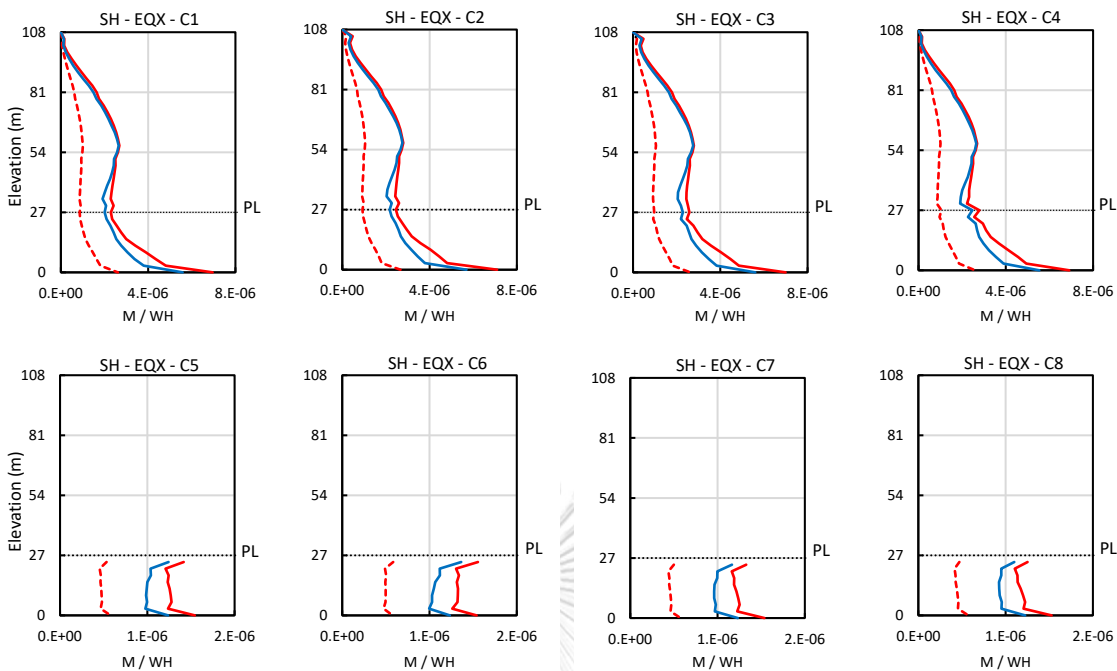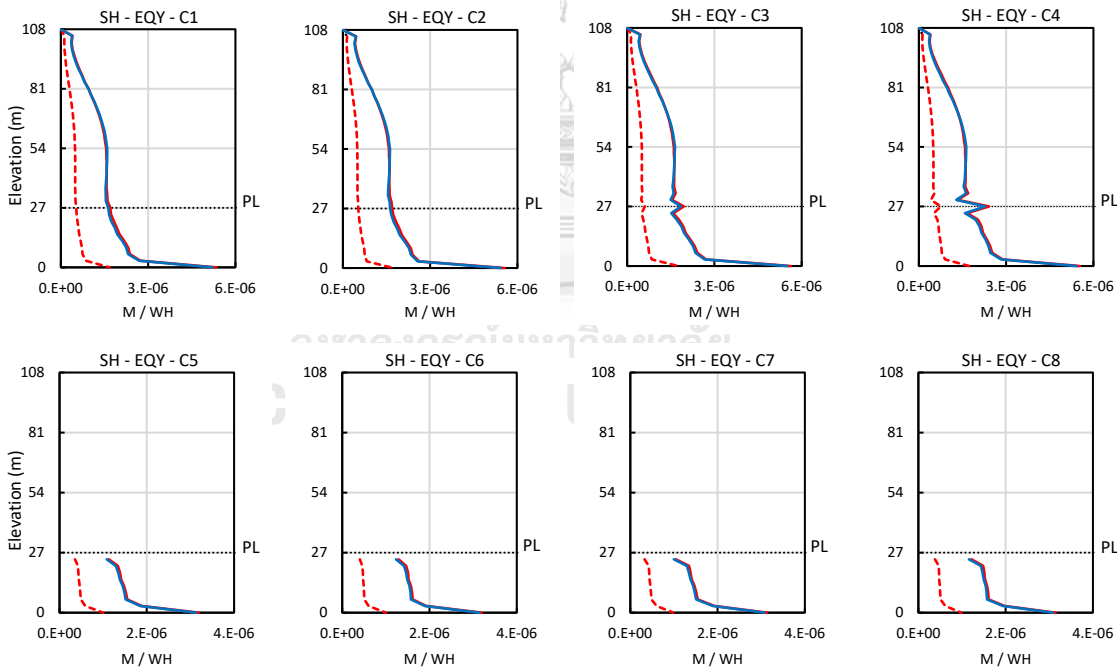
Figure B.12 Column bending moment for building SH located in Bangkok due to earthquake in (a) X-direction (EQX); (b) Y-direction (EQY).
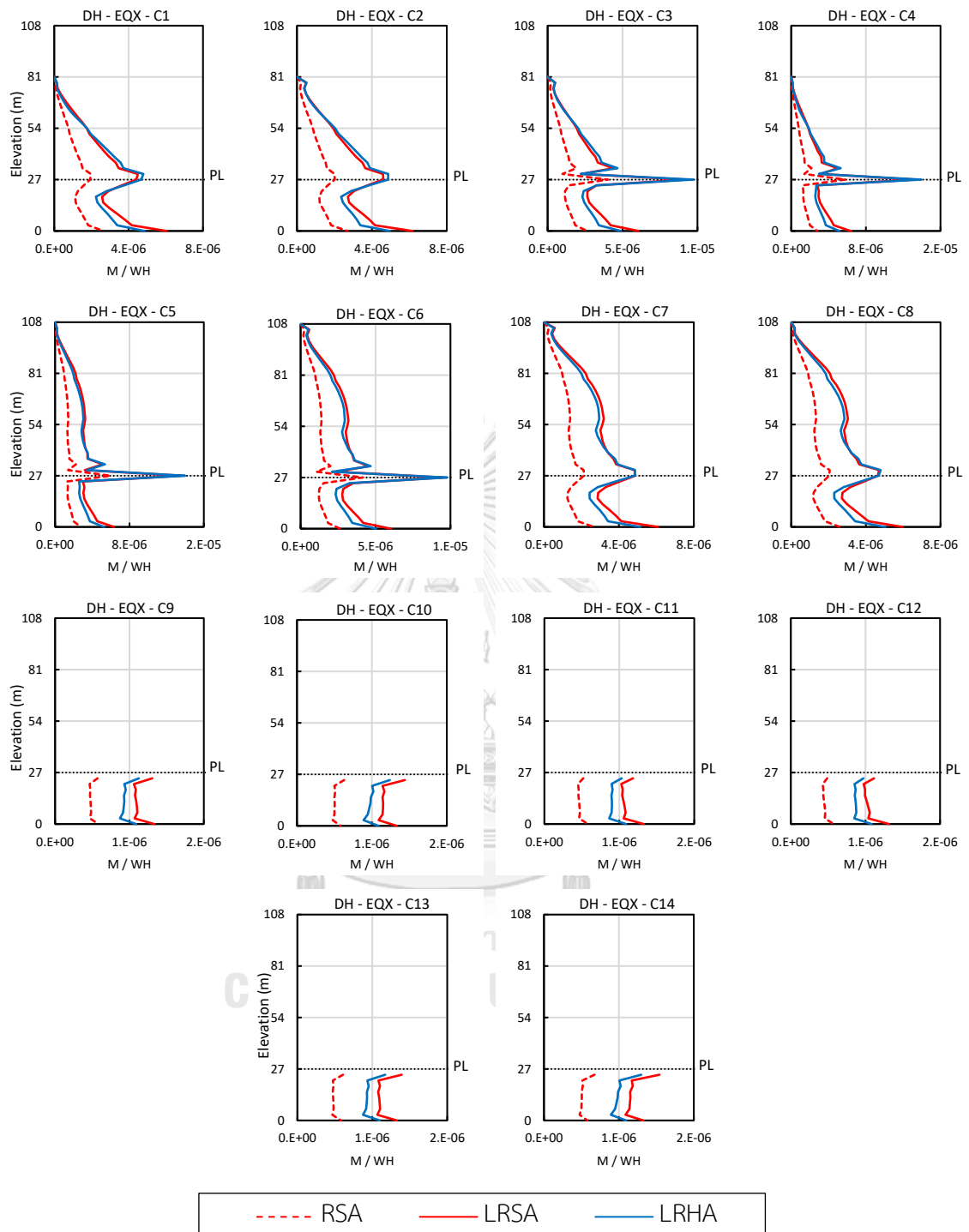
Figure B.13 Column bending moment for building DH located in Bangkok due to earthquake in X-direction (EQX).
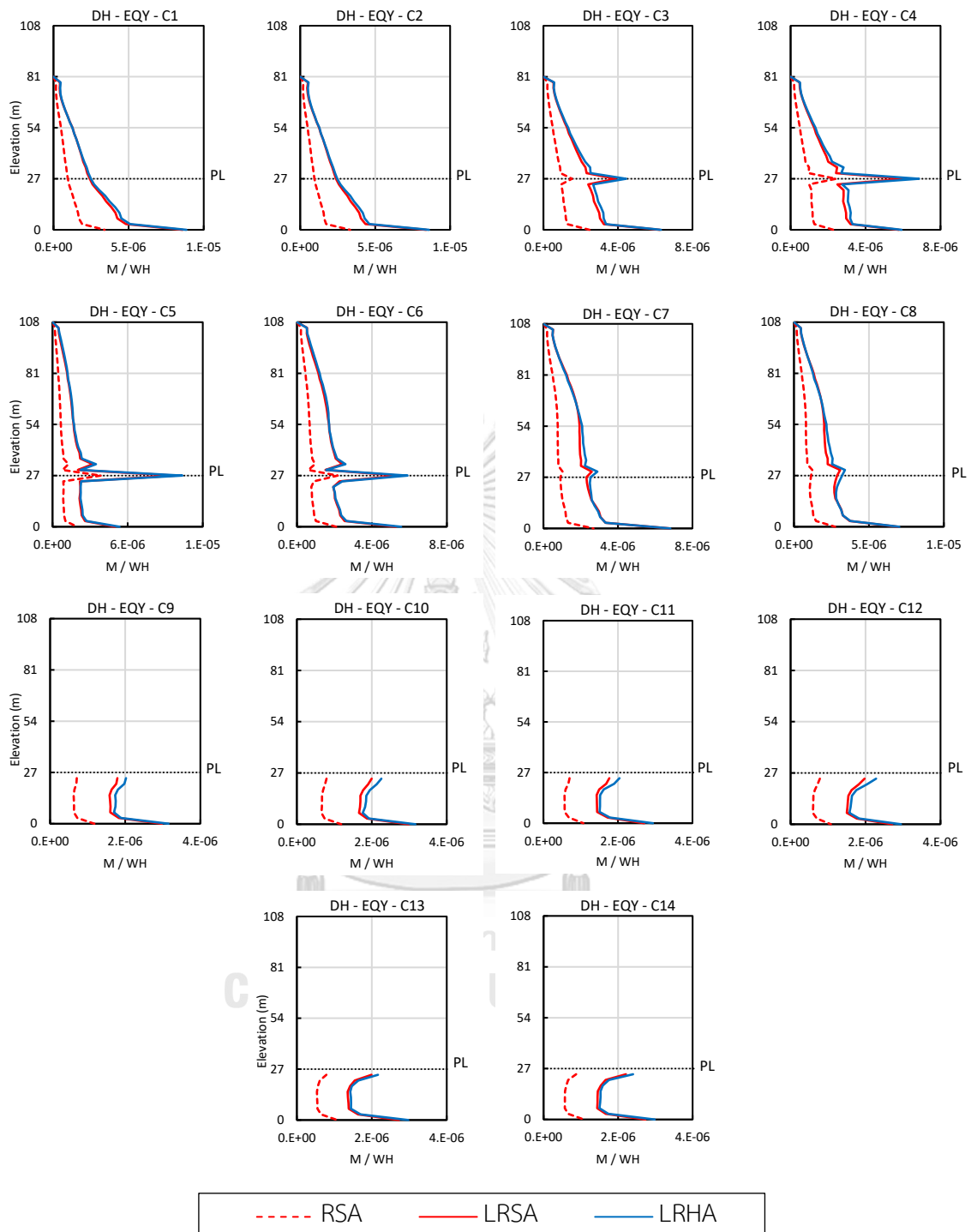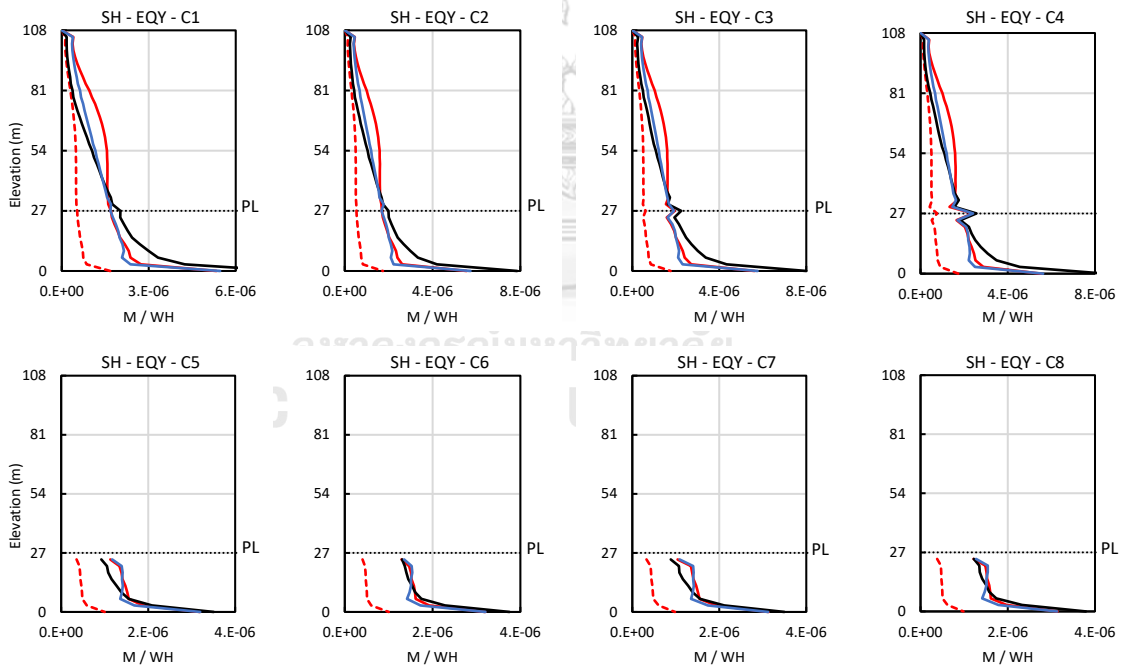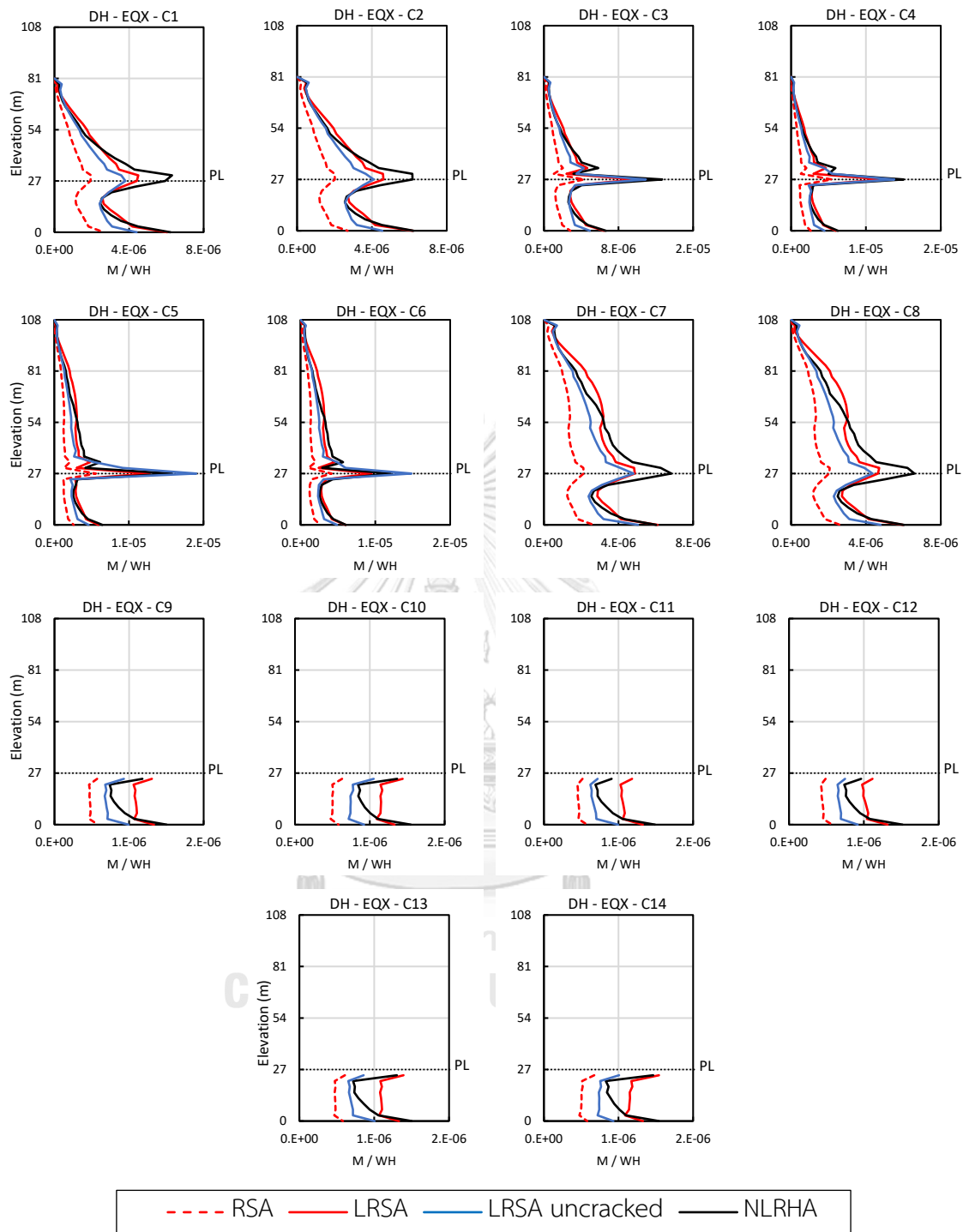
Figure B.14 Column bending moment of building DH located in Bangkok due to earthquake in Y-direction (EQY).
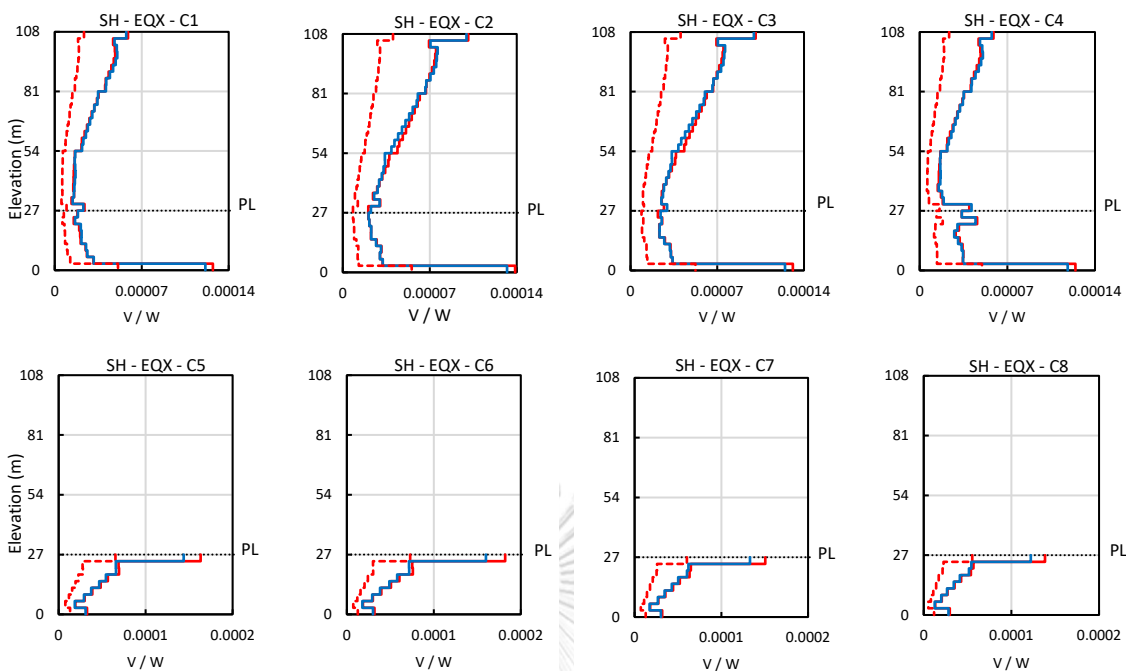
(a) Column shear forces due to EQX
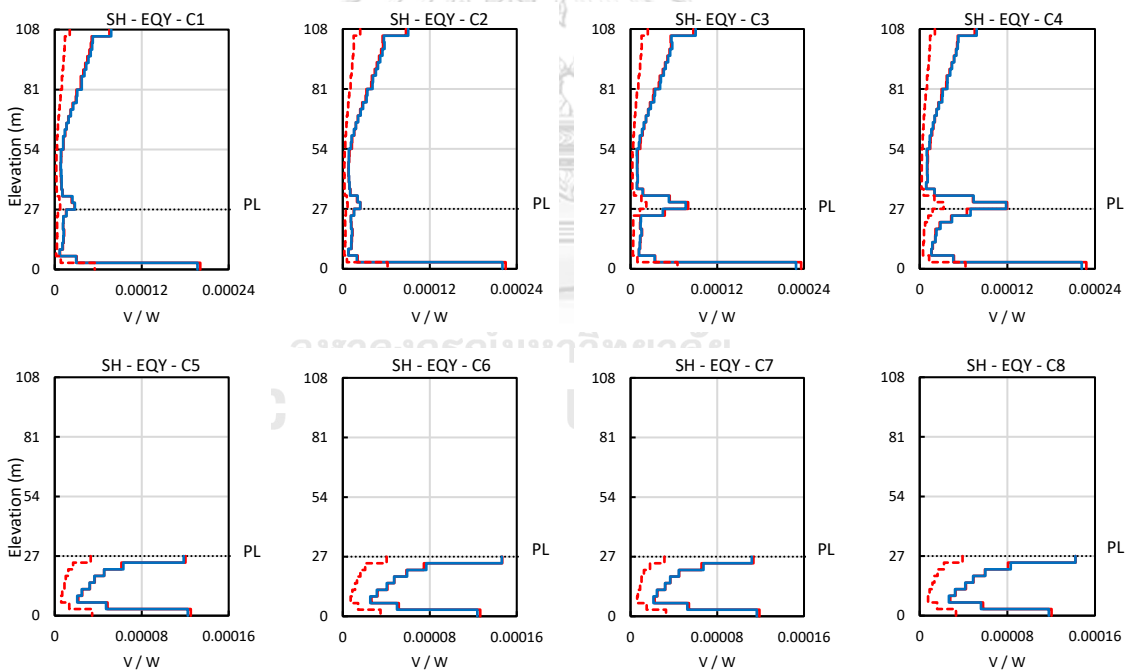
(b) Column shear forces due to EQY

Figure B.15 Column shear forces of building SH located in Chiang Mai due to earthquake in (a) X-direction (EQX); (b) Y-direction (EQY).
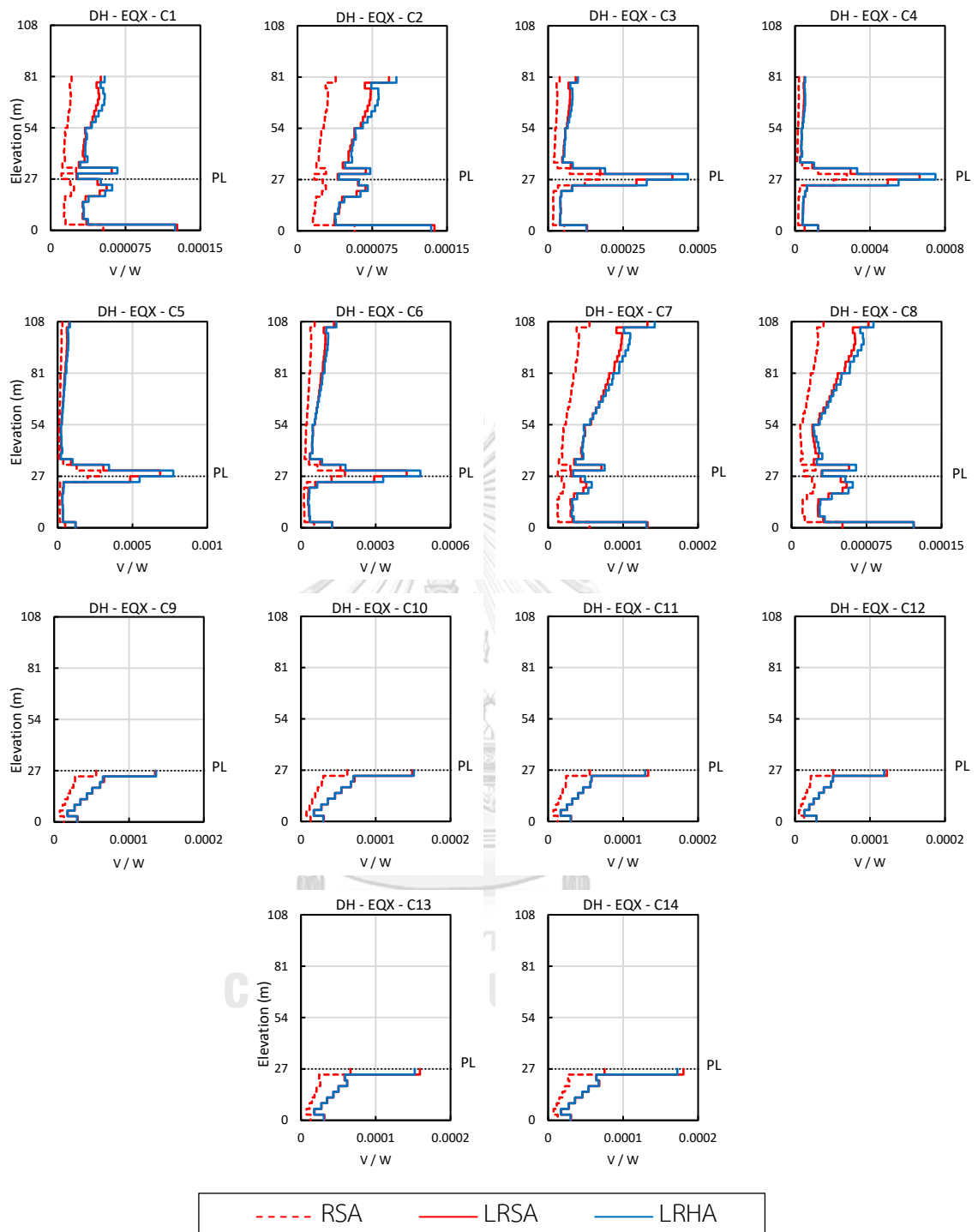
Figure B.16 Column shear forces of building DH located in Chiang Mai due to earthquake in X-direction (EQX).
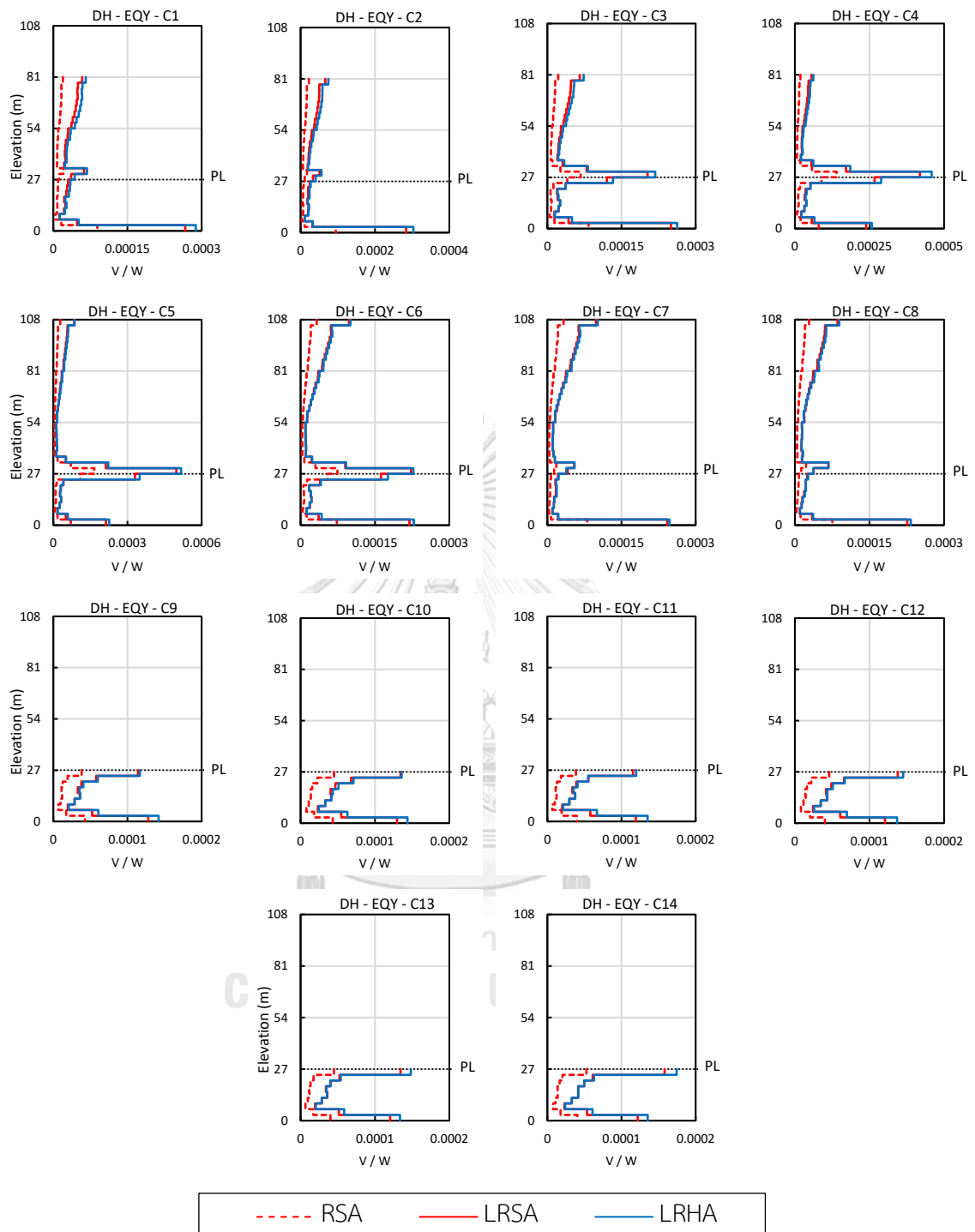
Figure B.17 Column shear forces of building DH located in Chiang Mai due to earthquake in Y-direction (EQY).

(a) Column bending moment due to EQX

(b) Column bending moment due to EQY

----- RSA ——— LRSA ——— LRHA
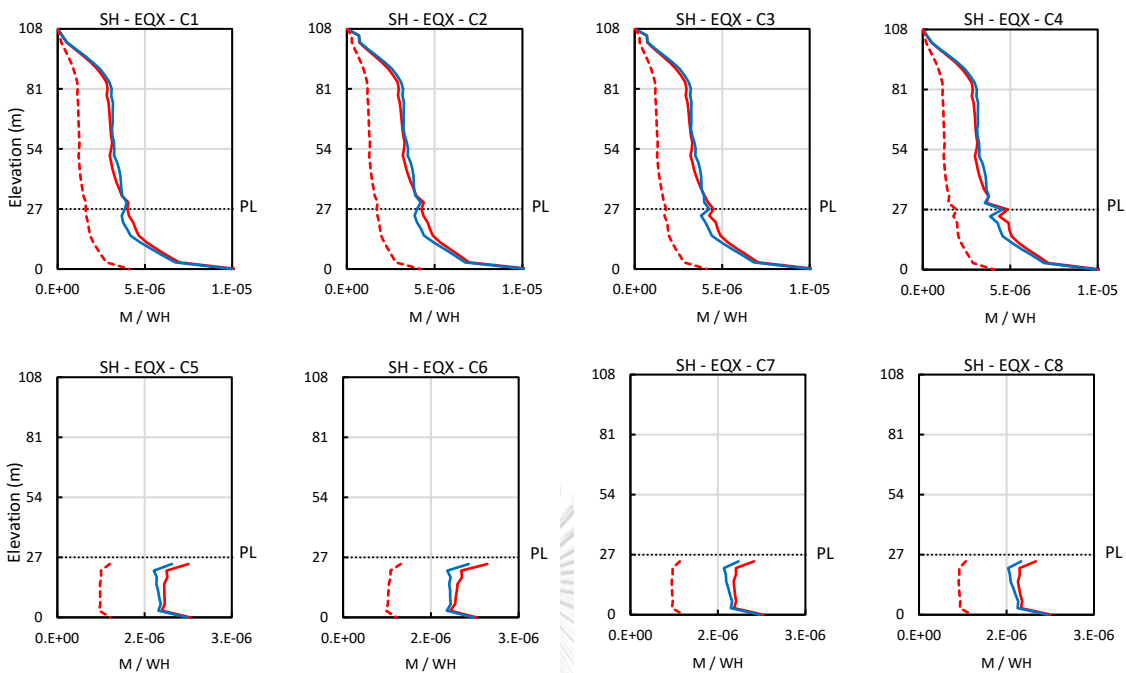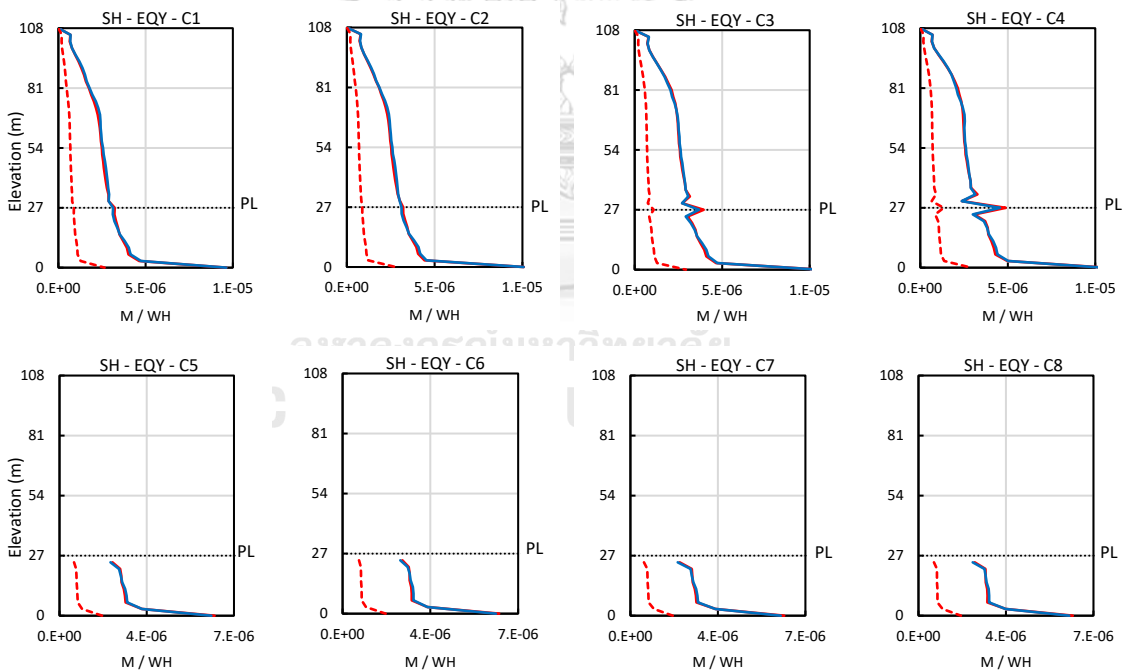
Figure B.18 Column bending moment for building SH located in Chiang Mai due to earthquake in (a) X-direction (EQX); (b) Y-direction (EQY).
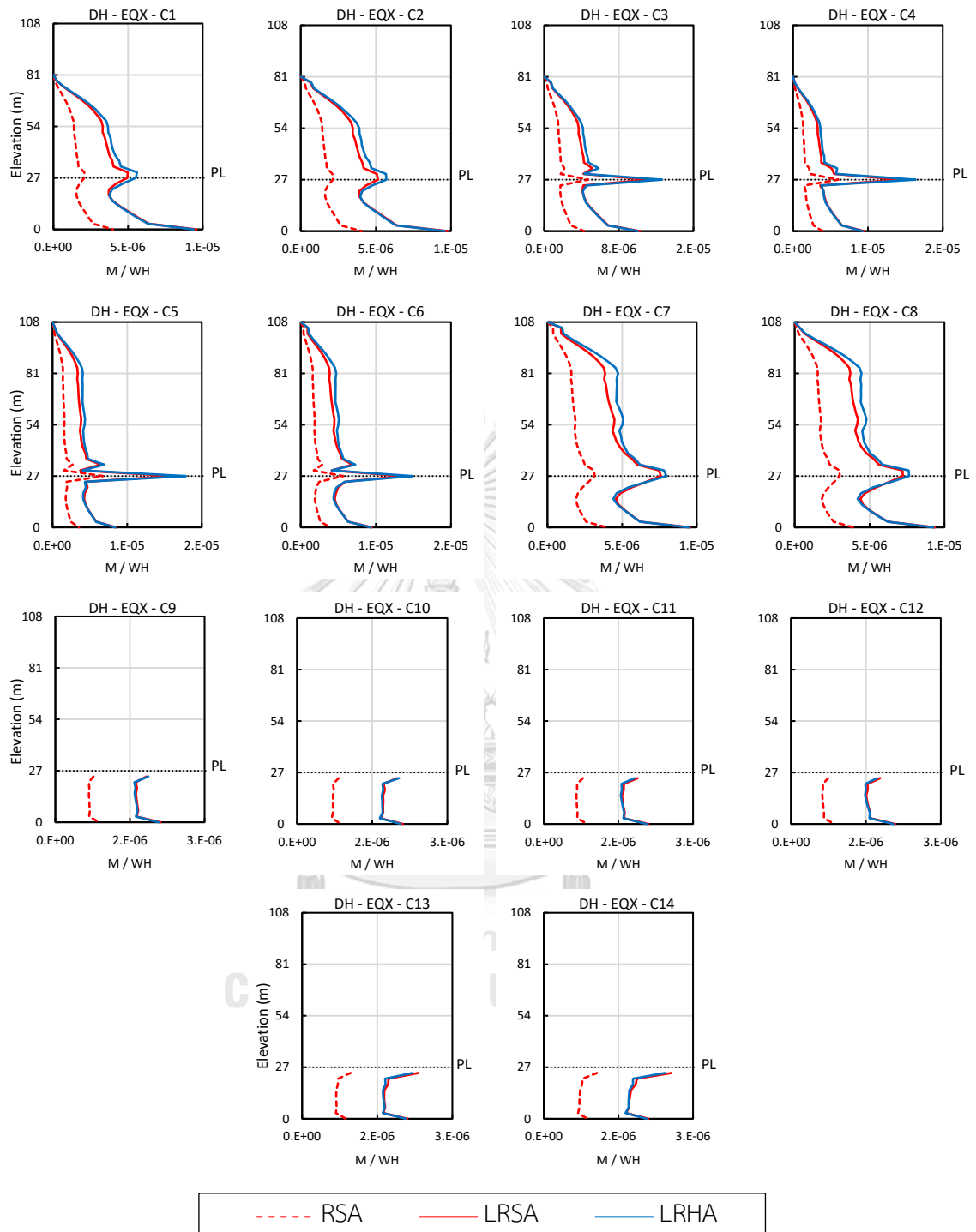
Figure B.19 Column bending moment for building DH located in Chiang Mai due to earthquake in X-direction (EQX).
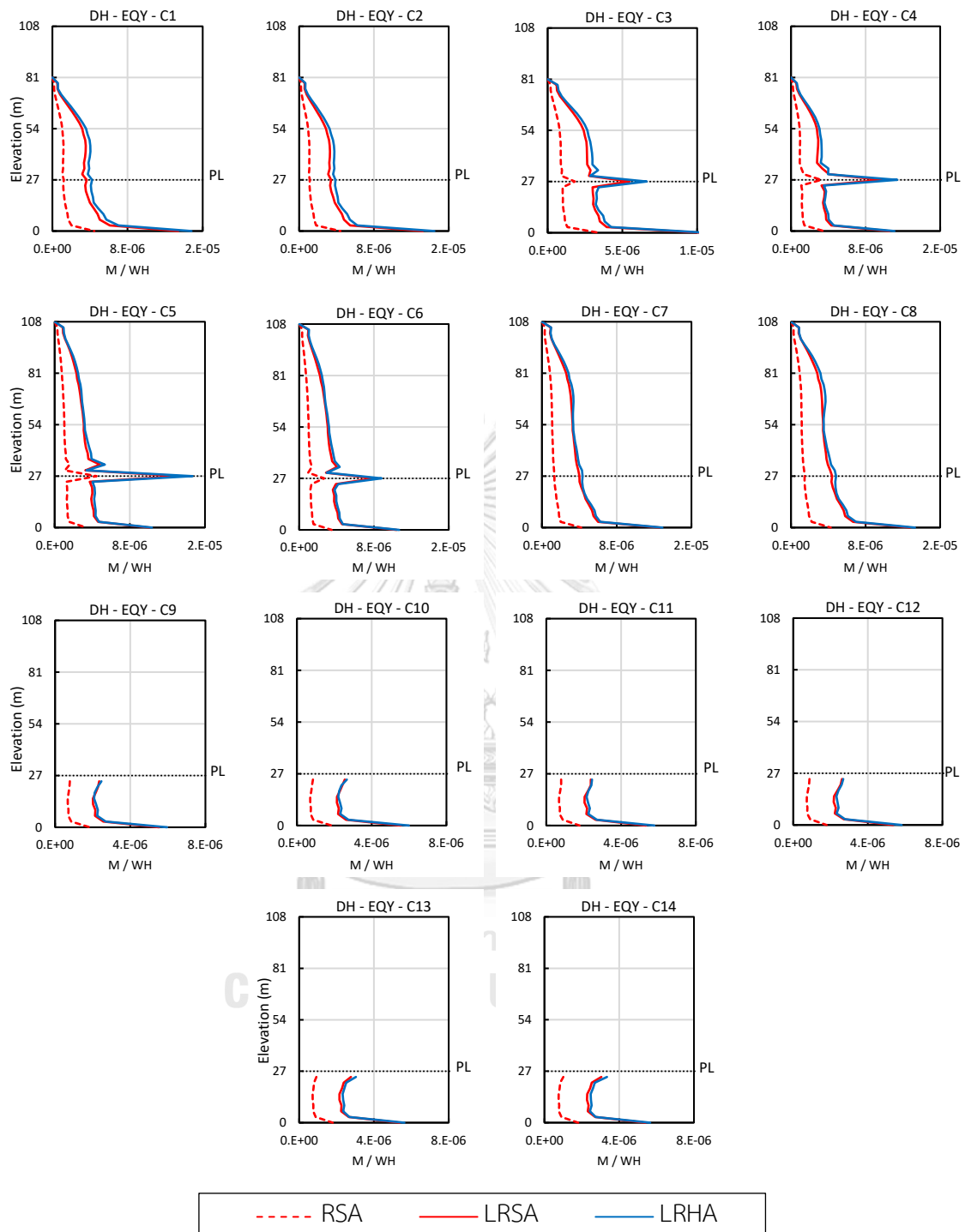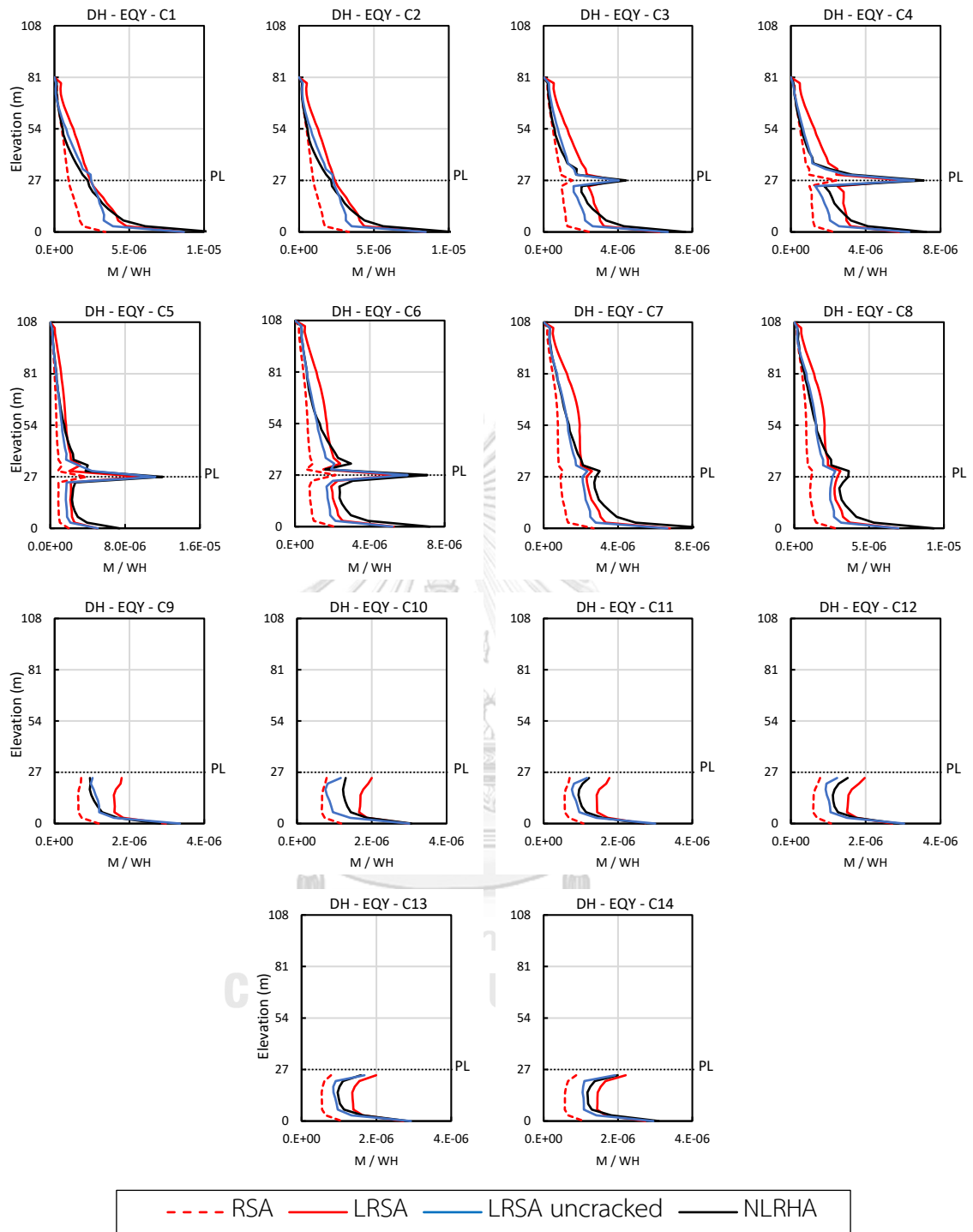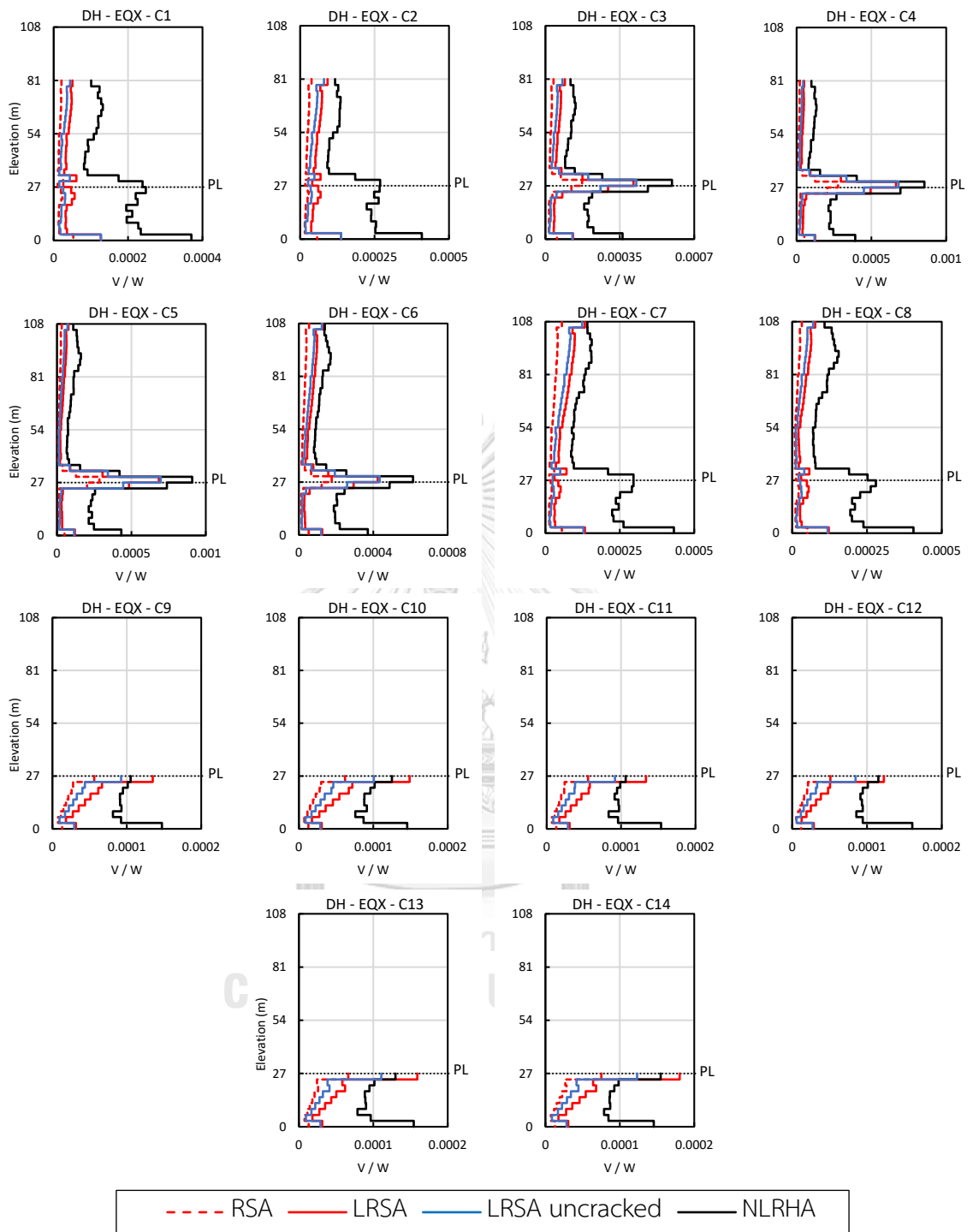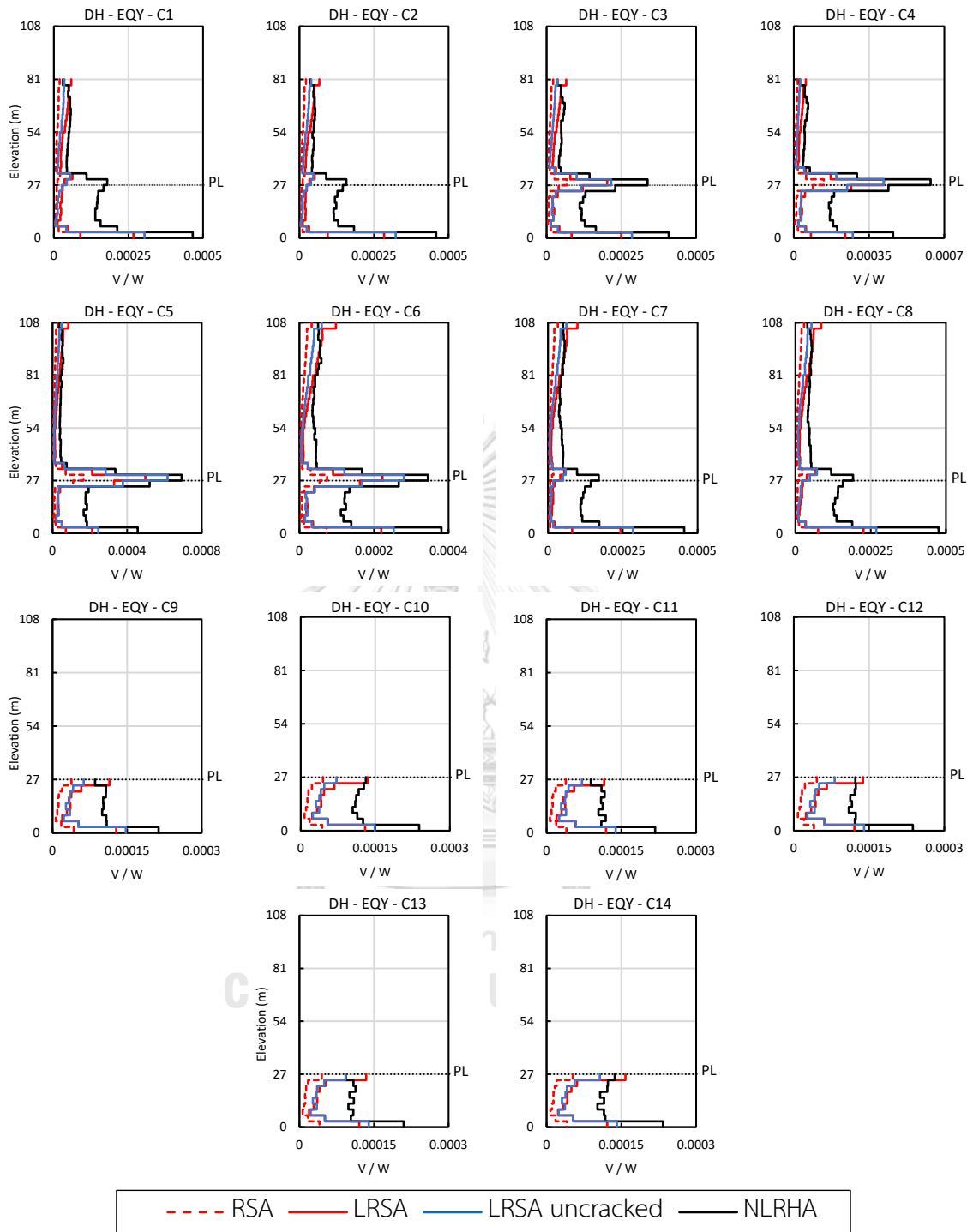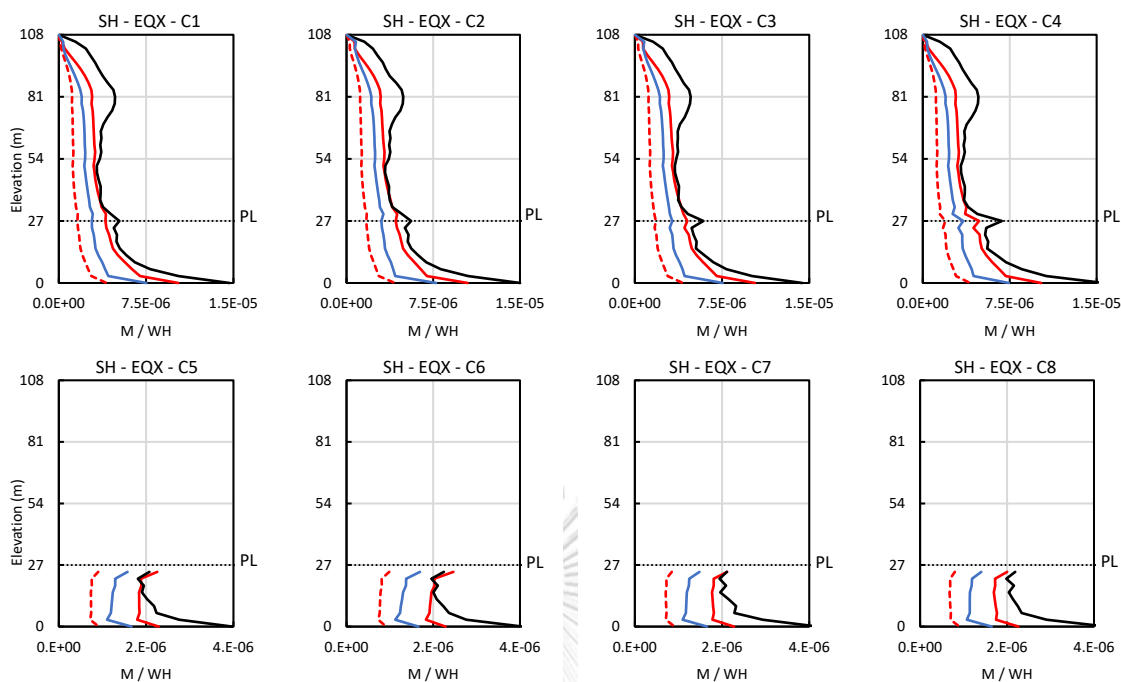
Figure B.20 Column bending moment for building DH located in Chiang Mai due to earthquake in Y-direction (EQY).

B.2 Diaphragm forces

In this section, diaphragm forces developed in diaphragm floors of the podium are presented (note that the podium consists of 9 stories). The forces are obtained along section cuts previously defined in ETBAS software. The section-cut locations are shown in the Figure B.21. Floors at the podium level are spanning between two main cantilever core walls aligned in the Y-direction. Hence, the interest is in the shear and bending moment in diaphragms resulted from an earthquake load in the Y-direction, while axial forces in diaphragms are obtained due to an earthquake in the X-direction. The peak response along all section cuts are shown in Figures B.22 to B.27. It should be noted that the slab elements were modelled using elastic shell element, and the demand forces along section cut are obtained by integrating the stress field determined from finite element analysis.
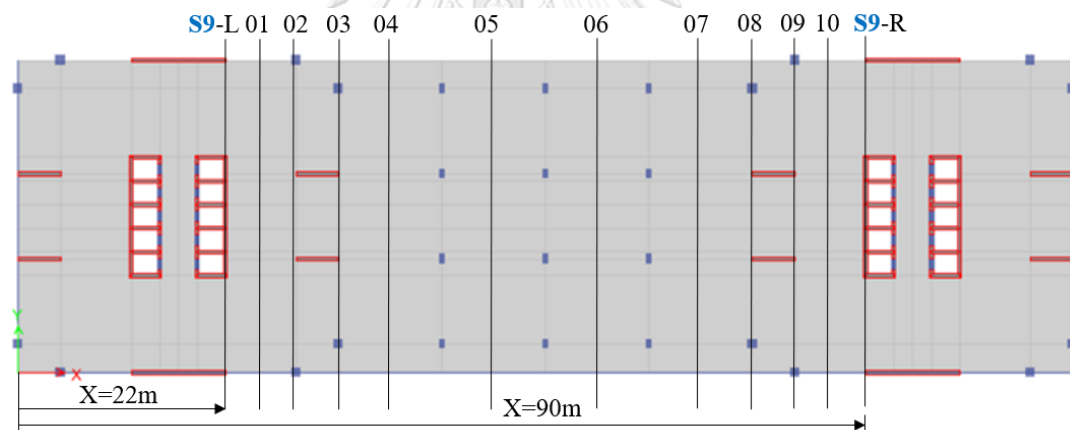
Figure B.21 Section-cut locations.

From figures below, the diaphragm demand forces that corresponds to SH building are similar to demand forces of a simply supported beam subjected to a uniform load. The out of synchronize behaviour of towers in DH building leads to significant contribution of axial forces in the podium floors as shown in Figure B.26 and B.27.

Story 9 - Shear Diagram (kN) - SH

Story 9 - Shear Diagram (kN) - DH

Story 8 - Shear Diagram (kN) - SH

Story 8 - Shear Diagram (kN) - DH

Story 7 - Shear Diagram (kN) - SH

Story 7 - Shear Diagram (kN) - DH

Story 6 - Shear Diagram (kN) - SH

Story 6 - Shear Diagram (kN) - DH

Story 5 - Shear Diagram (kN) - SH

Story 5 - Shear Diagram (kN) - DH

Location of section cut, X (m)

Location of section cut, X (m)
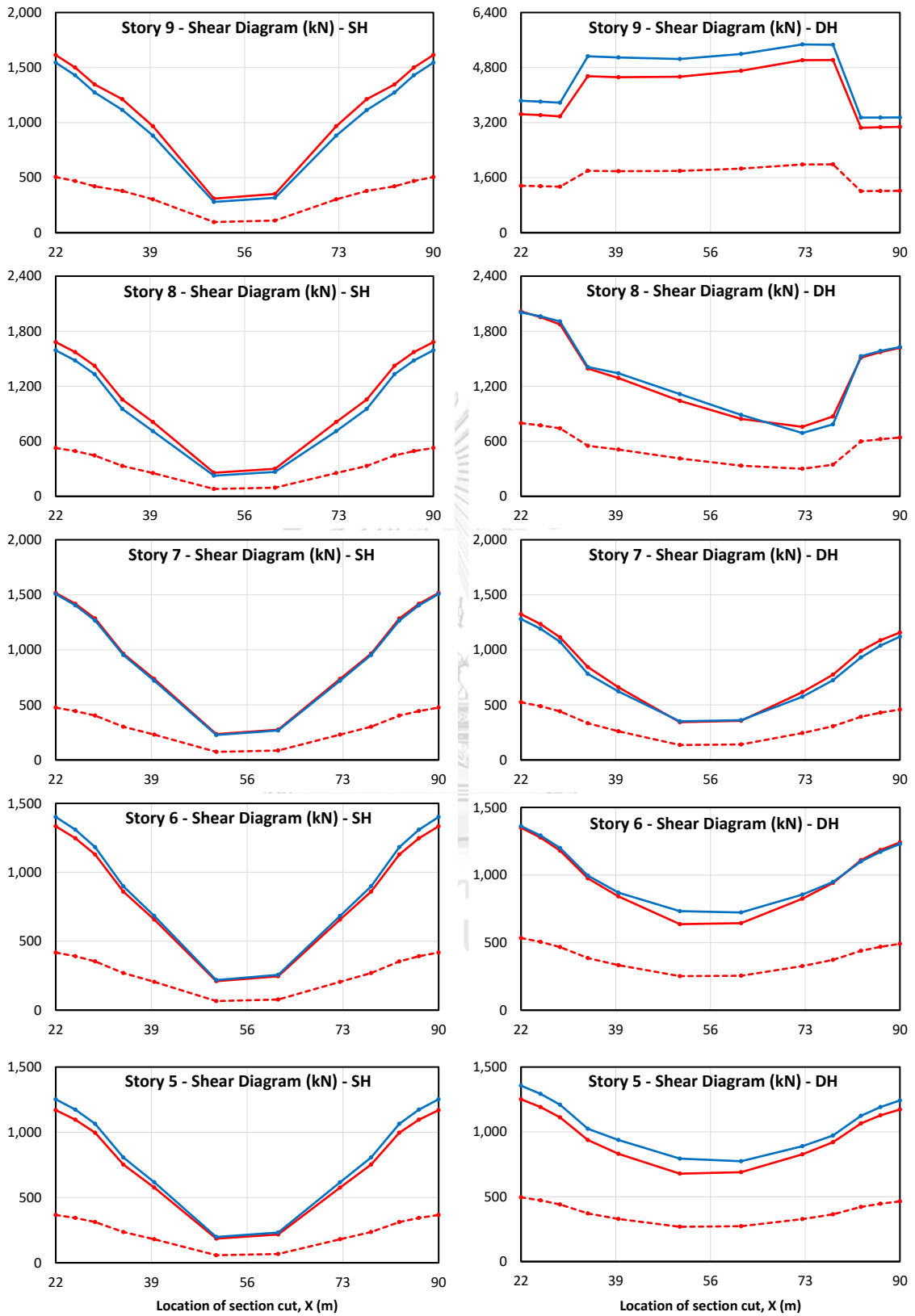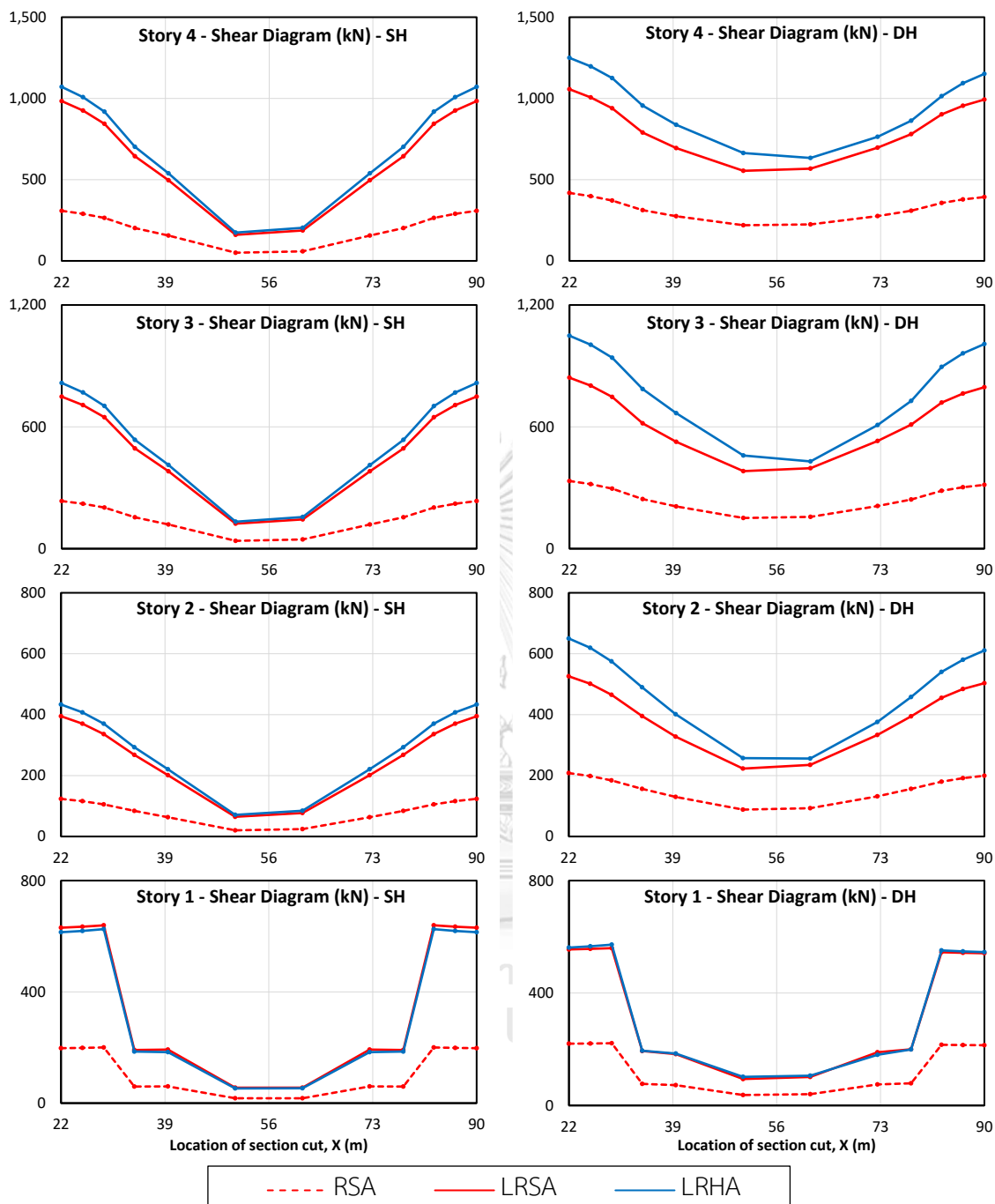
(Continued)

Figure B.22 Shear forces in diaphragms due to earthquake in the Y-direction for buildings SH and DH located in Bangkok.

Story 9 - Moment Diagram (kN.m) - SH

Story 9 - Moment Diagram (kN.m) - DH

Story 8 - Moment Diagram (kN.m) - SH

Story 8 - Moment Diagram (kN.m) - DH

Story 7 - Moment Diagram (kN.m) - SH

Story 7 - Moment Diagram (kN.m) - DH

Story 6 - Moment Diagram (kN.m) - SH

Story 6 - Moment Diagram (kN.m) - DH

Story 5 - Moment Diagram (kN.m) - SH

Story 5 - Moment Diagram (kN.m) - DH

Location of section cut, X (m)

Location of section cut, X (m)
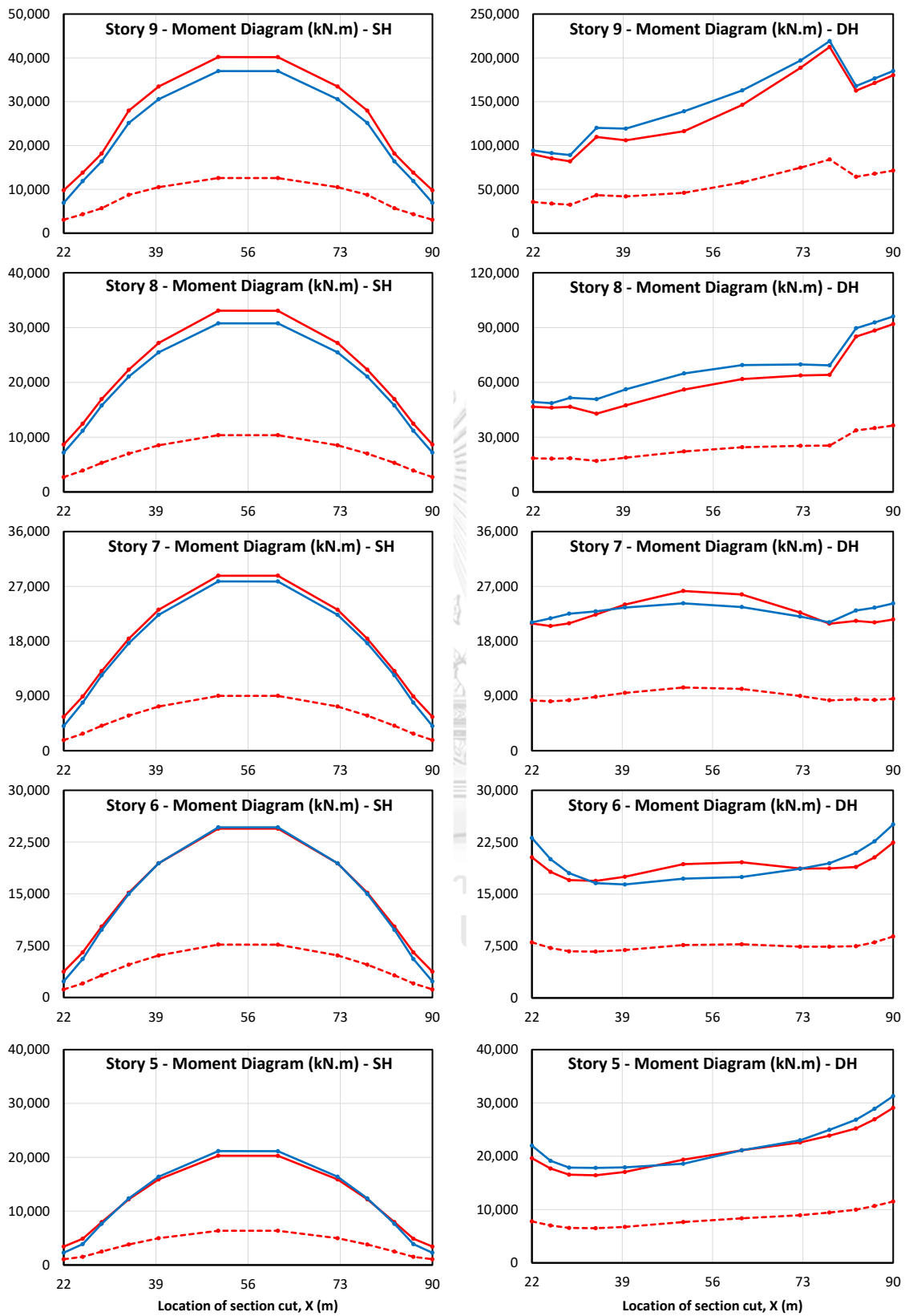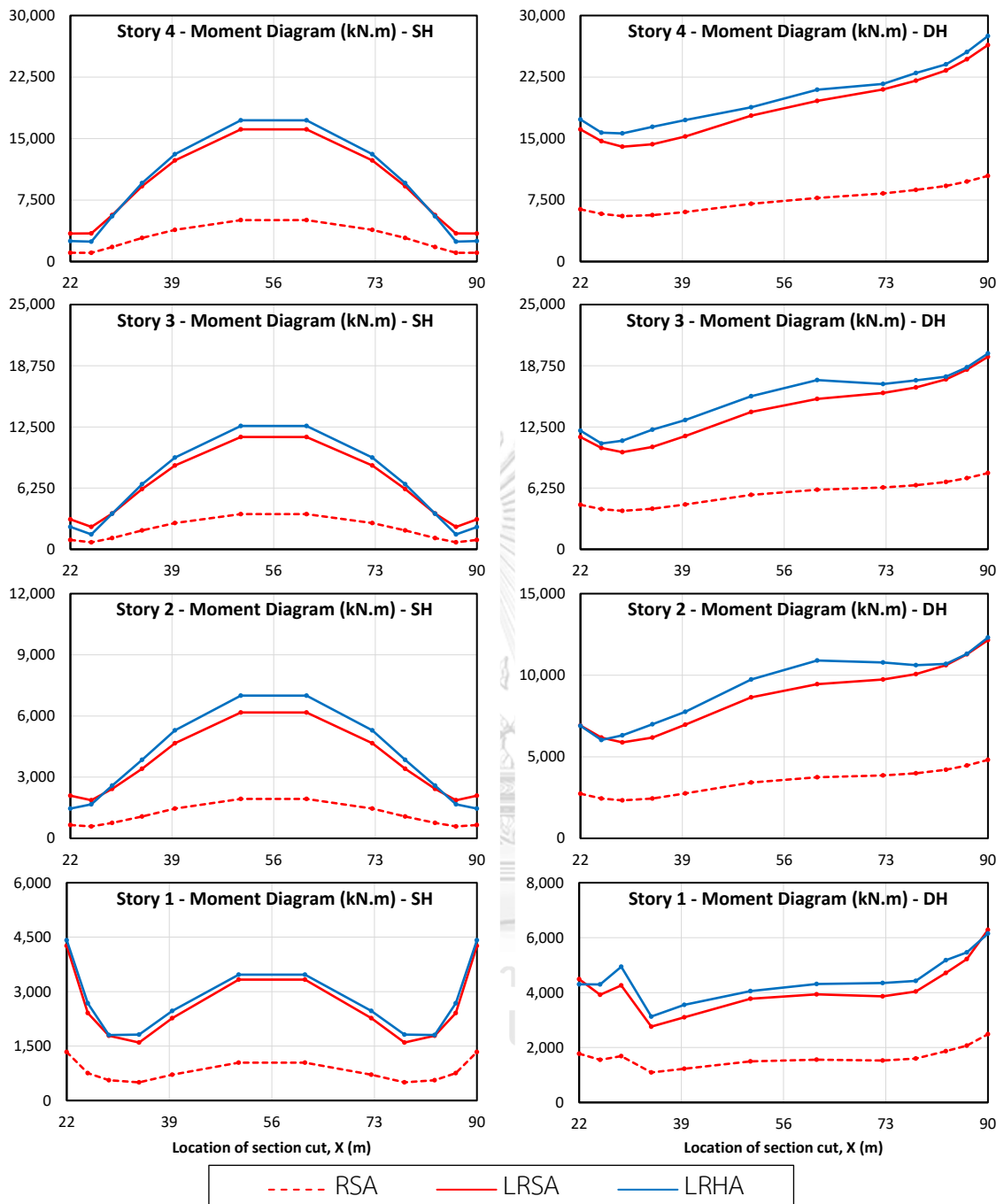
(Continued)

Figure B.23 Bending moment in diaphragms due to earthquake in the Y-direction for buildings SH and DH located in Bangkok.

Story 9 - Shear Diagram (kN) - SH

Story 9 - Shear Diagram (kN) - DH

Story 8 - Shear Diagram (kN) - SH

Story 8 - Shear Diagram (kN) - DH

Story 7 - Shear Diagram (kN) - SH

Story 7 - Shear Diagram (kN) - DH

Story 6 - Shear Diagram (kN) - SH

Story 6 - Shear Diagram (kN) - DH

Story 5 - Shear Diagram (kN) - SH

Story 5 - Shear Diagram (kN) - DH

Location of section cut, X (m)

Location of section cut, X (m)
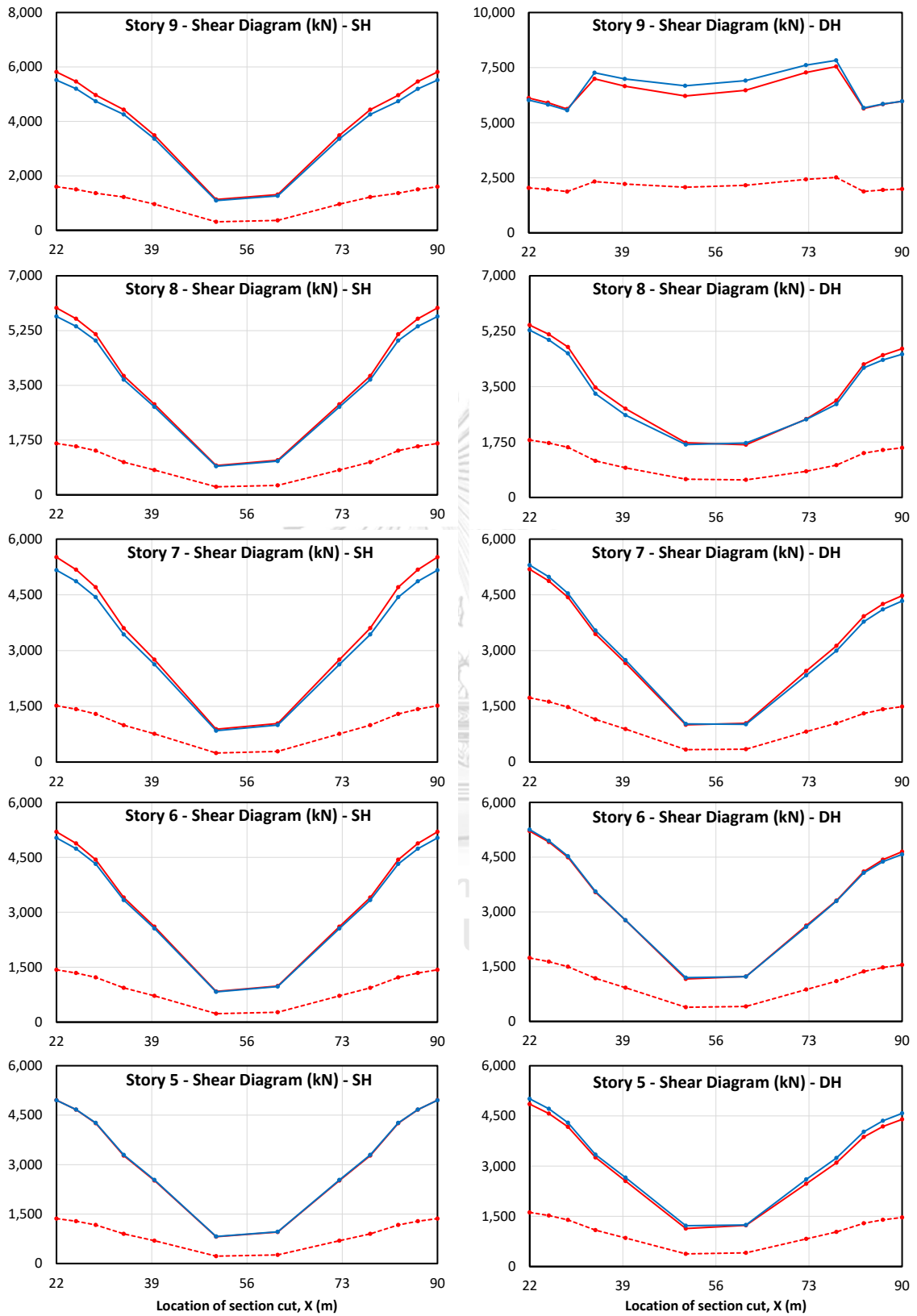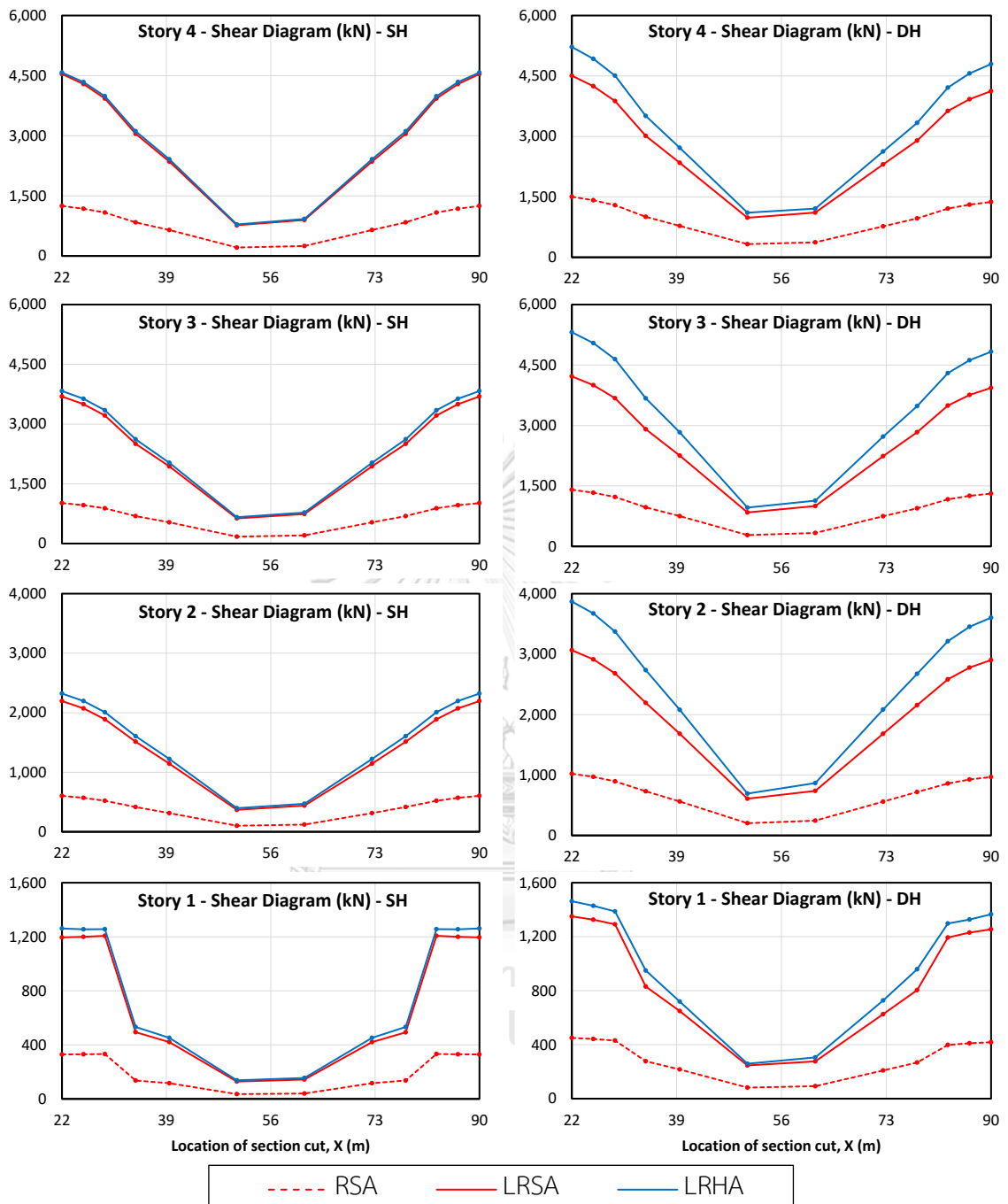
(Continued)

Figure B.24 Shear forces in diaphragms due to earthquake in the Y-direction for buildings SH and DH located in Chiang Mai.

Story 9 - Moment Diagram (kN.m) - SH

Story 9 - Moment Diagram (kN.m) - DH

Story 8 - Moment Diagram (kN.m) - SH

Story 8 - Moment Diagram (kN.m) - DH

Story 7 - Moment Diagram (kN.m) - SH

Story 7 - Moment Diagram (kN.m) - DH

Story 6 - Moment Diagram (kN.m) - SH

Story 6 - Moment Diagram (kN.m) - DH

Story 5 - Moment Diagram (kN.m) - SH

Story 5 - Moment Diagram (kN.m) - DH

Location of section cut, X (m)

Location of section cut, X (m)
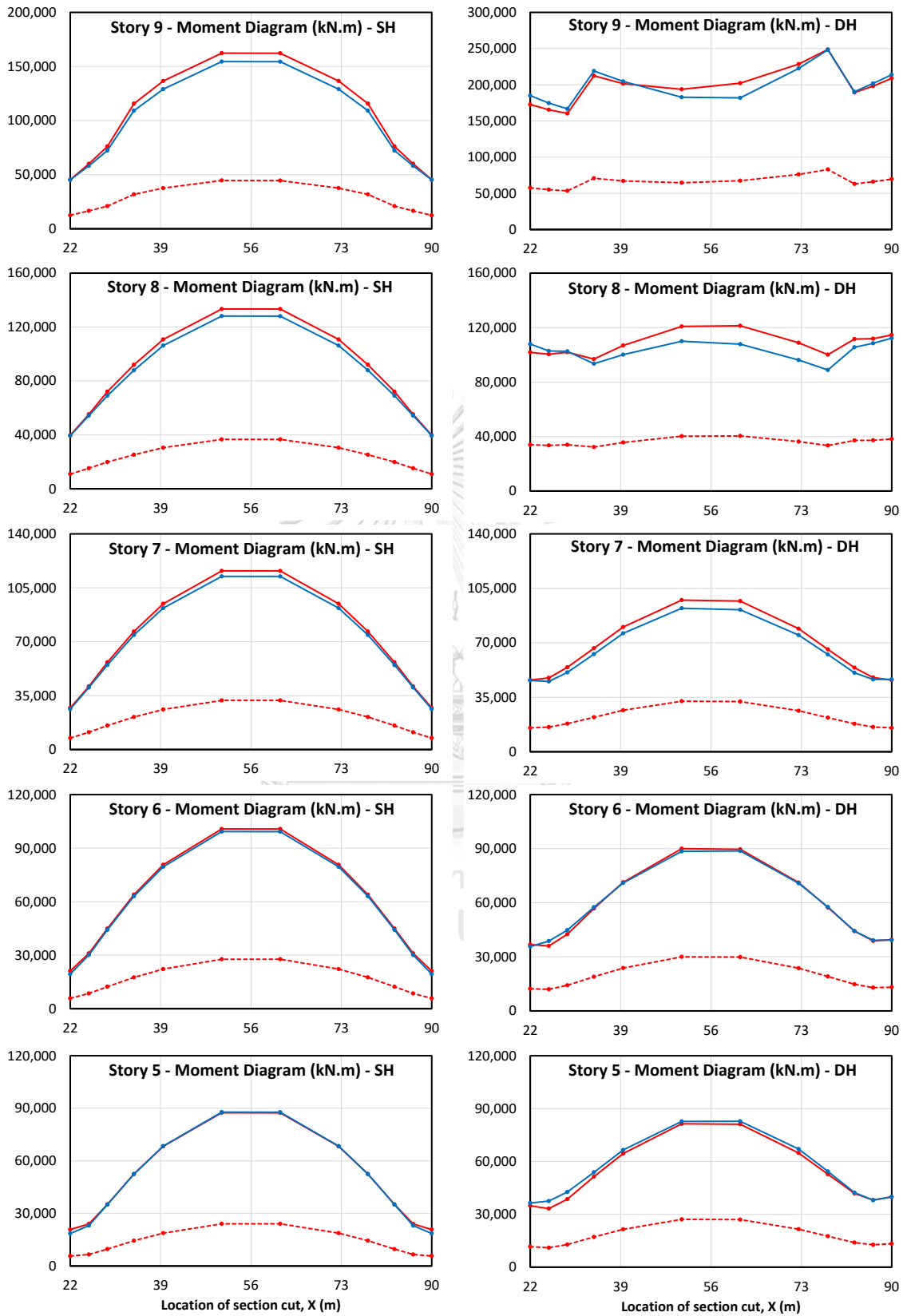
(Continued)
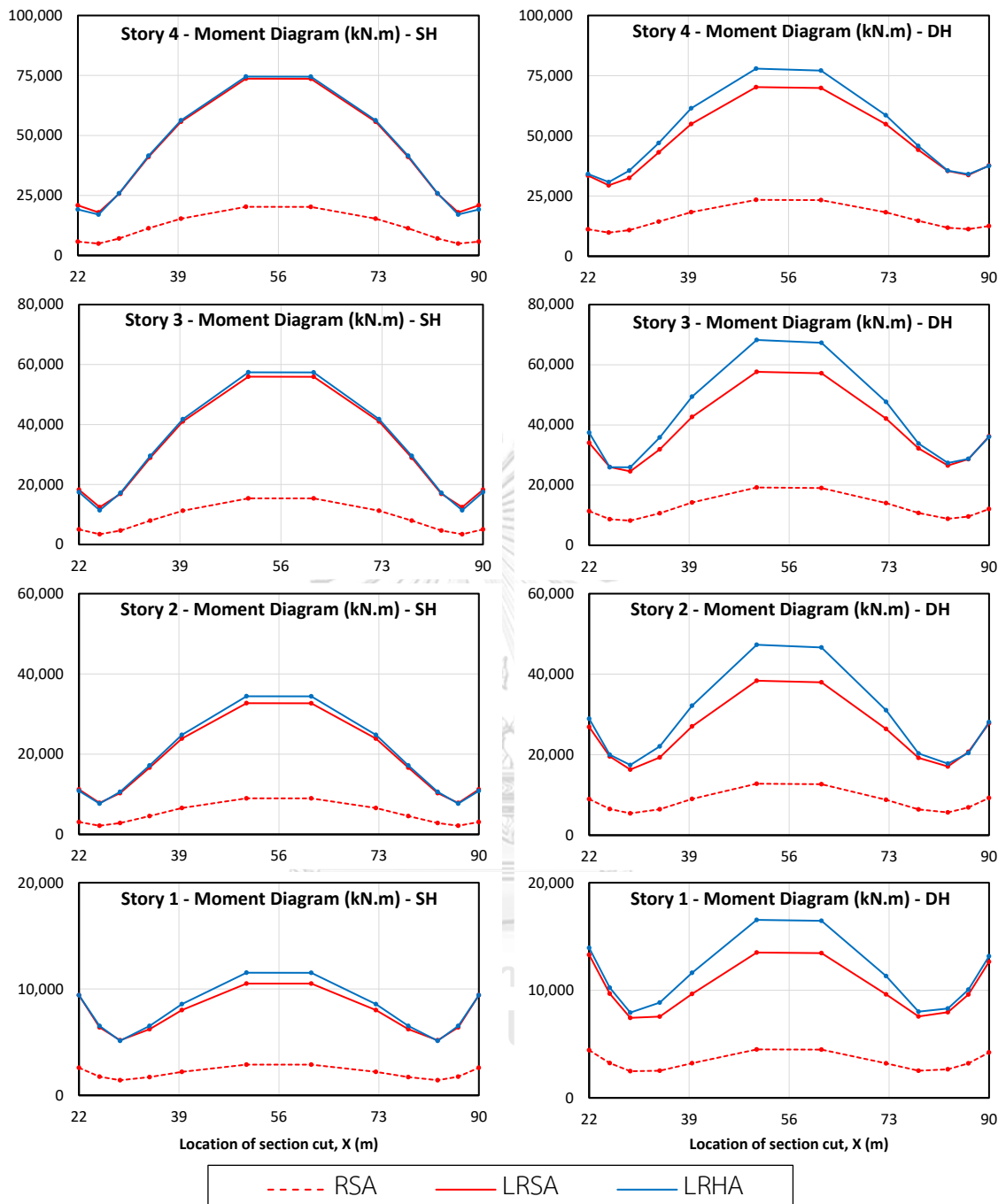
Figure B.25 Bending moment in diaphragms due to earthquake in the Y-direction for buildings SH and DH located in Chiang Mai.
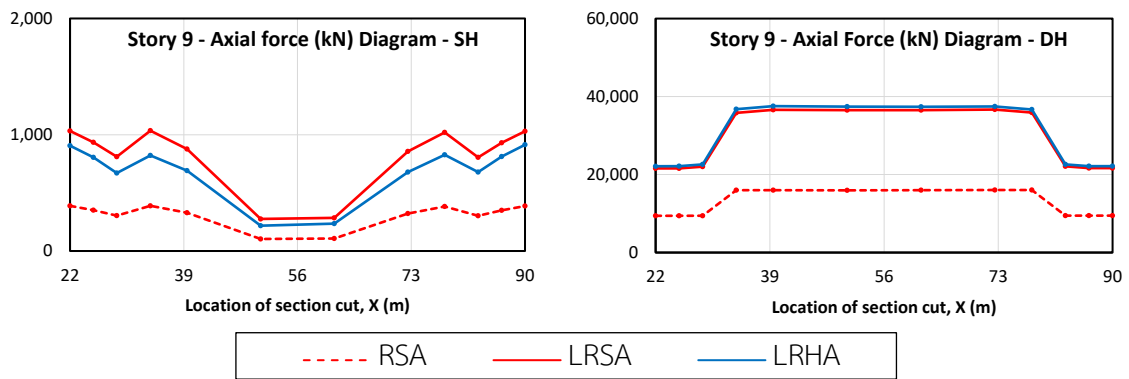
Figure B.26 Axial forces in diaphragms on the 9th floor of SH and DH buildings located in Bangkok due to earthquake in the X-direction.
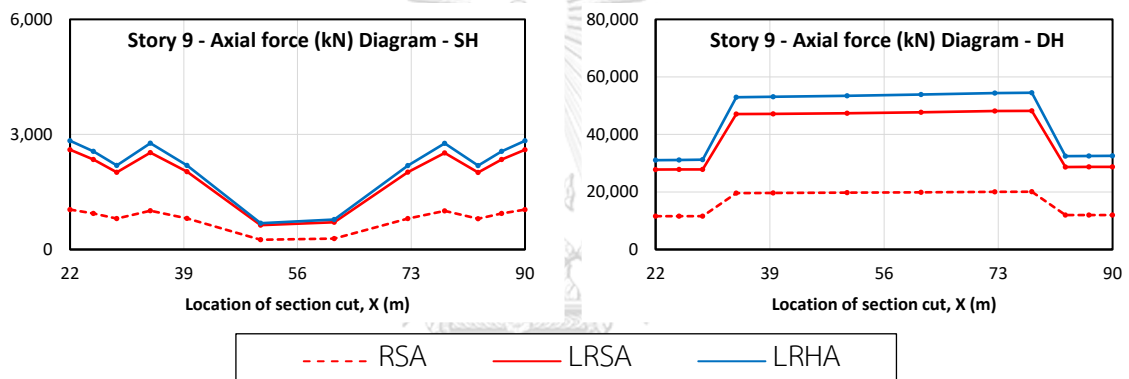
Figure B.27 Axial forces in diaphragms on the 9th floor of SH and DH buildings located in Chiang Mai due to earthquake in the X-direction.

APPENDIX C

LINEAR RESPONSE SPECTRUM ANALYSIS AND NONLINEAR RESPONSE HISTORY ANALYSIS

C.1 Vertical element forces

In this section, piers and columns forces are presented for the two buildings located in Bangkok and Chiang Mai. Results from LRSA$_{uncracked}$, LRSA, and RSA are compared to NLRHA results. Due to symmetrical response in both towers in building SH, and symmetry of structural configuration in towers, some of the structural elements are sharing the same demand forces. More details can be found in section 4.4 regarding methods described in this section.
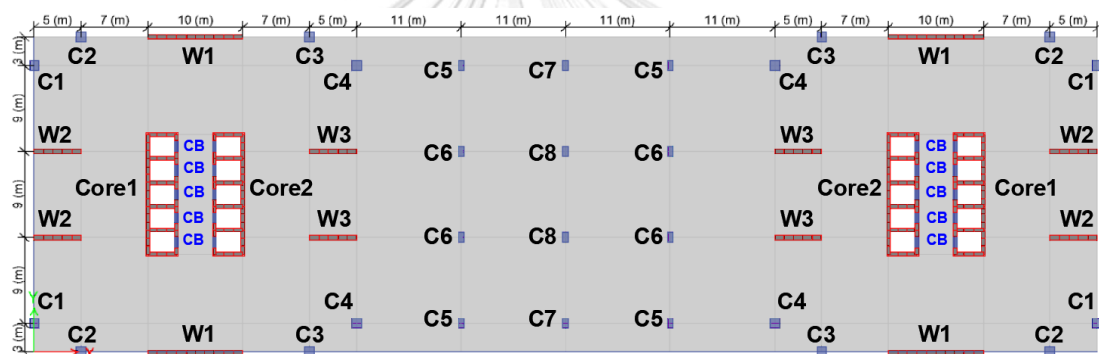
Figure C.1 Denotation of vertical members in building SH.
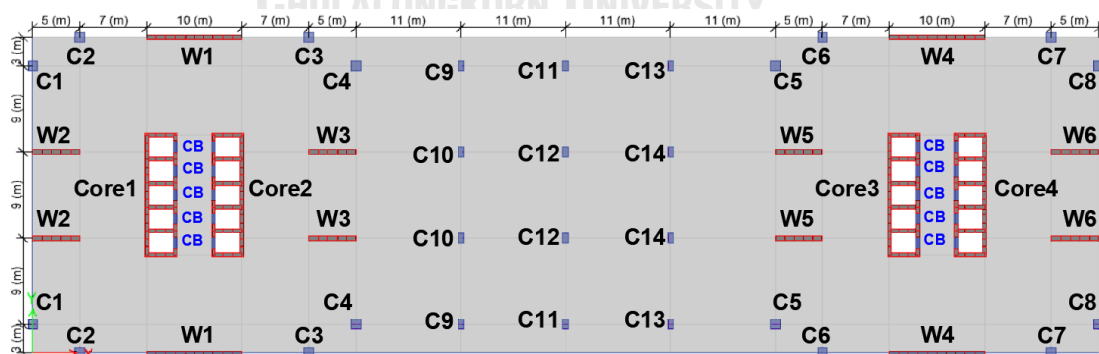
Figure C.2 Denotation of vertical members in building DH.

C.1.1 Wall forces
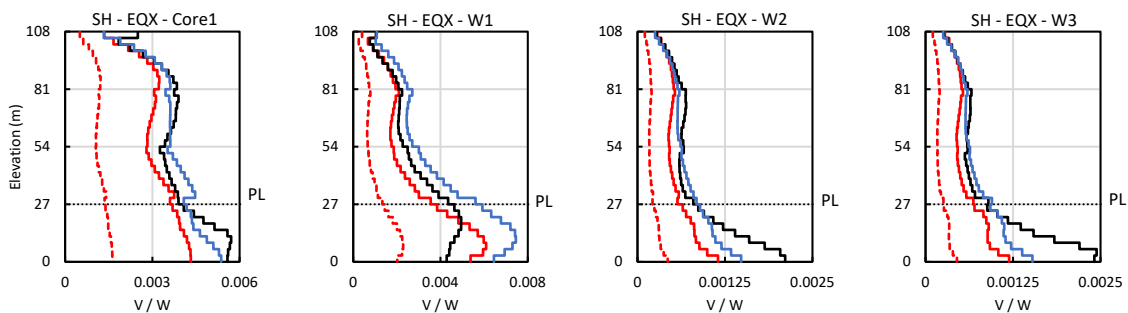
(a) Wall shear forces due to EQX
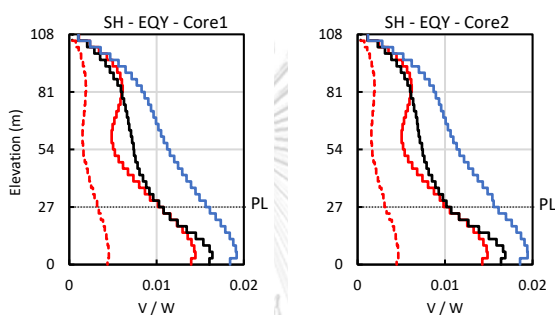
(b) Wall shear forces due to EQY
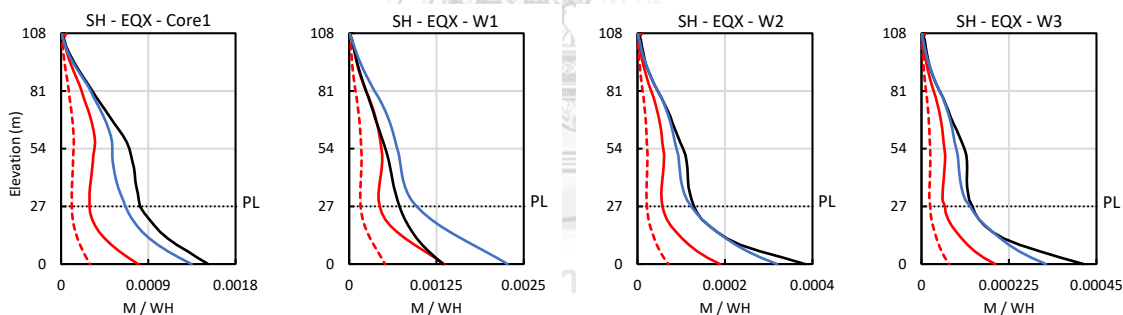
(c) Wall bending moment due to EQX
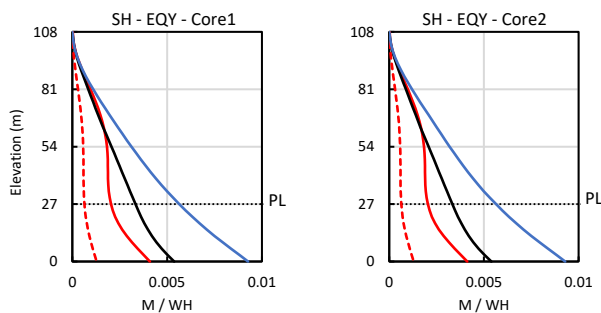
(d) Wall bending moment due to EQY

Figure C.3 Wall shear forces and bending moment of building SH located in Bangkok due to earthquake in X- and Y-direction.

(a) Wall shear forces due to EQX

(b) Wall shear forces due to EQY

- - - - RSA ——— LRSA ——— LRSA uncracked ——— NLRHA
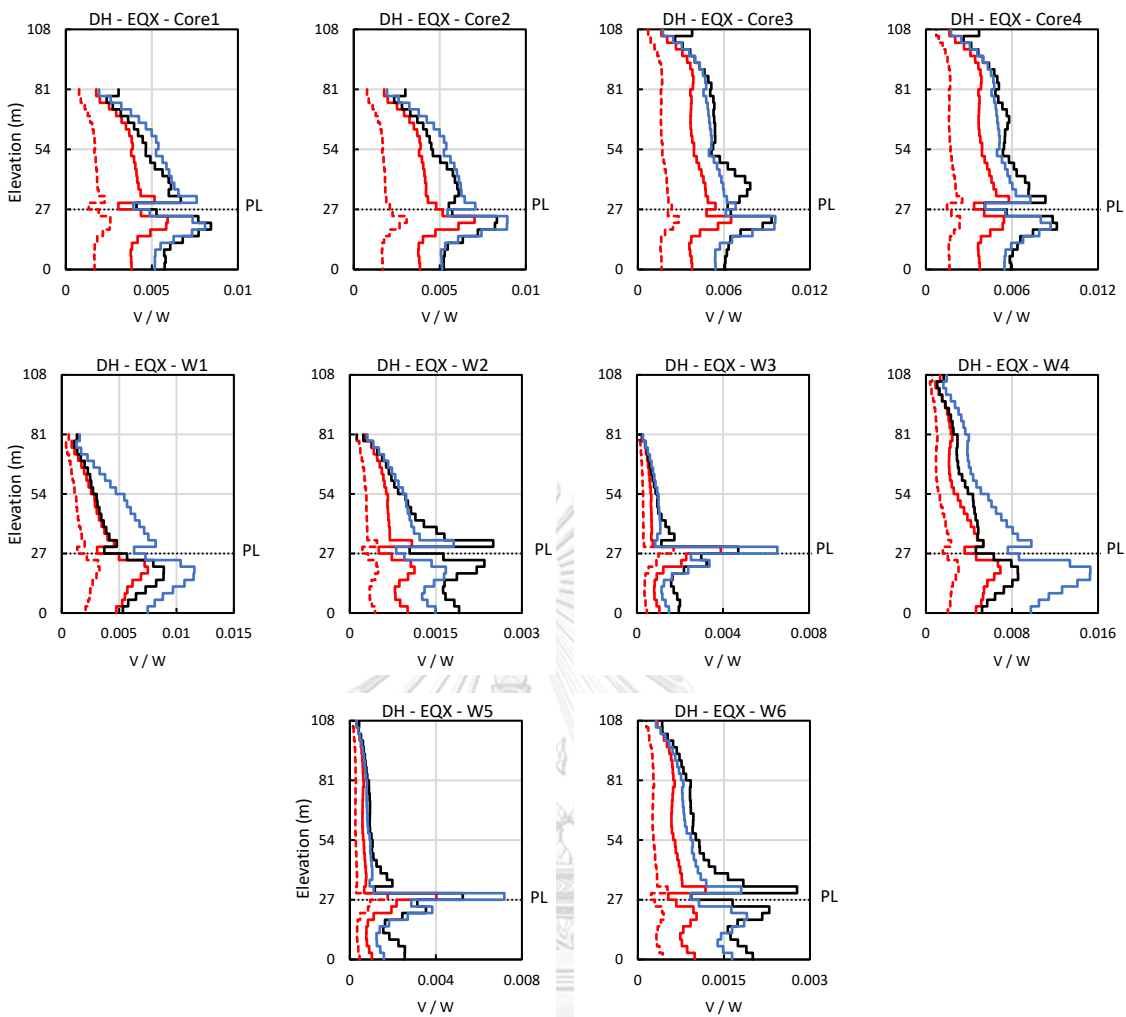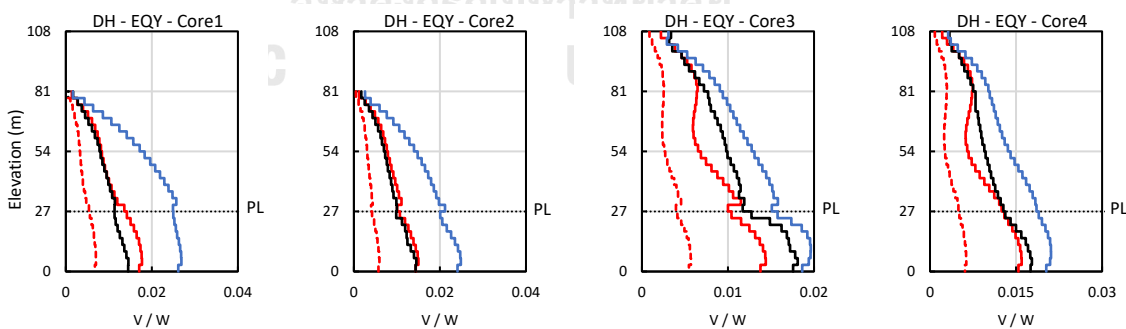
Figure C.4 Wall shear forces of building DH located in Bangkok due to earthquake in (a) X-direction (EQX); (b) Y-direction (EQY).

(a) Wall bending moment due to EQX

(b) Wall bending moment due to EQY

- - - - RSA ——— LRSA ——— LRSA uncracked ——— NLRHA
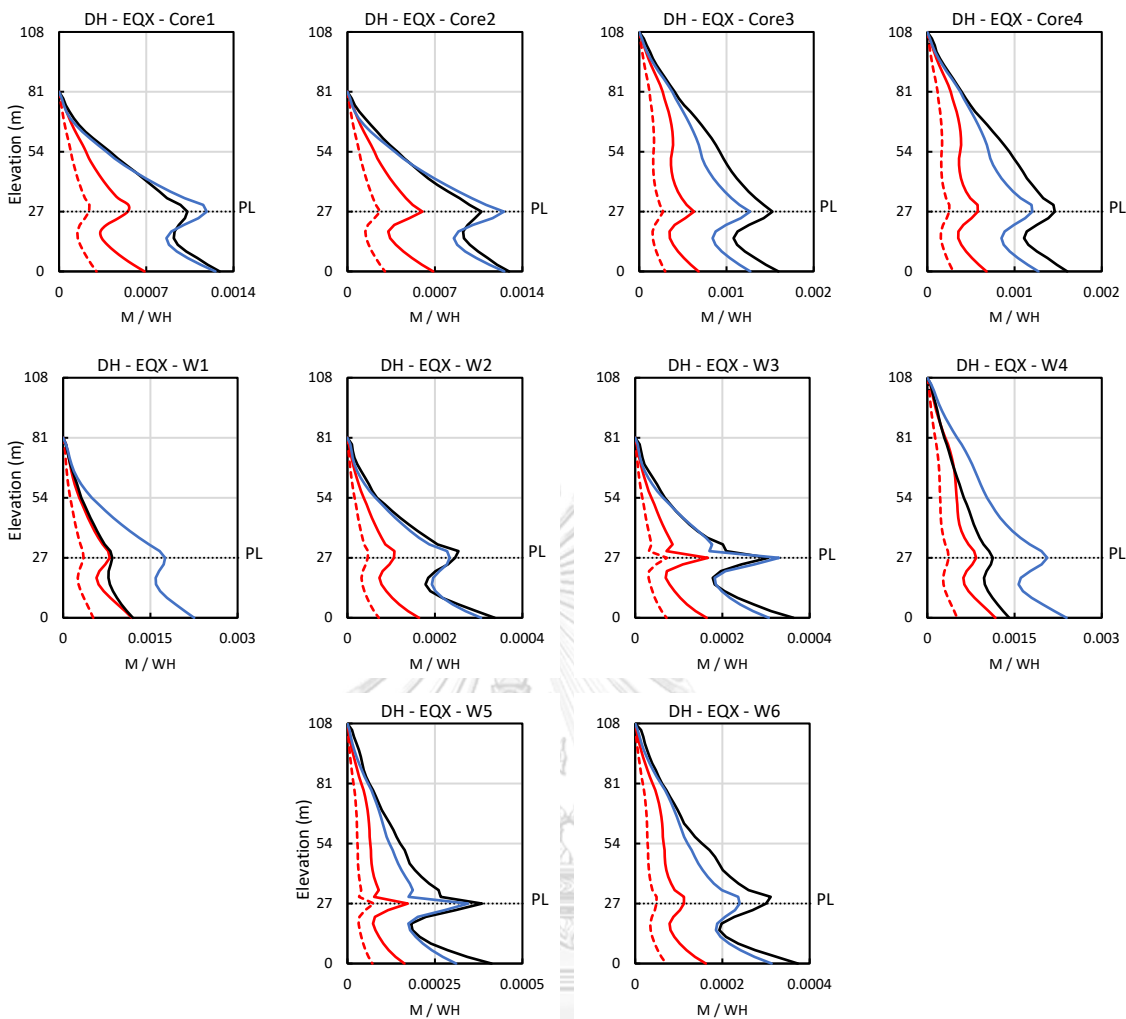
Figure C.5 Wall bending moment for building DH located in Bangkok due to earthquake in (a) X-direction (EQX); (b) Y-direction (EQY).

(a) Wall shear forces due to EQX

(b) Wall shear forces due to EQY

(c) Wall bending moment due to EQX

(d) Wall bending moment due to EQY

---- RSA ⎯⎯ LRSA ⎯⎯ LRSA uncracked ⎯⎯ NLRHA
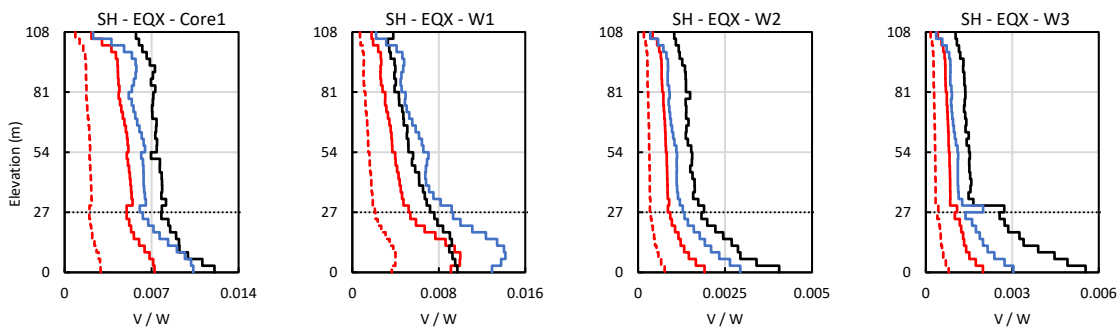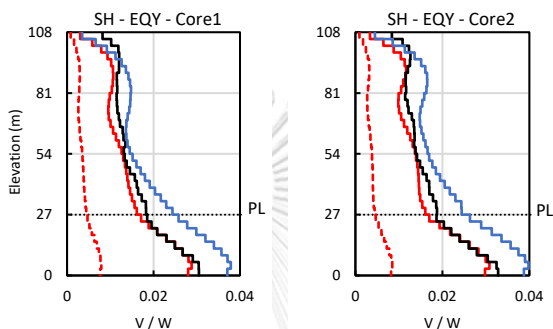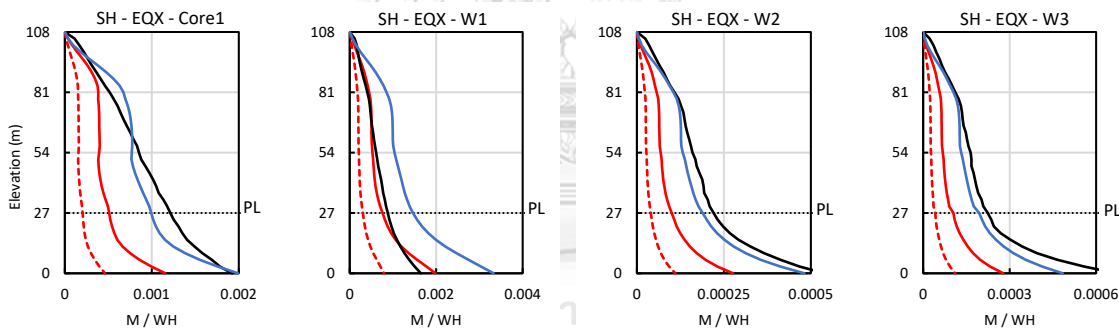
Figure C.6 Wall shear forces and bending moment in both directions for building SH located in Chiang Mai.

(a) Wall shear forces due to EQX

(b) Wall shear forces due to EQY

Figure C.7 Wall shear forces of building DH located in Chiang Mai due to earthquake in (a) X-direction (EQX); (b) Y-direction (EQY).

(a) Wall bending moment due to EQX

(b) Wall bending moment due to EQY

- - - RSA   —— LRSA   —— LRSA uncracked   —— NLRHA
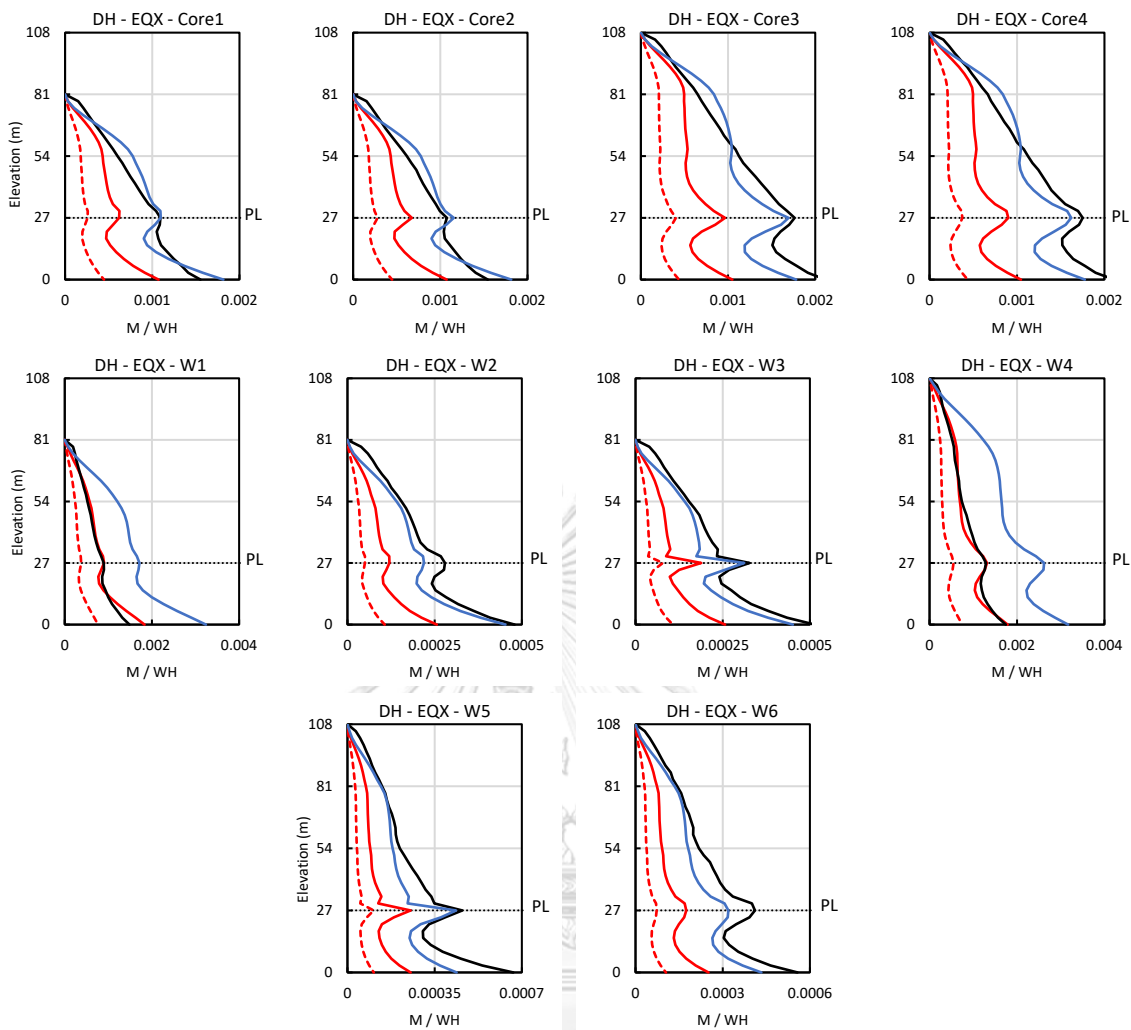
Figure C.8 Wall bending moment for building DH located in Chiang Mai due to earthquake in (a) X-direction (EQX); (b) Y-direction (EQY).

C.1.2 Column forces

(a) Column shear forces due to EQX

(b) Column shear forces due to EQY

- - - RSA ——— LRSA ——— LRSA uncracked ——— NLRHA
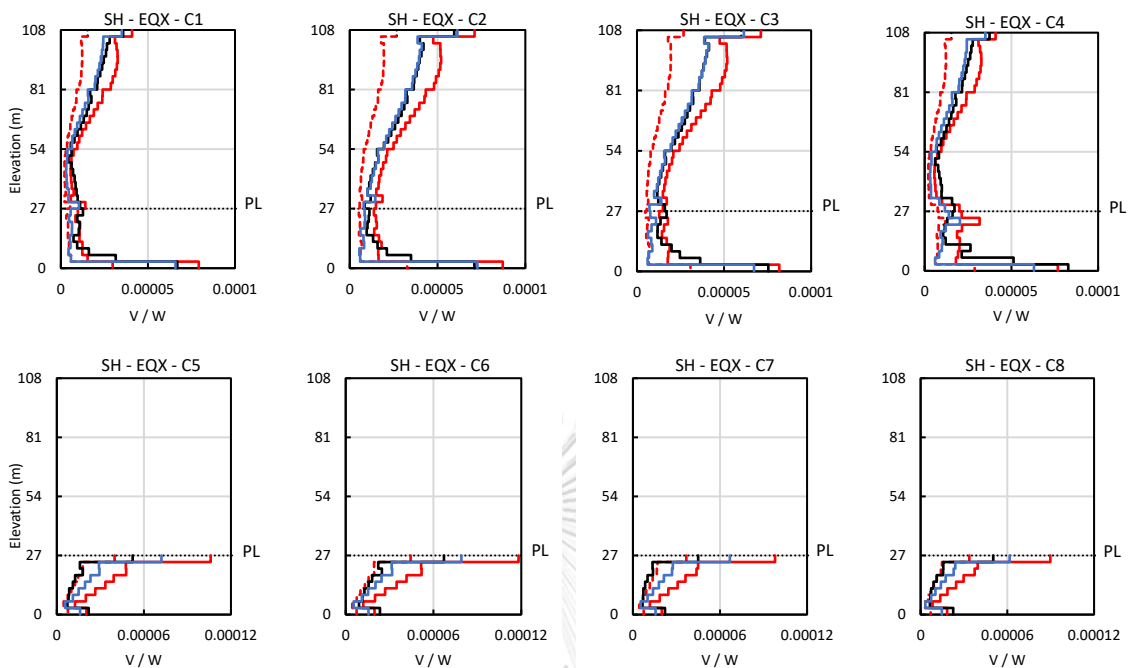
Figure C.9 Column shear forces of building SH located in Bangkok due to earthquake in (a) X-direction (EQX); (b) Y-direction (EQY).

Figure C.10 Column shear forces of building DH located in Bangkok due to earthquake in X-direction (EQX).

Figure C.11 Column shear forces of building DH located in Bangkok due to earthquake in Y-direction (EQY).

(a) Column bending moment due to EQX

(b) Column bending moment due to EQY

- - - - RSA   ——— LRSA   ——— LRSA uncracked   ——— NLRHA

Figure C.12 Column bending moment of building SH located in Bangkok due to earthquake in (a) X-direction (EQX); (b) Y-direction (EQY).

Figure C.13 Column bending moment of building DH located in Bangkok due to earthquake in X-direction (EQX).

Figure C.14 Column bending moment of building DH located in Bangkok due to earthquake in Y-direction (EQY).

(a) Column shear forces due to EQX

(b) Column shear forces due to EQY

---- RSA   —— LRSA   —— LRSA uncracked   —— NLRHA
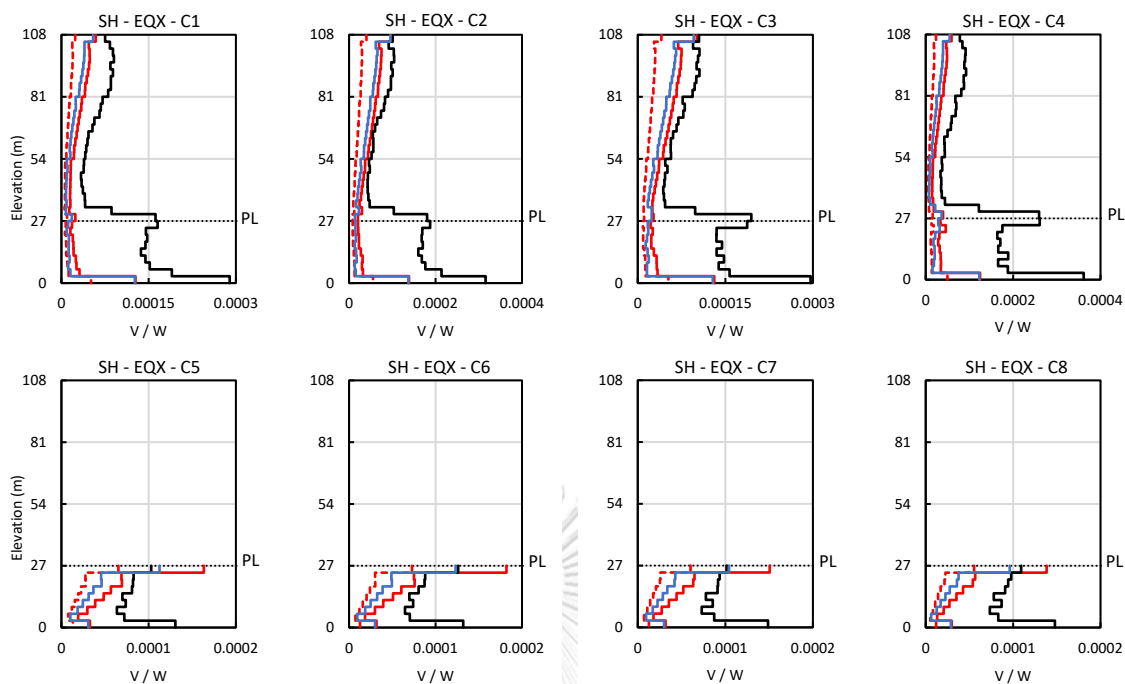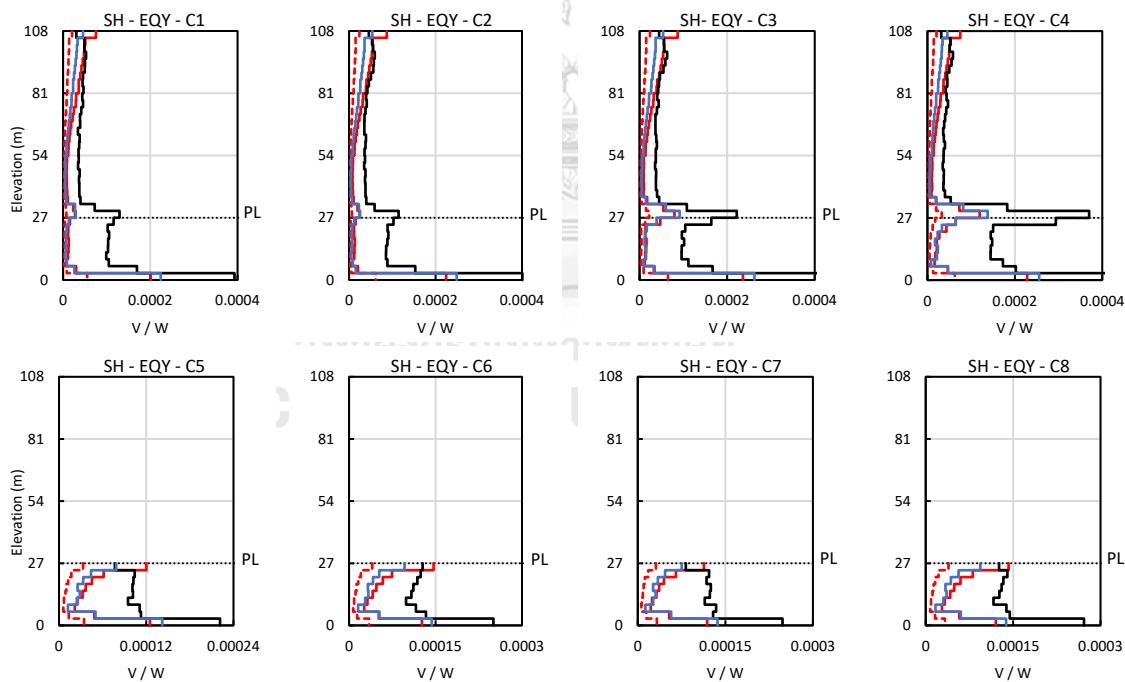
Figure C.15 Column shear forces of building SH located in Chiang Mai due to earthquake in (a) X-direction (EQX); (b) Y-direction (EQY).

Figure C.16 Column shear forces of building DH located in Chiang Mai due to earthquake in X-direction (EQX).

Figure C.17 Column shear forces of building DH located in Chiang Mai due to earthquake in Y-direction (EQY).

(a) Column bending moment due to EQX

(b) Column bending moment due to EQY

RSA ——— LRSA ——— LRSA uncracked ——— NLRHA
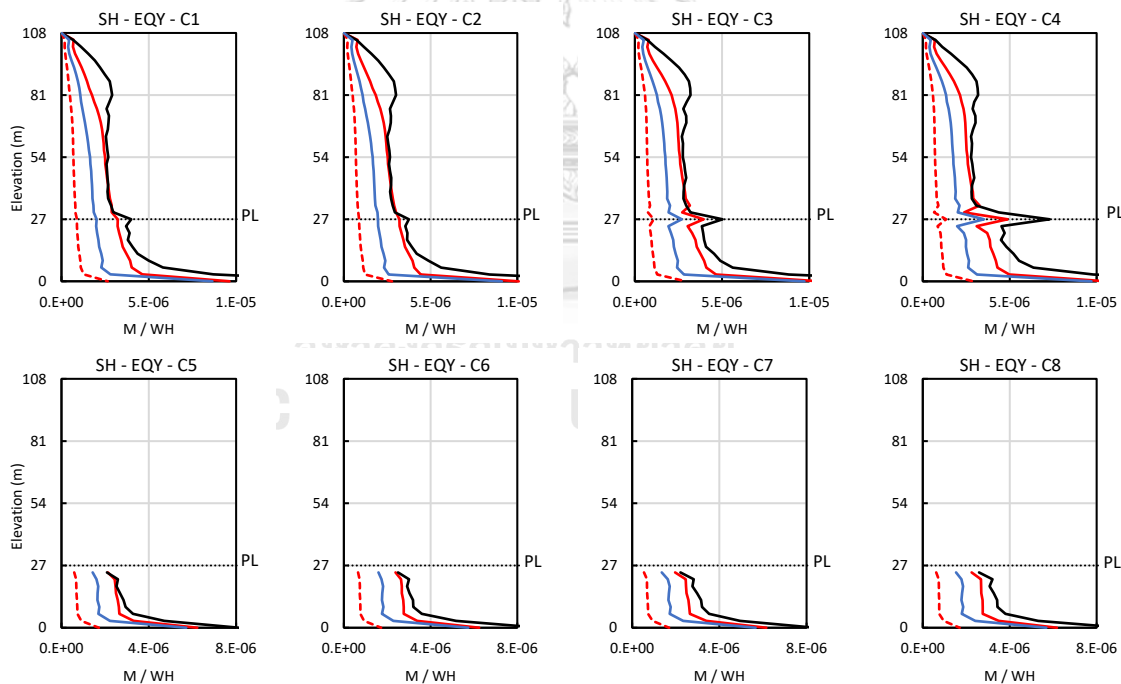
Figure C.18 Column bending moment of building SH located in Chiang Mai due to earthquake in (a) X-direction (EQX); (b) Y-direction (EQY).
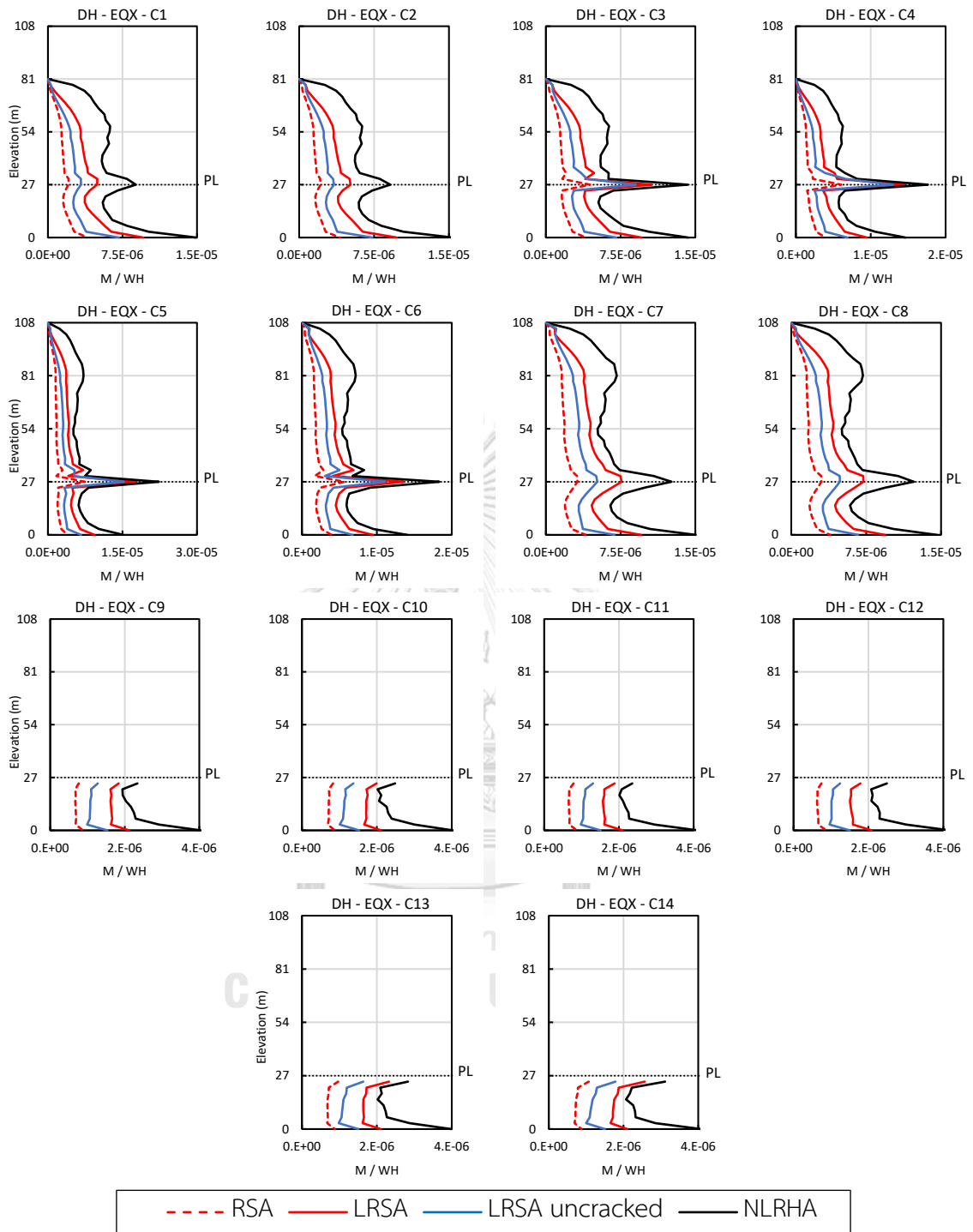
Figure C.19 Column bending moment of building DH located in Chiang Mai due to earthquake in X-direction (EQX).
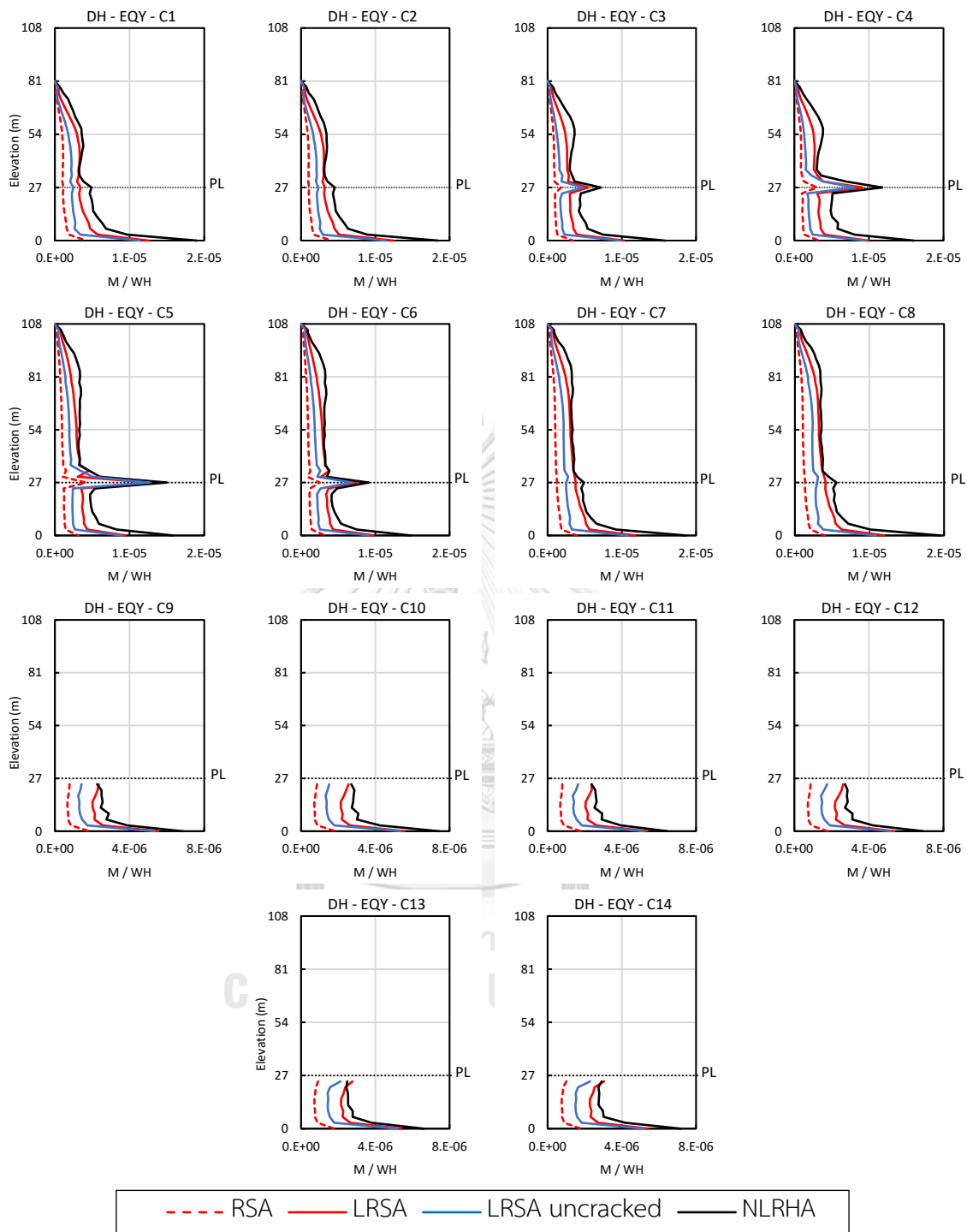
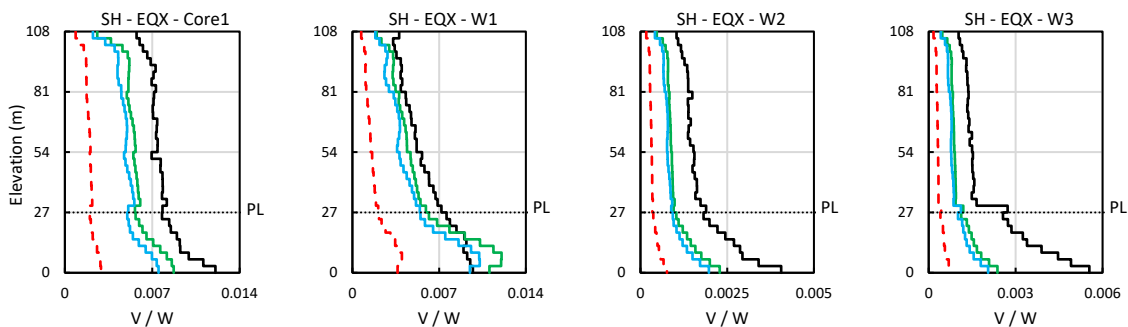Figure C.20 Column bending moment of building DH located in Chiang Mai due to earthquake in Y-direction (EQY).

C.2 Diaphragm forces

In this section, diaphragm forces developed in diaphragm floors of the podium are presented (note that the podium consists of 9 stories). The forces are obtained along section cuts previously defined in ETBAS and PERFORM-3D software. The section-cut locations are shown in the Figure C.21. Floors at the podium level are spanning between two main cantilever core walls aligned in the Y-direction. Hence, the interest is in the shear and bending moment in diaphragms resulted from an earthquake load in the Y-direction, while axial forces in diaphragms are obtained due to an earthquake in the X-direction. The peak response along all section cuts are shown in Figures C.22 to C.27. It should be noted that the slab elements were modelled using elastic shell element, and the demand forces along section cut are obtained by integrating the stress field determined from finite element analysis.
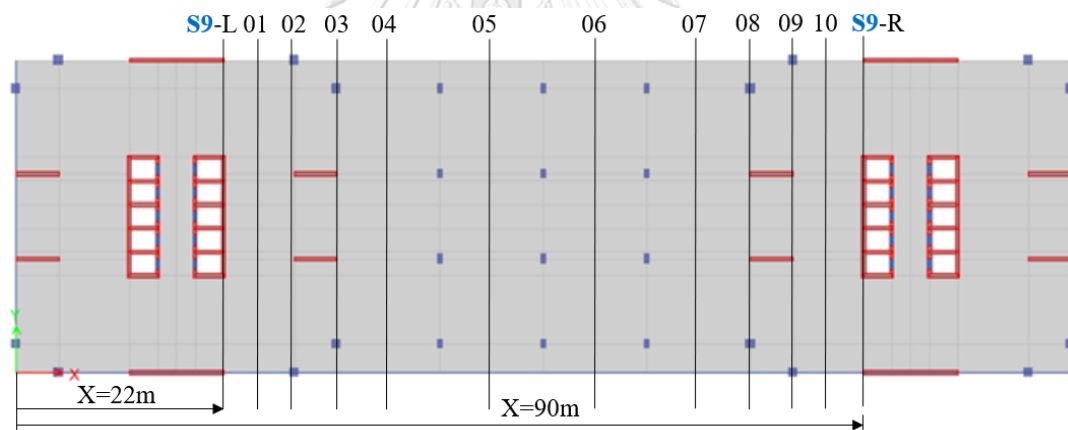
Figure C.21 Section-cut locations.

Story 9 - Shear Diagram (kN) - SH

Story 9 - Shear Diagram (kN) - DH

Story 8 - Shear Diagram (kN) - SH

Story 8 - Shear Diagram (kN) - DH

Story 7 - Shear Diagram (kN) - SH

Story 7 - Shear Diagram (kN) - DH

Story 6 - Shear Diagram (kN) - SH

Story 6 - Shear Diagram (kN) - DH

Story 5 - Shear Diagram (kN) - SH

Story 5 - Shear Diagram (kN) - DH

Location of section cut, X (m)

Location of section cut, X (m)
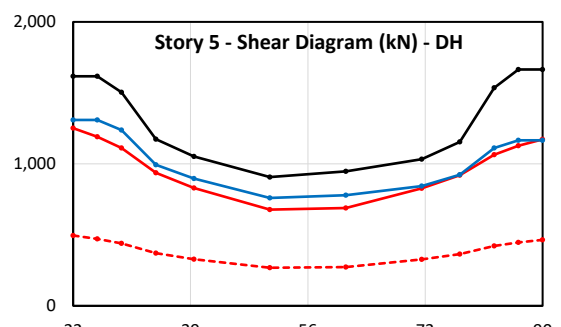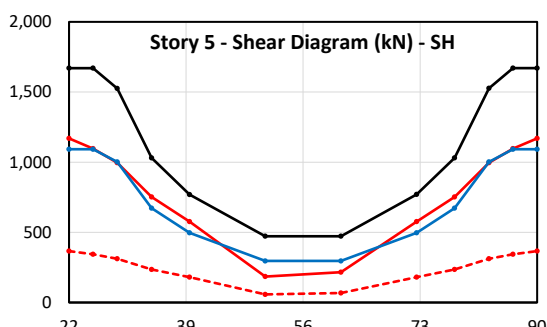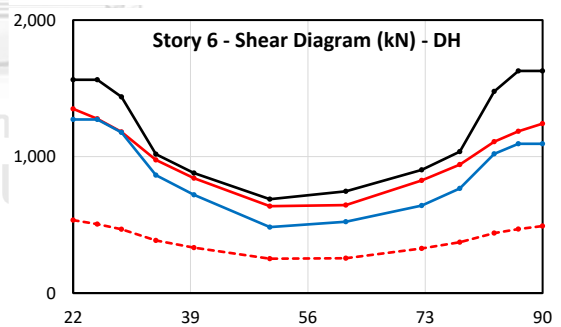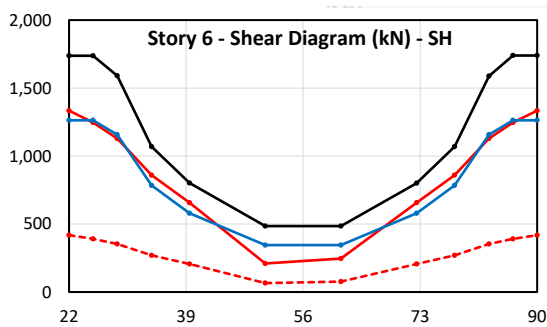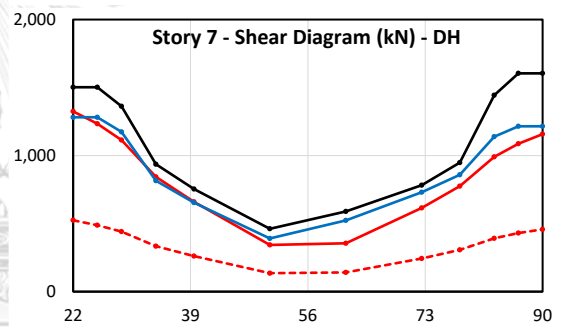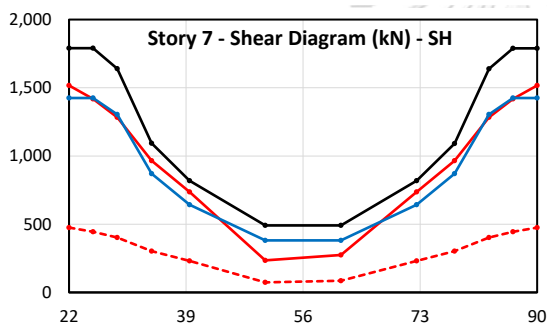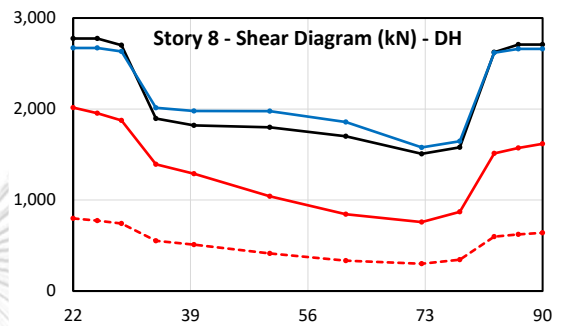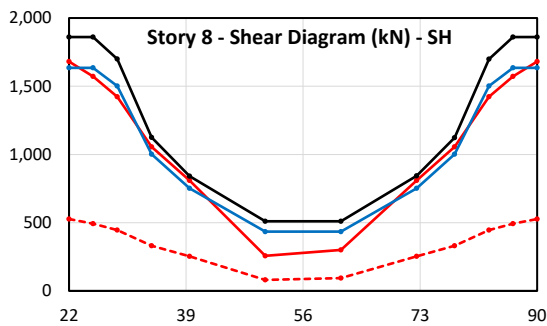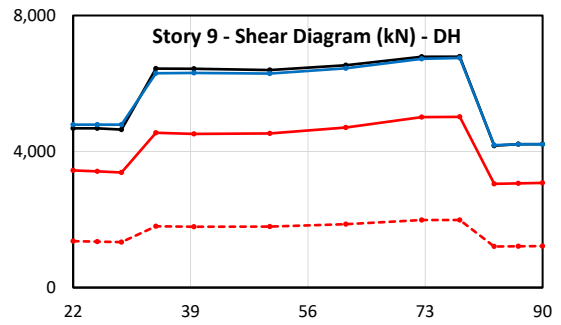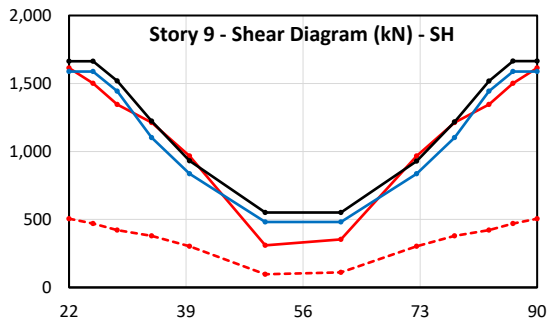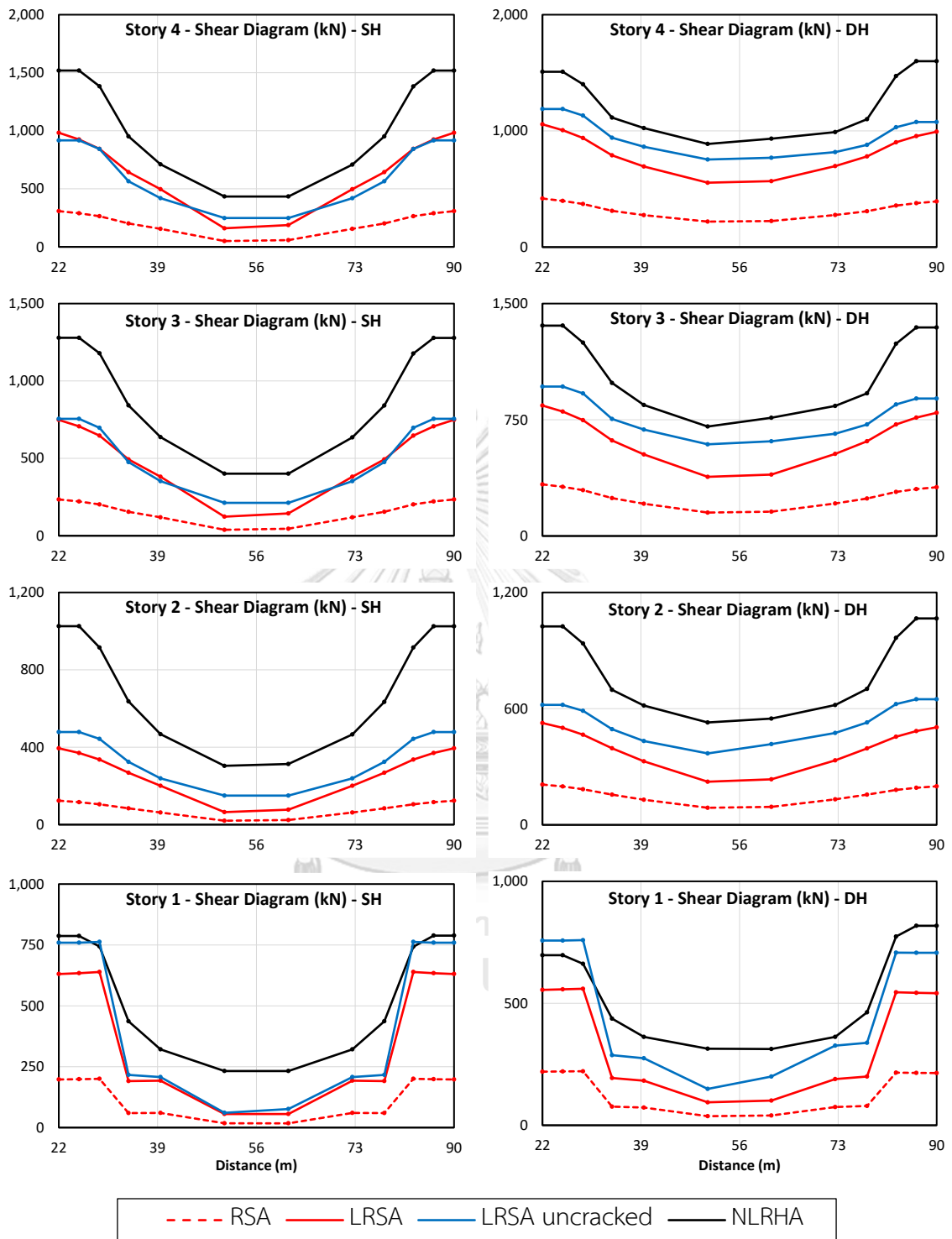
(Continued)

Figure C.22 Shear forces in diaphragms due to earthquake in the Y-direction for buildings SH and DH located in Bangkok.

Story 9 - Moment Diagram (kN.m) - SH

Story 9 - Moment Diagram (kN.m) - DH

Story 8 - Moment Diagram (kN.m) - SH

Story 8 - Moment Diagram (kN.m) - DH

Story 7 - Moment Diagram (kN.m) - SH

Story 7 - Moment Diagram (kN.m) - DH

Story 6 - Moment Diagram (kN.m) - SH

Story 6 - Moment Diagram (kN.m) - DH

Story 5 - Moment Diagram (kN.m) - SH

Story 5 - Moment Diagram (kN.m) - DH

Location of section cut, X (m)

Location of section cut, X (m)
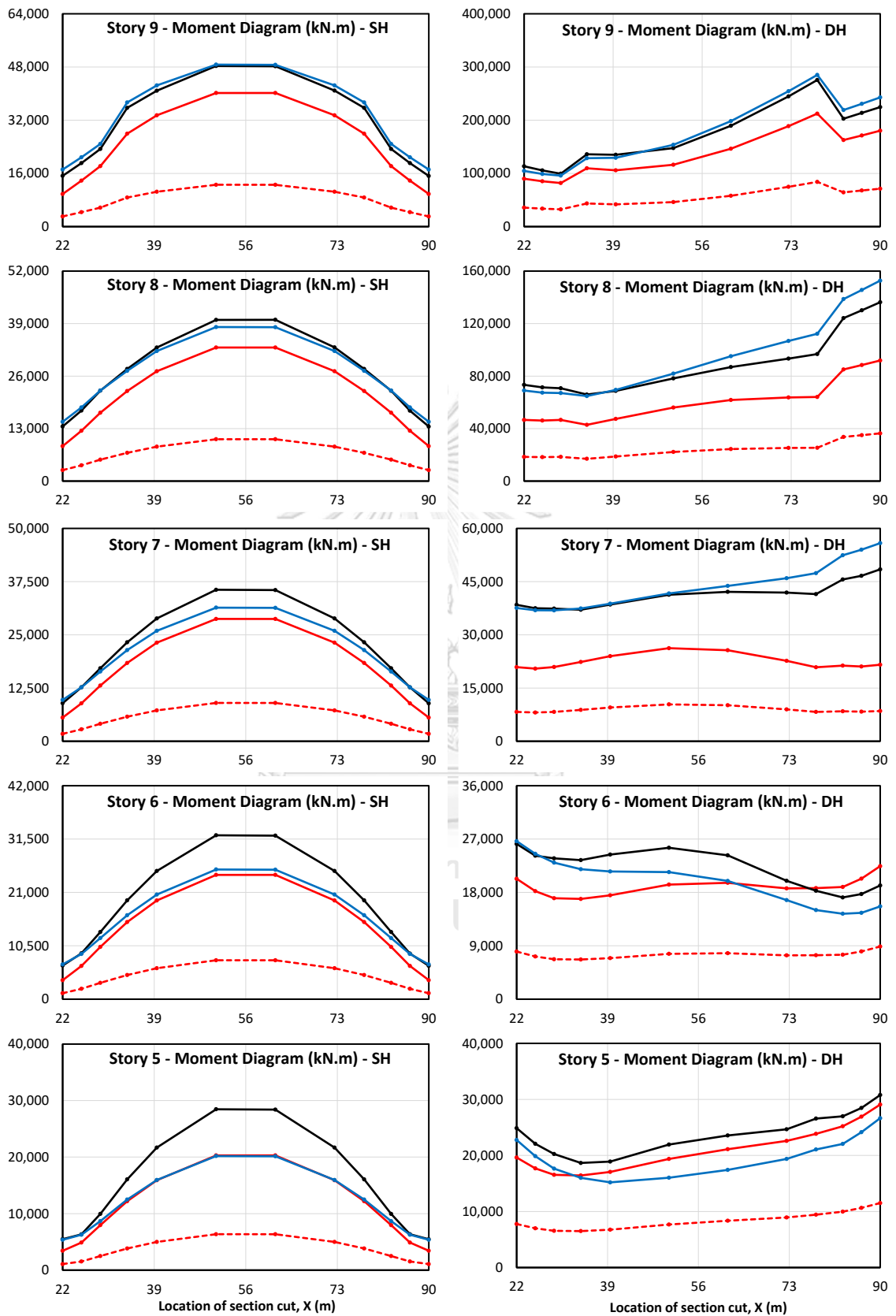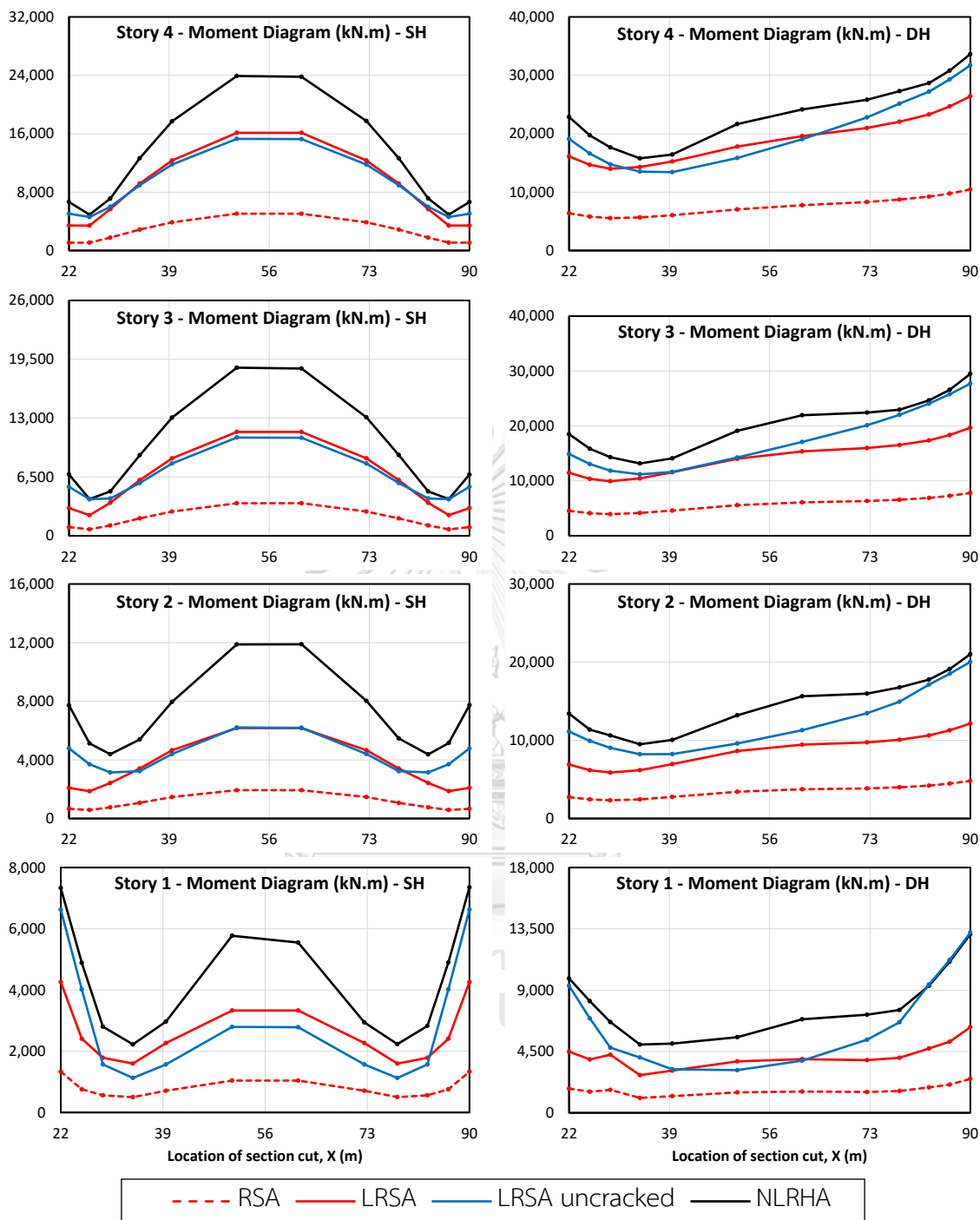
(Continued)

Figure C.23 Bending moment in diaphragms due to earthquake in the Y-direction for buildings SH and DH located in Bangkok.

Story 9 - Shear Diagram (kN) - SH

Story 9 - Shear Diagram (kN) - DH

Story 8 - Shear Diagram (kN) - SH

Story 8 - Shear Diagram (kN) - DH

Story 7 - Shear Diagram (kN) - SH

Story 7 - Shear Diagram (kN) - DH

Story 6 - Shear Diagram (kN) - SH

Story 6 - Shear Diagram (kN) - DH

Story 5 - Shear Diagram (kN) - SH

Story 5 - Shear Diagram (kN) - DH

Location of section cut, X (m)

Location of section cut, X (m)
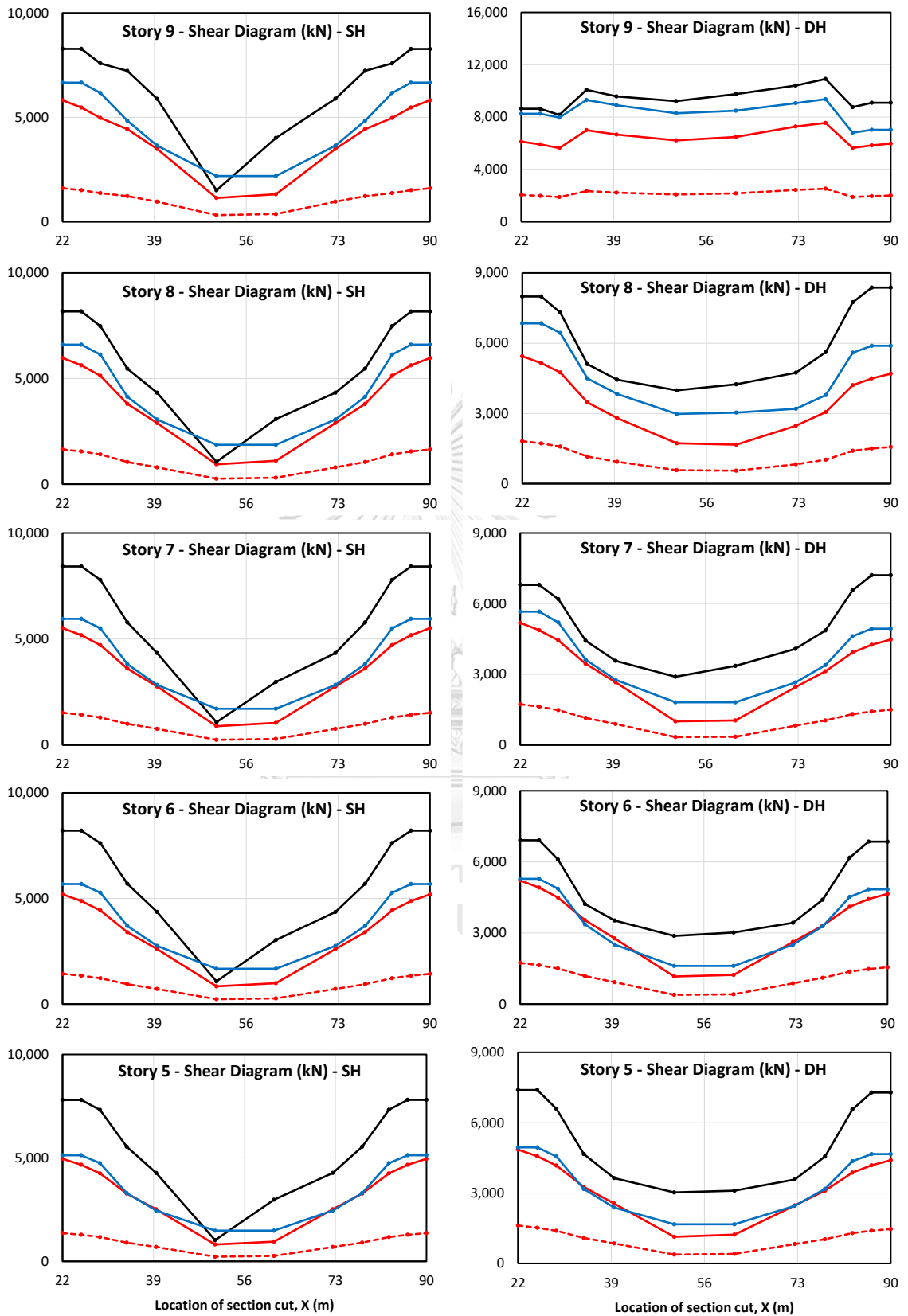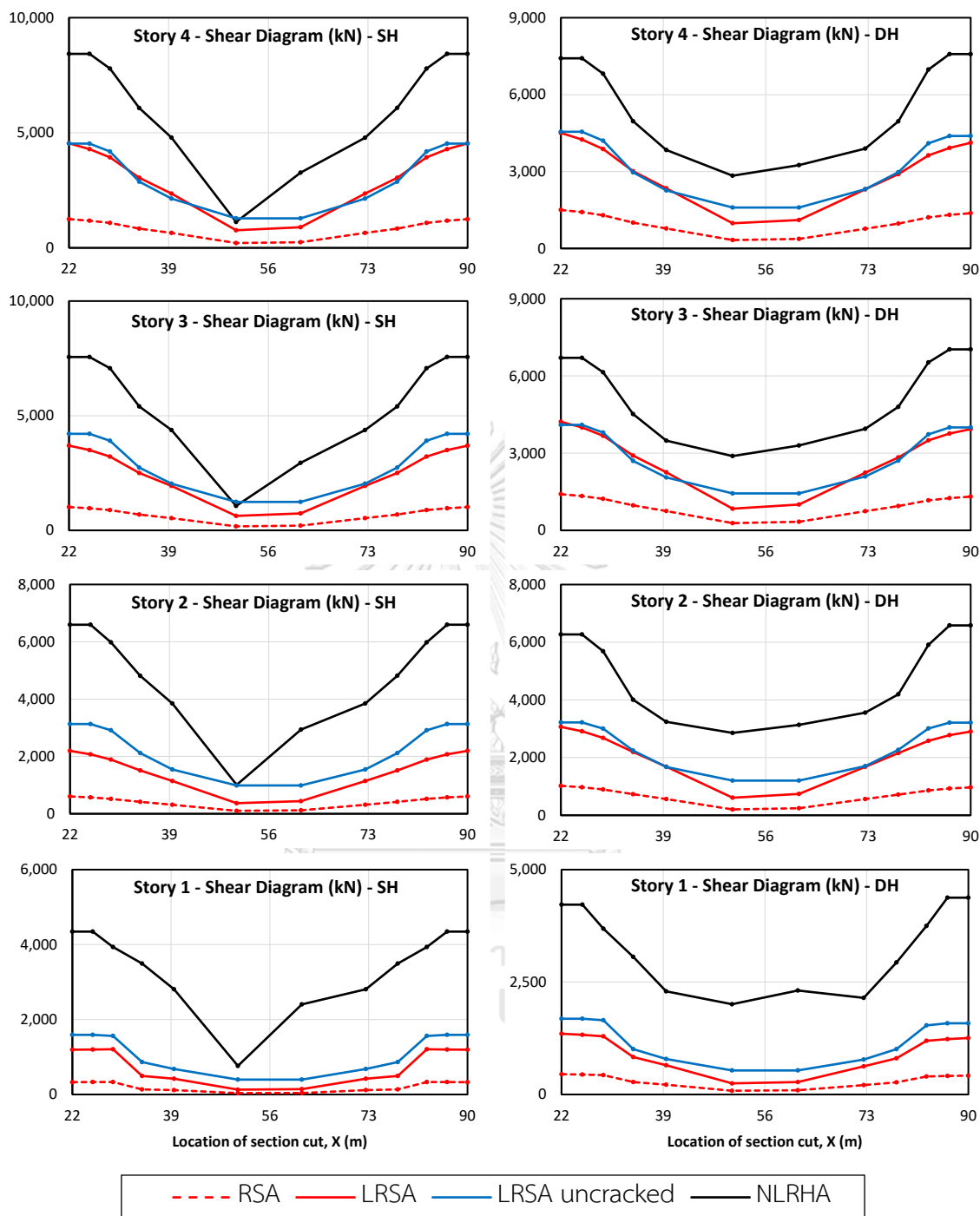
(Continued)

Figure C.24 Shear forces in diaphragms due to earthquake in the Y-direction for buildings SH and DH located in Chiang Mai.
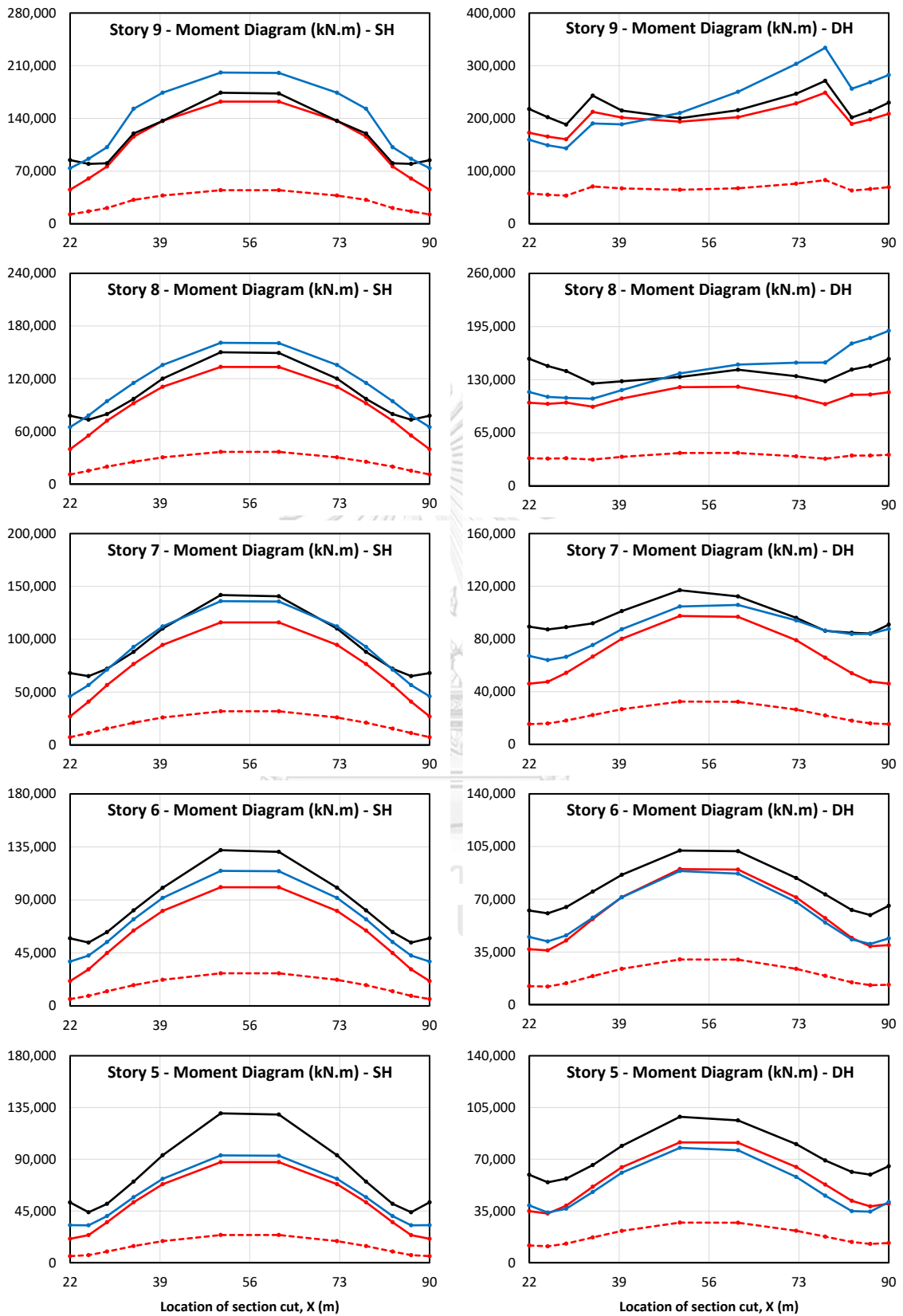
(Continued)
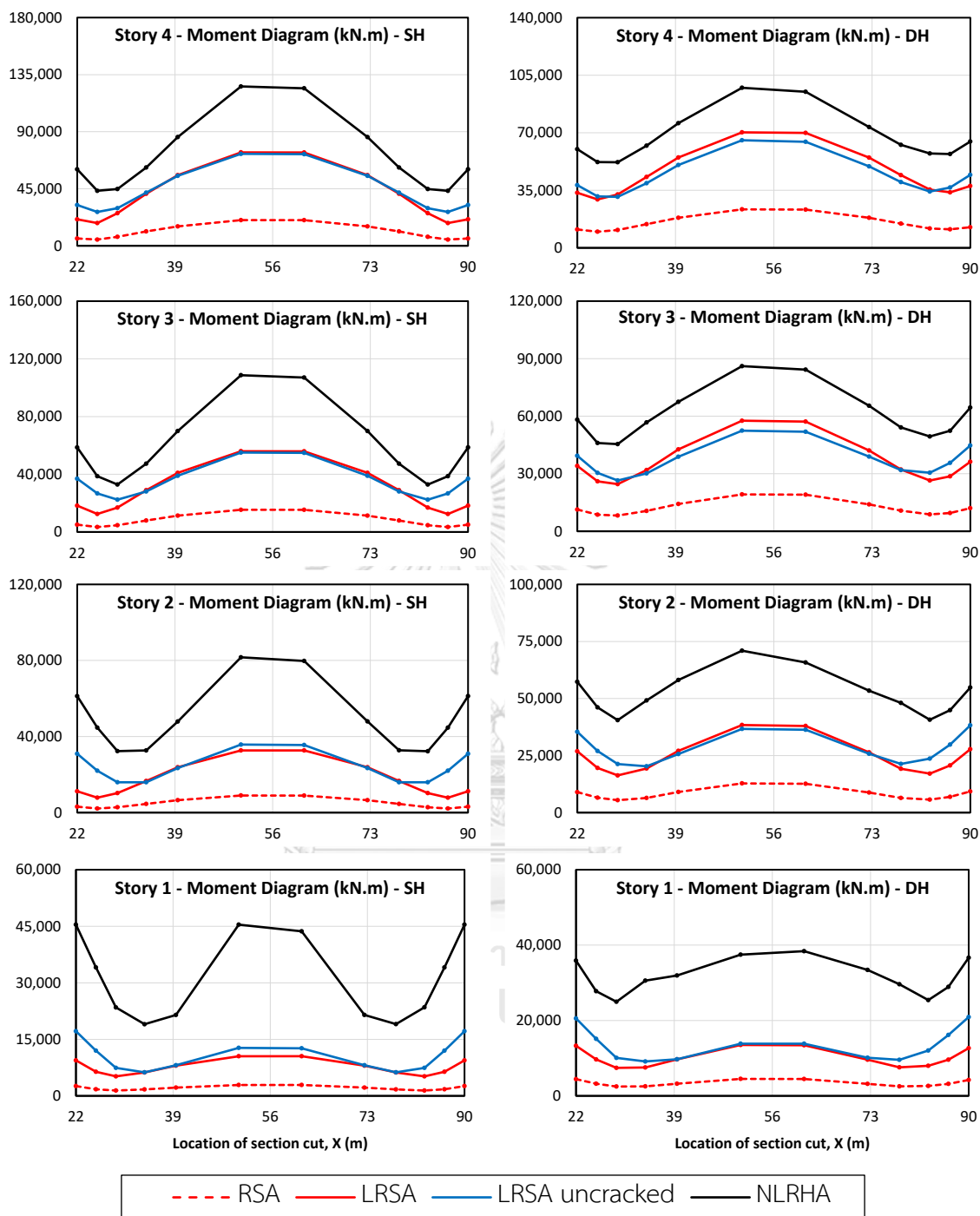
Figure C.25 Bending moment in diaphragms due to earthquake in the Y-direction for buildings SH and DH located in Chiang Mai.
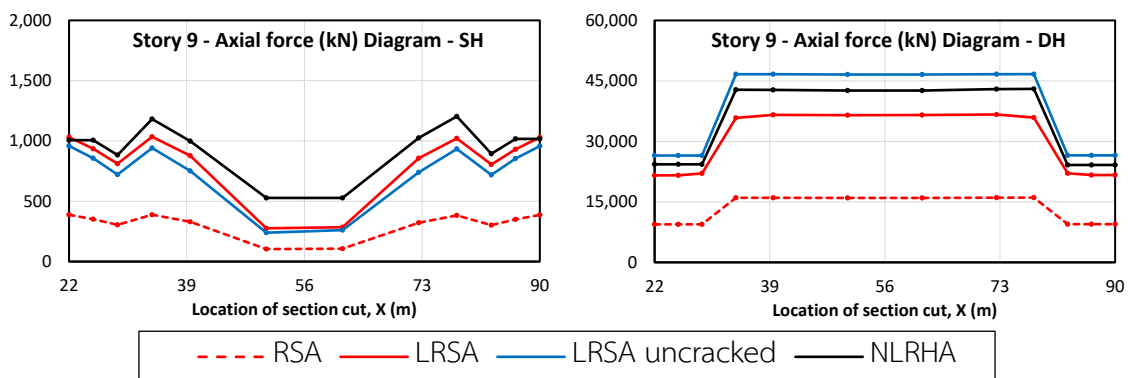
Figure C.26 Axial forces in diaphragms on the 9th floor of SH and DH buildings located in Bangkok due to earthquake in the X-direction.
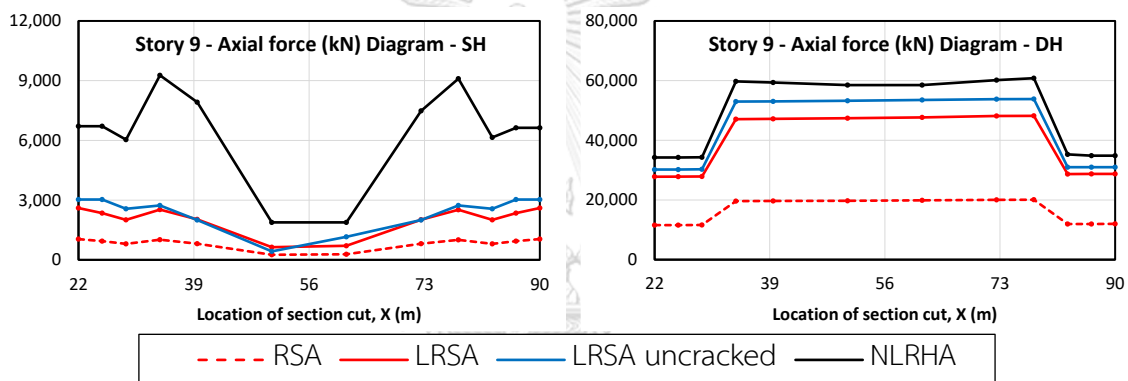
Figure C.27 Axial forces in diaphragms on the 9th floor of SH and DH buildings located in Chiang Mai due to earthquake in the X-direction.

APPENDIX D

MODIFIED RESPONSE SPECTRUM ANALYSIS

D.1 Vertical element forces

In this section, piers and columns forces are presented for the two buildings located in Bangkok and Chiang Mai. Results from RSA, and MRSA, are compared to NLRHA results. Due to symmetrical response in both towers in building SH, and symmetry of structural configuration in towers, some of the structural elements are sharing the same demand forces. More details can be found in section 4.6 regarding methods described in this section.
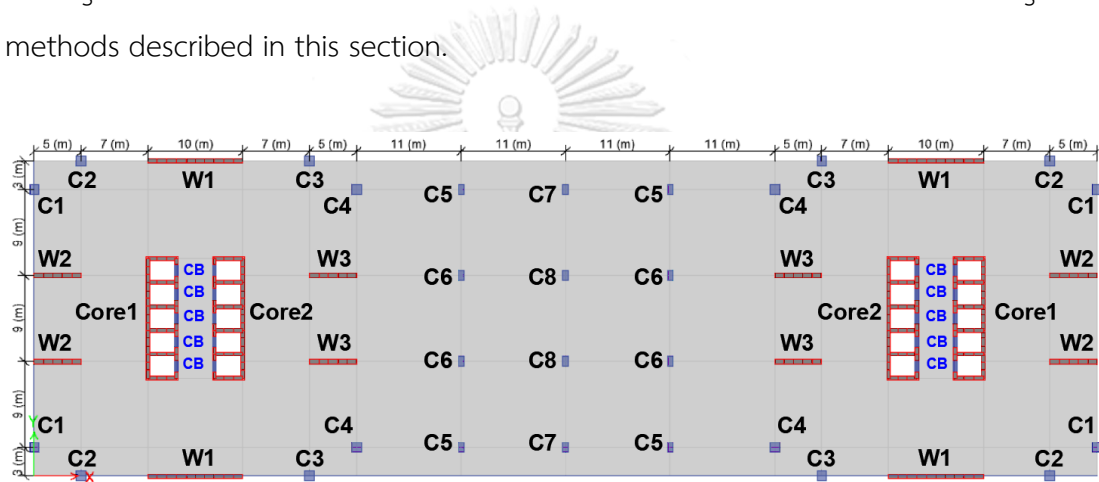
Figure D.1 Denotation of vertical members in building SH.
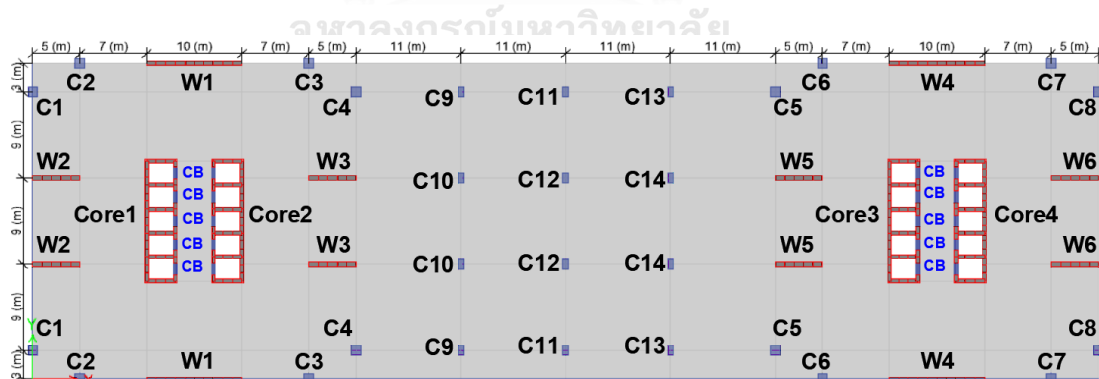
Figure D.2 Denotation of vertical members in building DH.

D.1.1 Wall forces
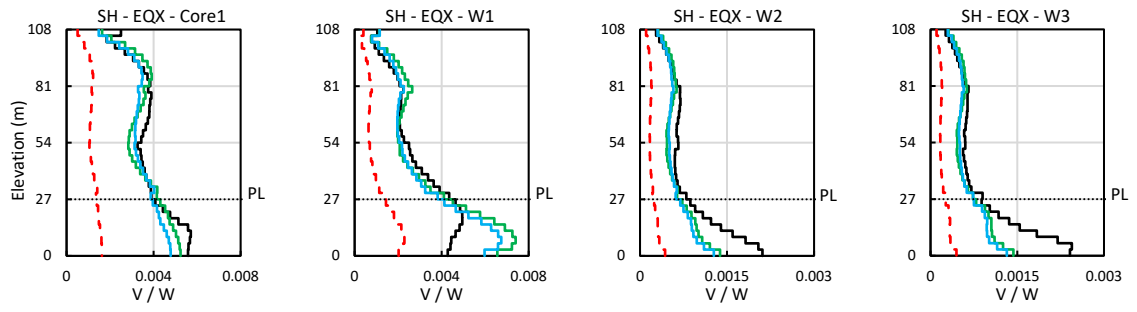
(a) Wall shear forces due to EQX
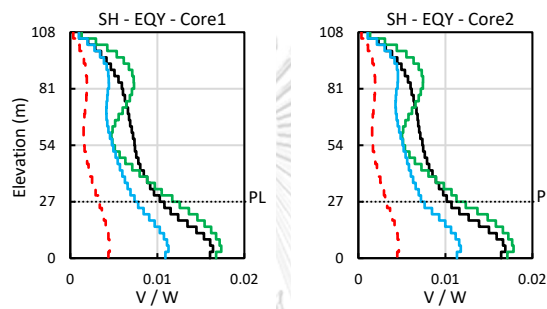
(b) Wall shear forces due to EQY

(c) Wall bending moment due to EQX

(d) Wall bending moment due to EQY

----- RSA ——— NLRHA ——— MRSA (HE) ——— MRSA (HI)
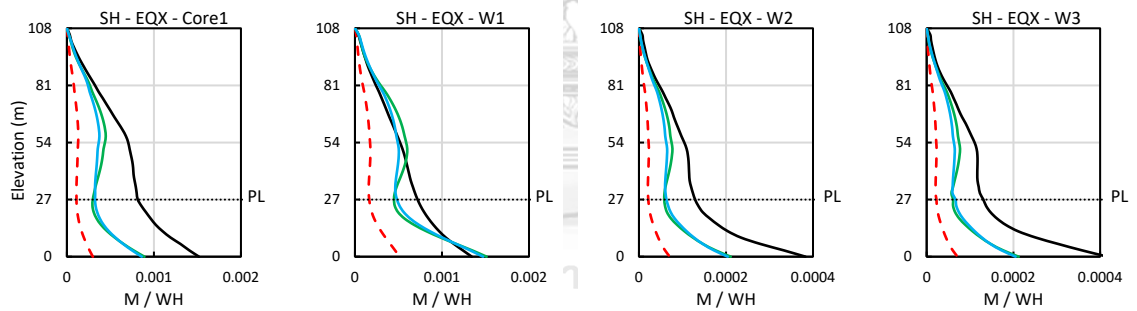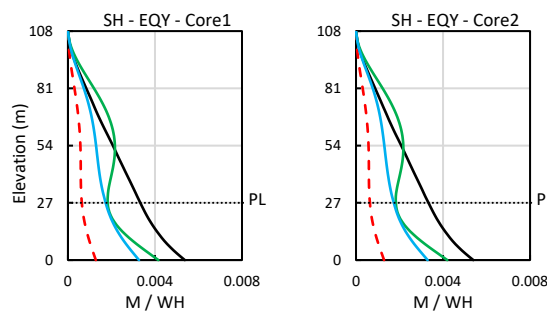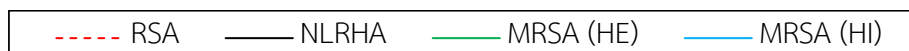
Figure D.3 Wall shear forces and bending moment of building SH located in Bangkok due to earthquake in X- and Y-direction.

(a) Wall shear forces due to EQX

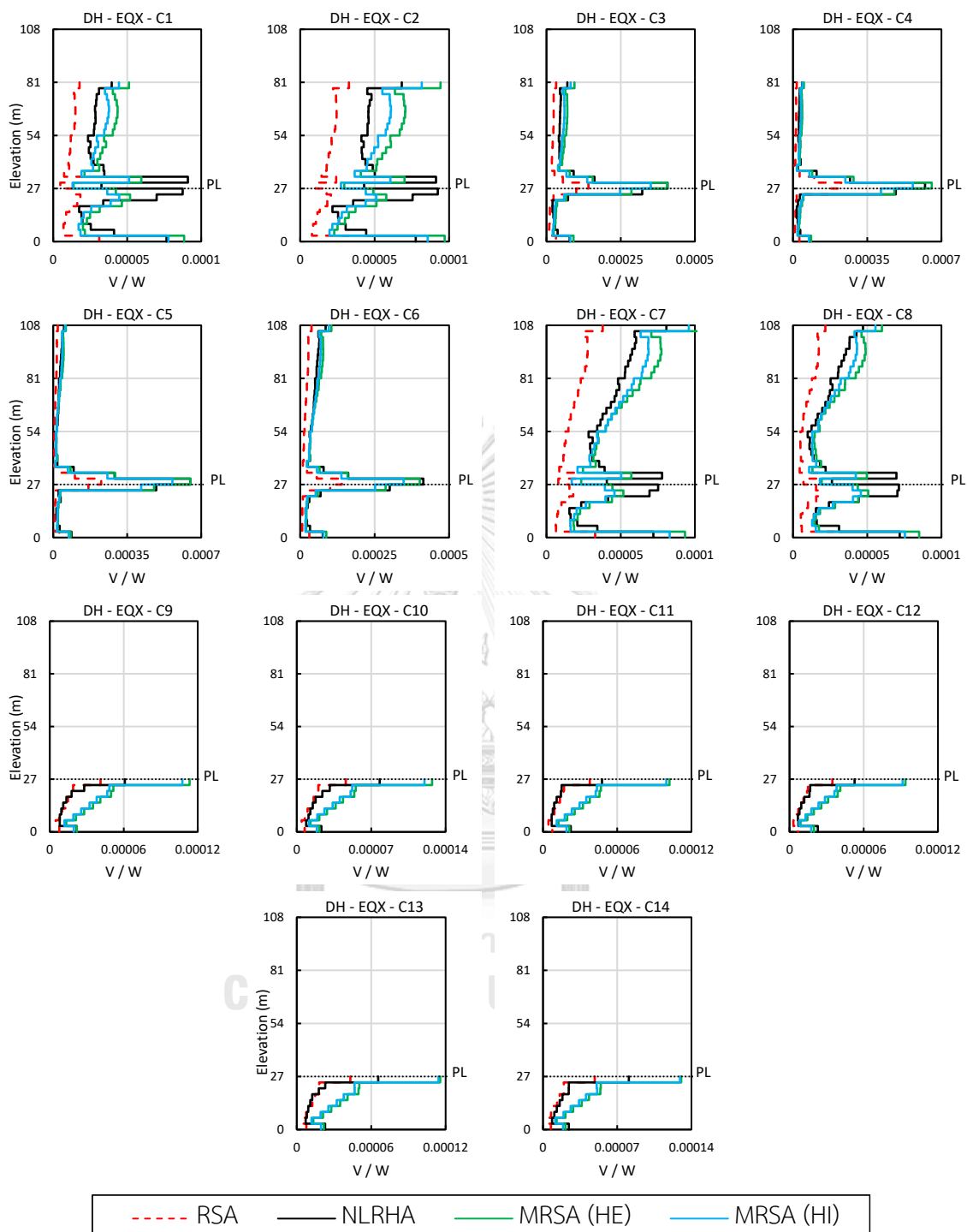(b) Wall shear forces due to EQY

RSA NLRHA MRSA (HE) MRSA (HI)
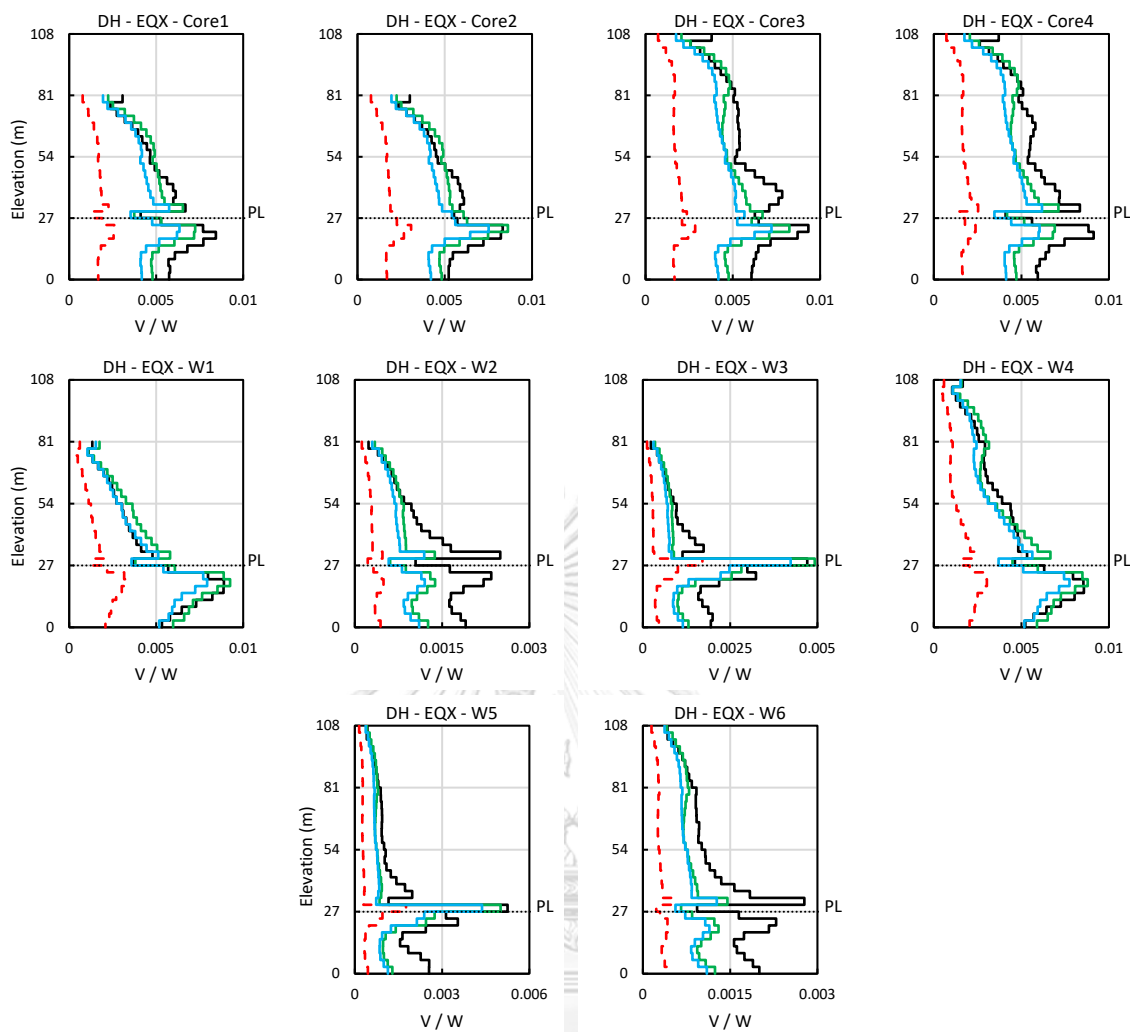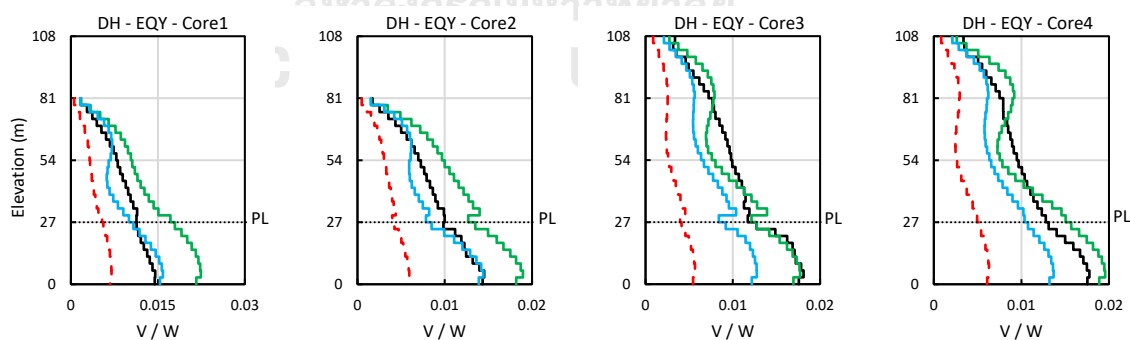
Figure D.4 Wall shear forces of building DH located in Bangkok due to earthquake in (a) X-direction (EQX); (b) Y-direction (EQY).
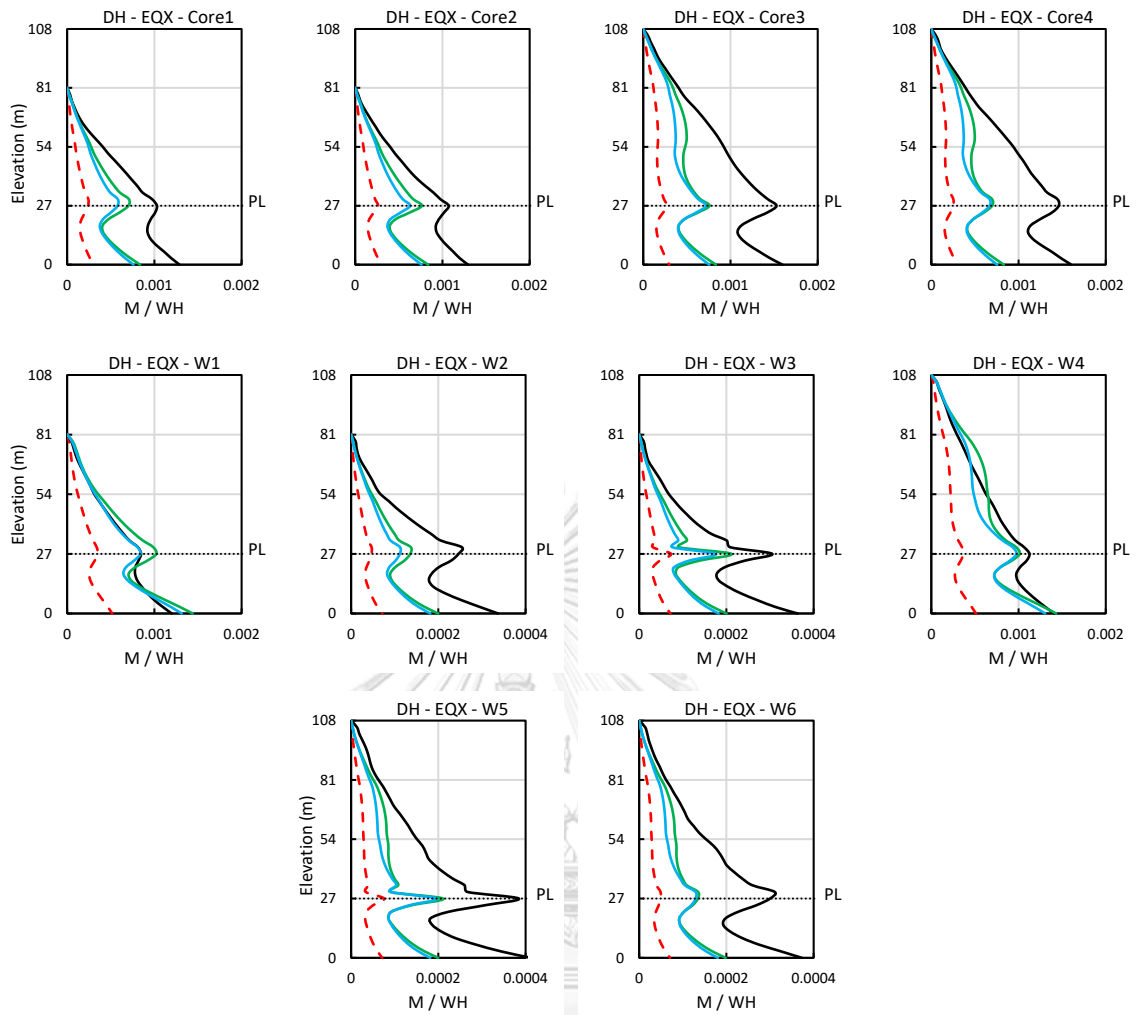
(a) Wall bending moment due to EQX
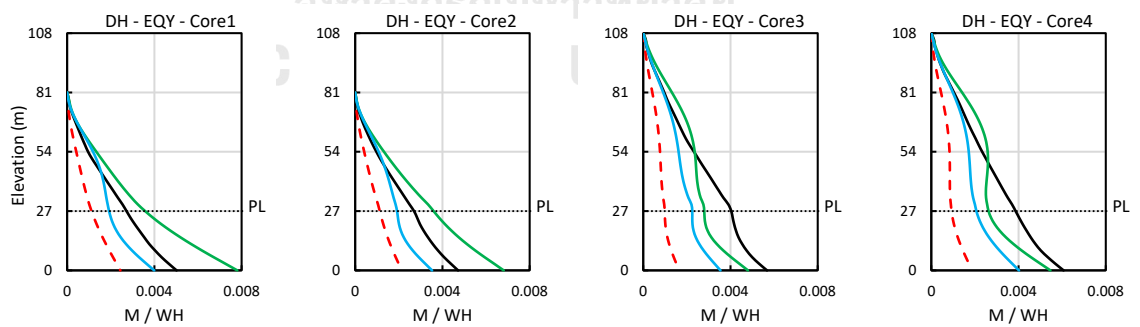
(b) Wall bending moment due to EQY
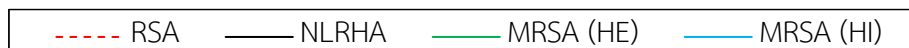
Figure D.5 Wall bending moment for building DH located in Bangkok due to earthquake in (a) X-direction (EQX); (b) Y-direction (EQY).
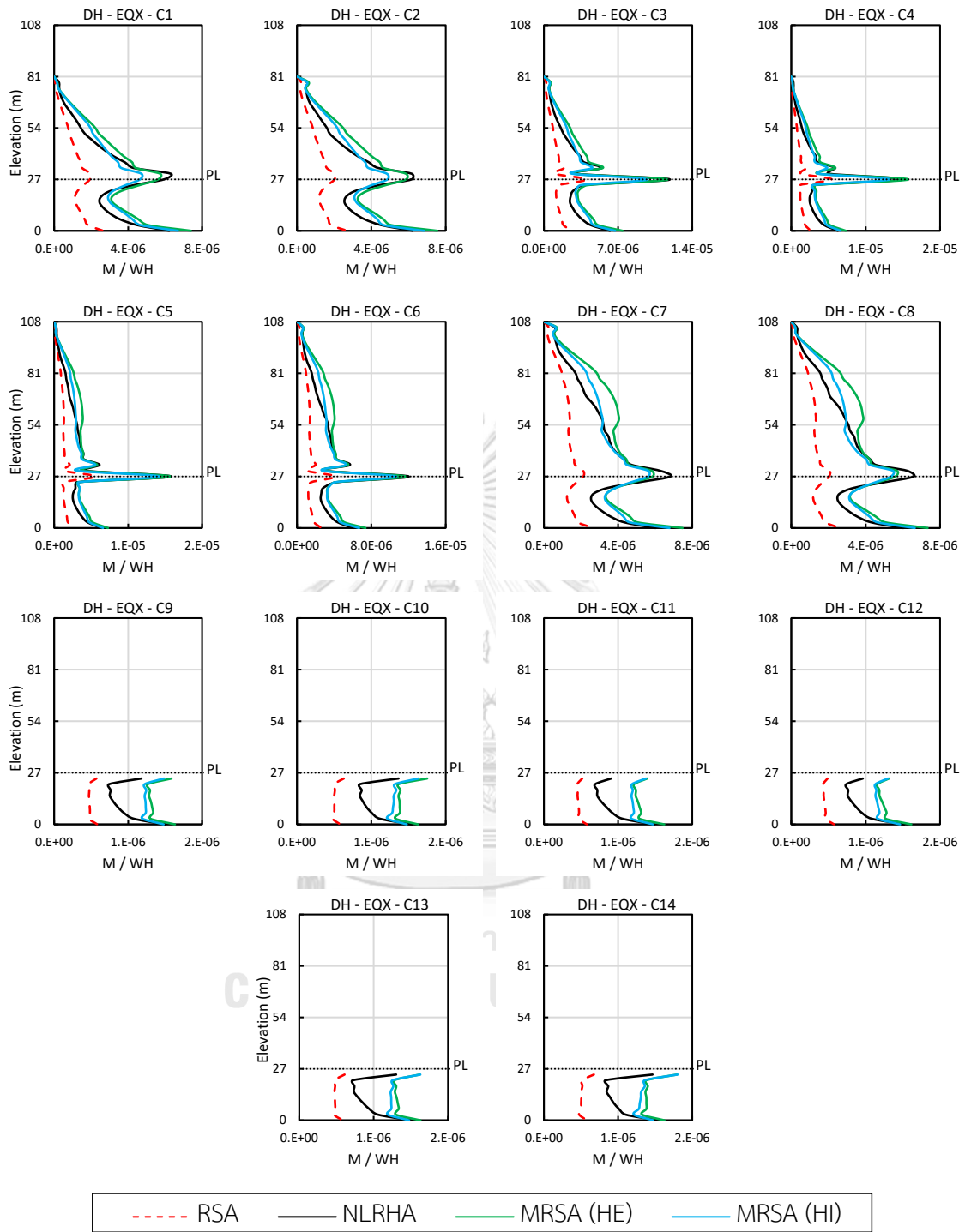
(a) Wall shear forces due to EQX
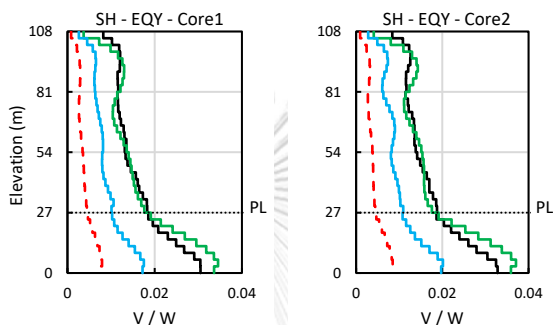
(b) Wall shear forces due to EQY
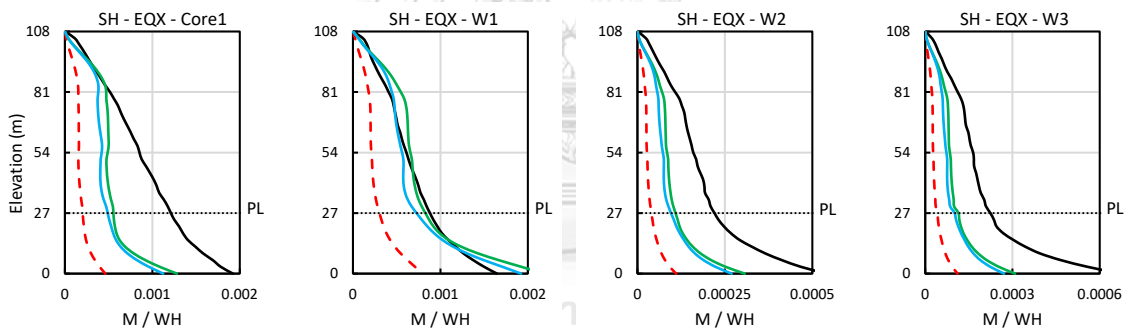
(c) Wall bending moment due to EQX
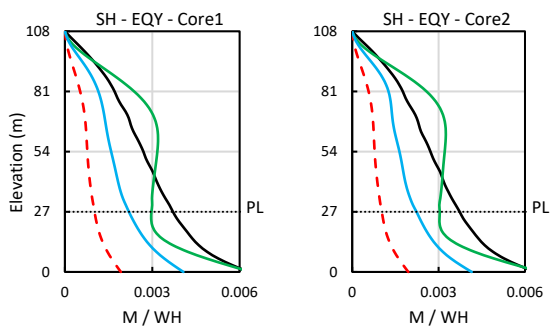
(d) Wall bending moment due to EQY
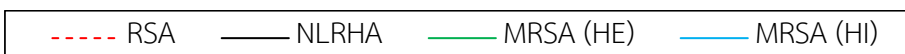
Figure D.6 Wall shear forces and bending moment of building SH located in Chiang Mai due to earthquake in X- and Y-direction.
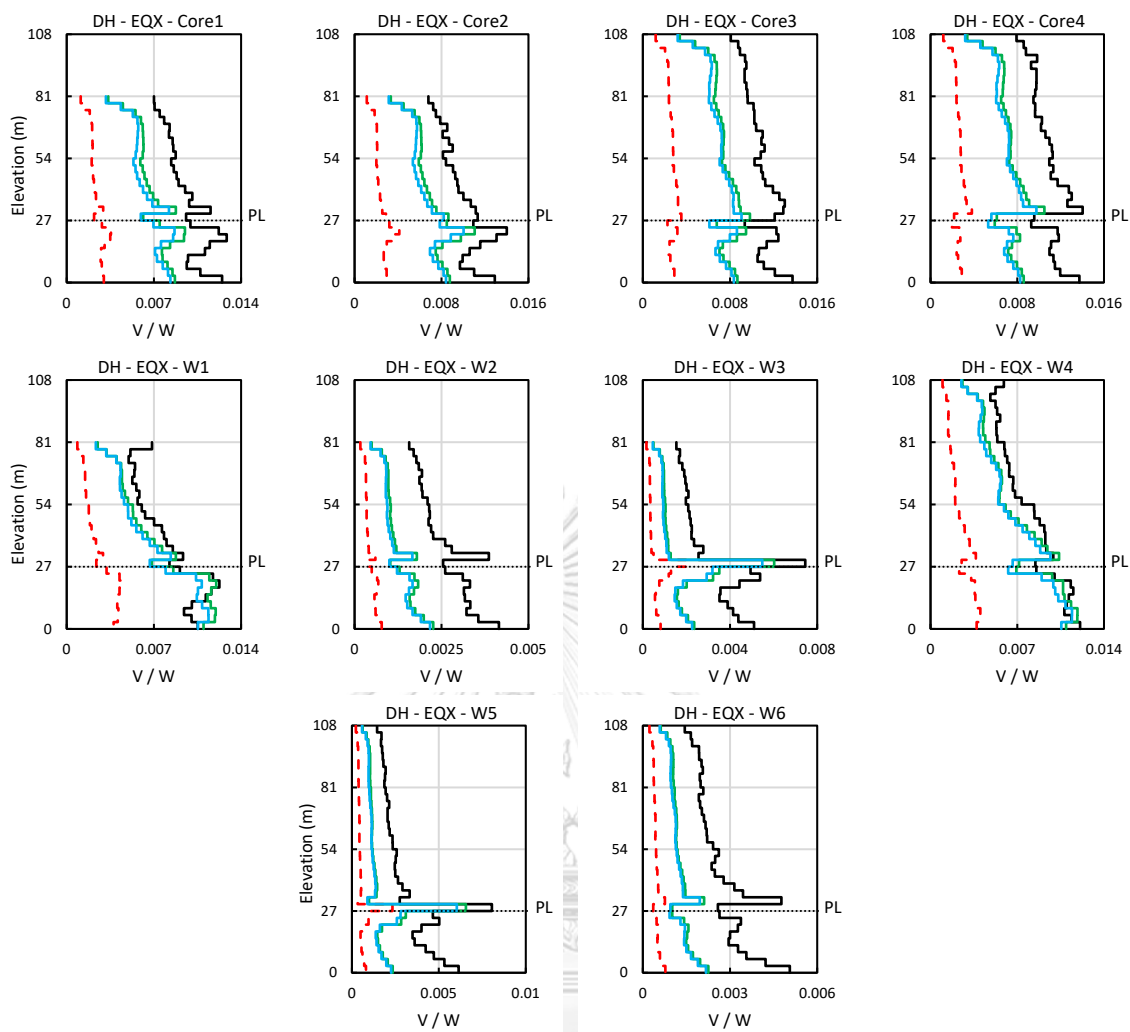
(a) Wall shear forces due to EQX
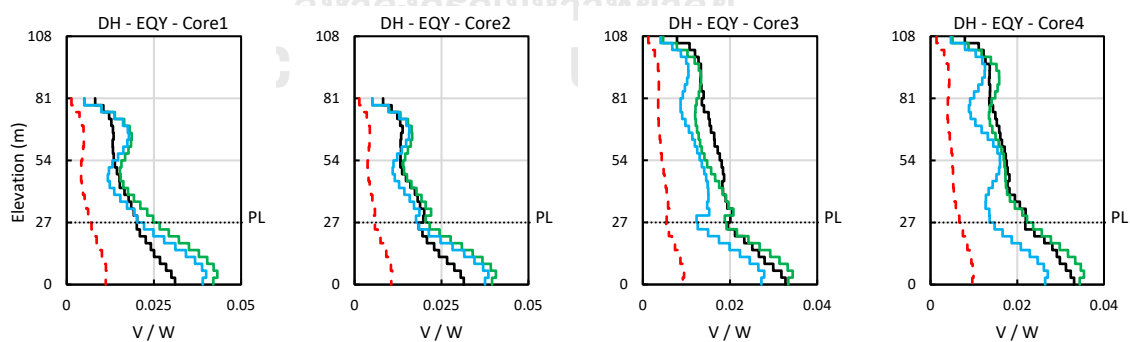
(b) Wall shear forces due to EQY
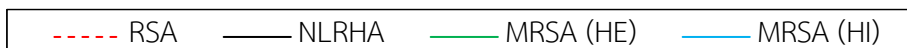
Figure D.7 Wall shear forces of building DH located in Chiang Mai due to earthquake in (a) X-direction (EQX); (b) Y-direction (EQY).

(a) Wall bending moment due to EQX

(b) Wall bending moment due to EQY

RSA — NLRHA — MRSA (HE) — MRSA (HI)
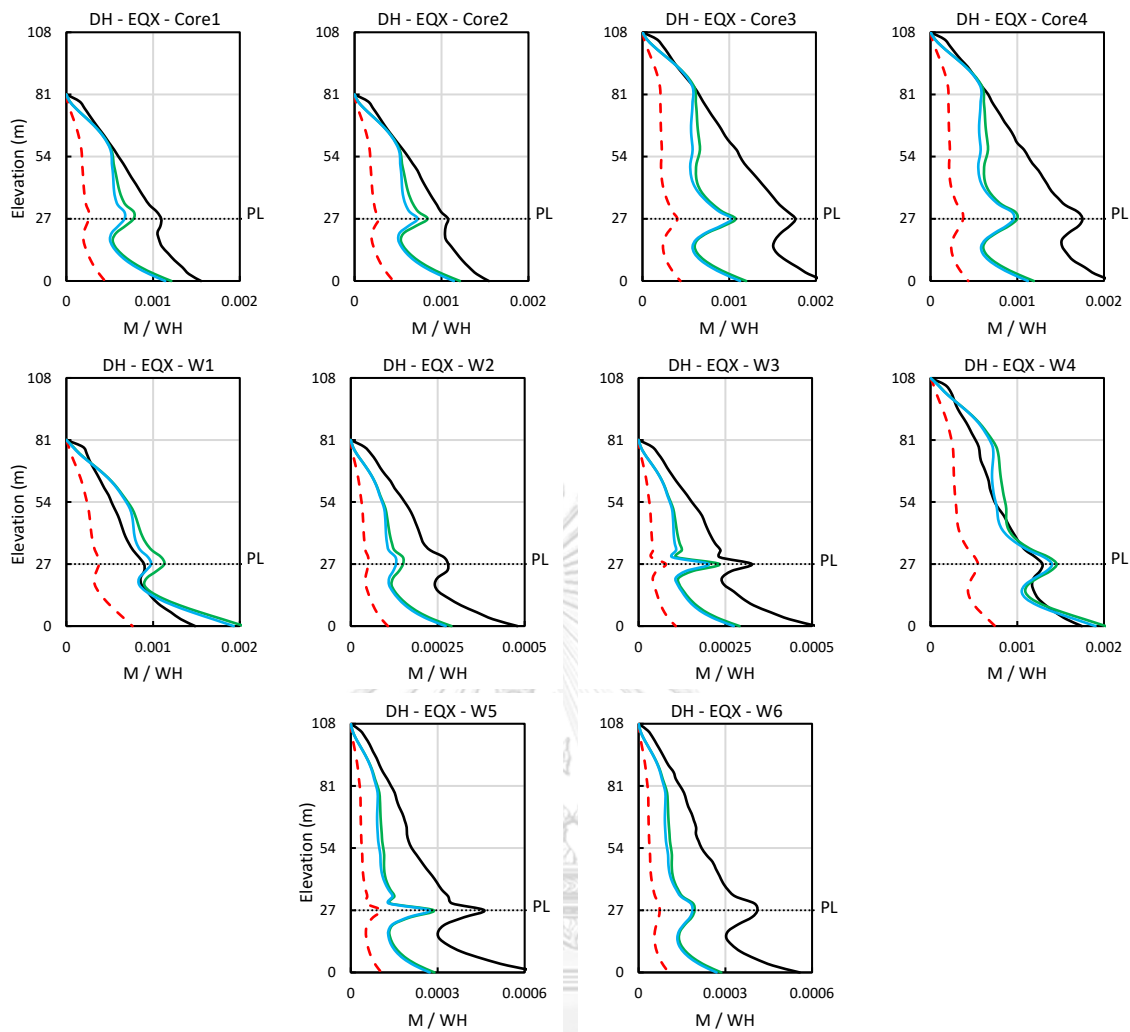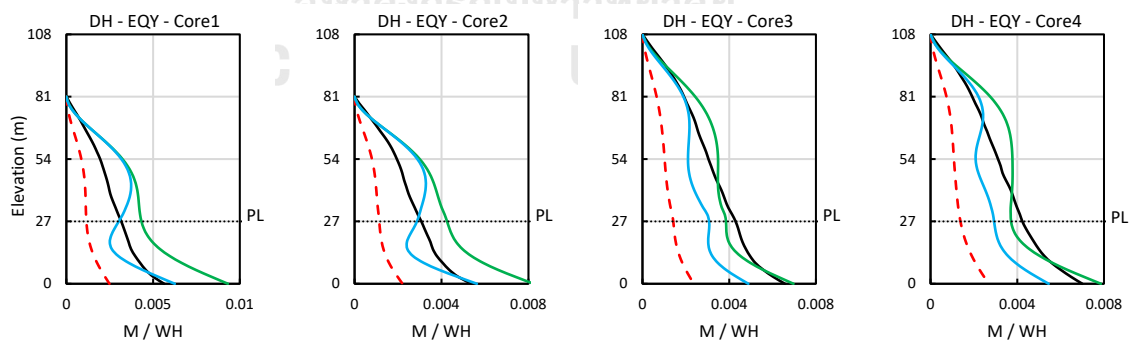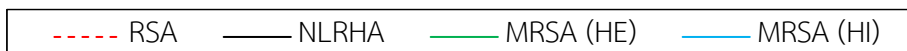
Figure D.8 Wall bending moment of building DH located in Chiang Mai due to earthquake in (a) X-direction (EQX); (b) Y-direction (EQY).

D.1.2 Column forces

(a) Column shear forces due to EQX

(b) Column shear forces due to EQY

---- RSA ——— NLRHA ——— MRSA (HE) ——— MRSA (HI)
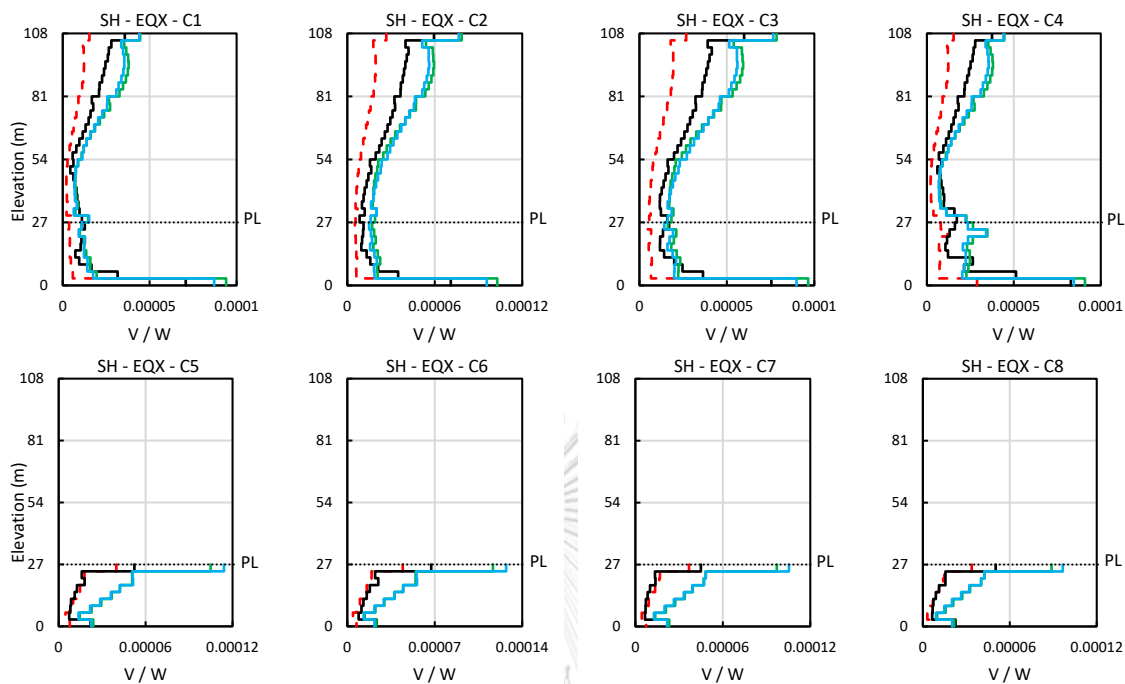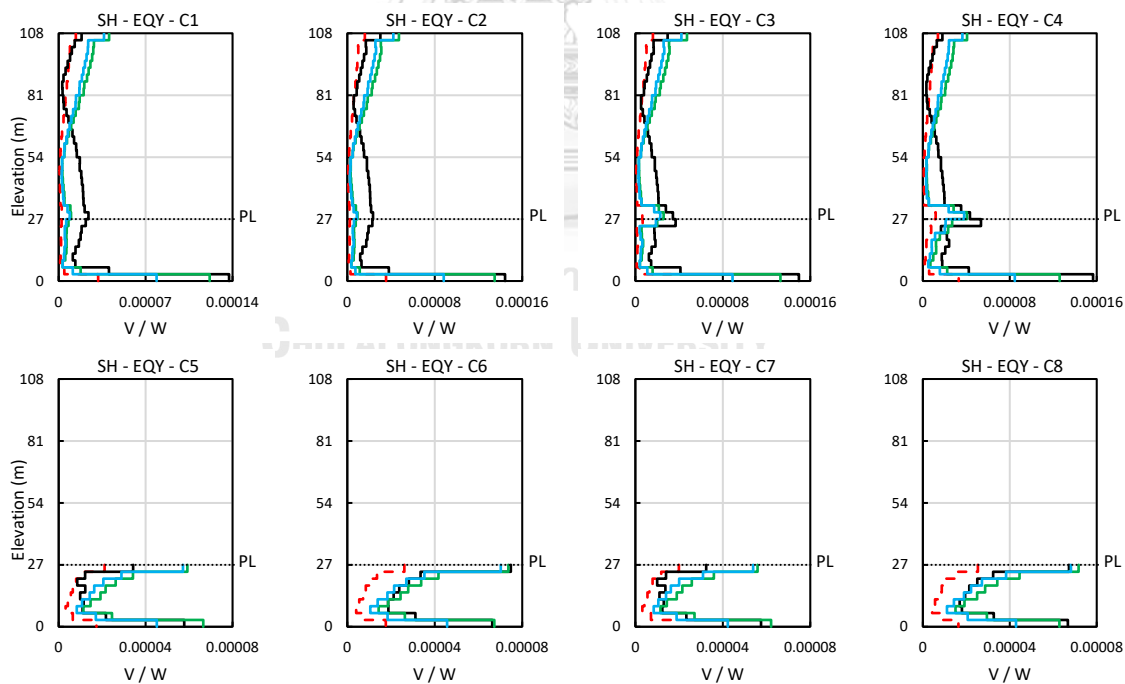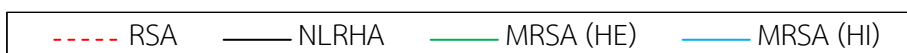
Figure D.9 Column shear forces of building SH located in Bangkok due to earthquake in (a) X-direction (EQX); (b) Y-direction (EQY).

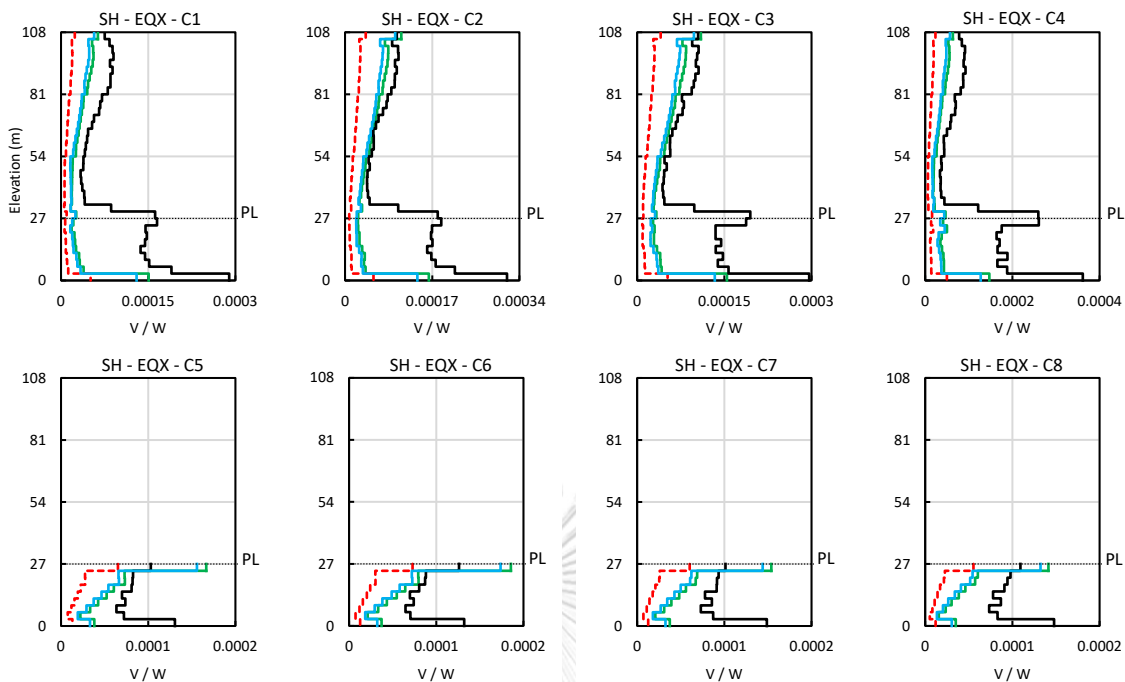Figure D.10 Column shear forces of building DH located in Bangkok due to earthquake in X-direction (EQX).
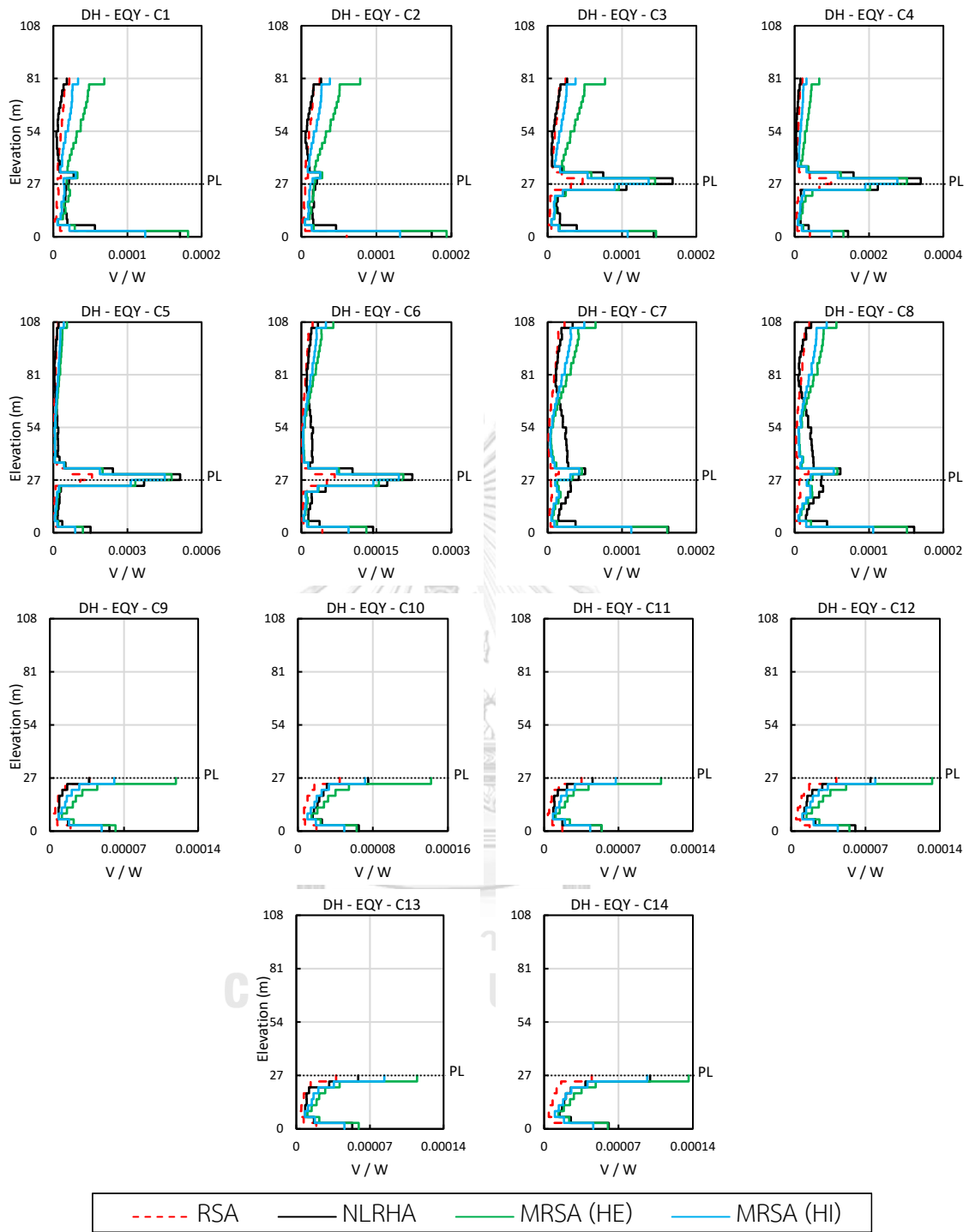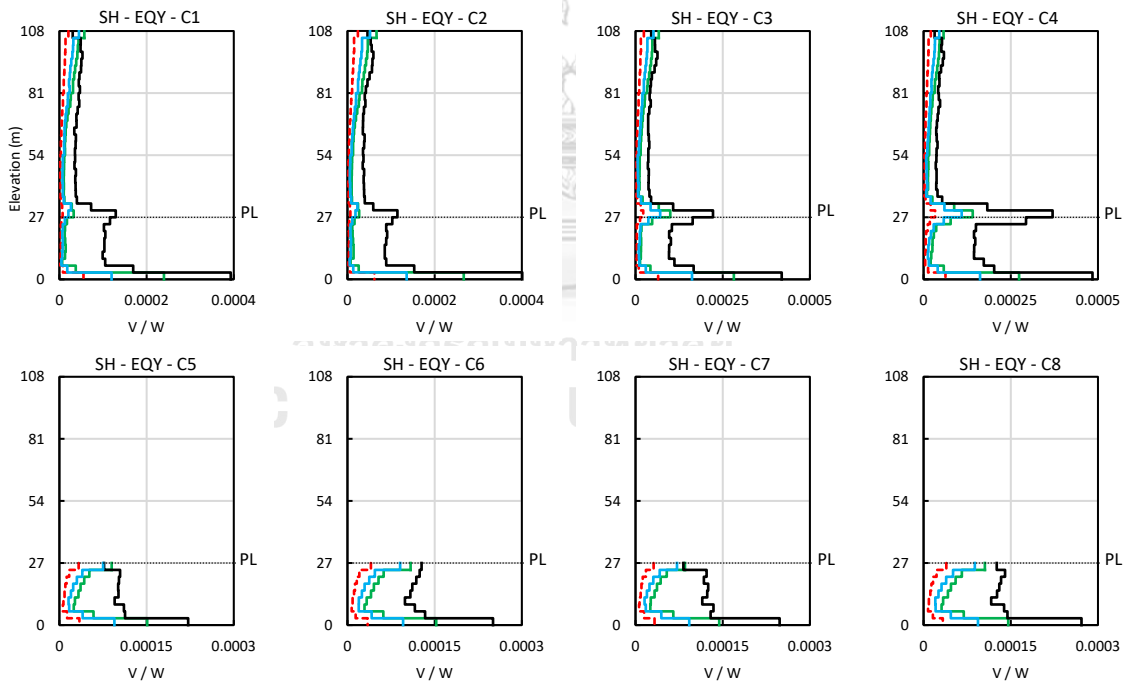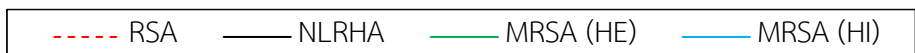
Figure D.11 Column shear forces of building DH located in Bangkok due to earthquake in Y-direction (EQY).

(a) Column bending moment due to EQX

(b) Column bending moment due to EQY

- - - - RSA ——— NLRHA ——— MRSA (HE) ——— MRSA (HI)
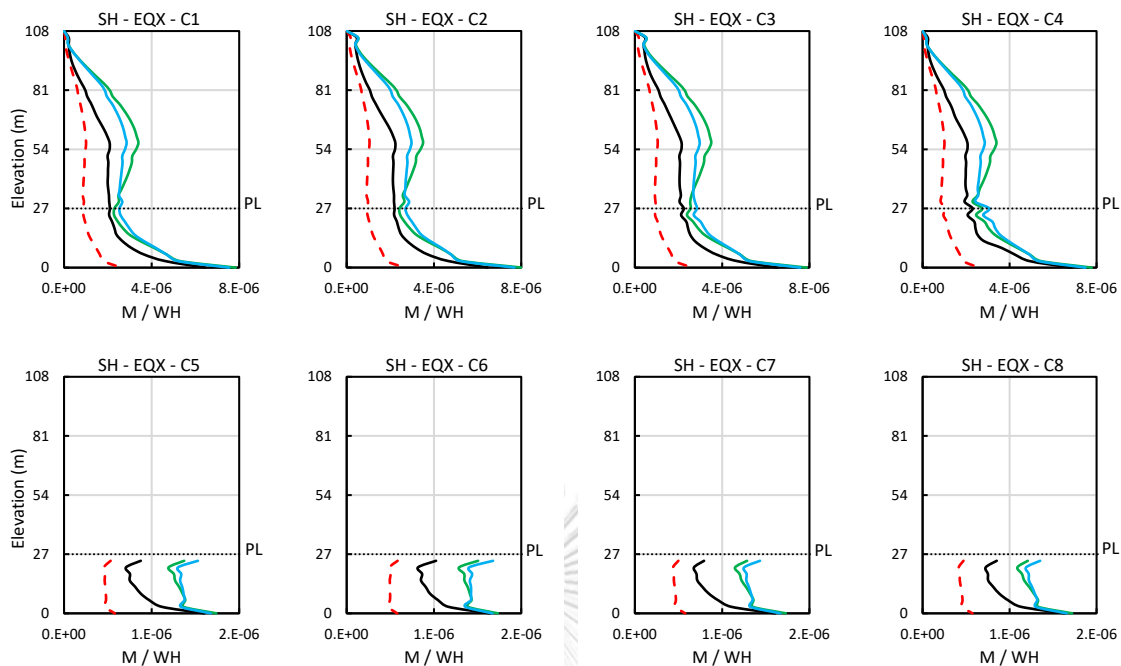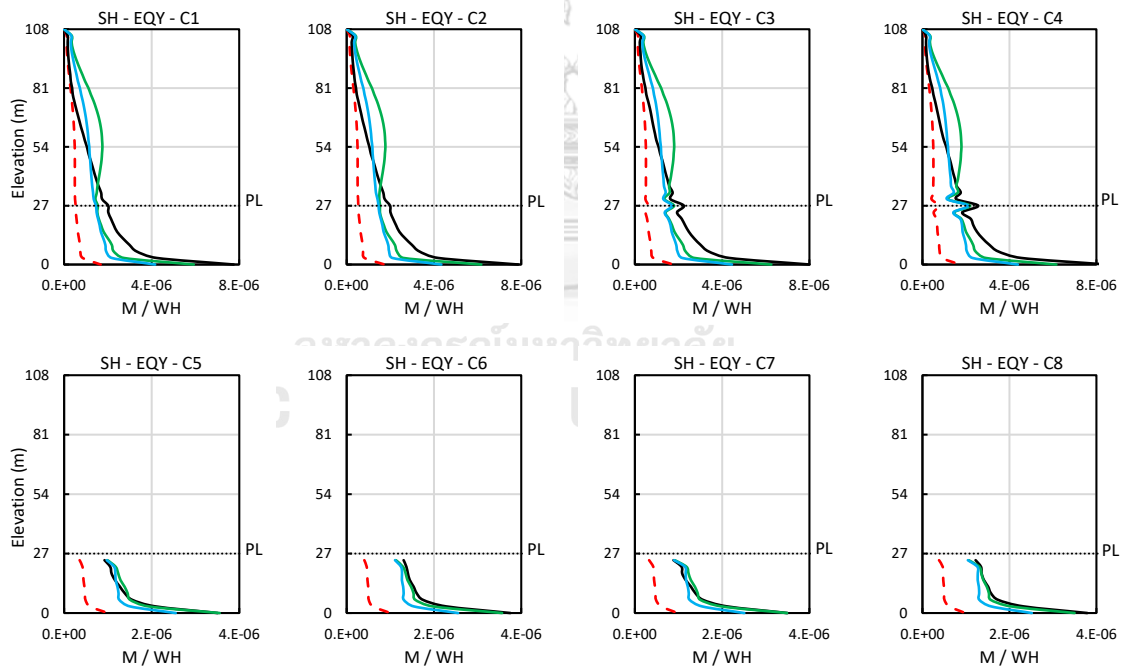
Figure D.12 Column bending moment of building SH located in Bangkok due to earthquake in (a) X-direction (EQX); (b) Y-direction (EQY).

Figure D.13 Column bending moment of building DH located in Bangkok due to earthquake in X-direction (EQX).
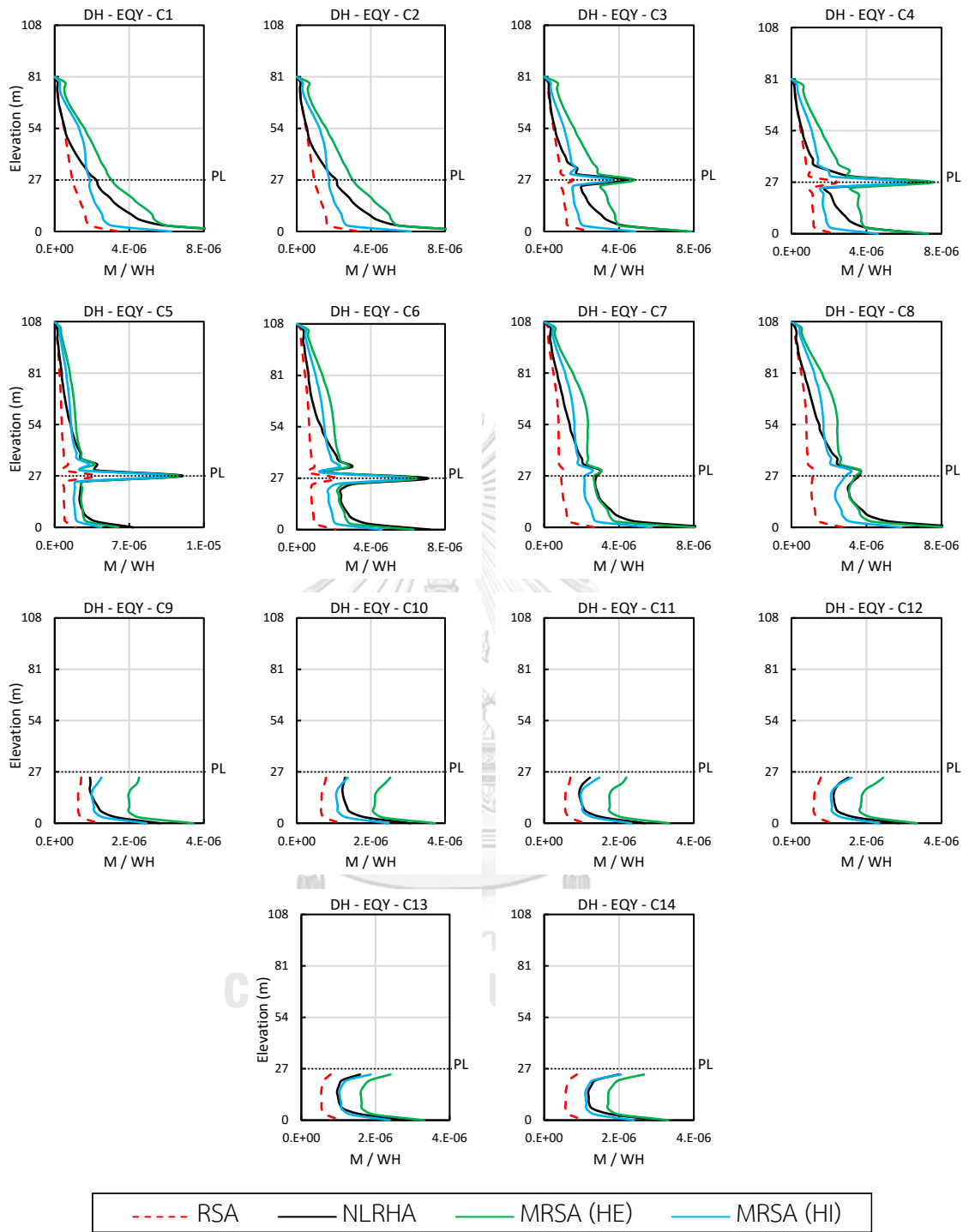
Figure D.14 Column bending moment of building DH located in Bangkok due to earthquake in Y-direction (EQY).

(a) Column shear forces due to EQX

(b) Column shear forces due to EQY

Figure D.15 Column shear forces of building SH located in Chiang Mai due to earthquake in (a) X-direction (EQX); (b) Y-direction (EQY).
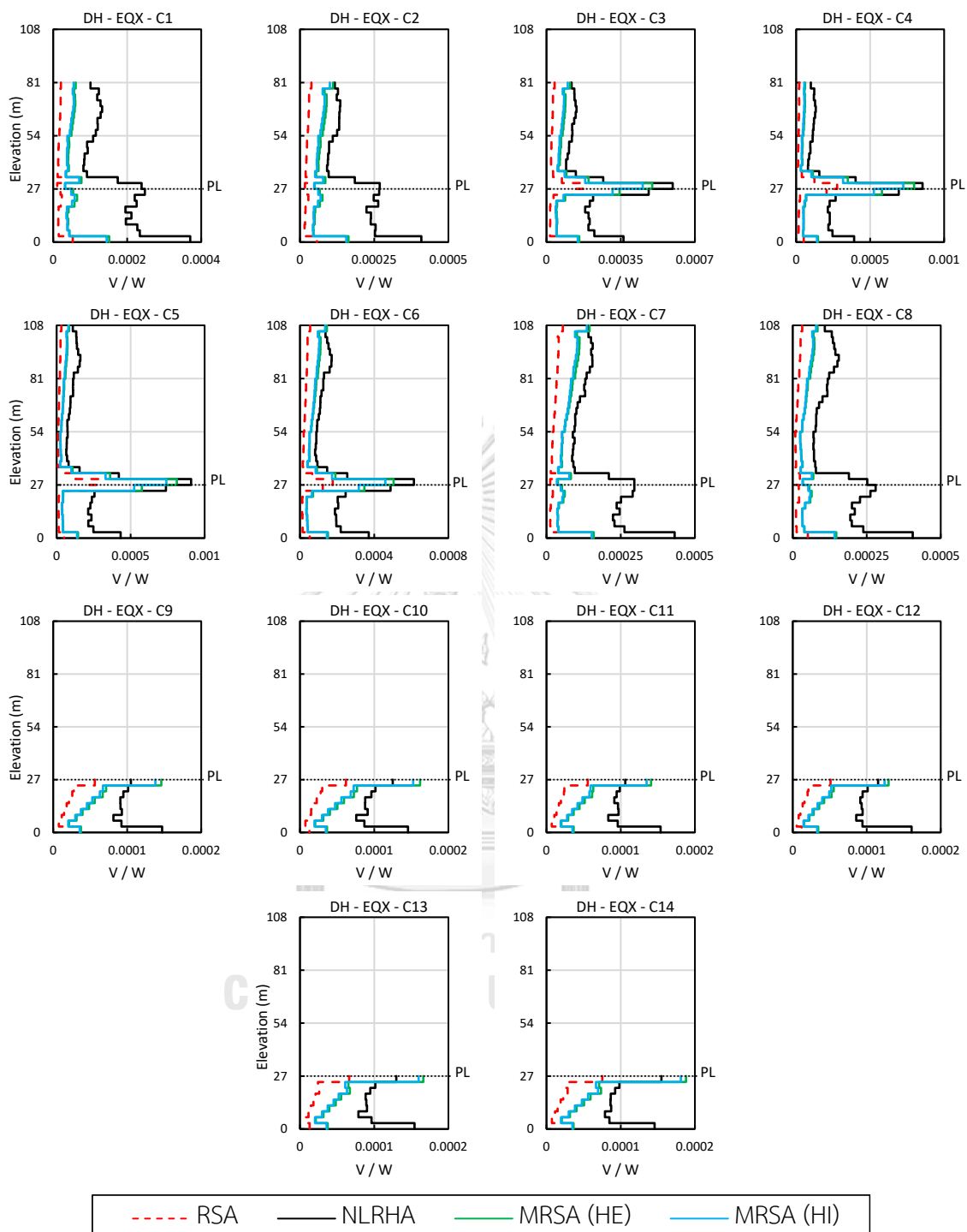
Figure D.16 Column shear forces of building DH located in Chiang Mai due to earthquake in X-direction (EQX).
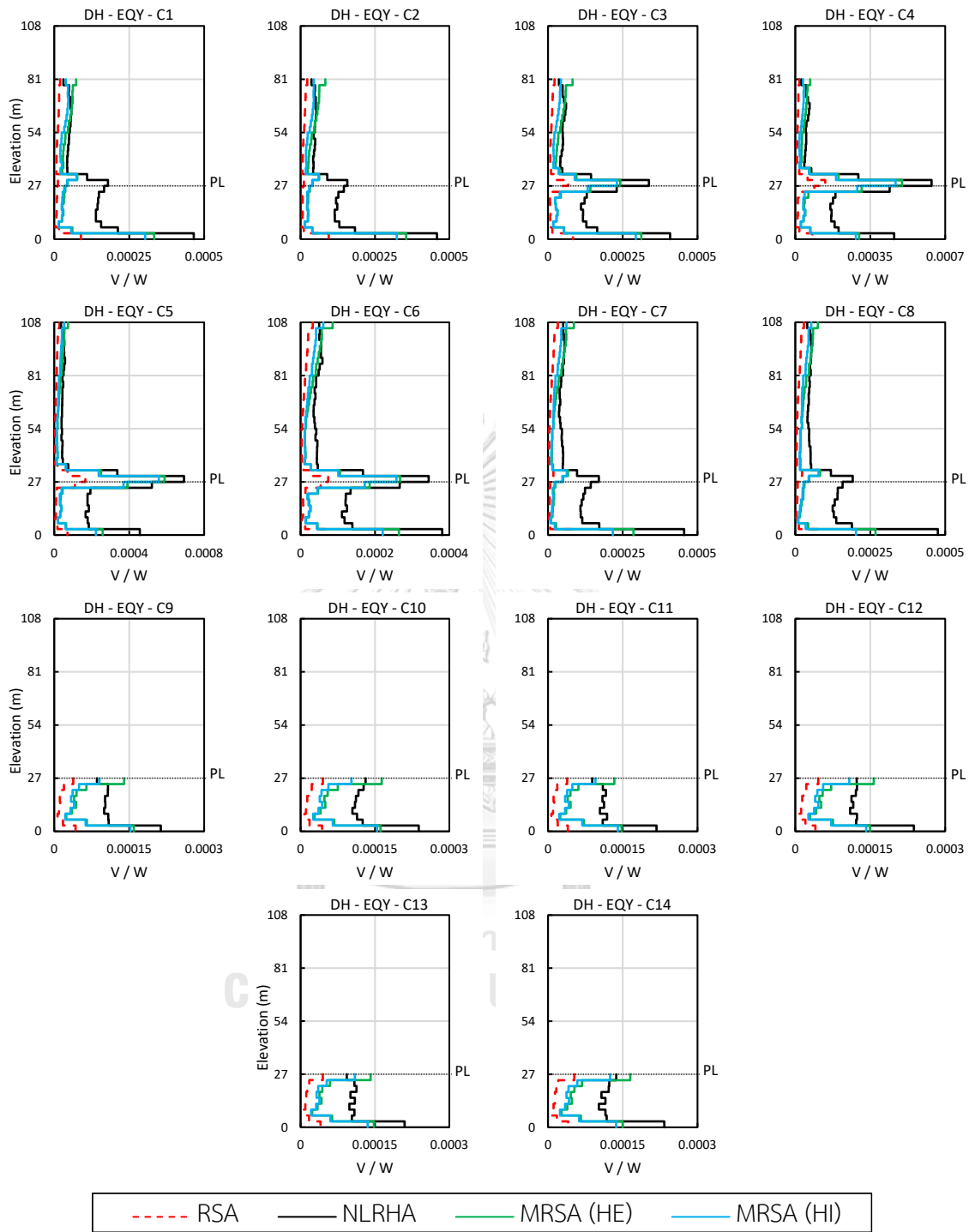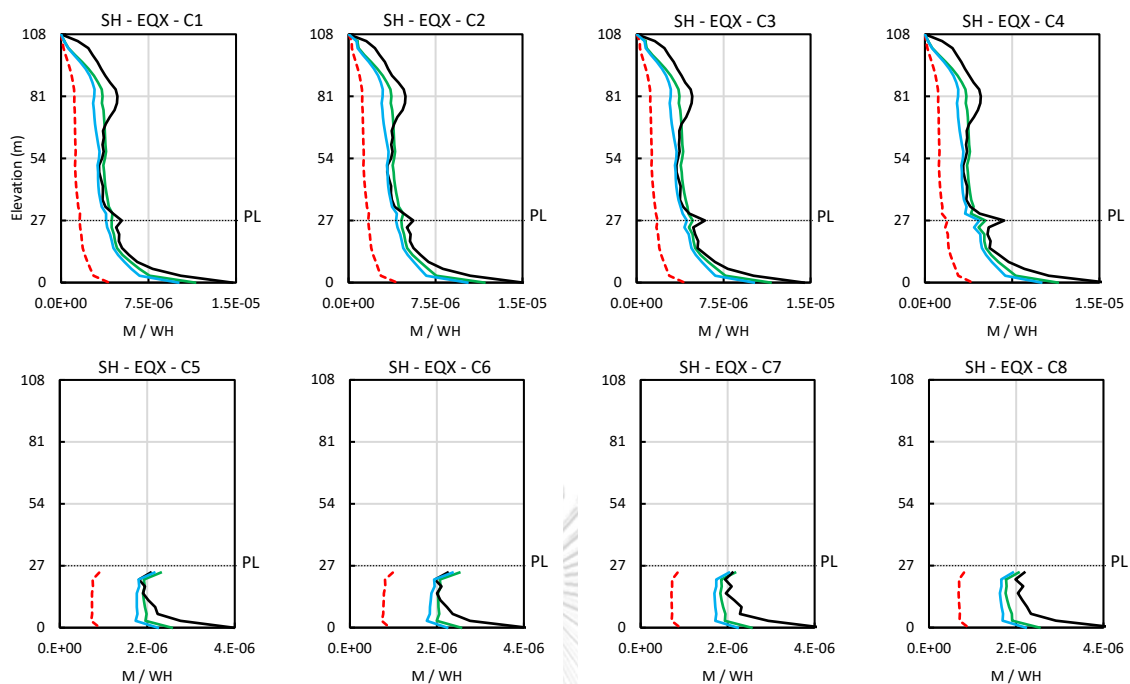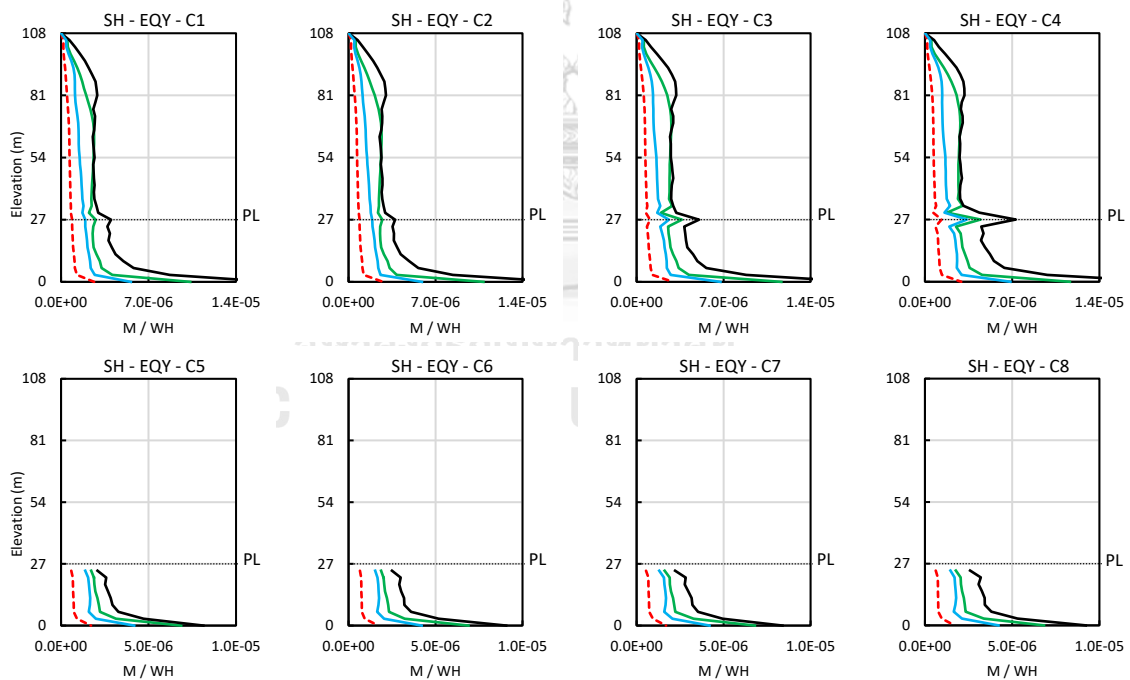
Figure D.17 Column shear forces of building DH located in Chiang Mai due to earthquake in Y-direction (EQY).

(a) Column bending moment due to EQX

(b) Column bending moment due to EQY

- - - - RSA ——— NLRHA ——— MRSA (HE) ——— MRSA (HI)

Figure D.18 Column bending moment of building SH located in Chiang Mai due to earthquake in (a) X-direction (EQX); (b) Y-direction (EQY).
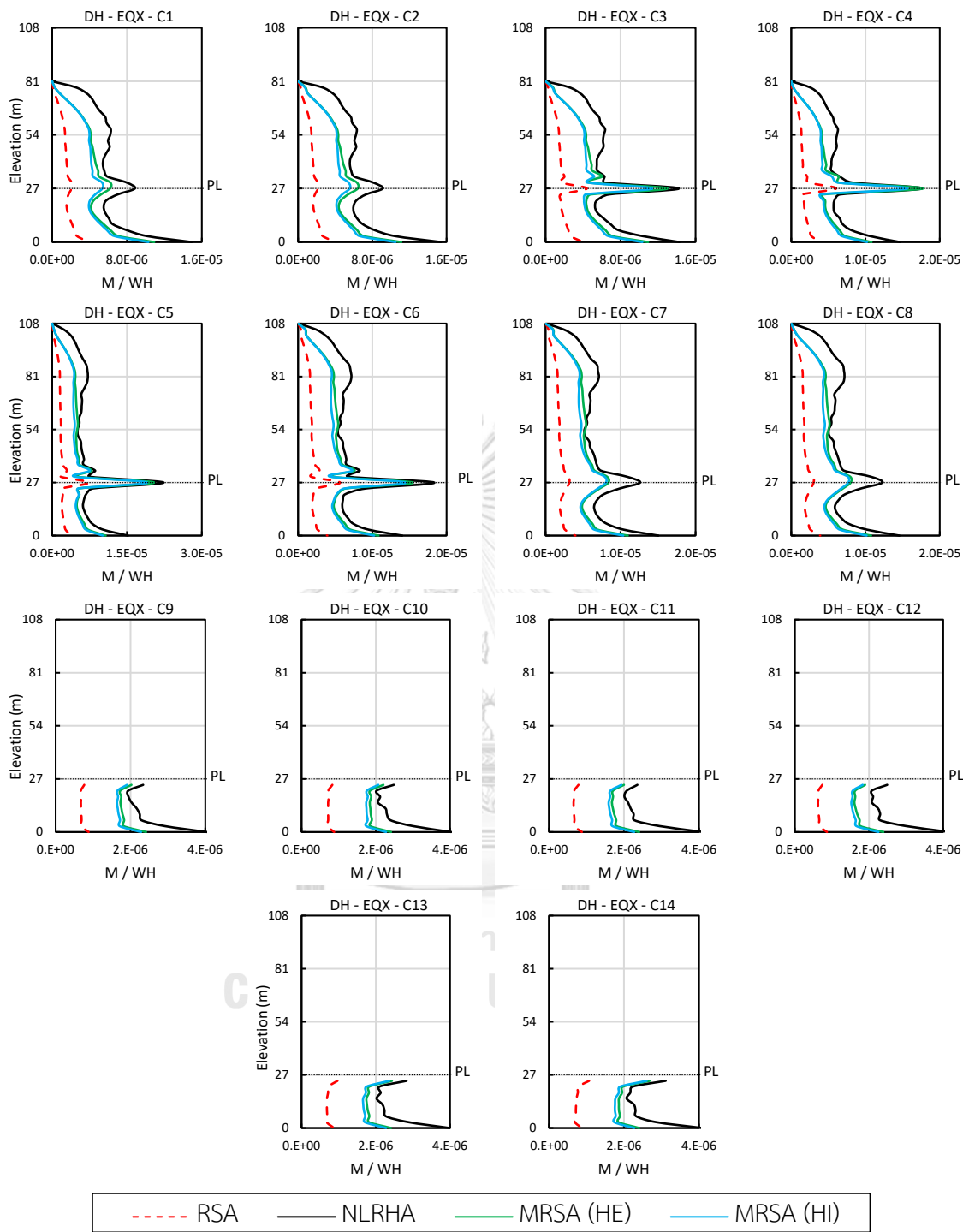
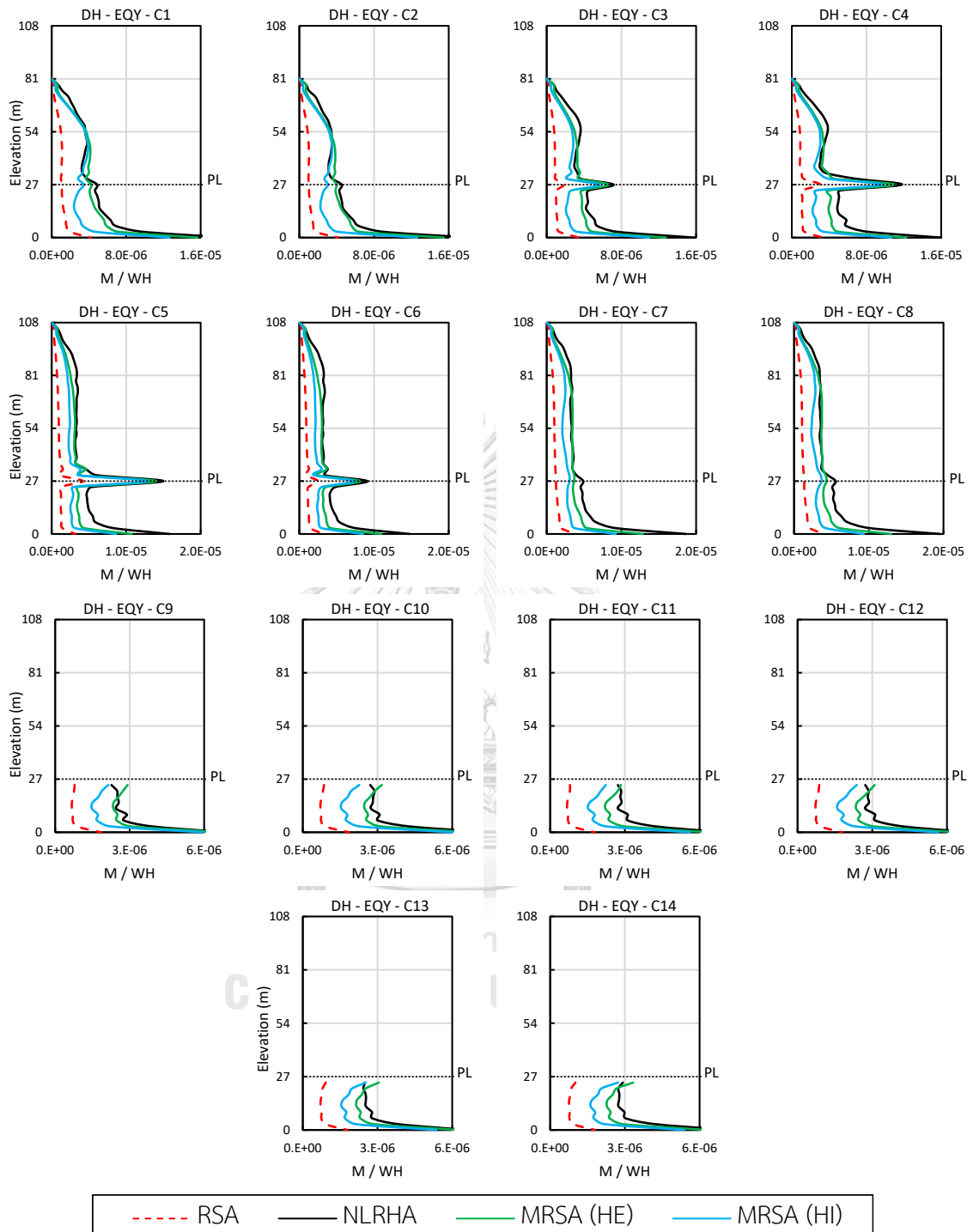Figure D.19 Column bending moment of building DH located in Chiang Mai due to earthquake in X-direction (EQX).

Figure D.20 Column bending moment of building DH located in Chiang Mai due to earthquake in Y-direction (EQY).

D.2 Diaphragm forces

In this section, diaphragm forces developed in diaphragm floors of the podium are presented (note that the podium consists of 9 stories). The forces are obtained along section cuts previously defined in ETBAS and PERFORM-3D software. The section-cut locations are shown in the Figure D.21. Floors at the podium level are spanning between two main cantilever core walls aligned in the Y-direction. Hence, the interest is in the shear and bending moment in diaphragms resulted from an earthquake load in the Y-direction, while axial forces in diaphragms are obtained due to an earthquake in the X-direction. The peak response along all section cuts are shown in Figures D.22 to D.25. It should be noted that the slab elements were modelled using elastic shell element, and the demand forces along section cut are obtained by integrating the stress field determined from finite element analysis.
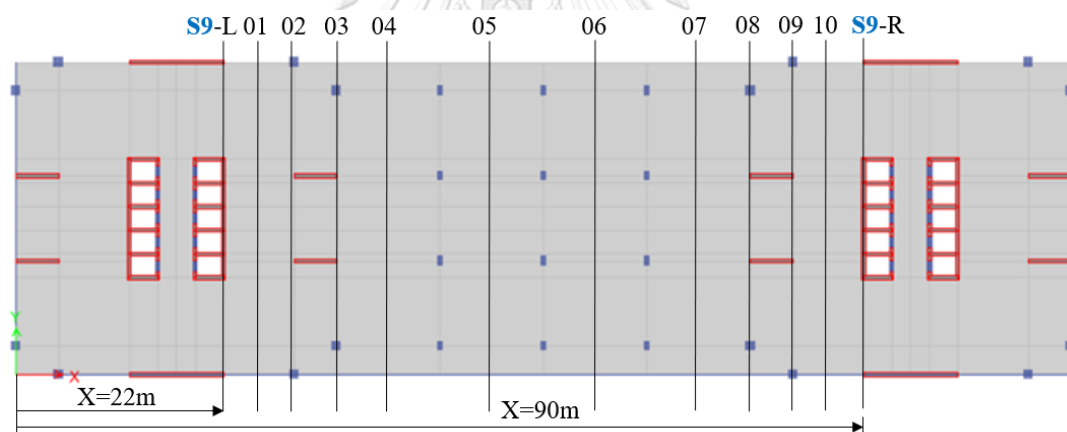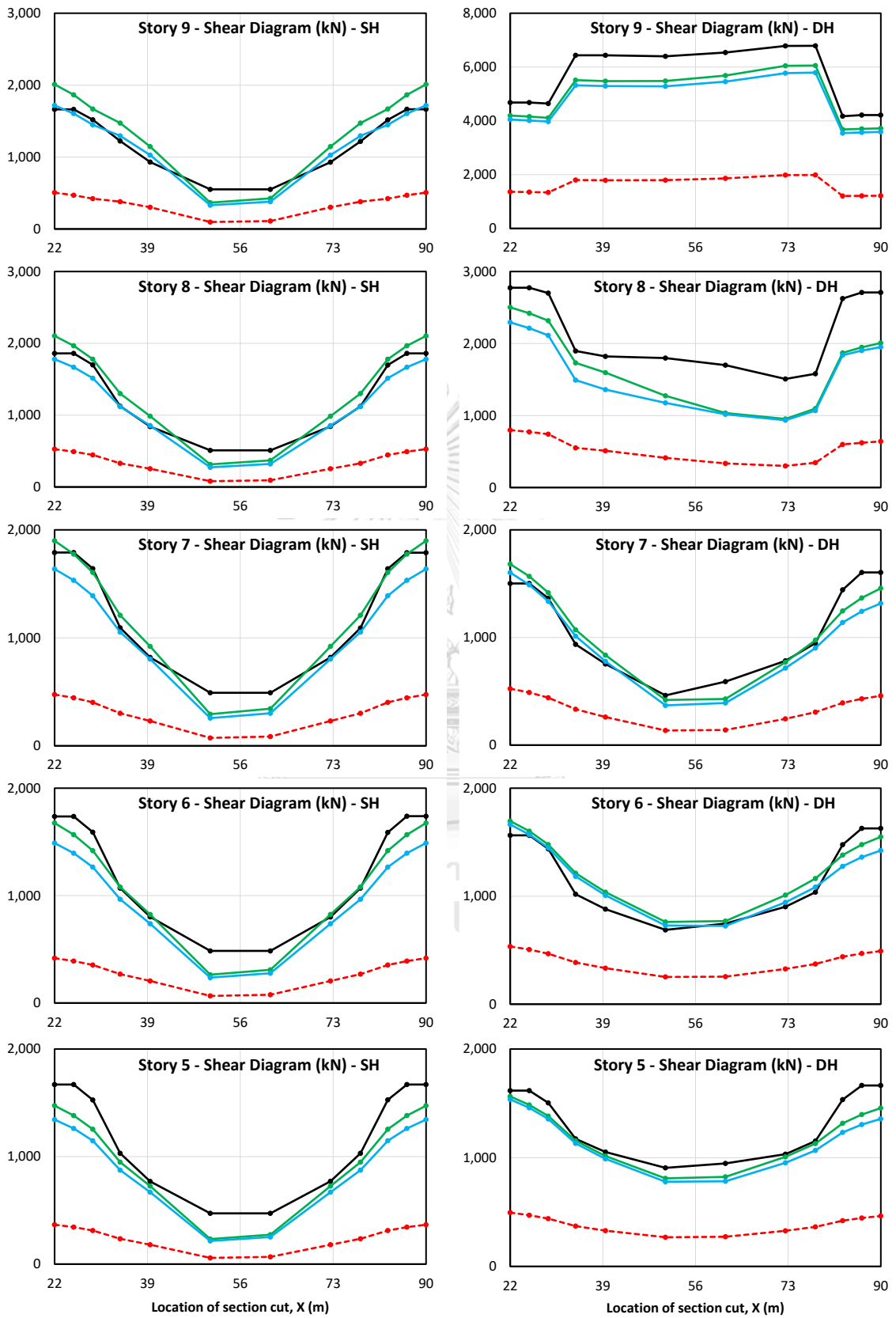

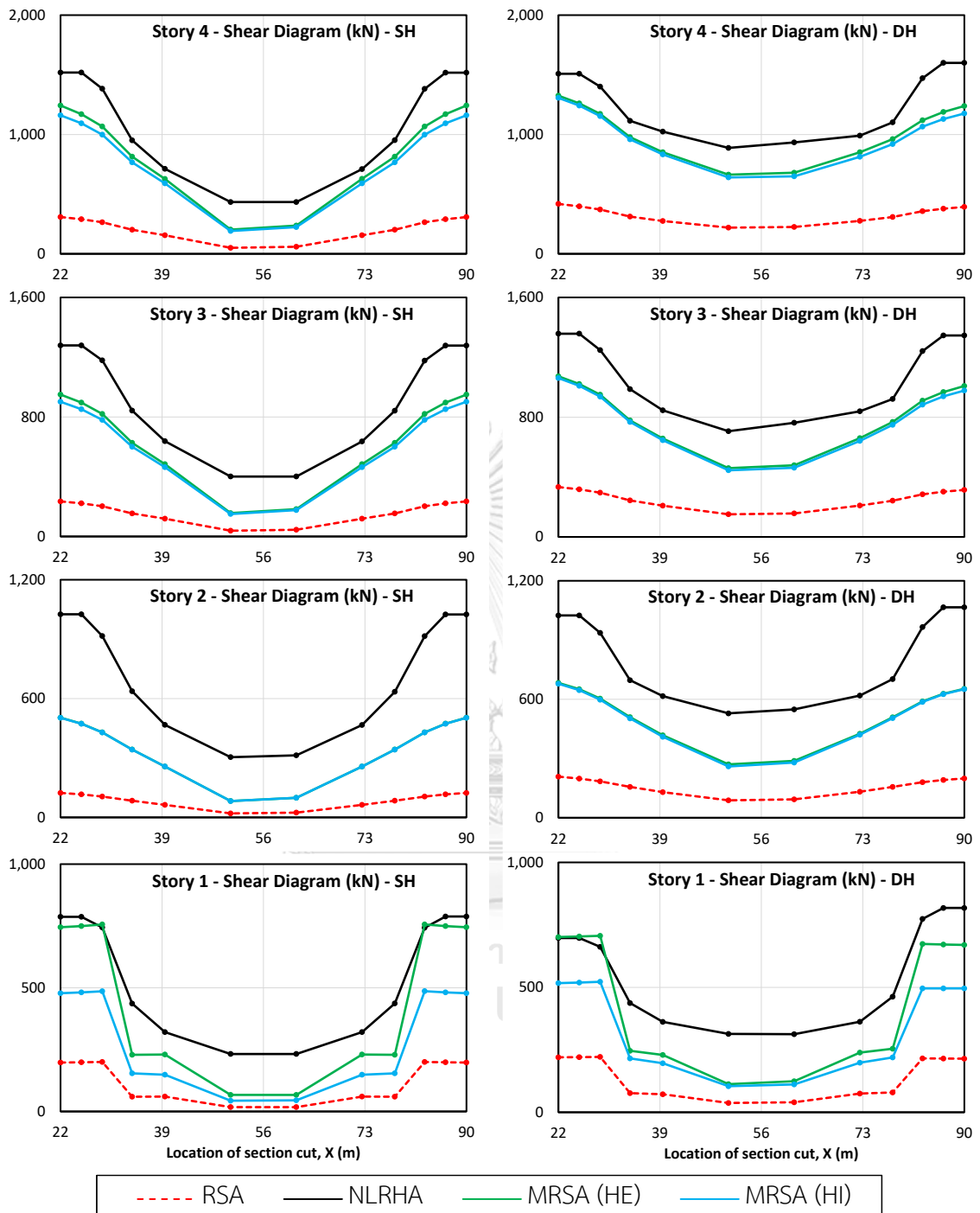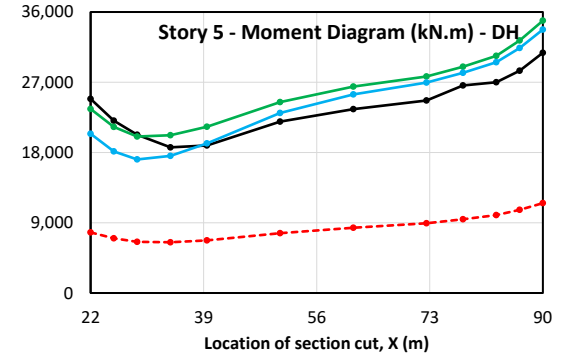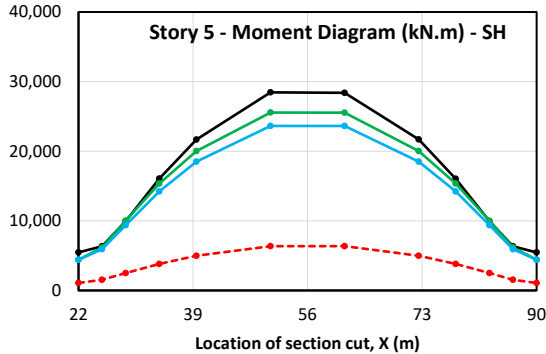Figure D.21 Section-cut locations.

(Continued)

Figure D.22 Shear forces in diaphragms due to earthquake in the Y-direction for buildings SH and DH located in Bangkok.

Story 9 - Moment Diagram (kN.m) - SH

Story 9 - Moment Diagram (kN.m) - DH

Story 8 - Moment Diagram (kN.m) - SH

Story 8 - Moment Diagram (kN.m) - DH

Story 7 - Moment Diagram (kN.m) - SH

Story 7 - Moment Diagram (kN.m) - DH

Story 6 - Moment Diagram (kN.m) - SH

Story 6 - Moment Diagram (kN.m) - DH

Story 5 - Moment Diagram (kN.m) - SH

Story 5 - Moment Diagram (kN.m) - DH

Location of section cut, X (m)

Location of section cut, X (m)
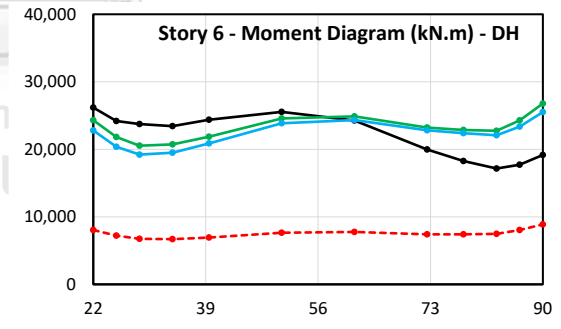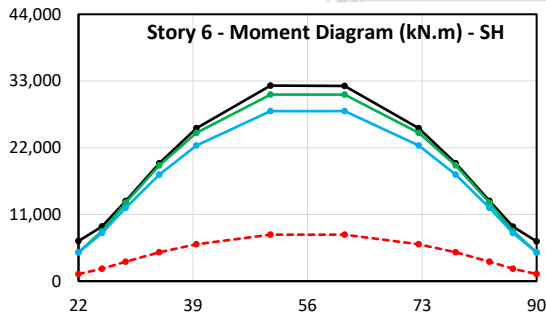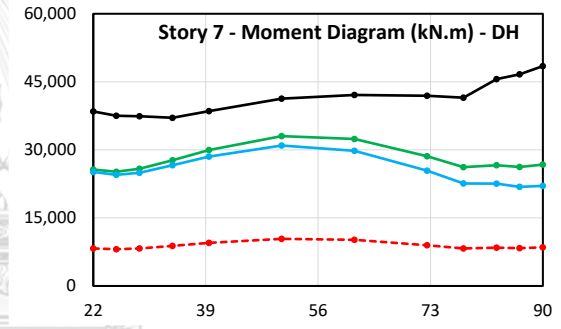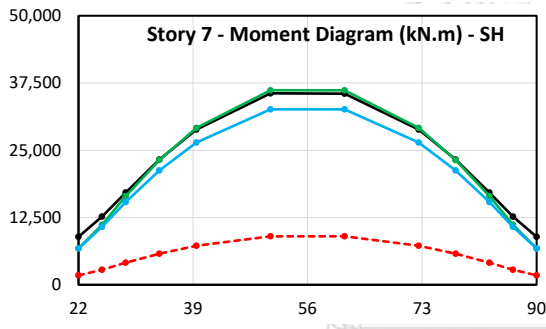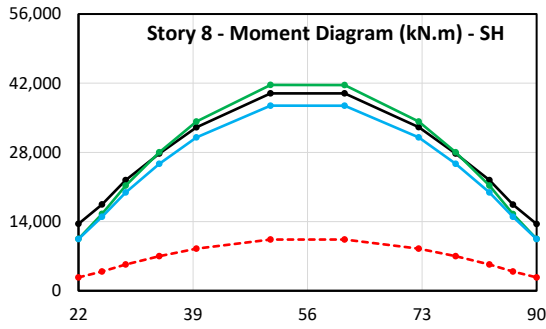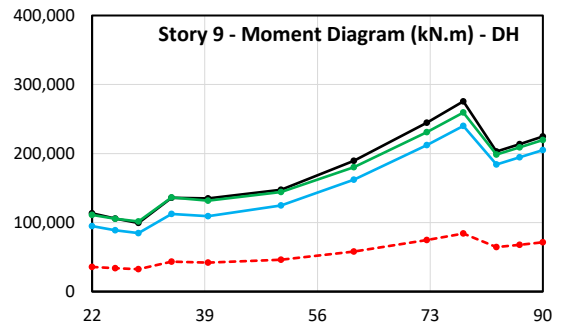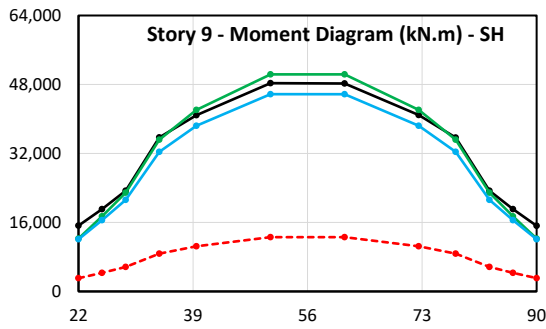
(Continued)

Figure D.23 Bending moment in diaphragms due to earthquake in the Y-direction for buildings SH and DH located in Bangkok.

(Continued)

Figure D.24 Shear forces in diaphragms due to earthquake in the Y-direction for buildings SH and DH located in Chiang Mai.

Story 9 - Moment Diagram (kN.m) - SH

Story 9 - Moment Diagram (kN.m) - DH

Story 8 - Moment Diagram (kN.m) - SH

Story 8 - Moment Diagram (kN.m) - DH

Story 7 - Moment Diagram (kN.m) - SH

Story 7 - Moment Diagram (kN.m) - DH

Story 6 - Moment Diagram (kN.m) - SH

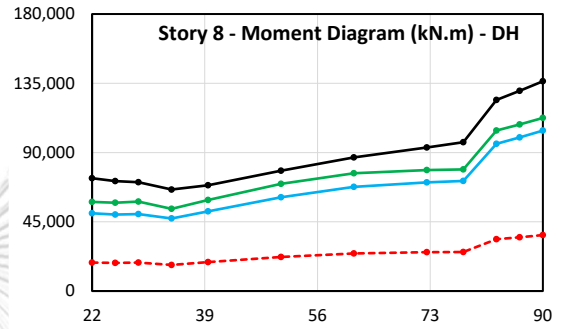Story 6 - Moment Diagram (kN.m) - DH

Story 5 - Moment Diagram (kN.m) - SH

Story 5 - Moment Diagram (kN.m) - DH

Location of section cut, X (m)

Location of section cut, X (m)

(Continued)
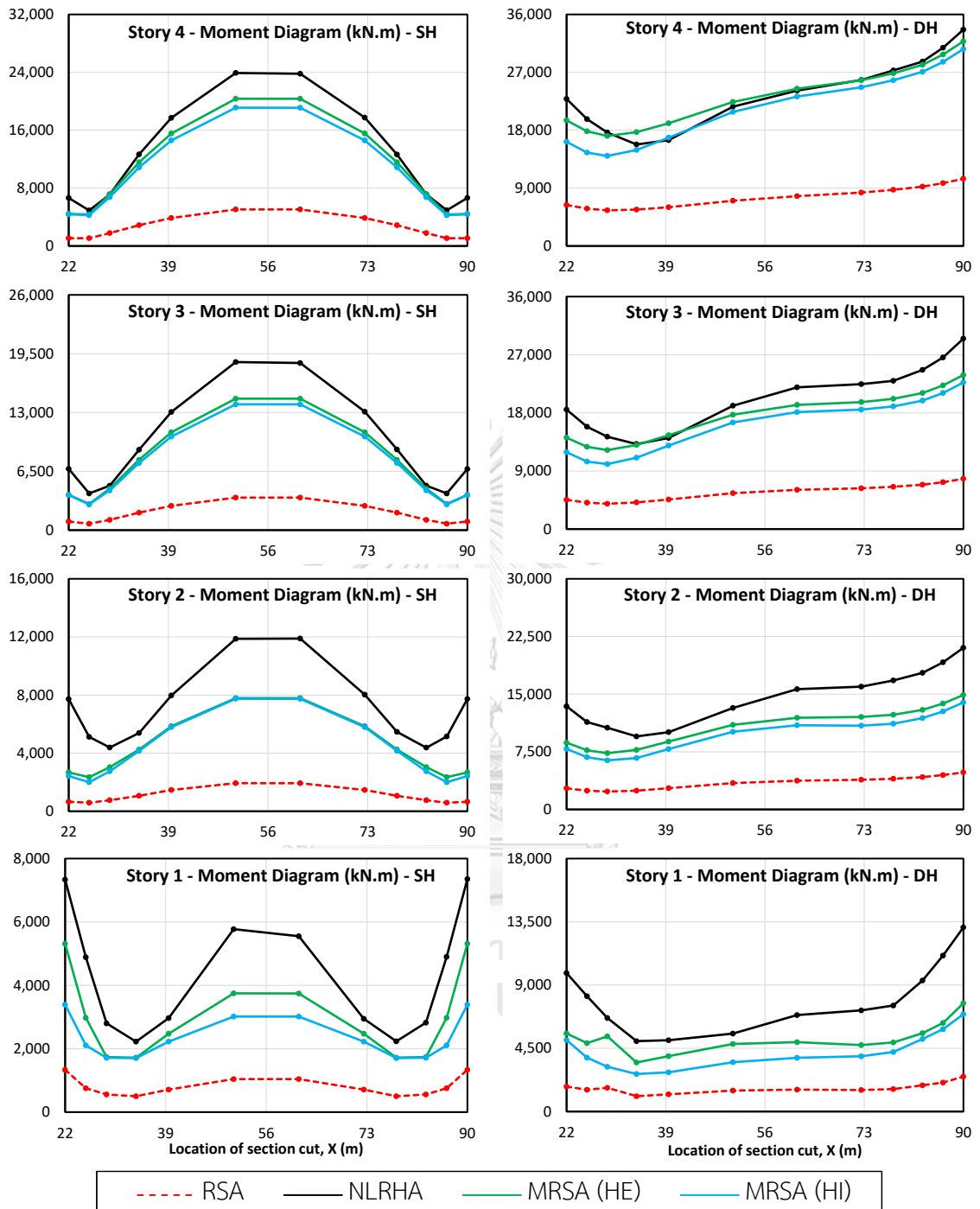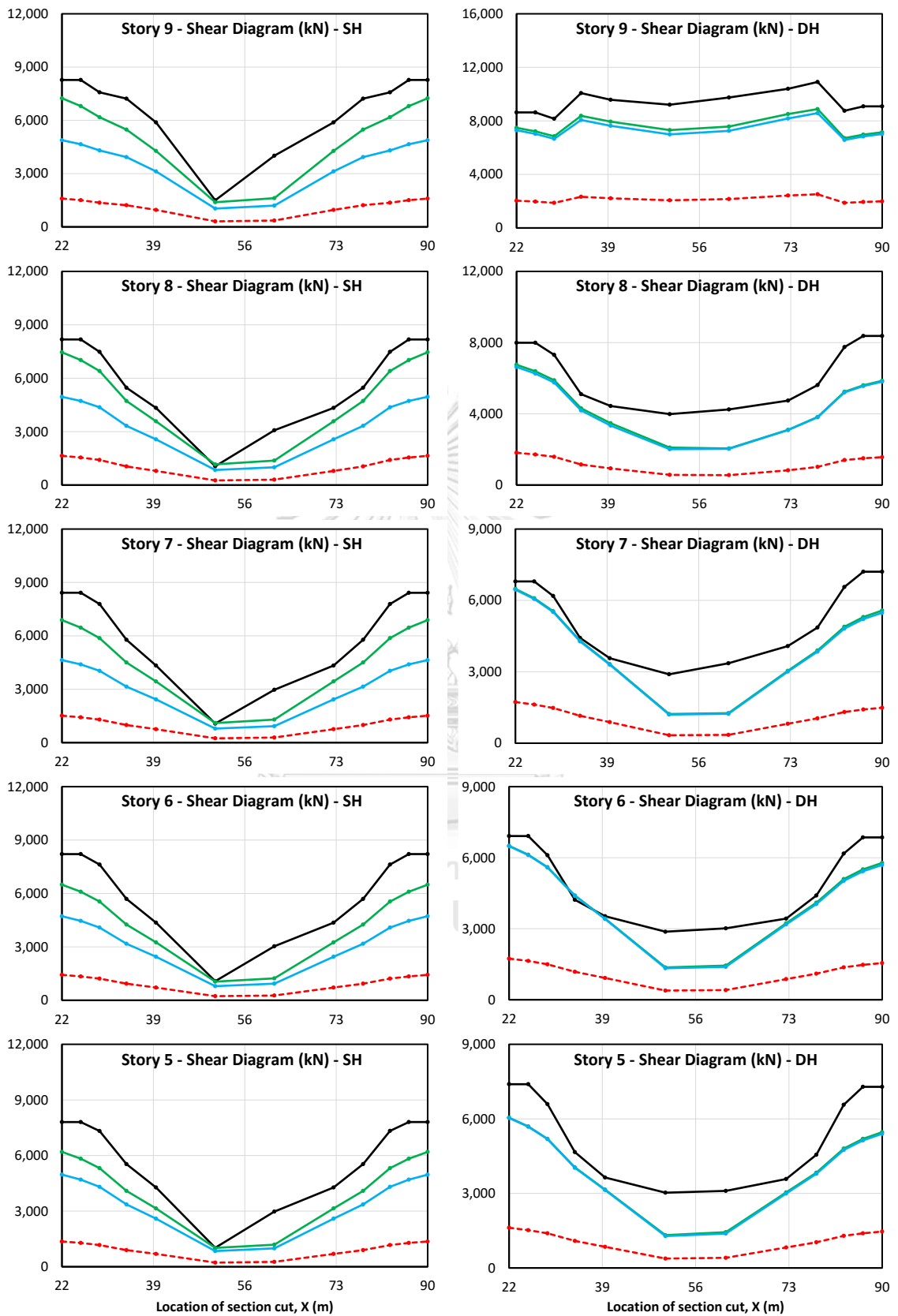
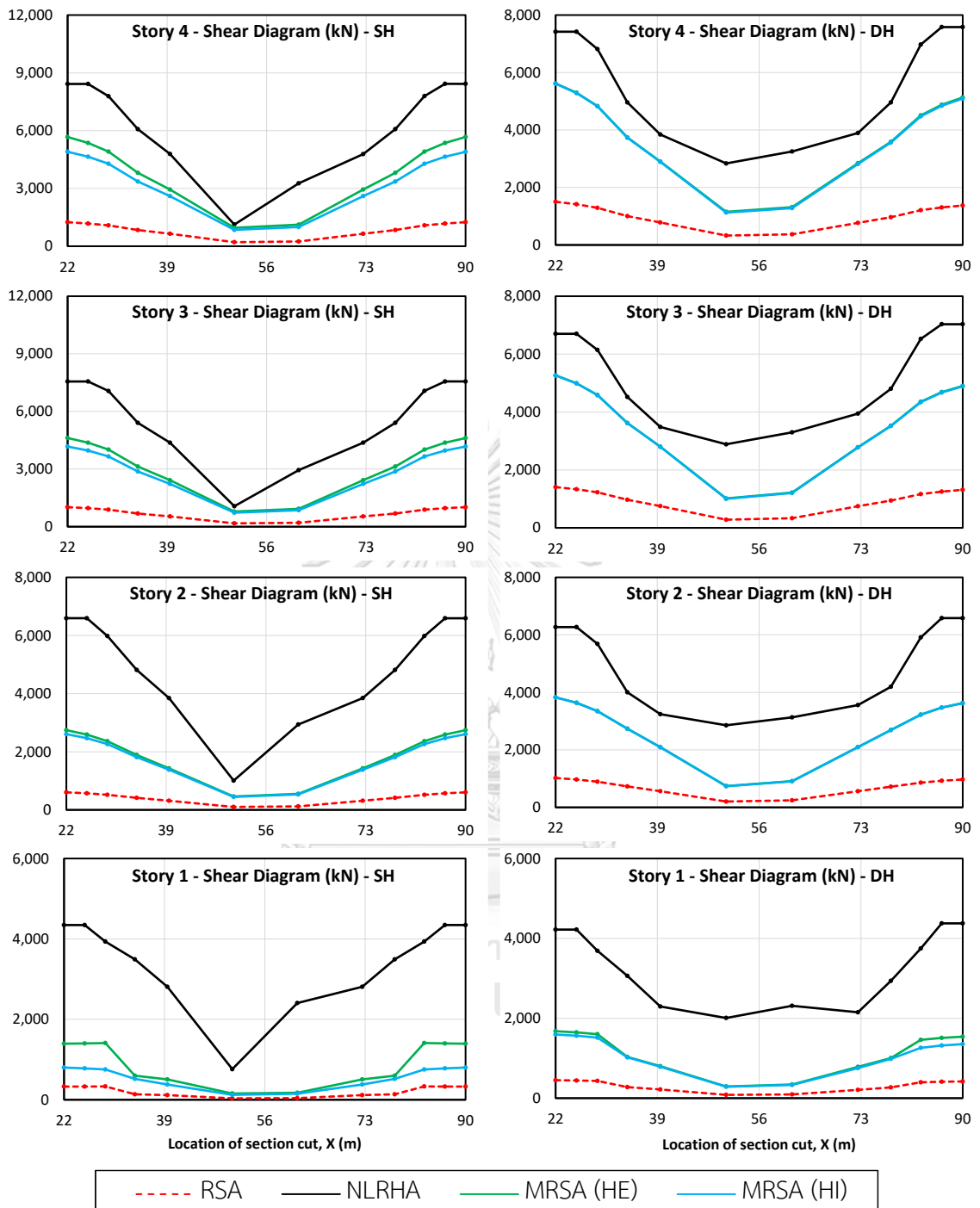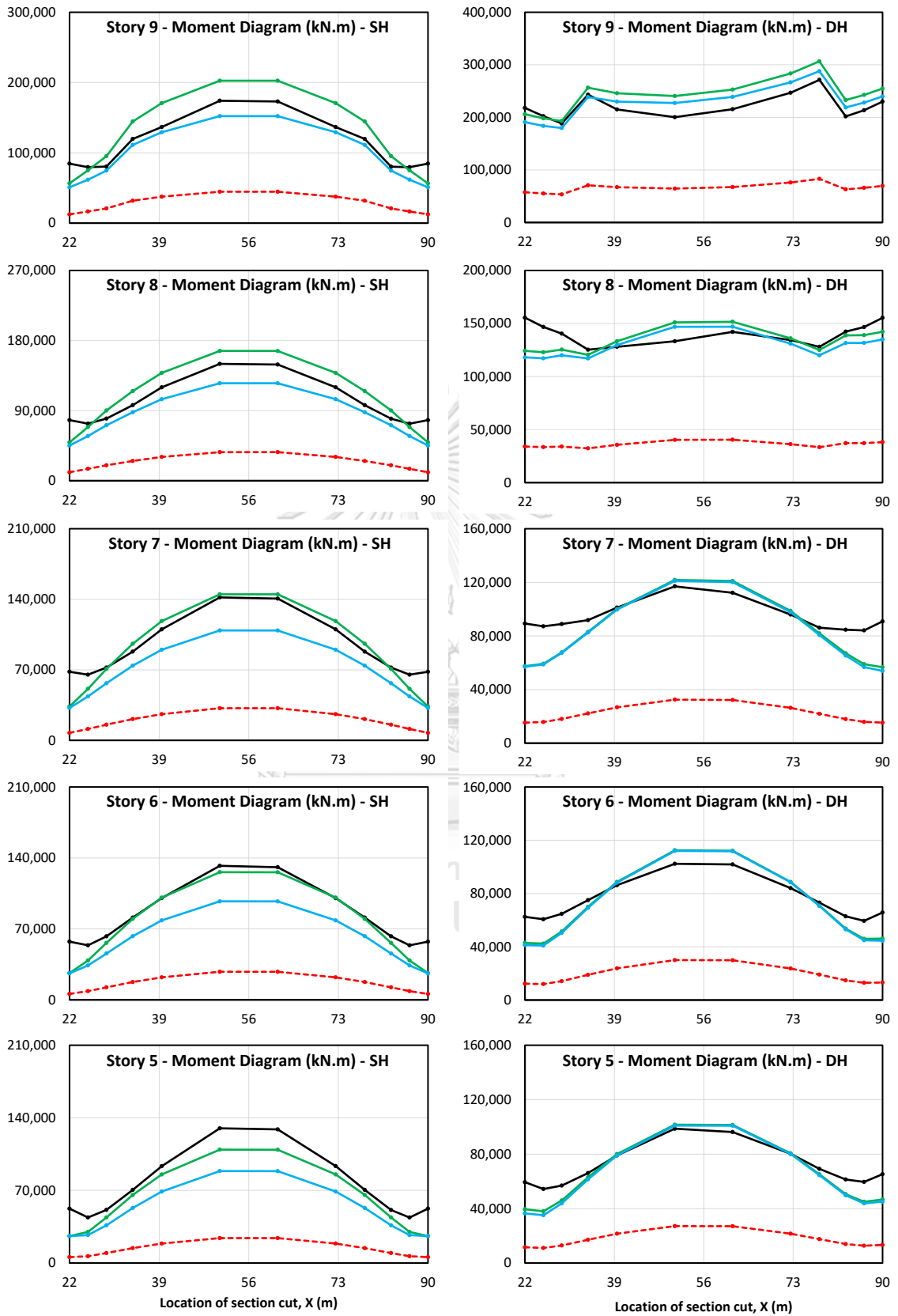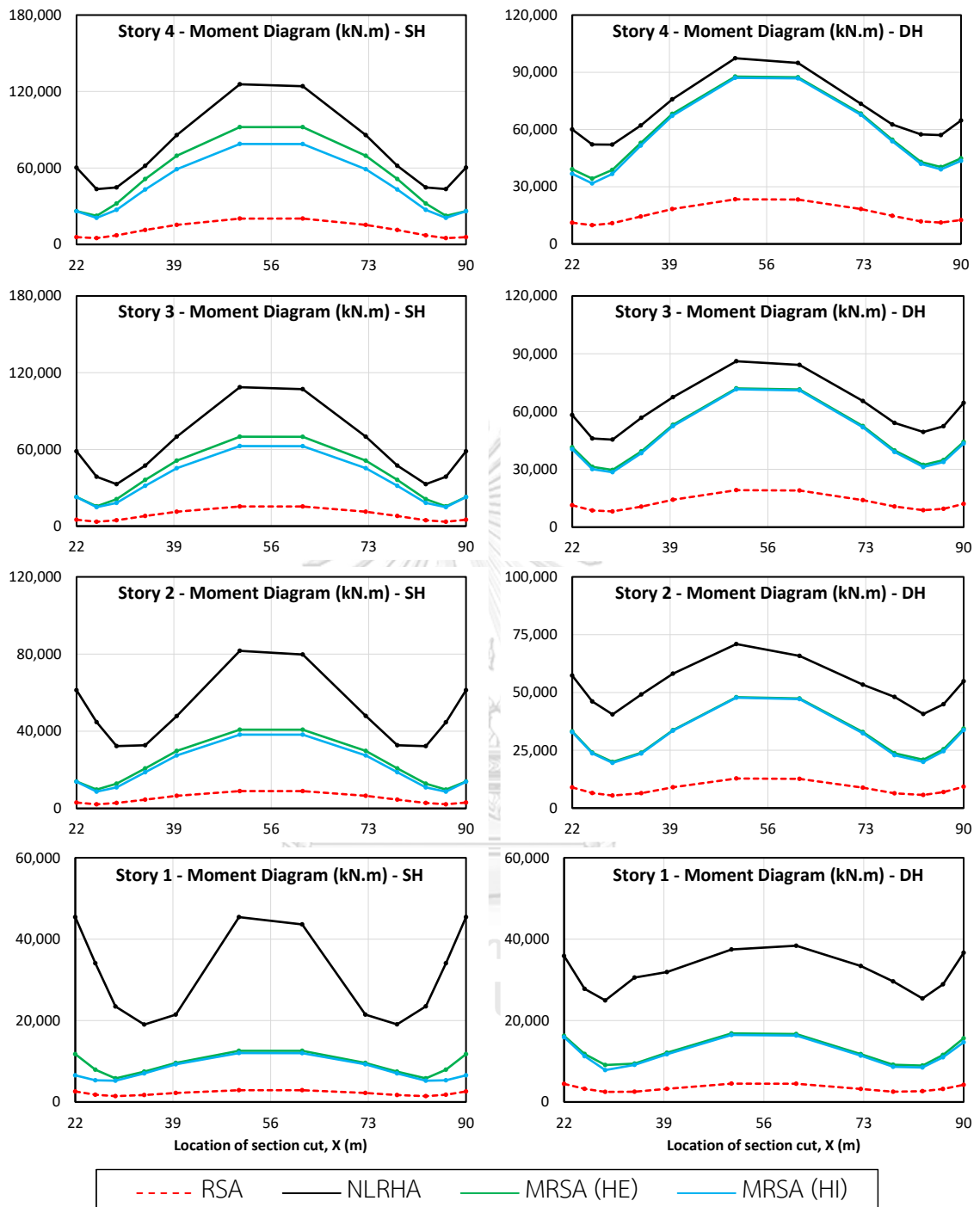Figure D.25 Bending moment in diaphragms due to earthquake in the Y-direction for buildings SH and DH located in Chiang Mai.

REFERENCES

American Concrete Institute. (2014). *Building Code Requirements for Structural Concrete (ACI 318M-14) and Commentary (ACI 318RM-14)*. Farmington Hills, USA.

American Concrete Institute. (2019). *Building Code Requirements for Structural Concrete (ACI 318-19) and Commentary (ACI 318R-19)*. Farmington Hills, USA.

American Society of Civil Engineers. (2013). *Seismic Evaluation and Retrofit of Existing Buildings*. ASCE/SEI 41-13. Reston, Virginia.

American society of Civil Engineers. (2016). *Minimum Design Loads and Associated Criteria for Buildings and Other Structures*. ASCE/SEI 7-16. Reston, Virginia.

Bangkok Metropolitan Administration. (2001). Bangkok Building Control Law, B.E. 2544. Retrieved from http://203.155.220.230/bmainfo/law/law.php?t=031

Blakeley, R. W. G., Cooney, R. C., & Megget, L. M. (1975). Seismic shear loading at flexural capacity in cantilever wall structures. *Bulletin of New Zealand National Society Earthquake Engineering, 8*(4), 278-290.

Boivin, Y., & Paultre, P. (2012). Seismic force demand on ductile reinforced concrete shear walls subjected to western North American ground motions: Part 2 - new capacity design methods. *Canadian Journal of Civil Engineering, 39*(7), 738-750. doi:10.1139/l2012-044

Canadian Standard Association. (2004). *Design of concrete structures*. CSA standard A23.3-04. Ontario, Canada.

Chao, S.-H., Goel, S., & Lee, S.-S. (2007). A Seismic Design Lateral Force Distribution Based on Inelastic State of Structures. *Earthquake Spectra, 23*. doi:10.1193/1.2753549

Chopra, A. K. (2012). *Dynamics of structures: theory and applications to earthquake*

engineering (4th ed.): Upper Saddle River, NJ: Pearson Prentice Hall.

Chopra, A. K., & Goel, R. K. (2002). A modal pushover analysis procedure for estimating seismic demands for buildings. *Earthquake Engineering and Structural Dynamics, 31*(3), 561-582.

Chopra, A. K., & Goel, R. K. (2002). A modal pushover analysis procedure for estimating seismic demands for buildings. *Earthquake Engineering & Structural Dynamics, 31*(3), 561-582.

Chopra, A. K., & Goel, R. K. (2004). A modal pushover analysis procedure to estimate seismic demands for unsymmetric-plan buildings. *Earthquake Engineering & Structural Dynamics, 33*(8), 903-927.

Chopra, A. K., & McKenna, F. (2016). Modeling viscous damping in nonlinear response history analysis of buildings for earthquake excitation. *Earthquake Engineering and Structural Dynamics, 45*(2), 193-211.

Cimellaro, G. P., Giovine, T., & Lopez-Garcia, D. (2014). Bidirectional pushover analysis of irregular structures. *Journal of structural engineering, 140*(9), 04014059.

Computers and Structures. (2018). *ETABS, Integrated Building Design Software, Version 18.0.1*. Berkeley, California.

Computers and Structures. (2018). *PERFORM-3D, Nonlinear Analysis and Performance Assessment of 3D Structures, Version 7.0.0*. Berkeley, California.

Department of Public Work and Town & Country Planning. (2018). *Seismic Resistant Design of Buildings and Structures, DPT 1301/1302-61*. Bangkok, Thailand.

Eibl, J., & Keintzel, E. (1988). Seismic shear forces in RC cantilever shear walls. *9th World conference on earthquake engineering*.

European Committee for Standardization. (2004). *Eurocode 8: Design of structures for earthquake resistance - Part 1: General rules, seismic actions and rules for*

buildings. Brussels, Belgium.

European Committee for Standardization. (2005). *Eurocode 8: Design of structures for earthquake resistance – Part 3: Assessment and retrofitting of buildingsr buildings*. Brussels, Belgium.

Fajfar, P. (2000). A nonlinear analysis method for performance-based seismic design. *Earthquake spectra, 16*(3), 573-592.

Fajfar, P., Marušić, D., & Peruš, I. (2005). Torsional effects in the pushover-based seismic analysis of buildings. *Journal of Earthquake Engineering, 9*(06), 831-854.

Filiatrault, A., D'Aronco, D., & Tinawi, R. (1994). Seismic shear demand of ductile cantilever walls: a Canadian code perspective. *Canadian Journal of Civil Engineering, 21*(3), 363-376. doi:10.1139/l94-039

Fleischman, R., Naito, C., Restrepo, J., Sause, R., & Ghosh, S. K. (2005). Seismic Design Methodology for Precast Concrete Diaphragms Part 1: Design Framework. *PCI Journal, 50*, 68-83. doi:10.15554/pcij.09012005.68.83

Haselton, C. B., Liel, A. B., Lange, S. T., & Deierlein, G. G. (2008). *Beam-column element model calibrated for predicting flexural response leading to global collapse of RC frame buildings* University of California, Berkeley, California.

Khy, K., & Chintanapakdee, C. (2017). Evaluation of seismic shear demands of RC core walls in Thailand determined by RSA procedure. *Engineering Journal, 21*(2), 151-172.

Khy, K., & Chintanapakdee, C. (2018). *Improved response spectrum analysis procedure for design of reinforced concrete tall buildings*. Retrieved from Bangkok:

Khy, K., Chintanapakdee, C., Warnitchai, P., & Wijeyewickrema, A. C. (2019). Modified response spectrum analysis to compute shear force in tall RC shear wall buildings. *Engineering Structures, 180*, 295-309.

doi:https://doi.org/10.1016/j.engstruct.2018.11.022

Kreslin, M., & Fajfar, P. (2012). The extended N2 method considering higher mode effects in both plan and elevation. *Bulletin of Earthquake Engineering, 10*(2), 695-715.

Luu, H., Léger, P., & Tremblay, R. (2013). Seismic demand of moderately ductile reinforced concrete shear walls subjected to high-frequency ground motions. *Canadian Journal of Civil Engineering, 41*(2), 125-135. doi:10.1139/cjce-2013-0073

Mander, J. B., Priestley, M. J., & Park, R. (1988). Theoretical stress-strain model for confined concrete. *Journal of Structural Engineering, ASCE, 114*(8), 1804-1826.

Ministry of Construction of China. (2001). *Code for Seismic Design of Buildings (GB50011-2001)*: China Architecture & Building Press, Beijing.

Moehle, J. P., Bozorgnia, Y., Jayaram, N., Jones, P., Rahnama, M., Shome, N., . . . Zareian, F. (2011). *Case studies of the seismic performance of tall buildings designed by alternative means, Task 12 Report for the Tall Buildings Initiative*. Berkeley, California: Pacific Earthquake Engineering Research Center, University of California.

Naish, D., Fry, A., Klemencic, R., & Wallace, J. (2013). Reinforced concrete coupling beams - Part II: Modeling. *ACI Structural Journal, 110*(6), 1067-1075.

Najam, F. A., & Warnitchai, P. (2018). A modified response spectrum analysis procedure to determine nonlinear seismic demands of high‑rise buildings with shear walls. *The Structural Design of Tall and Special Buildings, 27*(1), 1409.

Nakai, M., Koshika, N., Kawano, K., Hirakawa, K., & Wada, A. (2012). Performance-Based Seismic Design for High-Rise Buildings in Japan. *international Journal of High-Rise Buildings, 1*(3), 155-167.

National Building Code of Canada. (2010). *Commission on Building and Fire Codes, National Research Council of Canada*. Ottawa, Canada.

New Zealand Standard. (2006). *Concrete Structure Standard - Part 2: Commentary on the Design of Concrete Structures*. NZS 3101. Wellington, New Zealand.

Paulay, T., & Priestley, M. J. N. (1992). *Seismic Design of Reinforced Concrete and Masonry Buildings*. New York: John Wiley and Sons.

Priestley, M., Calvi, G., Kowalsky, M., & Powell, G. (2008). Displacement-Based Seismic Design of Structures *2007 New Zealand Society for Earthquake Engineering Conference*. Palmerston North, New Zealand.

Rejec, K., Isakovic, T., & Fischinger, M. (2012). Seismic shear force magnification in RC cantilever structural walls, designed according to Eurocode 8. *Bulletin of Earthquake Engineering, 10*(2), 567-586. doi:10.1007/s10518-011-9294-y

Reyes, J. C., & Chopra, A. K. (2011). Three-dimensional modal pushover analysis of buildings subjected to two components of ground motion, including its evaluation for tall buildings. *Earthquake Engineering & Structural Dynamics, 40*(7), 789-806.

Şahin, H., Alyamaç, K., & Erdoğan, A. (2013). Investigation of Dynamic Shear Amplification of Cantilever Wall Systems. *2nd International Balkans Conference on Challenges of Civil Engineering, BCCCE*.

Soleimani, S., Aziminejad, A., & Moghadam, A. (2017). Extending the concept of energy-based pushover analysis to assess seismic demands of asymmetric-plan buildings. *Soil Dynamics and Earthquake Engineering, 93*, 29-41.

Structural Engineers Association of North California. (2007). *Recommended Administrative Bulletin on the Seismic Design and Review of Tall Buildings using Non-Prescriptive Procedures*: Prepared for City of San Francisco Department of Building Inspection. San Francisco, California.

VITA

NAME	Tarek Youssef
DATE OF BIRTH	28 July 1995
PLACE OF BIRTH	Lebanon
INSTITUTIONS ATTENDED	M.Eng (2019-2020): Department of Civil Engineering, Chulalongkorn University, Thailand
	B.Eng. (2013-2017): Department of Civil Engineering, Rafik Hariri University, Lebanon
HOME ADDRESS	30M, Majdal Anjar, Bekaa, 1802, Lebanon

จุฬาลงกรณ์มหาวิทยาลัย
CHULALONGKORN UNIVERSITY